Site selection for offshore wind farms in Danish waters

Investigations of bird distribution and abundance

Energistyrelsen/Danish Energy Agency

This report has been prepared under the DHI Business Management System certified by Bureau Veritas to comply with ISO 9001 (Quality Management)

Site selection for offshore wind farms in Danish waters

Investigations of bird distribution and abundance

Prepared for	Energistyrelsen/Danish Energy Agency
Represented by	Mr Søren Keller

Authors	Henrik Skov, Lars O. Mortensen, Naomi Tuhuteru
Project manager	Henrik Skov
Quality supervisor	Mikael Kamp Sørensen

Project number	11823165
Approval date	18-09-2019
Revision	Final
Classification	Open ©

© Cover photo courtesy of Thomas W. Johansen

CONTENTS

0 Executive summary 1

1 Introduction 3

2 Methodology for bird investigations 5
2.1 Seabird survey data 5
2.1.1 North Sea 5
2.1.2 Southern Kattegat 6
2.1.3 Distance analysis 12
2.1.4 Establishment of geo-database on seabird survey data in the North Sea and Kattegat 14
2.2 Common Crane flight data at Krieger's Flak 14
2.3 Oceanographic dynamics of the coastal North Sea 14
2.4 Seabird distribution modelling 16
2.4.1 Background 16
2.4.2 Extraction of dynamic oceanographic co-variables 17
2.4.3 Model fitting 17
2.4.4 Model evaluation 18
2.4.5 Hydrodynamic modelling 18
2.4.6 Prediction of dynamic distributions of seabirds 18
2.5 Assessment of importance of areas to seabirds 19
2.5.1 Percentile contours 19
2.5.2 Determination of gradients in area importance 19
2.6 Assessment of migration patterns of Common Crane at Krieger's Flak 20
2.6.1 Assessment of the horizontal and vertical distribution of Common Crane 20
2.6.2 Assessment of cumulative collision risk with existing and planned projects 21

3 Results 23
3.1 Distribution models 23
3.1.1 North Sea 23
3.1.2 Southern Kattegat 44
3.2 Thor, Ringkøbing and Jammerbugt areas 68
3.2.1 Red-throated/Black-throated Diver 68
3.2.2 Northern Gannet 70
3.2.3 Common Scoter 72
3.2.4 Great Skua 74
3.2.5 Little Gull 74
3.2.6 Common Gull 76
3.2.7 Herring Gull 76
3.2.8 Sandwich Tern 77
3.2.9 Common Guillemot 77
3.2.10 Razorbill 78
3.2.11 Little Auk 78
3.3 Hesselø Area 79
3.3.1 Red-throated/Black-throated Diver 79
3.3.2 Red-necked Grebe 80
3.3.3 Mute Swan, Common Goldeneye, Greater Scaup 80
3.3.4 Common Eider, Common Scoter, Velvet Scoter 80
3.3.5 Herring Gull, Great Black-backed Gull 81
3.3.6 Black-legged Kittiwake 82
3.3.7 Razorbill 83
3.4 Krieger's Flak Area 84

3.4.1 Migration intensity of Common Crane 84
3.4.2 Horizontal and vertical distribution of Common Crane 84
3.4.3 Cumulative collision risk of Common Crane 90

4 Conclusions 94
4.1 Thor and Ringkøbing areas 94
4.2 Jammerbugt area 94
4.3 Hesselø area 94
4.4 Krieger's Flak area 95

5 References 96

A APPENDIX A – Hydrodynamic model – UKNS2 100
A.1 Water level 100
A.2 Currents 101
A.3 Salinity and water temperature 106

B APPENDIX B – Hydrodynamic model – DKBS2 108
B.1 Water Level 108
B.1.1 Measured water level 108
B.2 Circulation 111
B.2.1 Discharge through Danish straits 111
B.2.2 Measured current 112
B.3 Stratification 121
B.3.1 Measured salinity and water temperature 121
B.4 Conclusion 134
B.5 References 134

C APPENDIX C – Model Results 135
C.1 North Sea 135
C.1.1 Red-throated/Black-throated Diver 135
C.1.2 Common Scoter 137
C.2 Kattegat 139
C.2.1 Red-throated/Black-throated Diver 139
C.2.2 Common Eider 141
C.2.3 Common Scoter 143
C.2.4 Velvet Scoter 145
C.2.5 Black-legged Kittiwake 147
C.2.6 Razorbill 149

D APPENDIX D – Meta Data 151
D.1 North Sea – west coast 151
D.2 Jammerbugten 153
D.3 Kattegat 155

FIGURES

Figure 1 Overview of four regions designated for potential development of offshore wind farms. Thor forms part of the Ringkøbing area. The Danish Exclusive Economic Zone is indicated. 5
Figure 2 Seasonal coverage of aerial seabird survey data collected in the North Sea since 2000 and included in the investigation. Distance of surveyed transects (m) is summarized per 5 km^2. The 30 m depth contour is indicated. 7
Figure 3 Seasonal coverage of aerial seabird survey data collected in the southern part of Kattegat since 2000 and included in the investigation. Distance of surveyed transects (m) is summarized per 5 km^2. The 30 m depth contour is indicated. 8
Figure 4 Seasonal coverage of ship-based seabird survey data collected in the Kattegat since 1985 and included in the investigation. The 30 m depth contour is indicated. 9
Figure 5 Tracks of migrating Common Crane recorded by radar, rangefinder and satellite telemetry (Skov et al. 2015). 14
Figure 6 Mean patterns of surface salinity, temperature, frontal activity (current gradient) and eddy activity along the west coast of Jutland as estimated by DHIs North Sea model for the month of December 2018. 16
Figure 7 Profile lines (marked in green colour) used for the visualisation of density gradients across the four development areas in the North Sea and Kattegat. 20
Figure 8 Comparison of predicted versus observed numbers of Red-throated/Black-throated Diver *Gavia stellate/arctica* along the aerial transect lines in the North Sea. 24
Figure 9 Predicted mean monthly density (n/km^2) of Red-throated/Black-throated Diver *Gavia stellate/arctica* along the west coast of Denmark. 25
Figure 10 Predicted mean monthly density (n/km^2) of Red-throated/Black-throated Diver *Gavia stellate/arctica* along the coast of Skagerrak. 26
Figure 11 Areas of high habitat suitability to Red-throated/Black-throated Diver *Gavia stellate/arctica* predicted during the main months of occurrence along the west coast of Denmark. 27
Figure 12 Areas of high habitat suitability to Red-throated/Black-throated Diver *Gavia stellate/arctica* predicted during the main months of occurrence along the coast of Skagerrak. 28
Figure 13 Predicted gradients in the mean monthly density (n/km^2) of Red-throated/Black-throated Diver *Gavia stellate/arctica* along two profile lines crossing the Thor development area. 29
Figure 14 Predicted gradients in the mean monthly density (n/km^2) of Red-throated/Black-throated Diver *Gavia stellate/arctica* along the profile line crossing the Ringkøbing development area. 30
Figure 15 Predicted gradients in the mean monthly density (n/km^2) of Red-throated/Black-throated Diver *Gavia stellate/arctica* along two profile lines crossing the Jammerbugt development area. 31
Figure 16 Comparison of predicted versus observed numbers of Common Scoter *Melanitta nigra* along the aerial transect lines in the North Sea. 34
Figure 17 Predicted mean monthly density (n/km^2) of Common Scoter *Melanitta nigra* along the west coast of Denmark. 35
Figure 18 Predicted mean monthly density (n/km^2) of Common Scoter *Melanitta nigra* along the coast of Skagerrak. 36
Figure 19 Areas of high habitat suitability to Common Scoter *Melanitta nigra* predicted during the main months of occurrence along the west coast of Denmark. 37
Figure 20 Areas of high habitat suitability to Common Scoter *Melanitta nigra* predicted during the main months of occurrence along the coast of Skagerrak. 38
Figure 21 Predicted gradients in the mean monthly density (n/km^2) of Common Scoter *Melanitta nigra* along two profile lines crossing the Thor development area. 39
Figure 22 Predicted gradients in the mean monthly density (n/km^2) of Common Scoter *Melanitta nigra* along the profile line crossing the Ringkøbing development area. 40
Figure 23 Predicted gradients in the mean monthly density (n/km^2) of Common Scoter *Melanitta nigra* along two profile lines crossing the Jammerbugt development area. 41
Figure 24 Comparison of predicted versus observed numbers of Red-throated/Black-throated Diver *Gavia stellata{arctica* along the aerial transect lines in the southern Kattegat. 44
Figure 25 Predicted mean monthly density (n/km^2) of Red-throated/Black-throated Diver *Gavia stellata/arctica* in the southern Kattegat. 45

Figure 26 Areas of high habitat suitability to Red-throated/Black-throated Diver *Gavia stellata/arctica* predicted during the main months of occurrence in the southern Kattegat. 45
Figure 27 Predicted gradients in the mean monthly density (n/km^2) of Red-throated/Black-throated Diver *Gavia stellata/arctica* along two profile lines crossing the Hesselø development area. 46
Figure 28 Comparison of predicted versus observed numbers of Common Eider *Somateria mollissima* along the aerial transect lines in the southern Kattegat. 48
Figure 29 Predicted mean monthly density (n/km^2) of Common Eider *Somateria mollissima* in the southern Kattegat. 48
Figure 30 Areas of high habitat suitability to Common Eider *Somateria mollissima* predicted during the main months of occurrence in the southern Kattegat. 49
Figure 31 Predicted gradients in the mean monthly density (n/km^2) of Common Eider *Somateria mollissima* along two profile lines crossing the Hesselø development area. 50
Figure 32 Comparison of predicted versus observed numbers of Common Scoter *Melanitta nigra* along the aerial transect lines in the southern Kattegat. 52
Figure 33 Predicted mean monthly density (n/km^2) of Common Scoter *Melanitta nigra* in the southern Kattegat. 53
Figure 34 Areas of high habitat suitability to Common Scoter *Melanitta nigra* predicted during the main months of occurrence in the southern Kattegat. 53
Figure 35 Predicted gradients in the mean monthly density (n/km^2) of Common Scoter *Melanitta nigra* along two profile lines crossing the Hesselø development area. 54
Figure 36 Comparison of predicted versus observed numbers of Velvet Scoter *Melanitta fusca* along the aerial transect lines in the southern Kattegat. 56
Figure 37 Predicted mean monthly density (n/km^2) of Velvet Scoter *Melanitta fusca* in the southern Kattegat. 57
Figure 38 Areas of high habitat suitability to Velvet Scoter *Melanitta fusca* predicted during the main months of occurrence in the southern Kattegat. 57
Figure 39 Predicted gradients in the mean monthly density (n/km^2) of Velvet Scoter *Melanitta fusca* along two profile lines crossing the Hesselø development area. 58
Figure 40 Comparison of predicted versus observed numbers of Black-legged Kittiwake *Rissa tridactyla* along the ship-based transect lines in the southern Kattegat. 60
Figure 41 Predicted mean monthly density (n/km^2) of Black-legged Kittiwake *Rissa tridactyla* in the southern Kattegat. 61
Figure 42 Areas of high habitat suitability to Black-legged Kittiwake *Rissa tridactyla* predicted during the main months of occurrence in the southern Kattegat. 61
Figure 43 Predicted gradients in the mean monthly density (n/km^2) of Black-legged Kittiwake *Rissa tridactyla* along one profile line crossing the Hesselø development area. 62
Figure 44 Comparison of predicted versus observed numbers of Razorbill *Alca torda* along the ship-based transect lines in the southern Kattegat. 64
Figure 45 Predicted mean monthly density (n/km^2) of Razorbill *Alca torda* in the southern Kattegat. 65
Figure 46 Areas of high habitat suitability to Razorbill *Alca torda* predicted during the main months of occurrence in the southern Kattegat. 65
Figure 47 Predicted gradients in the mean monthly density (n/km^2) of Razorbill *Alca torda* along one profile line crossing the Hesselø development area. 66
Figure 48 Observed densities of Red-throated/Black-throated Diver *Gavia stellate/arctica* split by season 69
Figure 49 Observed densities of Northern Gannet *Morus bassanus* split by season. 71
Figure 50 Observed densities of Common Scoter *Melanitta nigra* split by season. 73
Figure 51 Observed densities of Little Gull *Hydrocoloeus minutus* split by season. 75
Figure 52 Observed densities of Common Gull *Larus canus* split by season. 76
Figure 53 Observed densities of Common Guillemot *Uria aalge* split by season 77
Figure 54 Observed densities of Red-throated/Black-throated Diver *Gavia stellate/arctica* split by season 79
Figure 55 Observed densities of Red-necked Grebe *Podiceps grisegena* split by season. 80
Figure 56 Observed densities of Herring Gull *Larus argentatus* and Great Black-backed Gull *Larus marinus* during winter. 81
Figure 57 Observed densities of Black-legged Kittiwake *Rissa tridactyla* split by season. 82

Figure 58 Observed densities of Razorbill *Alca torda* split by season. 83
Figure 59 Migration tracks of Common Crane collected in the region during the Krieger's Flak baseline (Skov et al. 2015). Upper panel: spring and autumn 2013 - GPS-telemetry tagged birds are indicated by orange lines, radar-based tracks are marked by blue lines, and rangefinder-based tracks by red lines. Lower panel: GPS-telemetry tagged birds 2014-2015. 85
Figure 60 Migration tracks of ten GPS-tagged Common Crane collected in the study region during 2011-2012 (Courtesy Swedish University of Agricultural Sciences). Tracks over the sea are lines combining adjoining GPS positions logged on land, and do not show actual flight paths. 86
Figure 61 Sampled migration directions of Common Crane at Falsterbo, autumn 2013 (Skov et al. 2015). Numbers on the Y-axes refer to sample size (number of recordings by laser rangefinder). Each wedge represents a sector of 15°. The mean direction is indicated by the black line running from the centre of the graph to the outer edge. The arcs extending to either side represent the 95% confidence limits of the mean direction. 86
Figure 62 Frequency distribution of altitude measurements of Common Crane by laser rangefinder at the Swedish south coast, at the Danish coast and at FINO 2 during the Kriegers Flak baseline, autumn 2013 (Skov et al. 2015). 87
Figure 63 Height measurements of 11 GPS-tagged Common Crane 2013-2015. Krieger's Flak is located at latitude 55.00° N. 88
Figure 64 GAMM response curves for the Common Crane based on data from both spring and autumn collected during the Krieger's Flak baseline (Skov et al. 2015). The values of the environmental predictors are shown on the X-axis and the response on the Y-axis is on the scale of the linear predictor. The degree of smoothing is indicated in the title of the Y-axis. The shaded areas and the dotted lines show the 95% Bayesian confidence intervals. 89
Figure 65 Average altitude for Common Crane in relation to distance from the coast of Sweden during autumn and from the coast of Germany during spring predicted during different visibility and wind directions for the spring and autumn seasons. All other predictor variables are set to mean values within the species-specific data set. The lines are the predicted flight altitudes and the black rectangle indicates the rotor swept area by 10 MW turbines. The line dividing the rectangle indicates the height of a 3 MW turbine. 91
Figure 66 Overview of planned, consented and built offshore wind farms in the Arkona Basin. 93
Figure 67 The cumulative number of Common Crane predicted to collide annually with wind farms in the Arkona Basin during different periods between 2000 and 2023. The Kriegers Flak A and B wind farms have been added to 2022 and 2023. The wind farms include all commissioned, consented and planned wind farms. The PBR threshold indicative of the limit for a sustainable mortality of Common Crane is indicated. 93

Figure A- 1 Comparison of measured and modelled water level at Helgoland. In the lower panel bias-corrected scatter plot and performance measures for the year 2011 are given. 100
Figure A- 2 Comparison of observed and modelled currents at FINO1 in the subsurface layer (at 8m depth). Data source: FINO1 ©Bundesamt für Seeschifffahrt und Hydrographie (BSH), Germany, sponsored by BMWi (Bundesministerium für Wirtschaft und Energie) and PTJ (Projektträger Jülich, Forschungszentrum Jülich). 102
Figure A- 3 Comparison of observed and modelled currents at FINO1 in the bottom layer (at 28m depth). Data source: FINO1 ©Bundesamt für Seeschifffahrt und Hydrographie (BSH), Germany, sponsored by BMWi (Bundesministerium für Wirtschaft und Energie) and PTJ (Projektträger Jülich, Forschungszentrum Jülich). 103
Figure A- 4 Comparison of observed and modelled currents at FINO3 in the surface layer (at 4m depth). Data source: FINO3 ©Bundesamt für Seeschifffahrt und Hydrographie (BSH), Germany, sponsored by BMWi (Bundesministerium für Wirtschaft und Energie), PTJ (Projektträger Jülich, Forschungszentrum Jülich), SH (Schleswig-Holstein) and EU (European Union). 104
Figure A- 5 Comparison of observed and modelled currents at FINO3 in the bottom layer (at 18m depth). Data source: FINO3 ©Bundesamt für Seeschifffahrt und Hydrographie (BSH), Germany, sponsored by BMWi (Bundesministerium für Wirtschaft und Energie), PTJ

(Projektträger Jülich, Forschungszentrum Jülich), SH (Schleswig-Holstein) and EU (European Union). 105
Figure A- 6 Comparison of measured and modelled salinity (top) and water temperature (bottom) at FINO1 station 106

Figure B- 1 Location of applied tide gauge stations 108
Figure B- 2 Comparison of measured and modelled water level at Aarhus 109
Figure B- 3 Comparison of measured and modelled water level at Hornbæk 109
Figure B- 4 Comparison of measured and modelled water level at Korsør 109
Figure B- 5Comparison of measured and modelled water level at Gedser 110
Figure B- 6 Instantaneous discharge at Great Belt, Øresund and Little Belt shown exemplary for 2011. Positive numbers represent outflow (northward), negative numbers inflow (southward) events. 111
Figure B- 7 Scatter plots of instantaneous discharges at Great Belt (horizontal axes) vs Øresund and Little Belt (vertical axes) for the year 2011. 111
Figure B- 8 Location of available current measurement stations. 112
Figure B- 9 Comparison of measured and modelled current at Väderöarna station at depth 4m. 113
Figure B- 10 Comparison of measured and modelled current at Väderöarna station at depth 28m. 114
Figure B- 11 Comparison of measured and modelled current at Läsö Ost Boj at depth 2m. 115
Figure B- 12 Comparison of measured and modelled current at FINO2 station at depth 5m. 116
Figure B- 13 Comparison of measured and modelled current at FINO2 station at depth 20m 117
Figure B- 14 Comparison of measured and modelled current at BSH Arkona Becken station at depth 5-6m 118
Figure B- 15 Comparison of measured and modelled current at BSH Arkona Becken station at depth 40m. 119
Figure B- 16 Comparison of measured and modelled current at Huvudskär Ost Boj at depth 2m. 120
Figure B- 17 Location of salinity and temperature measurement stations. 121
Figure B- 18 Comparison of measured and modelled salinity (top) and water temperature (bottom) at AA17 station 122
Figure B- 19 Comparison of measured and modelled salinity (top) and water temperature (bottom) at NOR7715 station 123
Figure B- 20 Comparison of measured and modelled salinity (top) and water temperature (bottom) at NOR403 station 124
Figure B- 21 Comparison of measured and modelled salinity (top) and water temperature (bottom) at Anholt E station 125
Figure B- 22 Comparison of measured and modelled salinity (top) and water temperature (bottom) at VSJ20925 station 126
Figure B- 23 Comparison of measured and modelled salinity (top) and water temperature (bottom) at ARH70117 station 127
Figure B- 24 Comparison of measured and modelled salinity (top) and water temperature (bottom) at FYN6100051 station 128
Figure B- 25 Comparison of measured and modelled salinity (top) and water temperature (bottom) at FYN6700053 station 129
Figure B- 26 Comparison of measured and modelled salinity (top) and water temperature (bottom) at FOE-B12 station 130
Figure B- 27Comparison of measured and modelled salinity (top) and water temperature (bottom) at KBH431 station. 131
Figure B- 28 Comparison of measured and modelled salinity (top) and water temperature (bottom) at BY2 station. 132
Figure B- 29 Comparison of measured and modelled salinity (top) and water temperature (bottom) at BY5 station. 133

Figure C- 1 Response curves for presence absence model parts for Red-throated/Black-throated Diver *Gavia stellate/arctica* in the North Sea. 136
Figure C- 2 Response curves for positive model parts for Red-throated/Black-throated Diver *Gavia stellate/arctica* in the North Sea. 136
Figure C- 3 Response curves for presence absence model parts for Common Scoter *Melanitta nigra* in the North Sea. 138
Figure C- 4 Response curves for positive model parts for Common Scoter *Melanitta nigra* in the North Sea. 138
Figure C- 5 Response curves for presence absence model parts for Red-throated/Black-throated Diver *Gavia stellata/arctica* in the southern Kattegat. 140
Figure C- 6 Response curves for positive model parts for Red-throated/Black-throated Diver *Gavia stellata/arctica* in the southern Kattegat. 140
Figure C- 7 Response curves for presence absence model parts for Common Eider *Somateria mollissima* 142
Figure C- 8 Response curves for positive model parts for Common Eider *Somateria mollissima* 142
Figure C- 9 Response curves for presence absence model parts for Common Scoter *Melanitta nigra* 144
Figure C- 10 Response curves for positive model parts for Common Scoter *Melanitta nigra* 144
Figure C- 11 Response curves for presence absence model parts for Velvet Scoter *Melanitta fusca* 146
Figure C- 12 Response curves for positive model parts for Velvet Scoter *Melanitta fusca* 146
Figure C- 13 Response curves for presence absence model parts for Black-legged Kittiwake *Rissa tridactyla* 147
Figure C- 14 Response curves for positive model parts for Black-legged Kittiwake Rissa tridactyla 148
Figure C- 15 Response curves for presence absence model parts for Razorbill *Alca torda* 150
Figure C- 16 Response curves for positive model parts for Razorbill *Alca torda* 150

TABLES

Table 1 Seabird survey data included in the study. 10
Table 2 Distance corrections applied for the aerial survey data for the North Sea and Kattegat for each species and data provider 13
Table 3 Model overview indicating the bird species modelled, databases used and both dynamic and static predictors used for the North Sea and Kattegat study areas. 18
Table 4 Statistics on the predicted abundance of Red-throated/Black-throated Diver *Gavia stellate/arctica* in the Thor development area in comparison to the rest of the Danish part of the North Sea. 32
Table 5 Statistics on the predicted abundance of Red-throated/Black-throated Diver *Gavia stellate/arctica* in the Ringkøbing development area in comparison to the rest of the Danish part of the North Sea 32
Table 6 Statistics on the predicted abundance of Red-throated/Black-throated Diver *Gavia stellate/arctica* in the Jammerbugt development area in comparison to the rest of the Danish part of the North Sea 33
Table 7 Statistics on the predicted abundance of Common Scoter *Melanitta nigra* in the Thor development area in comparison to the rest of the Danish part of the North Sea. 42
Table 8 Statistics on the predicted abundance of Common Scoter *Melanitta nigra* in the Ringkøbing development area in comparison to the rest of the Danish part of the North Sea. 42
Table 9 Statistics on the predicted abundance of Common Scoter *Melanitta nigra* in the Jammerbugt development area in comparison to the rest of the Danish part of the North Sea. 43
Table 10 Statistics on the predicted abundance of Red-throated/Black-throated Diver *Gavia stellata/arctica* in the Hesselø development area in comparison to the rest of the southern Kattegat. 47
Table 11 Statistics on the predicted abundance of Common Eider *Somateria mollissima* in the Hesselø development area in comparison to the rest of the southern Kattegat. 51
Table 12 Statistics on the predicted abundance of Common Scoter *Melanitta nigra* in the Hesselø development area in comparison to the rest of the southern Kattegat. 55

Table 13 Statistics on the predicted abundance of Velvet Scoter *Melanitta fusca* in the Hesselø development area in comparison to the rest of the southern Kattegat. 59
Table 14 Statistics on the predicted abundance of Black-legged Kittiwake *Rissa tridactyla* in the Hesselø development area in comparison to the rest of the southern Kattegat.....63
Table 15 Statistics on the predicted abundance of Razorbill *Alca torda* in the Hesselø development area in comparison to the rest of the southern Kattegat. 67

Table A- 1 List of predictor variables included in the initial distribution models 107

Table C- 1 Smooth terms, adjusted R-squared and evaluation statistics for the distribution models for Red-throated/Black-throated Diver *Gavia stellate/arctica* in the North Sea. F statistics and the approximate significance for the smooth terms and t-statistic and the significance for the parametric terms are shown. 135
Table C- 2 Smooth terms, adjusted R-squared and evaluation statistics for the distribution models for Common Scoter *Melanitta nigra* in the North Sea. F statistics and the approximate significance for the smooth terms and t-statistic and the significance for the parametric terms are shown.....137
Table C- 3 Smooth terms, adjusted R-squared and evaluation statistics for the distribution models for Red-throated/Black-throated Diver *Gavia stellata/arctica* in the southern Kattegat. F statistics and the approximate significance for the smooth terms and t-statistic and the significance for the parametric terms are shown. 139
Table C- 4 Smooth terms, adjusted R-squared and evaluation statistics for the distribution models for Common Eider *Somateria mollissima* in the southern Kattegat. F statistics and the approximate significance for the smooth terms and t-statistic and the significance for the parametric terms are shown. 141
Table C- 5 Smooth terms, adjusted R-squared and evaluation statistics for the distribution models for Common Scoter *Melanitta nigra* in the southern Kattegat. F statistics and the approximate significance for the smooth terms and t-statistic and the significance for the parametric terms are shown.....143
Table C- 6 Smooth terms, adjusted R-squared and evaluation statistics for the distribution models for Velvet Scoter *Melanitta fusca* in the southern Kattegat. F statistics and the approximate significance for the smooth terms and t-statistic and the significance for the parametric terms are shown.....145
Table C- 7 Smooth terms, adjusted R-squared and evaluation statistics for the distribution models for Black-legged Kittiwake *Rissa tridactyla*. F statistics and the approximate significance for the smooth terms and t-statistic and the significance for the parametric terms are shown.....147
Table C- 8 Smooth terms, adjusted R-squared and evaluation statistics for the distribution models for Razorbill *Alca torda* in the southern Kattegat. F statistics and the approximate significance for the smooth terms and t-statistic and the significance for the parametric terms are shown. 149

0 Executive summary

In connection with the Danish Energy Agency's screening for new areas for development of offshore wind farms, four gross areas have been identified for the upcoming 800 MW offshore wind farms, consisting of the areas Thor/Ringkøbing (North Sea), Jammerbugt, Hesselø and Krieger's Flak. As part of the screening, this report provides reviews and analyses of existing knowledge of bird occurrence in the four areas with the aim to strengthen the basis for decision-making for the location of future offshore wind farms. The key species investigated in the four areas are:

Ringkøbing/Thor and Jammerbugt: Red-/Black-throated Diver, Common Scoter

Hesselø: Red-/Black-throated Diver, Common Eider, Common Scoter, Velvet Scoter, Black-legged Kittiwake, Razorbill

Krieger's Flak: Common Crane

The existing database for assessing bird occurrence in the four areas is extensive both in terms of geographical and temporal coverage. The reviewed database contains all data after 2000 which have been collected with standardized methods at international and nationwide Danish waterbird counts, dedicated counts carried out in planned offshore wind turbine projects and designation of areas worthy of protection etc. The review concluded that further surveys will not appreciably increase safety in the assessment of bird occurrence in the four areas. Following this, efforts to supplement existing data on bird occurrence in the four areas has therefore focused on the collection of all existing data in geo-databases of waterbird densities and the establishment of detailed maps of the main species spread in and around the areas. The review further concluded that key species for assessment of the ornithological importance and sensitivity of the Thor/Ringkøbing and Jammerbugt development areas were Red-throated/Black-throated Diver and Common Scoter, while the migration of Common Crane was the key feature of interest in relation to the development area on Krieger's Flak. Thus, detailed analyses and models were developed for these species and scenarios.

It can largely be said that the lack of knowledge of certain species / subsections in the four gross areas is due to the fact that existing data have not been collected and put into a marine biological context in the gross areas. Due to the wide spread of surveillance data, efforts have been required to collect these data in geo-databases and to produce fine-scale density maps for use in the EIA context. In connection with the baseline investigations for the Krieger's Flak OWF project the flight behaviour of migrating Common Crane was investigated using satellite telemetry, rangefinder and radar tracking. These unique data provided high resolution tracks showing flight trajectories and altitudes as Common Cranes cross the Krieger's Flak area during different meteorological conditions. The data have been made available for the assessment of the new gross Krieger's Flak development area.

Accurate assessment of habitat use by seabirds requires highly dynamic, fine-resolution data both for species and the environment. Hence, we have used time series of post-processed hydrodynamic variables from DHI's North Sea model to link observations of seabirds to the hydrodynamic variables which most influence the distribution of seabirds. Both the Ringkøbing/Thor and Jammerbugt development areas are located at the interface between the Jutland Current and North Sea water masses with the strongest gradient in surface salinity found in the eastern (Ringkøbing/Thor) and south eastern (Jammerbugt) parts. The links between the distribution of seabirds and oceanographic conditions were established using dynamic species distribution models which coupled observations of seabirds to flow and hydrographic variables based on closest match in space and time.

The validation of the developed species distribution models shows that a high predictive accuracy has been achieved in the distribution models of the Red-throated and Black-throated Diver and the Common Scoter in the areas targeted for offshore wind farms in the Danish part of the North Sea. The Thor wind farm area constitutes the northernmost part of the much larger Ringkøbing area, which extends to the north western Horns Rev area. As both divers and Common Scoter display highest densities towards the north western Horns Rev the southern half of the Ringkøbing area overlaps with high densities of

divers (>0.75 birds/km^2) and scoters (>50 birds/km^2), hold relatively large numbers of birds in comparison with their total population size and therefore has a high risk for severe displacement of these species. Densities of scoters are much lower in the northern part of the Ringkøbing and Thor areas, and high densities of divers in Thor are limited to the easternmost 5 km of the dedicated wind farm area.

Although the concentration of Common Scoter in Ringkøbing and Thor areas is predicted to be persistent across seasons the densities of divers in both areas only reach densities above 0.75 birds/km^2 during the period preceding spring migration in April. Yet, although peak numbers are limited in time potential population effects of displacement may still be significant depending on available food resources in the areas which the birds are displaced into.

The dedicated wind farm area in Jammerbugt is located in the same type of marine habitat as the north eastern part of the Ringkøbing area and the Thor area, and densities of divers and scoters are therefore similar. Accordingly, densities of divers are comparable to these areas, and higher densities of divers in the Jammerbugt area are also confined to the month of April. More than half of the central part of the wind farm area has high habitat quality to divers during April. The densities of Common Scoter reach medium level in the southern half of the wind farm area.

With the exception of Black-legged Kittiwake during the winter period the dedicated wind farm area Hesselø hosts low densities of seabirds, including divers and seaducks. As the Black-legged Kittiwake has low sensitivity towards displacement from offshore wind farms the Hesselø site should be considered as the most suitable of the four proposed sites due to overall low levels of impacts on birds foreseen for this site.

With respect to Krieger's Flak and the Arkona Basin, the cumulative impact from all projects in the region means that 1,466 Common Cranes have the potential to collide annually with the existing, consented and planned offshore wind farms in the near future. Compared to the estimated PBR threshold of 1,887 birds, the combined collision impact on the Swedish-Norwegian population of Common Crane equals 77.7 % of the PBR threshold. As the collision mortality is clearly below the PBR threshold the population will most likely be capable of compensating the loss of birds imposed by the 18 projects by 2023. With additional offshore wind farm projects in the region the collision mortality may, however approach a level which is not sustainable by the population.

1 Introduction

DHI has been commissioned by the Danish Energy Agency to provide an updated data basis on the occurrence of birds in four gross areas for offshore wind turbines and an assessment of the suitability of the areas in relation to the areas' sensitivity and protection value for birds. The results of this work will be used as an improved basis for selecting areas for offshore wind turbines and for implementing future EIA studies.

In connection with the Danish Energy Agency's screening for new areas for use in offshore wind, four gross areas have been identified for the upcoming 800 MW offshore wind farms, consisting of the areas Thor/Ringkøbing (North Sea), Jammerbugt, Hesselø and Krieger's Flak. For a possible final designation of areas for new offshore wind farms, the Danish Energy Agency, in cooperation with COWI A / S, has initiated a closer screening of the gross areas. As part of screening, existing knowledge of bird occurrence in the four gross areas of offshore wind should be supplemented in order to strengthen the basis for decision-making for the location of future offshore wind farms.

The main purpose of the task is to provide a modern and adequate data basis on the occurrence of birds that can or can with great certainty confirm or deny whether an offshore wind farm is compatible with the protection concerns of the bird species that occur in the four areas.

Rather than an in-depth treatment of the occurrence of all bird species in the four areas The Danish Energy Agency has stressed that, for resource reasons the task has been delimited to provide supplementary bird data for the key bird species determined by their sensitivity to displacement, barrier effects and collision with offshore wind turbines and the relative importance of the areas. DHI has therefore focused the work on the following four project activities mentioned in chronological order:

1. Prioritizing the collection of supplementary information based on the occurrence and sensitivity of birds

2. Evaluation of data needs

3. Establishment of area-covering and detailed distribution maps of waterbird densities in the North Sea and central Kattegat, and an assessment of flight behavior and collision risk for migrating Common Crane at Krieger's Flak

4. Assessment of the suitability of the areas as offshore wind farms in relation to birds

The key species investigated in the four areas are:

Ringkøbing/Thor and Jammerbugt: Red-/Black-throated Diver, Common Scoter

Hesselø: Red-/Black-throated Diver, Common Eider, Common Scoter, Velvet Scoter, Black-legged Kittiwake, Razorbill

Krieger's Flak: Common Crane

The existing data base for assessing bird occurrence in the four areas is extensive both in terms of geographical and temporal coverage. Following a review of all existing data after 2000, which have been collected with standardized methods at international and nationwide Danish waterbird counts, dedicated counts carried out in planned offshore wind turbine projects and designation of areas worthy of protection etc. The review concluded that further surveys will not appreciably increase safety in the assessment of bird occurrence in the four areas. Following this, efforts to supplement existing data on bird occurrence in the four areas has therefore focused on the collection of all existing

data in geo-databases of waterbird densities and the establishment of detailed maps of the main species spread in and around the areas.

It can largely be said that the lack of knowledge of certain species / subsections in the four gross areas is due to the fact that existing data have not been collected and put into a marine biological context in the gross areas. Due to the wide spread of surveillance data, efforts have been required to collect these data in geo-databases and to produce fine-scale density maps for use in the EIA context.

2 The site selection process for the new Danish offshore wind farms

Based on the Danish Energy Agency's screening, four potential areas have been identified for establishing new offshore wind farms (Figure 1):

- Thor and Ringkøbing (North Sea)
- Jammerbugten
- Hesselø
- Krieger's Flak

COWI has been commissioned to establish an economic ranking of the four areas by performing a fine screening, which takes into account the seabed conditions, environmental and space conditions, most obvious network connection and wind resource within the given area. The updated assessment of the occurrence of birds in the four gross areas feed into the overall ranking system.

In 2014, COWI carried out a validation of meso-scale wind data for coastal projects in Denmark. The conclusion from the validation was that the meso-scale data generated is in such good agreement with actual measurements that they can be used directly in the wind resource assessments for Danish offshore wind turbine projects.

A sensitivity analysis of the environmental and planning effects of establishment of the four wind farms is carried out in two steps:

- Step 1, where selected environmental and planning conditions which can be influenced by the establishment of offshore wind turbines are mapped in GIS.
- Step 2, which produces GIS maps that rank the sensitivity of different areas (and sub-areas) facing the establishment of an offshore wind farm at each site (with associated landing corridors).

Based on the GIS maps of the prevalence of the selected environmental and planning conditions, scoring values and weights the overall sensitivity to the establishment and operation of offshore wind farms at each site is calculated using a GIS model. The environmental and planning conditions in the four potential offshore wind farms (with associated landing corridors) is being described, and the suitability of the sites with regard to the establishment of an offshore wind farm is ranked based on the results of the sensitivity analysis. To the extent possible, sub-areas are ranked within the sites in order to identify the areas that least harm the environment.

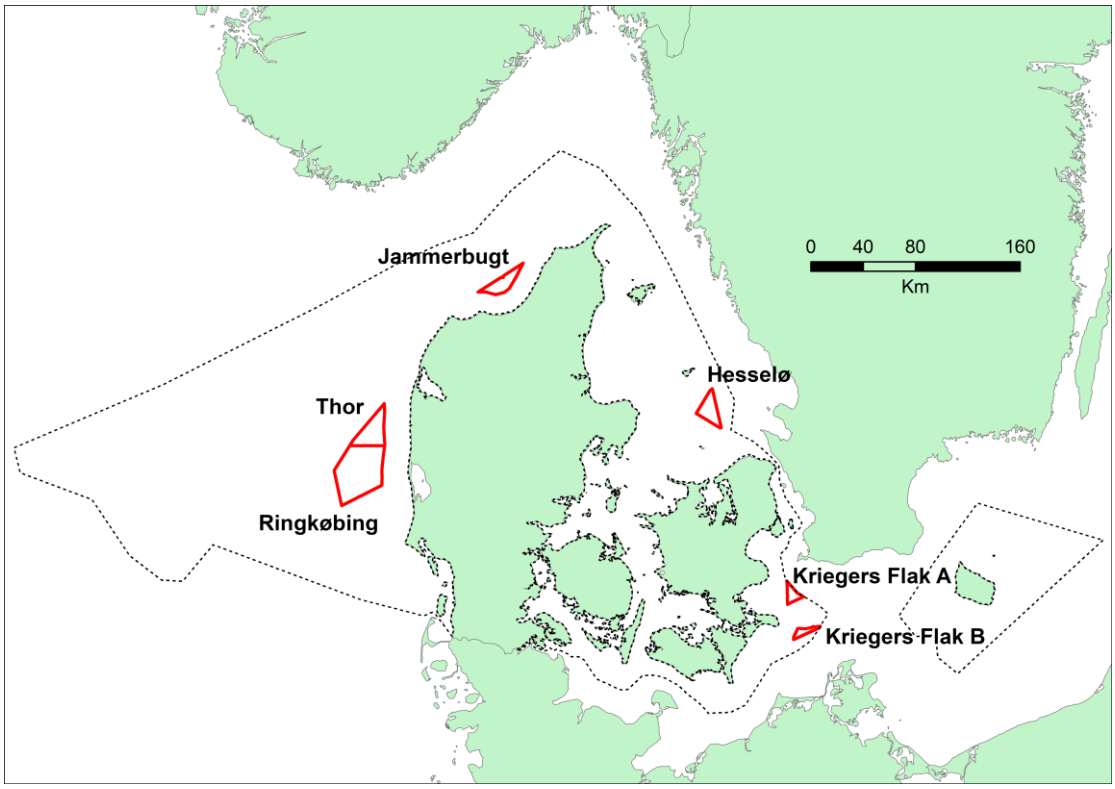

Figure 1 Overview of four regions designated for potential development of offshore wind farms. Thor forms part of the Ringkøbing area. The Danish Exclusive Economic Zone is indicated.

2 Methodology for bird investigations

2.1 Seabird survey data

2.1.1 North Sea

An overview of the received and processed 77 data sets from visual aerial transect surveys of seabirds is provided were received and processed:

- Two NOVANA surveys
- 49 surveys in particular Horns Rev I and II
- 10 surveys in particular Horns Rev III
- Three dedicated surveys for pockets
- Surveys related to EIAs for the North Sea South and the North Sea North

In addition, there is a very large set of historical material with ship-based survey data from 1986-1993, which among other things contains information on the species composition of pockets and oak birds that are difficult to species-determined from aircraft.

An overview of the spatial seasonal coverage of surveys included in this investigation is given in Figure 2. In the North Sea intensive coverage has only been achieved in the Horns Rev region due to baseline and monitoring programmes related to Horns Rev 1 and 2. The region off the Danish west coast, including the proposed gross areas for

Ringkøbing and Thor wind farms has only been surveyed during the spring season, whereas virtually no coverage has been achieved in the other seasons. In the Jammerbugt including the proposed gross area for the wind farm the best coverage has also been achieved in other seasons than winter.

It is concluded that a very large amount of survey data exists on the occurrence of seabirds in the Danish parts of the North Sea. Gaps in survey coverage along the west coast is seasonal, which means that lack of knowledge of seabird distribution and abundance during certain periods can be compensated for by predictive modelling using couplings between seabird distribution and the marine biological conditions found along the west coast. Further surveys are not expected to provide greater certainty in the assessment of the importance of the areas to seabirds.

2.1.2 Southern Kattegat

The area is covered by NOVANA surveys in 2004 (not full coverage of the Hesselø area), 2008, 2012, 2013 and 2016. In addition, for waterbirds, from the Swedish side, data from aerial waterbird surveys in 2017-2019 were also made available by Lund University. In order to cover pelagic seabirds and species which are difficult to identify to species from airplane like grebes and auks historic standardised ship-based line transect survey data kept in the European Seabirds at Sea Database (ESASD) were also included.

In the southern Kattegat the best coverage of the region around the proposed Hesselø site has been obtained during winter (Figure 3, Figure 4). During spring, good coverage has only been achieved east of the site in the Swedish part. Very limited data were obtained during the autumn season.

It is concluded that a large amount of data exists on the occurrence of seabirds in the region around the Hesselø site, particularly during the winter season.

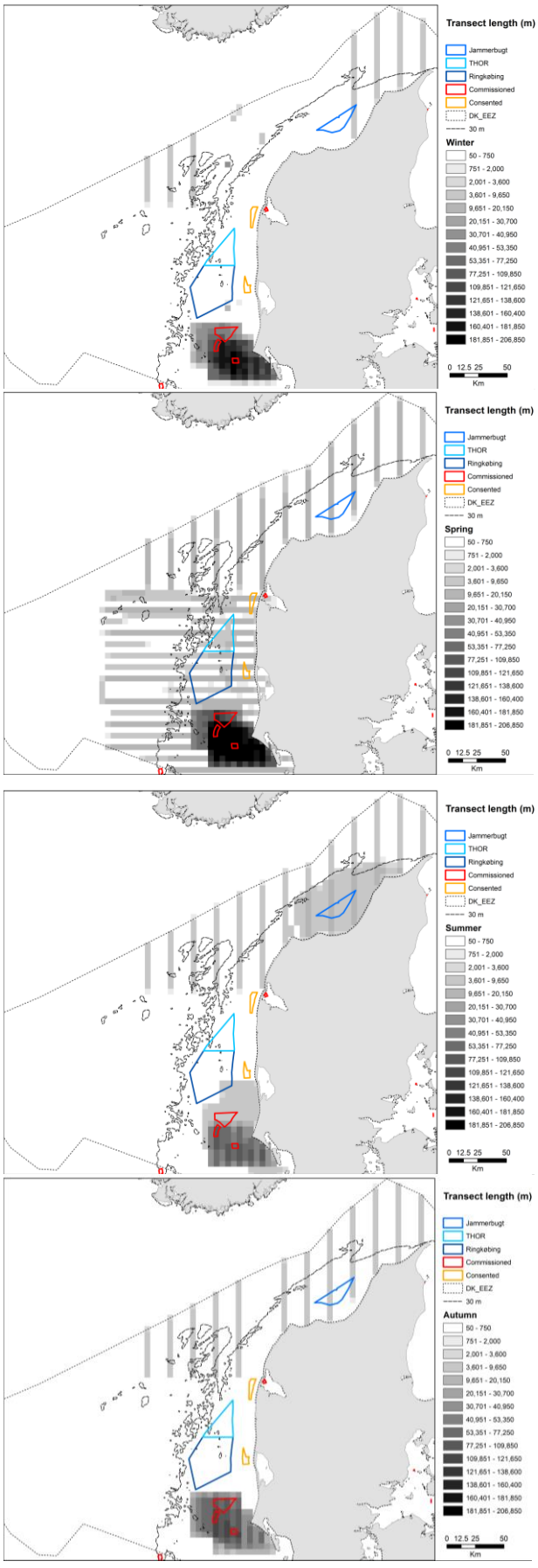

Figure 2 Seasonal coverage of aerial seabird survey data collected in the North Sea since 2000 and included in the investigation. Distance of surveyed transects (m) is summarized per 5 km^2. The 30 m depth contour is indicated.

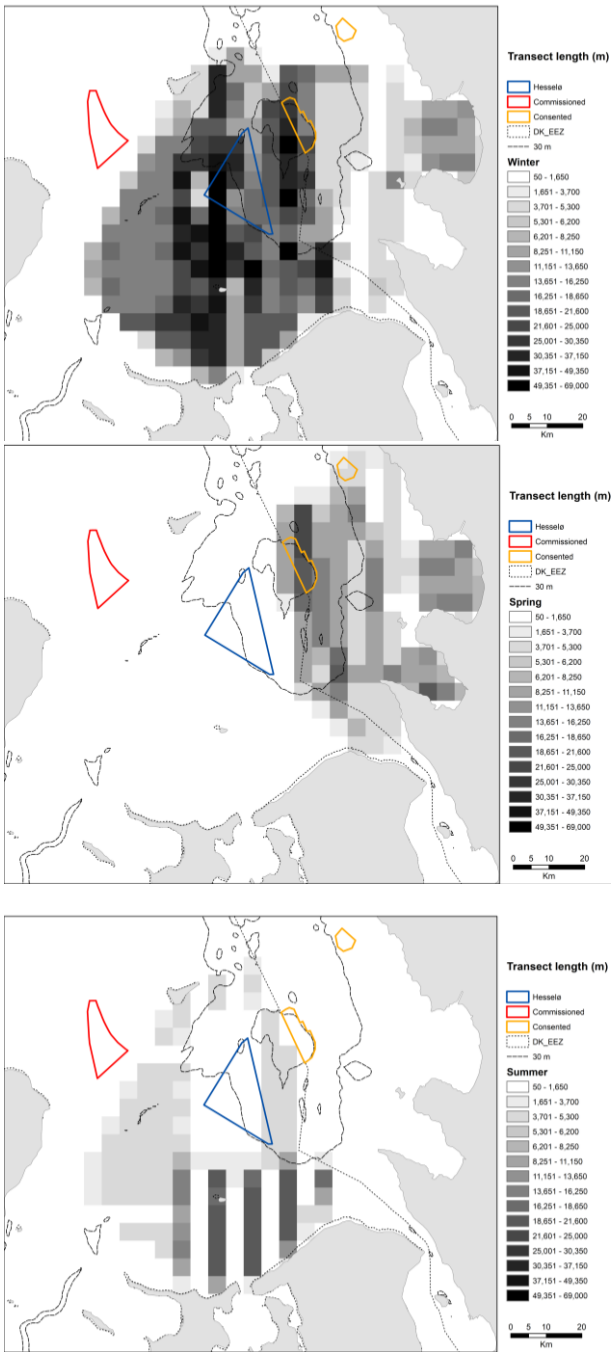

Figure 3 Seasonal coverage of aerial seabird survey data collected in the southern part of Kattegat since 2000 and included in the investigation. Distance of surveyed transects (m) is summarized per 5 km^2. The 30 m depth contour is indicated.

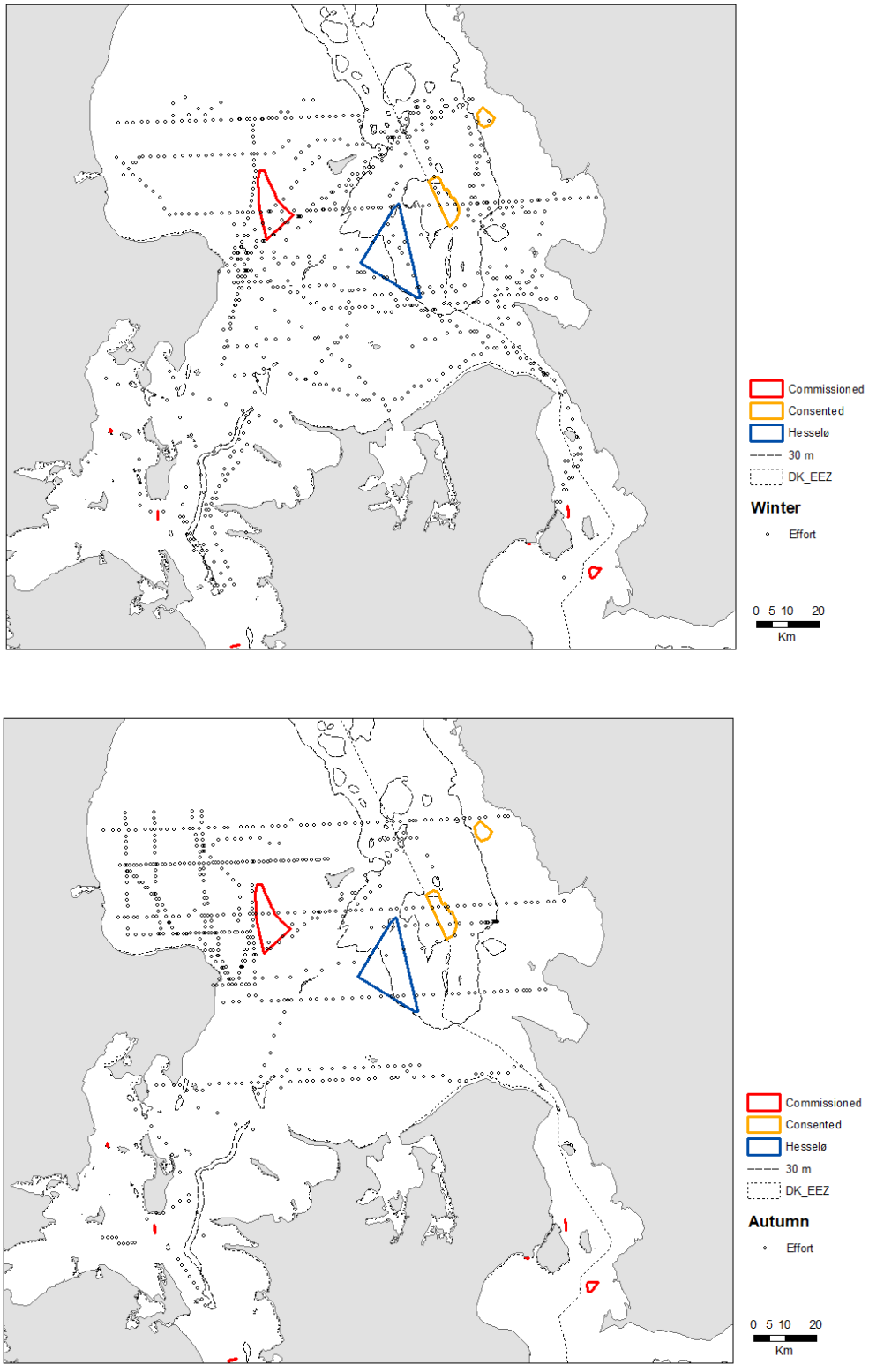

Figure 4 Seasonal coverage of ship-based seabird survey data collected in the Kattegat since 1985 and included in the investigation. The 30 m depth contour is indicated.

Table 1 Seabird survey data included in the study.

Area	Period	Method	Source
North Sea and Skagerrak	Aug 2012 and winter 2013	Aerial line transect survey	AU/DEC – Novana
North Sea and Skagerrak	Five surveys 2006-2008 Apr 2008, Apr 2009, Apr/May 2016, Aug 2011, Aug 2012, Aug 2013	Aerial line transect survey Aerial line transect survey Aerial line transect survey Aerial line transect survey	AU/DEC – dedicated surveys for divers and seaducks
Horns Rev	Aug 1999, Sep 1999, Nov 1999, Feb 2000, Mar 2000, Apr 2000, Aug 2000, Oct 2000, Dec 2000, Feb 2001, Mar 2001, Apr 2001, Aug 2001, Sep 2001, Jan 2002, Mar 2002, Apr 2002, Aug 2002, Feb 2003, Mar 2003, Apr 2003, Sep 2003, Dec 2003, Feb 2004, Mar 2004, May 2004, Sep 2004, Nov 2005, Feb 2006, Apr 2006, May 2006, Jan 2007, Feb 2007, Mar 2007, Apr 2007, Mar 2011, Mar 2011, Apr 2011, Oct 2011, Nov 2011, Jan 2012, Feb 2012, Mar 2012, Mar 2012, Apr 2012	Aerial line transect survey	AU/DCE – surveys undertaken for Vattenfall (Horns Rev 1) and Ørsted (Horns Rev 2)
North Sea	Jan 2013, Feb 2013, Mar 2013, Apr 2013, May 2013, Jun 2013, Jul 2013, Aug 2013, Sep 2013, Nov 2013	Aerial line transect survey	Orbicon – surveys undertaken for ENDK in relation to baseline connected to EIA assessment for the Horns Rev 3 offshore wind farm
	Nov 2013, Feb 2014, Mar 2014, Apr 2014	Aerial line transect survey	Niras – surveys undertaken for ENDK in relation to baseline connected to EIA assessment for the Vestkysten N + S offshore wind farm

Area	Period	Method	Source
Central Kattegat	Winter 2004, Winter 2008, Aug 2012, Winter 2013, Winter 2016	Aerial line transect survey	AU/DEC – Novana
Central Kattegat	Autumn and winter 1987-1993	Ship-based line transect survey	European Seabirds at Sea Database
Central Kattegat	Spring 2017, Winter 2018, Spring 2018, Winter 2019	Aerial line transect survey	Lund University – National waterbird survey

2.1.3 Distance analysis

The raw survey data in the compiled data base was distance corrected following standard distance sampling techniques (Buckland et al. 2001) conducted using the Distance package in R (https://cran.r-project.org/web/packages/Distance). The analyses were conducted in line with Winiarski et al. (2014). As the behaviour of seabirds, i.e. whether sitting or flying cannot be safely assessed during aerial surveys distance detection functions were calculated for all birds. In the distance analysis all birds are assumed to be detected in the distance band closest to the airplane/ship, further away detectability decreases with increasing distance from the airplane/ship. A set of different detection function models were fitted. Half normal, hazard rate and uniform detection functions were fitted, and Cosine adjustment terms were added to the models as well as Hermite polynomials (for Half-normal detection function) and simple polynomial (for the hazard rate detection function). Bird abundance and sea state were available as covariates in the models. Finally, the best fitting function was chosen on the basis of the smallest Akaike Information Criterion (AIC) values (Burnham and Anderson 2002).

Detection functions were calculated separately for each species, survey platform and data provider for the North Sea and Kattegat. Estimated detection functions were used to estimate species-specific detection probability and effective strip widths (ESW), which represent the width within which the expected number of detected seabirds would be the same as the numbers actually detected within the full width of 432 m (airplane) or 300 m (ship). The abundance of each species in each segment was thereafter corrected using the correction factors listed in Table 2.

Table 2 Distance corrections applied for the aerial survey data for the North Sea and Kattegat for each species and data provider.

	AU/DCE			Niras			Orbicon			Lund Univ.		
	Detect. Probabil.	SE	ESW	Detect. Probabil.	SE	ESW	Detect. Probabil.	SE	ESW	Detect. Probabil.	SE	ESW
NORTH SEA												
Red-throated/Black-throated Diver	0.31/0.32	0.02/0.004	465/475	0.63	0.17	141	0.15	0.008	307	X	X	X
Common Scoter	0.35/0.28	1.85/0.10	540/431	0.62	0.04	221	0.20	0.006	301	X	X	X
KATTEGAT												
Red-throated/Black-throated Diver	0.34	0.05	329	X	X	X	X	X	X	0.49	91.7	245
Common Eider	0.24	0.01	359	X	X	X	X	X	X	0.51	427	255
Common Scoter	0.50	0.05	743	X	X	X	X	X	X	0.30	0.17	302
Velvet scoter	0.38	0.23	365	X	X	X	X	X	X	1*	0*	-*
Black-legged Kittiwake	-	-	-	X	X	X	X	X	X	-	-	-
Razorbill	-	-	-	X	X	X	X	X	X	-	-	-

2.1.4 Establishment of geo-database on seabird survey data in the North Sea and Kattegat

The corrected abundance was merged with the effort data and species-specific densities (birds/km^2) were calculated. The data was finally re-segmented (mean density) into approximately 1 km segments, by adding up segments until 1000 m was reached. Data with a resolution coarser than 1.5 km (survey segments) or highly variable original resolution were not included in further analyses and simulations. The hydrodynamic variables described below were extracted to the corrected survey data based on position and time.

2.2 Common Crane flight data at Krieger's Flak

In connection with the baseline investigations for the Krieger's Flak OWF project the flight behaviour of migrating Common Crane was investigated using satellite telemetry, rangefinder and radar tracking (Skov et al. 2015). These unique data provided high resolution tracks showing flight trajectories and altitudes as Common Cranes cross the Krieger's Flak area during different meteorological conditions (Figure 5). The data have been made available for the assessment of the new gross Krieger's Flak development area.

Eight Common Cranes were equipped with high-resolution GPS satellite transmitters. Radar tracking of migrating Common Crane was carried out from the FINO 2 research platform in the German part of Krieger's Flak, where tracking was done using a high-performance solid-state radar (SCANTER 5000) with enhanced capacity for tracking over long distances and suppression of sea clutter. In addition, laser rangefinders were used to collect 3-D flight data from the FINO 2 platform, from the Falsterbo Rev Lighthouse and from the coasts of eastern Denmark and southern Sweden.

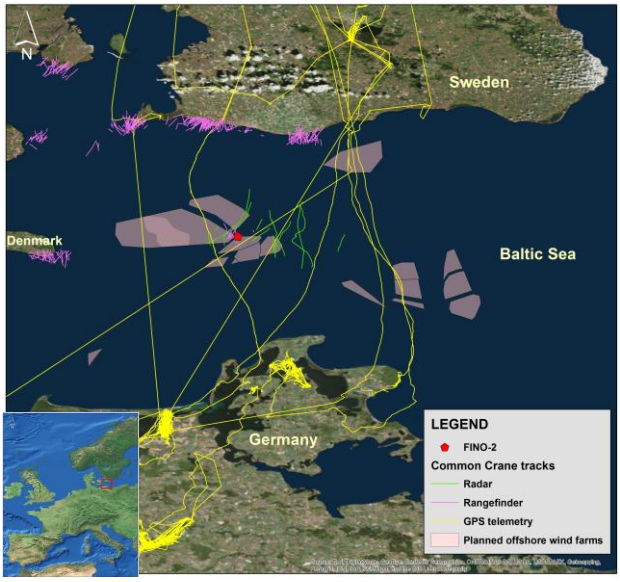

Figure 5 Tracks of migrating Common Crane recorded by radar, rangefinder and satellite telemetry (Skov et al. 2015).

2.3 Oceanographic dynamics of the coastal North Sea

The potential development areas at Ringkøbing/Thor and Jammerbugt are located in the coastal environment off the Jutland coast which share oceanographic characteristics with the entire Danish coastal region of the North Sea. Two main water masses are found in the region: Continental Coastal Water and Central North Sea Water (Lee 1980, Becker et al. 1983). The Central North Sea Water in the area can be divided into 2 slightly differing water masses, a surface layer and a bottom layer component; the bottom water component of the Central North Sea

Water is found in the valley of the river Elbe and areas to the northwest of here in the westernmost part of the Danish North Sea. Continental Coastal Water (CCW) is a mixture of water from the Atlantic and water from the English Channel, together with water from the rivers Rhine, Meuse and Ems, and run-off from the river Elbe (Becker et al. 1992). Along the Danish west coast the CCW has often been referred to as the Jutland Current (Nielsen 1999). Further differentiation of water masses in the CCW/Jutland Current is challenging due to the high variability in the area, and the strong yearly variation in temperature and salinity. The Jutland Current covers a large part of the surface water area off the Wadden Sea, and can be traced almost 100 km offshore, although the core of the current with low salinity and high concentations of nutrients are typically found within 40 km distance from the Wadden Sea. North of Horns Rev at the latitude of Henne Strand the Jutland Current bends towards the coast and can be followed as a 10-20 km wide surface water mass along the entire length of the Jutland coast to Skagen (Nielsen 1999).

As the marine environment of the potential development areas at Ringkøbing and in Jammerbugt are influenced by the Jutland Current in the same way as the area around Horns Rev it has been possible to integrate all existing data from the comprehensive baseline investigations associated with the Horns Rev 1, 2 and 3 offshore wind farms into the seabird distribution models for the development areas. This analytical approach has made it possible to predict the distribution and density of seabird at Ringkøbing and Jammerbugt even in seasons when only limited seabird surveys have been carried out.

The interface between the Jutland Current and the North Sea water mass gives rise to dynamic and productive frontal zone in which three different types of hydrographic fronts can be found; river plume, thermal and upwelling fronts. The seasonal thermal front, i.e. the boundary between the stratified and well-mixed water, can be observed along the 20-30 m depth contours (Munk 1993), and its position can be roughly determined from the water depth and maximum tidal velocity. The existence of the upwelling fronts is especially prevalent at Horns Rev (Skov & Thomsen 2008) and is steered by tidal currents and the topographical characteristics of Horns Rev. A permanent feature is the salinity or river plume front off the Wadden Sea, which is produced by the inflow of fresh water from the rivers to the North Sea.

Here, we have used the time series of post-processed hydrodynamic variables from DHI's North Sea model to link observations of seabirds to the hydrodynamic variables which most influence the distribution of seabirds. Examples of the mean patterns of surface salinity, frontal and eddy activity are visualised in Figure 6. Both the Ringkøbing/Thor and Jammerbugt development areas are located at the interface between the Jutland Current and North Sea water masses with the strongest gradient in surface salinity found in the eastern (Ringkøbing/Thor) and southeastern (Jammerbugt) parts. The zones with the strongest frontal activity along the west coast are located around Horns Rev, in the inner part of Jammerbugt and in deep waters of the Skagerrak over the slopes of the Norwegian Trench.

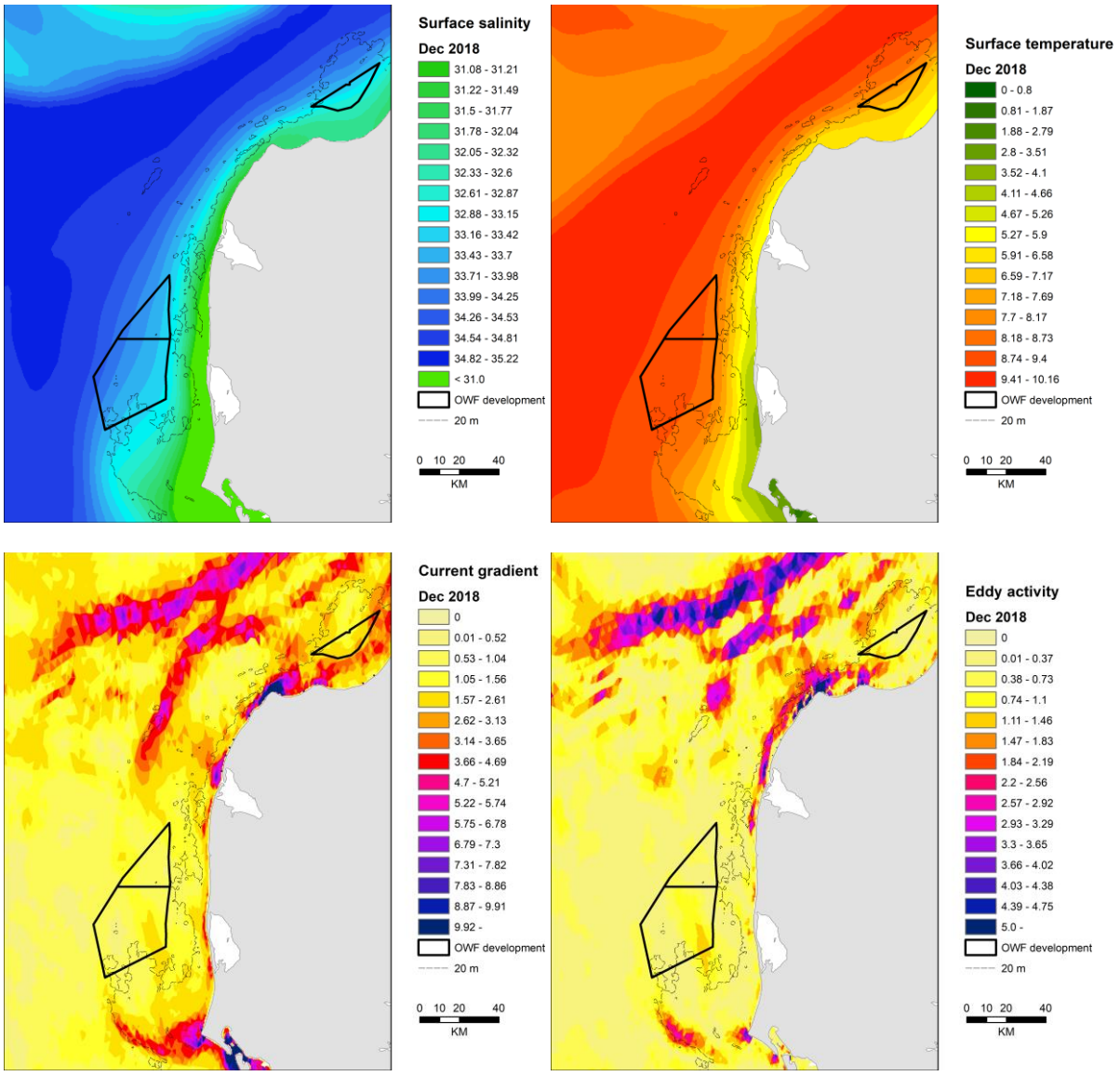

Figure 6 Mean patterns of surface salinity, temperature, frontal activity (current gradient) and eddy activity along the west coast of Jutland as estimated by DHIs North Sea model for the month of December 2018.

2.4 Seabird distribution modelling

2.4.1 Background

The use of distribution models for interpolating fragmented survey data into useful maps of mean densities of seabirds is well established, yet the majority of marine distribution models are made at a relatively coarse resolution and covering relatively large extents (Bailey & Thompson 2009, Maxwell et al. 2009). Terrestrial applications of distribution models typically assume that the physical environment exerts a dominant control over the natural distribution of a species. Obviously, the transfer of distribution models from land to sea means that the validity of model assumptions and predictive performance will be affected by the unique physical properties of marine habitats (Robinson et al. 2011). As a consequence, the detailed resolution of the distribution of marine species requires that the dynamic coupling to their physical environment is determined.

However, synoptic dynamic data on driving habitat parameters such as currents and hydrographic structures are often very difficult to obtain; the descriptions of key habitat features typically stem from correlations with static parameters such as water depth and distance to land (Skov et al. 2003, MacLeod & Zuur 2005, Cama et al. 2012). The fine-scale distribution of marine top predators like seabirds has been shown to correlate with physical oceanographic properties such as fronts, upwellings and eddies, which enhance the probability of predators encountering prey (Schneider & Duffy 1985, Skov & Prins 2001, Fauchald et al. 2011) exhibiting spatial dynamics and oscillations at different frequencies.

To accurately describe the distribution of seabirds over time, one needs to be able to take account of the actual habitat components realised during each observation. In the absence of these dynamic characteristics of seabird habitats, static distribution models of seabirds are unlikely to resolve the true variation in the distribution of the birds. In other words, if high resolution distribution models are based on static factors or mean values rather than in situ values for dynamic factors, predicted densities will rarely match the observed densities. Thus, accurate assessment of habitat use by seabirds requires highly dynamic, fine-resolution data both for species and the environment. Likewise, the application of static rather than dynamic distribution models in studies like this aiming at identifying potential conflicts between developing areas for offshore wind and conservation interests in terms of high densities of sensitive species of seabirds may result in an overestimate of densities in the periphery of species aggregations and an underestimate of densities within aggregations, leading to less accurate assessments.

2.4.2 Extraction of dynamic oceanographic co-variables

The dynamic oceanographic co-variables were extracted from validated, regional oceanographic models covering the North Sea and Kattegat respectively (see chapter 3.3.4. and Appendices A and B). These regional models are developed and maintained by DHI and are part of DHI´s operational Water Forecast service. The modelled co-variables cover the full analysis area and all observations in both time and space. The stored temporal resolution of the variables is 1 hour and the spatial resolution within the analysis are is about 3-5 km for the North Sea and 1-3 km for Kattegat. The co-variables consist of modelled state variables such as current velocity-components, salinity and water temperature as well as post-processed variables such as current gradient and vorticity. The dynamic oceanographic co-variables applied as predictors during the fitting of the models are listed in chapter 3.3.2 (Table 3).

The dynamic oceanographic co-variables are extracted for each observation at the relevant location and time. For the North Sea analysis, hourly values of the oceanographic co-variables were applied. For the Kattegat analysis however, seasonal means were applied. The extraction of these co-variables from the large binary model files and the merging of the observations and the extracted co-variables was done using Python script whilst taking into account the different data formats and map projections.

2.4.3 Model fitting

Models were made for the Red-throated/Black-throated Diver and the Common Scoter in the North Sea and Kattegat. Moreover, the following species were also modelled for Kattegat: Common Eider, Velvet Scoter, Black-legged Kittiwake and the Razorbill. Instead of using only static predictors such as depth, dynamic predictors such as current gradient were included in the model to predict bird distribution. The dynamic predictors included: current gradient, current speed, absolute vorticity, salinity gradient and water depth (Table 3).

Generalized additive (mixed) models (GA(M)Ms) were fitted using the “mgcv” and “MuMIn” package in R statistics (Wood, 2004; Burnham, 2002) for each bird species to be modelled. The model that provided the best fit was used. Due to zero-inflation a two-step GA(M)M model was fitted. This consisted of a presence absence binomial model and a positive gamma model. Initially all predictors, both static and dynamic, were included as smooth terms in the ´full´ model as listed in Table 3. Predictors which were deemed uninfluential or resulted in unrealistic ecological responses were excluded in a stepwise manner based on expert judgement and AIC scores. The allowed degree of freedom was restricted to a maximum

of 5 degrees of freedom (k = 5). Finally, the prediction form both the absence presence and positive model were combined to yield the final distribution. A correlogram was used to assess potential residual autocorrelation.

2.4.4 Model evaluation

Predictive accuracy of the North Sea models was evaluated using observed data from NIRAS which was not included in the model´s dataset. The predictive accuracy of the distribution models was evaluated by fitting the model on 70% of the randomly selected data and predicting on 30% of the remaining data.

2.4.5 Hydrodynamic modelling

To be able to describe the dynamic distribution of the key species the observed distribution patterns were related to the dynamic environment by statistical models as described above. Information of the dynamic environment was extracted from DHI's hydrodynamic models for the Inner Danish Waters (DKBS Ver. 2) and the North Sea (HDUKNS Ver. 3). The different hydrodynamic model outputs and validation are described in Appendix A.

2.4.6 Prediction of dynamic distributions of seabirds

Final models fitted were used to predict and map the distributions and densities of all modelled bird species in the North Sea and Kattegat study area in a spatial resolution of 3 km. Moreover, the frequency of high densities and model uncertainty was mapped.

Table 3 Model overview indicating the bird species modelled, databases used and both dynamic and static predictors used for the North Sea and Kattegat study areas.

Study area	Modelled Species	Database Source	Predictors	
			Dynamic	**Static**
North Sea	Divers (*Gaviidae*)	Århus University aerial surveys Orbicon aerial surveys for calibration, Niras aerial surveys for validation	Current gradient, current speed, chlorophyll, absolute vorticity, salinity and salinity gradient	Water depth
	Common Scoter (*Melanitta nigra*)	Århus University aerial surveys Orbicon aerial surveys for calibration, Niras aerial surveys for validation	Current speed, salinity	Water depth, slope and aspect
	Divers (*Gaviidae*)	Århus University aerial surveys Lund aerial surveys	Current gradient, current speed, chlorophyll, absolute vorticity, salinity and salinity gradient	Water depth
	Common Scoter (*Melanitta nigra*)	Århus University aerial surveys Lund aerial surveys	Current speed	
	Velvet Scoter (*Melanitta fusca*)	Århus University aerial surveys Lund aerial surveys	Current speed	
	Common Eider	Århus University aerial surveys	Current speed	

Kattegat	(*Somateria mollissima*)	Lund aerial surveys		
	Black-legged Kittiwake (*Rissa tridactyla*)	ESAS Ship surveys	Current gradient, current speed, chlorophyll, absolute vorticity, salinity and salinity gradient	Water depth
	Razorbill (*Alca torda*)	ESAS Ship surveys	Current gradient, current speed, chlorophyll, absolute vorticity, salinity and salinity gradient	Water depth

2.5 Assessment of importance of areas to seabirds

2.5.1 Percentile contours

In order to outline the areas of highest habitat suitability we used the 90th percentile in the predicted densities, as it is generally considered a robust and transparent method, and as it is widely established as a useful upper threshold. The use of the 90th percentile is in line with Embling *et al*. (2010) and Heinänen & Skov (2015), who investigated the use of a range of percentiles for selection of candidate areas for protection of harbour porpoises in British waters.

2.5.2 Determination of gradients in area importance

To further analyse the degree of overlap between the proposed development regions and areas of elevated seabird densities gradients in predicted densities of seabirds across each of the development regions were visualised (Figure 7).

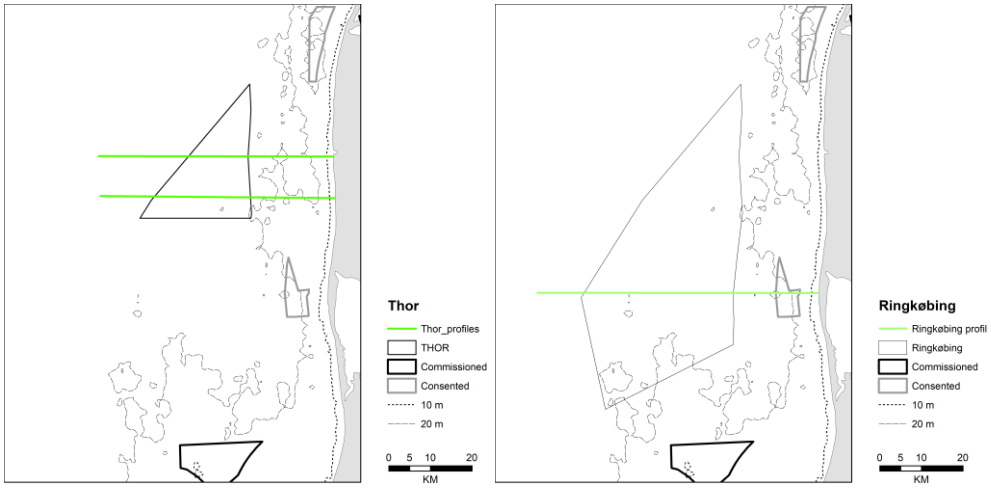

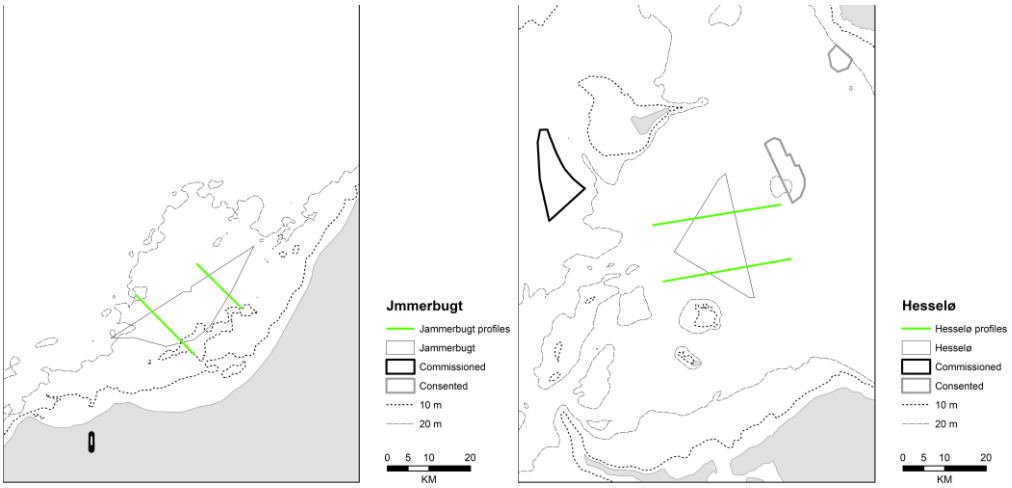

Figure 7 Profile lines (marked in green colour) used for the visualisation of density gradients across the four development areas in the North Sea and Kattegat.

2.6 Assessment of migration patterns of Common Crane at Krieger's Flak

2.6.1 Assessment of the horizontal and vertical distribution of Common Crane

In order to generalise the satellite tracking, radar and rangefinder observations flight models were developed which coupled flight heights to weather parameters using Generalised Additive Mixed Models. These models are suitable for explaining the differences in flight altitude related to wind and weather conditions (wind speed, air pressure, relative humidity, clearness and temperature) and distance to land. If the flight altitude of Common Crane changes significantly with weather conditions the probability for collision will most likely also vary at the site, and the overall collision mortality will depend on the frequency of adverse conditions which cause the birds to fly at rotor height. To be able to model the non-linear relationships (between the altitude and predictor variables), non-normally distributed errors and also account for the spatial and temporal autocorrelation (non-independencies in the residuals) in the data we used the semi-parametric and data driven generalized additive mixed modelling approach (GAMMs, Wood 2006, Zuur et al. 2009). Species-specific GAMMs with a suitable error distribution, either a Tweedie error distribution (with a log link and a power parameter between 1 and 2, Shono 2008) or a gamma distribution (with log a link) were fitted. To account for the temporal and spatial autocorrelation in the data we include the date (day and month) as a random term and a first order autocorrelation structure, corAR1, grouped by the individual tracks. The random effect and correlation structure were needed as one of the assumptions of the statistical method is that the samples (within the rangefinder, GPS telemetry or radar tracks) are independent of each other. This assumption is naturally violated as the succeeding samples in the various tracks are highly dependent on the previous samples.

We included distance to departure coast, clearness and humidity as smooth functions. Wind speed was included as a smooth function and directions as a factor variable. The models were fitted using R version 2.13.0 (R Development Core Team, 2004) and the "mgcv" package (Wood, 2006).

The predictive accuracy of the models was evaluated by using a split sample approach, fitting the model on 70% of the tracks and evaluating the models on the remaining 30%. The agreement between the observed and predicted altitudes was tested using the Spearman's rank correlation coefficient. The model fit was also assessed by the adjusted R-square values (variance explained) and an inspection of the residuals. We further used the models (based on all tracks) for predicting the average flight altitude at Krieger's Flak during average weather conditions (in the species-specific data set) during tail, head and cross winds.

2.6.2 Assessment of cumulative collision risk with existing and planned projects

The behavioural responses of migrating cranes were decomposed into micro, meso and macro avoidance using the framework proposed by Cook et al. (2014) and further elaborated on by May (2015). According to May (2015) macro avoidance generally reflects the displacement of flying birds from the wind farm perimeter, while meso avoidance reflects the aversive flight behaviour of the birds towards individual turbines. Micro avoidance reflects the last second behavioural response of the birds in or near the rotor-swept zone in order to avoid collision with the rotor blades. Macro and meso avoidance rates of migrating cranes were measured by the radar and rangefinder tracking at the Baltic 2 wind farm, while in the absence of detailed recordings from the rotor-swept zones of the wind farm the micro avoidance rate was taken from Winkelmann (1992) who reported a rate of 0.92 for birds at land-based wind farms. The macro avoidance zone was defined as the area around the wind farm, while the meso avoidance zone was defined as the rotor zone including a 10 m buffer (Cook et al. 2014). The geometry of the rotor zone was determined in real time by aligning the rotor perpendicularly to the direction of the wind at the time of the bird crossing. The rotor zone had a width of 13.5 m (chord width of the rotor blades + 10 m). All crane tracks recorded as intersecting the wind farm perimeter including the buffer around the rotor zone were classified as non-macro avoidance, and tracks recorded as intersecting a rotor zone plus buffer area were classified as non-meso avoidance.

Macro and meso avoidance rates were estimated by summarizing the number of tracks recorded as intersecting and non-intersecting using either radar or laser rangefinder using the following formula:

$$\text{Avoidance rate} = \frac{(N\ tracks\ non{-}intersecting)}{(N\ tracks\ non{-}intersecting)+(N\ tracks\ intersecting)}$$

The overall avoidance displayed by the cranes to the Baltic 2 wind farm was calculated by integrating the specific macro, meso and micro avoidance rates as:

$$\text{Total avoidance} = 1 - ((1 - macro)\ x\ (1 - meso)\ x\ (1 - micro))$$

The number of annual collisions of Common Crane at the Baltic 2 wind farm was estimated using the Band (2012) collision model for single transits of the same individual, which has been widely applied to land-based and offshore wind farms in order to assess likely collision risks for migrating birds. The Band model provides predictions of the number of birds likely to be killed annually due to collisions with the specified design conditions (Table 1) using a range of parameters relating to the flight behaviour and morphological details of the species (Table 3) and the estimated avoidance rates from the behavioural records at the wind farm.

The Band collision model is split into five stages. Stage A assembles data on the number of flights which, in the absence of birds being displaced or taking other avoiding action, or being attracted to the windfarm, are potentially at risk from wind farm turbines. Stage B uses the flight activity data to estimate the potential number of bird transits through rotors of the windfarm. Stage C calculates the probability of collision during a single bird rotor transit. Stage D multiplies these to yield the potential collision mortality rate for the bird species in question, allowing for the proportion of time that turbines are not operational, assuming current bird use of the site and that no avoiding action is taken. Finally, stage E allows for the proportion of birds likely to avoid the windfarm or its turbines, either because they have been displaced from the site or because they take evasive action.

The collision estimates are thus derived by combining the 5 stages. Stage A defines flight activity of birds, which is used in Stage B for estimating the “flux” of birds trough the rotors due to the passage rates. In stage C the probability of collision during a single transit is calculated based on the wind turbine and bird characteristics. The investigations were undertaken during the entire spring season, and annual collision estimates were derived by multiplying the estimates from the spring seasons by two. The proportion of up- and down-wind is also taken into account. The proportion was set to 50 % for both autumn and spring seasons based on the historic weather statistics from Falsterbo, Sweden (downloaded from www.SMHI.se). Stage B and C are further combined in Stage C by multiplying the number of bird transits with the single transition collision risk and the proportion of time the windfarm is

operating, which gives the number of collisions per month assuming no avoidance reactions. In Stage D the number of collisions is multiplied by the overall avoidance rate to yield the final collision estimate per month.

Indications of potential population level effects on account of the estimated collision rates of Common Cranes at the Baltic 2 offshore wind farm were assessed using thresholds for sustainable removal following the Potential Biological Removal (PBR) concept. In addition, population level effects of estimated collision rates related to the construction of planned offshore wind farms in Danish, German and Swedish parts of the western Baltic Sea were also assessed. Almost all Common Cranes migrating across the region are recruited from the Swedish-Norwegian population. The Swedish and Norwegian population of Common Crane is estimated to 75,000 and 9,000 individuals, respectively. Of these, all 84,000 birds were set to cross the wind farm development region in the western Baltic Sea, although smaller numbers occasionally pass both east and west of this region (Swanberg 1987). The PBR approach which defines the threshold of additional annual mortality, which could be sustained by a population, is widely used to guide conservation and management of long-lived species like marine mammals (Wade 1998) and has been demonstrated as a useful tool to assess impacts of fisheries by-catch mortality on birds (Žydelis et al. 2009). Although PBR should only be used to derive indications of potential unsustainable impacts on populations, the metric accounts for potential bias due to density dependence, uncertainty in estimates of the population size and stochasticity (Wade 1998, Taylor et al. 2000, Milner-Gulland & Akcakaya 2001). Additive mortality exceeding PBR would indicate potentially overexploited populations.

If the aim of metrics in population modelling is to test whether or not the conservation objectives of a site will be met, for example on the integrity of the SPA network for Common Crane, any approach used must typically be capable of assessing whether the resultant additional mortality will mean a population can be maintained at its current level. For this reason, PBR has its limitations in its application (Cook & Robinson 2015, Green et al. 2016). Wade (1998) demonstrated that if the additional mortality resulting from a project is equal to that obtained from estimates of PBR, populations can reach equilibrium at a point well below the carrying capacity of the available habitat. PBR is calculated using the following general equation (Wade 1998):

$$PBR = \frac{1}{2} R_{\max} N_{\min} f$$

where R_{max} is maximum recruitment rate, N_{min} is minimum population size for a range of years (Prange 2005), and f is recovery factor used to account for uncertainty in population growth rate and population size. Maximum recruitment rate is calculated considering maximum annual population growth rate:

$$R_{max} = \lambda_{max} - 1$$

where λ_{max} is maximum annual population growth rate, which is solved using the equation suggested by Niel & Lebreton (2005), which requires only adult bird annual survival probability (S_{ad}) and age of first reproduction (α):

$$\lambda_{\max} = \exp\left(\left(\alpha + \frac{S_{ad}}{\lambda_{\max} - S_{ad}}\right)^{-1}\right)$$

For minimum population size (N_{min}) Wade (1998) suggested using the lower bound of the 60% confidence interval of a given population estimate. As only one number was available as population estimate for Common Crane, we followed Dillingham & Fletcher (2008) and estimated N_{min} using the 20th percentile of the population estimate assuming coefficient of variation $CV_{\bar{N}} = 0.05$.

The population recovery factor f, used to account for uncertainty in population growth rate and population size, ranges between 0.1 and 1. Dillingham & Fletcher (2008) suggested a recovery factor f = 0.7 for increasing populations, f = 0.5 for stable populations, f = 0.3 for declining, f = 0.1 for rapidly declining.

Several thresholds were defined in order to inform the assessment of potential population effects on Common Crane. The PBR threshold for a stable population (f = 0.5) was estimated at 1,887 birds, while the threshold for an increasing population (f = 0.7) was assesses at 2,642 birds. Annual survival probability was set to 0.9 and age of first reproduction to 4 (Robinson 2005). The final PBR values are

sensitive to the f value assumed, with an increase in f from 0.1 to 0.5 reflecting a five-fold increase in the PBR value estimated. However, the value selected is rarely based on empirical evidence and indeed in this case there was a notable absence of information on recent changes in anthropogenic sources of mortality of relevance to Common Crane. The value of 10 % annual mortality mentioned in Robinson (2005) originates from studies of Sandhill Cranes Grus canadensis in the 1970'es (Johnsgard 1983). Hence, little evidence exists of the current influence of a number of potential additive mortality factors on mortality and survival rates in Common Cranes. These factors include:

- Impairment of breeding habitats due to decline in area of wetlands caused by climatic changes;
- Impairment of breeding habitats due to decline in area of wetlands caused by drainage and agricultural practices;
- Disturbance during breeding from increased anthropogenic activities
- Increased disturbance during non-breeding from increased anthropogenic activities
- Increased mortality due to collisions with power lines and wind farms

Accordingly, a significant degree of precaution was built into the assessment. A 50 % of the PBR threshold for a stable population was used as a threshold below which significant impacts at population level are not likely. A stable population was used as a reference population in a precautionary fashion in view of the most likely population development over the future 10-year period of wind energy production in the region. This approach is also corroborated by the recent population trend. Following the steep increase in the population of Common Crane between 1980 and 2000, the population stabilised after 2000 (Prange 2005).

3 Results

3.1 Distribution models

3.1.1 North Sea

3.1.1.1 Red-throated/Black-throated Diver

The results of the distribution models for Red-throated and Black-throated Diver are shown in Appendix C.1.1. The presence/absence part of the models indicate that the species prefer areas away from shipping lanes and wind farms characterised by a combination of low water depth, high productivity, high surface salinity and low current speed. These features are typically found in the interface between the estuarine Jutland Current with low saline riverine water and the high saline North Sea water mass. The validation of the model's predictive is illustrated in Figure 8, which shows that the predicted numbers of divers along the aerial transect lines in the North Sea are comparable to the observed numbers.

The positive part of the models stresses the importance of the intermediate depth areas with 15m – 30m water depth away from wind farms located at the interface between high surface salinity and high productivity. The predicted mean monthly densities in Figure 9 and Figure 10 and the areas of high habitat suitability in Figure 11 and Figure 12 show zones of persistent higher densities (> 0.75 birds/km^2) and habitat quality in the interface, which follows the 15m-30m depth zone. The density of 0.75 has been chosen as a cut-off value for higher densities both because of the small size of the diver populations and densities recorded in other parts of the range. Due to the wide area of shallow water and the extent of the Jutland Current the zone is around 40 km wide in the area just north of Horns Rev. The Jutland Current bends towards the coast at Ringkøbing Fjord and extends over a 20 km wide area along the Jutland coast from here to Skagen.

The distribution of divers follows this pattern, which means that at the latitude of the southern part of the Ringkøbing development area low densities of divers are predicted close to the coast and in the North Sea, while higher densities are predicted in the interface which extends from 5 to 40 km offshore through the area. In the northern part of the Ringkøbing area and at the Thor development area low densities of divers are still predicted close to the coast and in the North Sea, while higher densities are predicted in the interface which here extends into the eastern part of the Thor area. The densities in both the Ringkøbing and the Thor area are highest during the month of April. A large part (50%-75%) of the development area in Jammerbugt is located in the area of high habitat suitability to divers during the months of February and April.

Figure 13, Figure 14, Figure 15 and Table 4, Table 5 and Table 6 provide more details on the importance of the Thor, Ringkøbing and Jammerbugt areas to divers. In the Thor area during February, March and April higher densities of divers extends from 3 km off the coast and westwards approximately 5 km into the Thor area. During the same months, higher densities of divers in the Ringkøbing area are predicted in two zones, one zone 7-18 km off the coast and another zone further offshore 32-50 km from the coast which is associated with the frontal region in the western part of Horns Rev. The latter zone of high habitat quality overlaps with the central southern part of the gross area for the Ringkøbing wind farm extending over a distance of 20 km inside the perimeter. In the Jammerbugt area the overlap with higher densities of divers is strongest in the central part of the wind farm area. Densities above 0.75 birds/km^2 in the three wind farm areas are confined to the month of April. During May, higher densities at the Thor site are only found closer to the coast at 3-6 km distance from the coast.

The model results classify approximately 10% of the Danish part of the North Sea as of high habitat suitability throughout winter and spring periods. Similarly, a large part of the Ringkøbing area has high habitat suitability (38.1% - 42.3%) throughout February, March and April. Compared to these figures the dynamics of the Thor and Jammerbugt areas in terms of high habitat suitability are much more pronounced and differs for Thor between 3.0 % in May and 37.4 % in April and for Jammerbugt between 0% in March and 72.5% in February.

The validation results (Appendix C) indicate that the presence-absence part of the model describes the input densities reasonably well with an AUC value of 0.63, while the predicted densities due to the high resolution only describes a small proportion of the variation in observed densities. The validation of the ability of the model to predict densities independently from the input data indicates that the model predictions provide a reliable generalisation of the densities over the modelled region with a Sperman's correlation coefficient of 0.1.

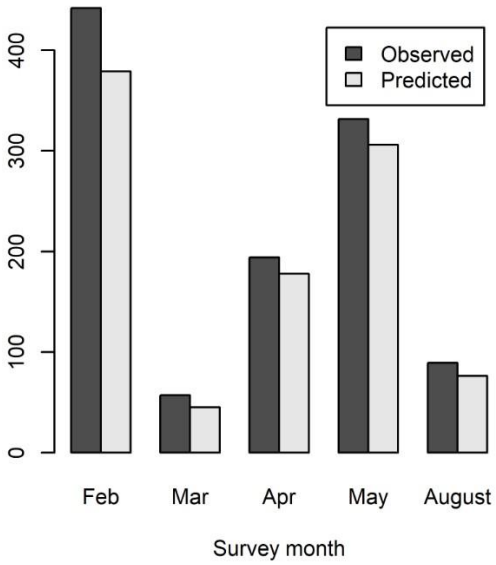

Figure 8 Comparison of predicted versus observed numbers of Red-throated/Black-throated Diver *Gavia stellate/arctica* along the aerial transect lines in the North Sea.

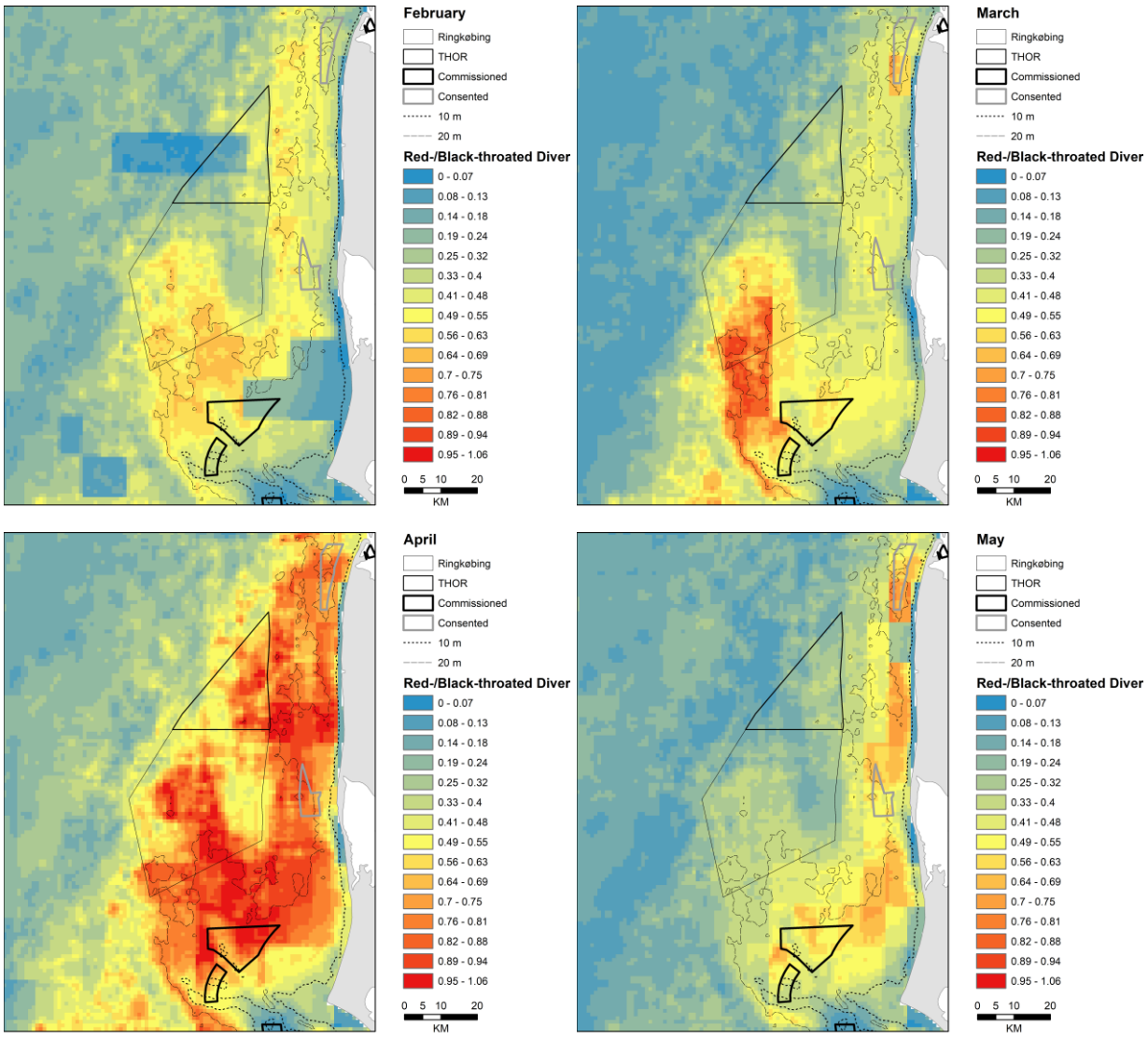

Figure 9 Predicted mean monthly density (n/km^2) of Red-throated/Black-throated Diver *Gavia stellate/arctica* along the west coast of Denmark.

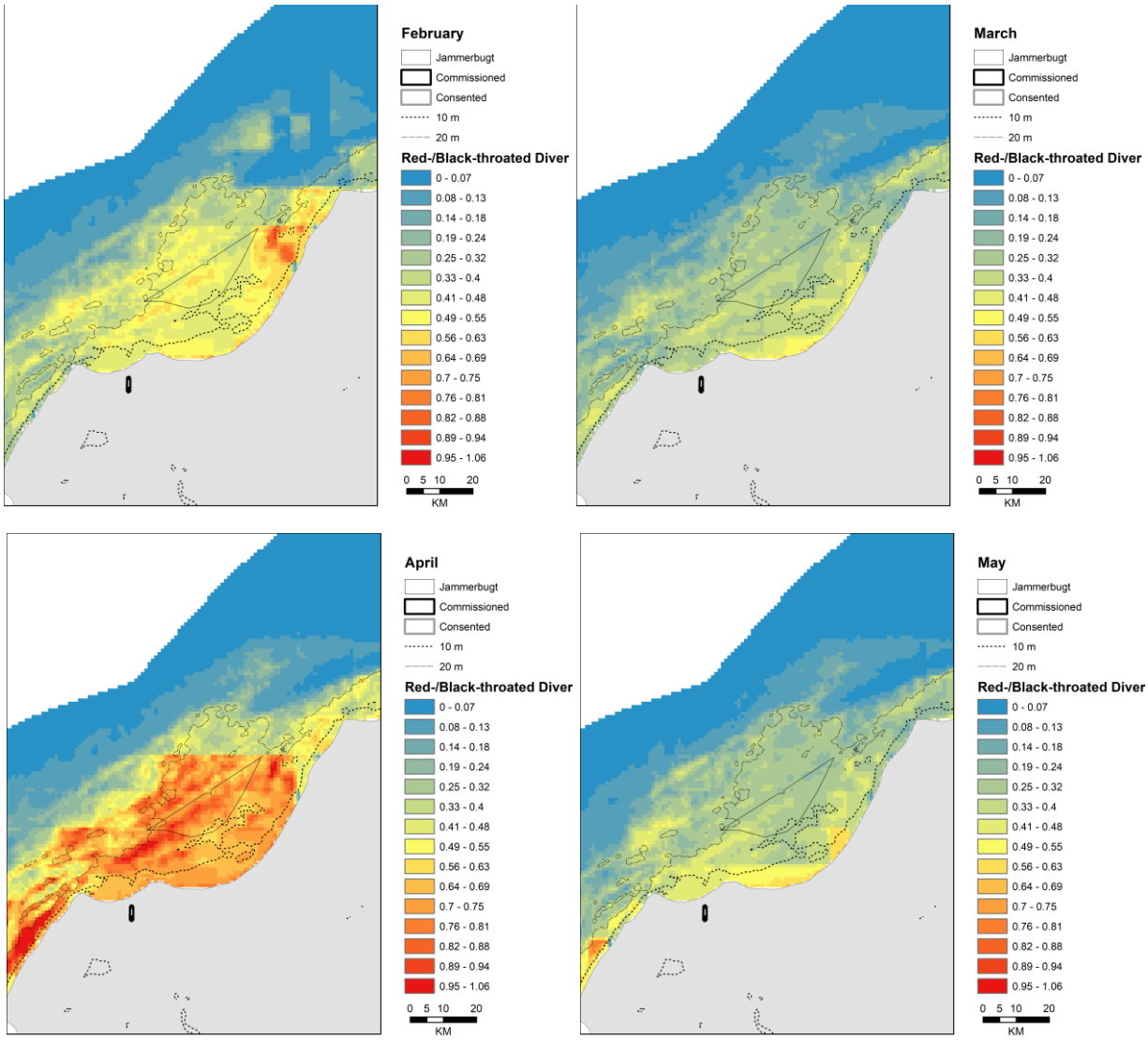

Figure 10 Predicted mean monthly density (n/km^2) of Red-throated/Black-throated Diver *Gavia stellate/arctica* along the coast of Skagerrak.

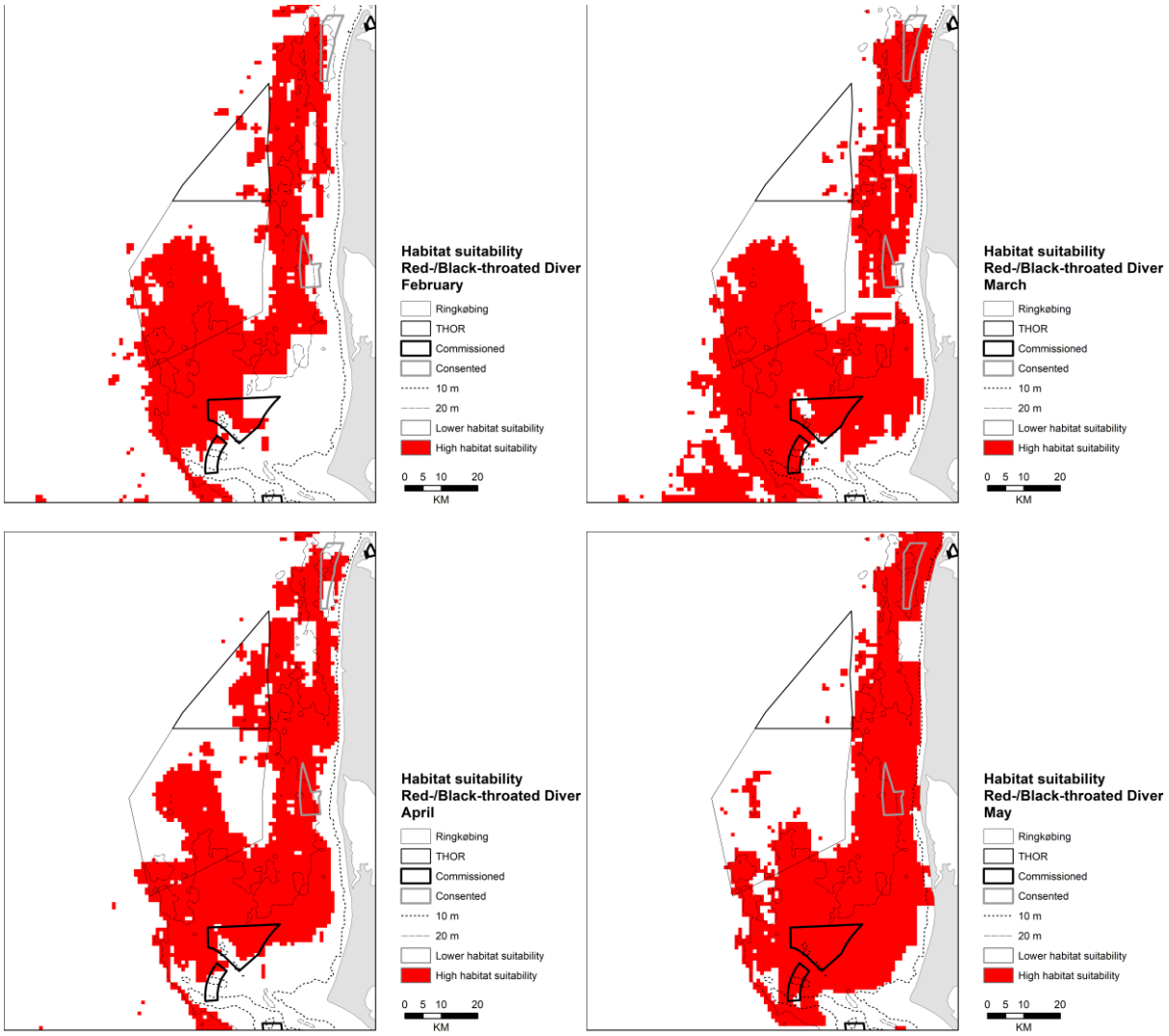

Figure 11 Areas of high habitat suitability to Red-throated/Black-throated Diver *Gavia stellate/arctica* predicted during the main months of occurrence along the west coast of Denmark.

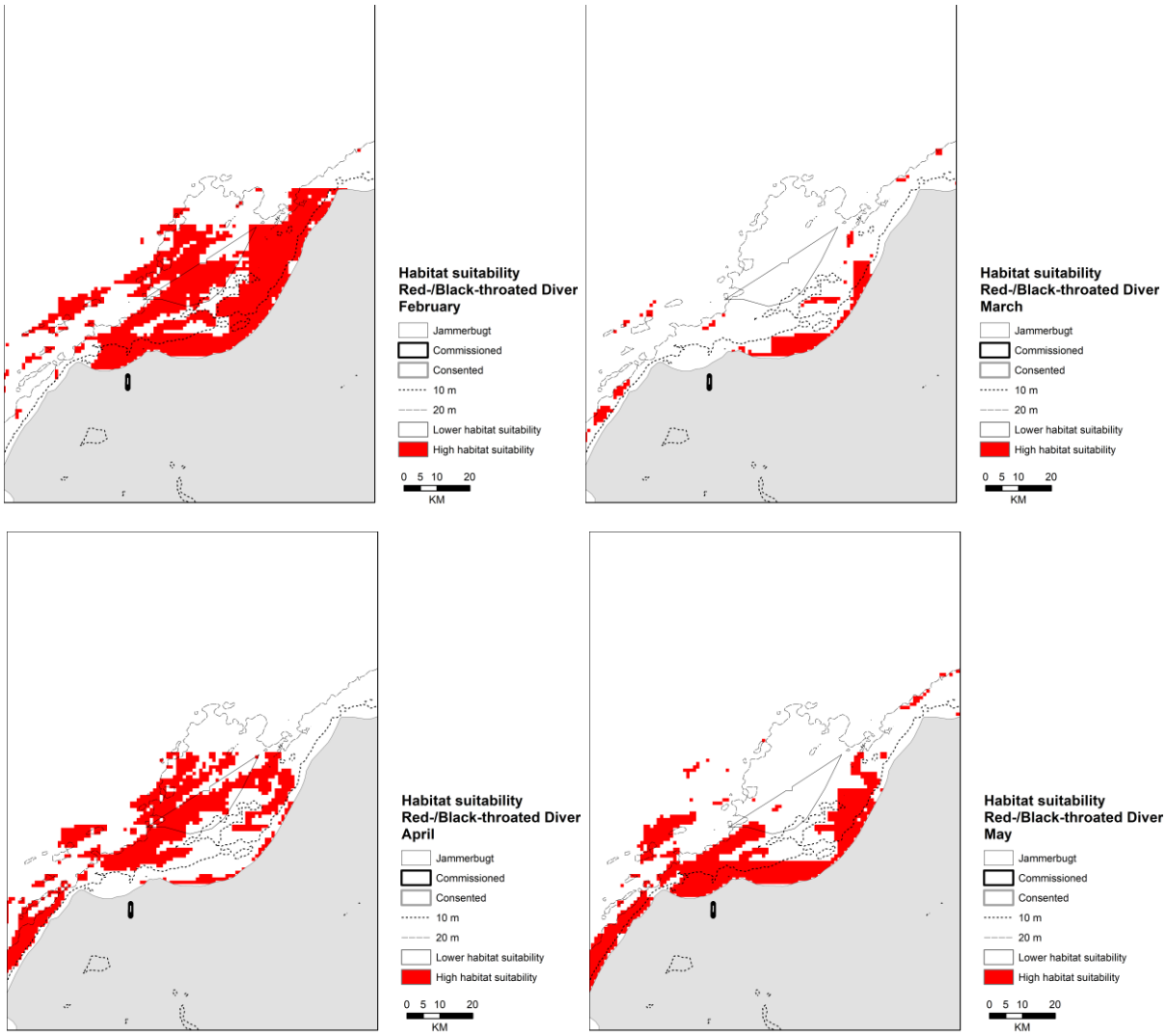

Figure 12 Areas of high habitat suitability to Red-throated/Black-throated Diver *Gavia stellate/arctica* predicted during the main months of occurrence along the coast of Skagerrak.

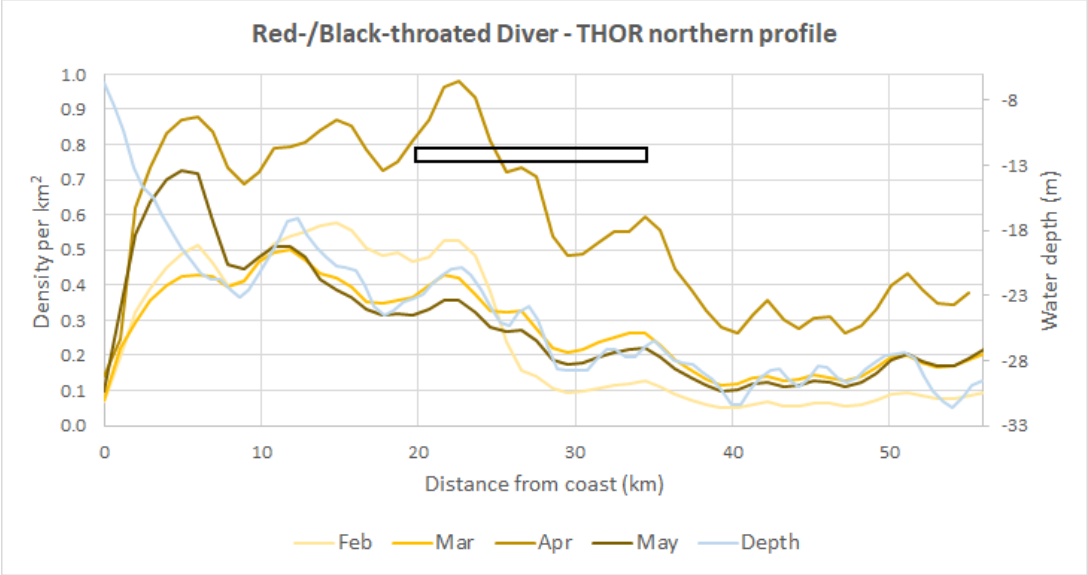

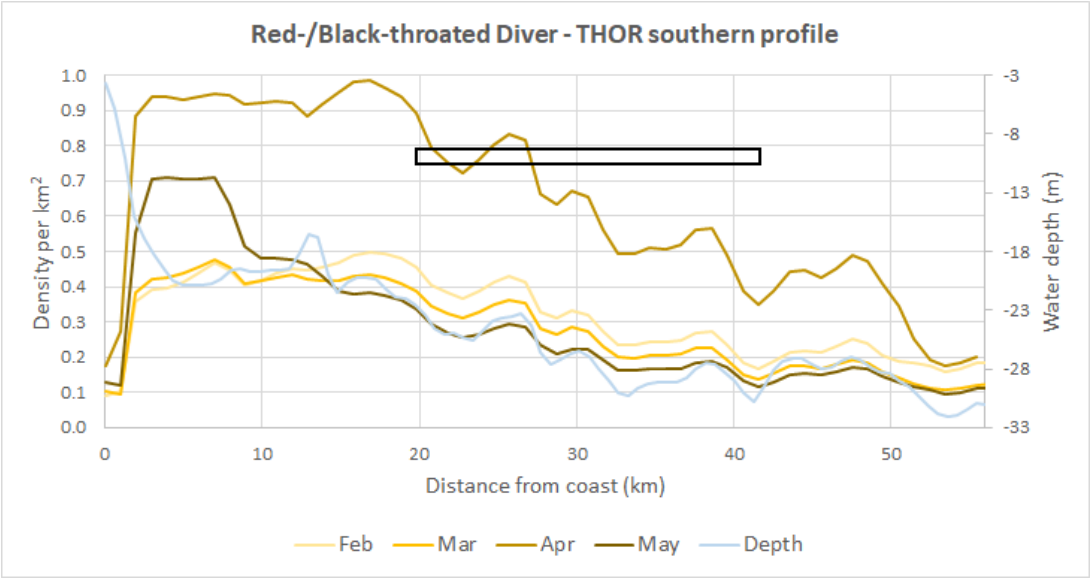

Figure 13 Predicted gradients in the mean monthly density (n/km^2) of Red-throated/Black-throated Diver *Gavia stellate/arctica* along two profile lines crossing the Thor development area.

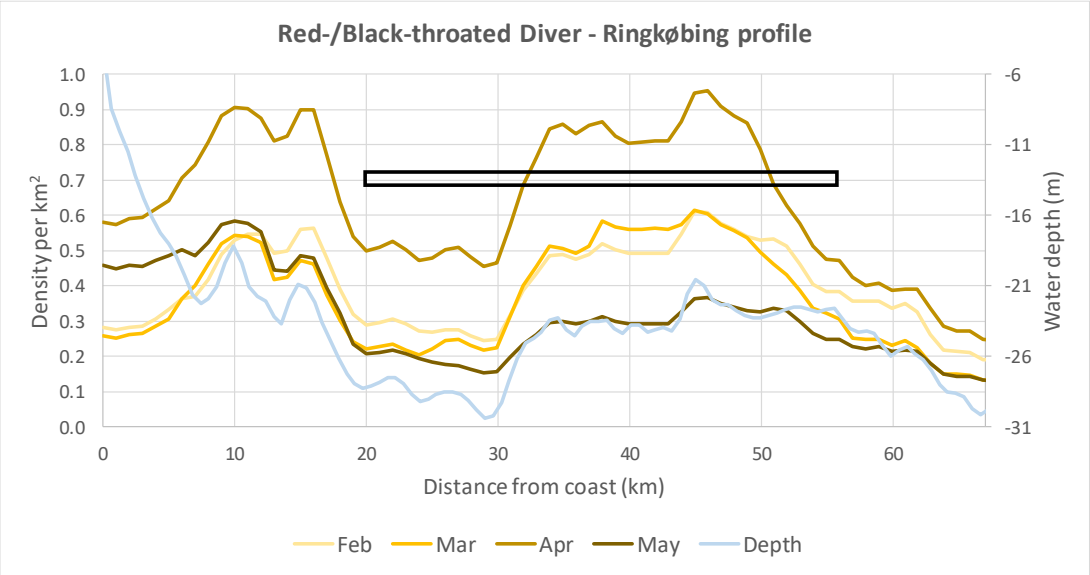

Figure 14 Predicted gradients in the mean monthly density (n/km^2) of Red-throated/Black-throated Diver *Gavia stellate/arctica* along the profile line crossing the Ringkøbing development area.

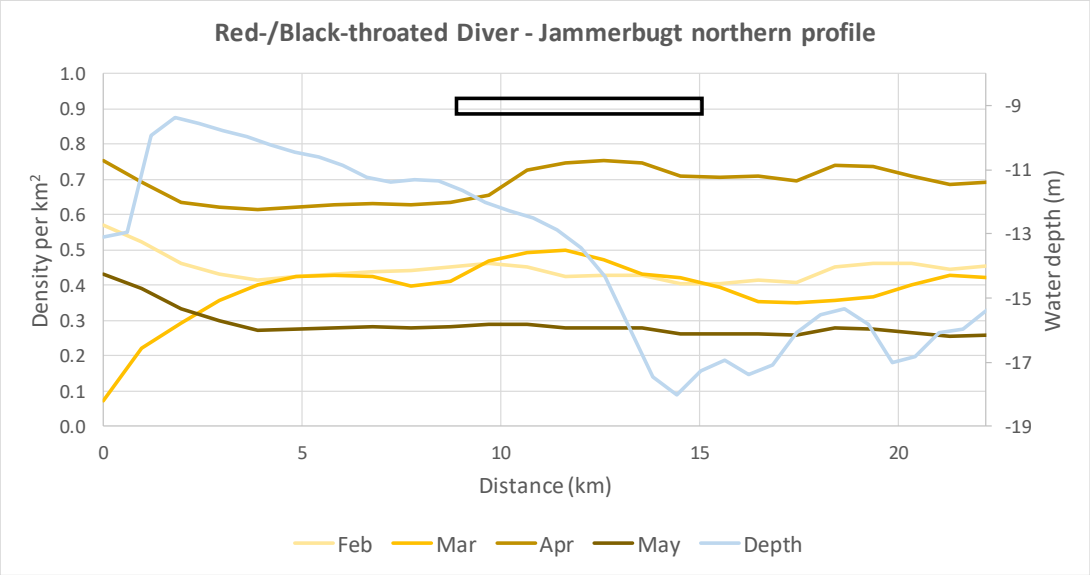

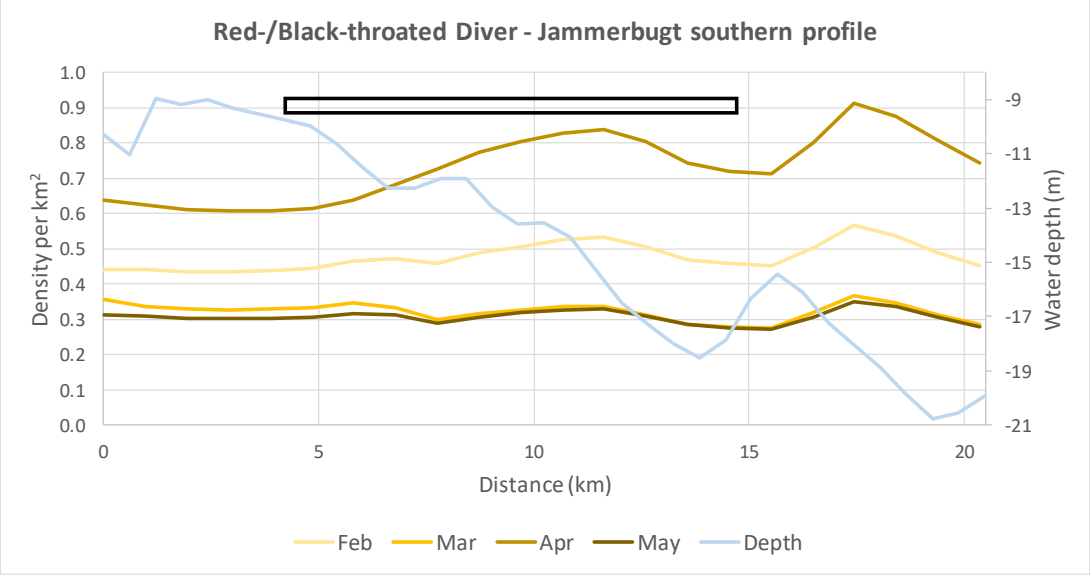

Figure 15 Predicted gradients in the mean monthly density (n/km^2) of Red-throated/Black-throated Diver *Gavia stellate/arctica* along two profile lines crossing the Jammerbugt development area.

Table 4 Statistics on the predicted abundance of Red-throated/Black-throated Diver *Gavia stellate/arctica* in the Thor development area in comparison to the rest of the Danish part of the North Sea.

Area	Feb	Mar	Apr	May
Total number of grid cells	58216	58216	58216	58216
High habitat suitability	5885	5799	5633	5713
% High habitat suitability	10.1	10.0	9.7	9.8
Thor area (km^2)	462	462	462	462
Danish NS area (km^2)	58216	58216	58216	58216
Thor % area	0.79	0.79	0.79	0.79
Thor area High habitat suitability (km^2)	72	26	173	14
Thor area % High habitat suitability	15.6	5.6	37.4	3.0
Thor area % High habitat suitability of total Danish NS area	1.2	0.4	3.1	0.2
Mean density NS	0.208	0.188	0.282	0.2
Total number NS	12109	10945	16417	11643
Mean density Thor area	0.301	0.288	0.305	0.235
Total number Thor area	139	133	141	109

Table 5 Statistics on the predicted abundance of Red-throated/Black-throated Diver *Gavia stellate/arctica* in the Ringkøbing development area in comparison to the rest of the Danish part of the North Sea

Area	Feb	Mar	Apr	May
Total number of grid cells	58216	58216	58216	58216
High habitat suitability	5885	5799	5633	5713
% High habitat suitability	10.1	10.0	9.7	9.8
Ringkøbing area (km^2)	1707	1707	1707	1707
Danish NS area (km^2)	58216	58216	58216	58216
Ringkøbing % area	2.93	2.93	2.93	2.93
Ringkøbing area High habitat suitability (km^2)	722	650	707	259
Ringkøbing area % High habitat suitability	42.3	38.1	41.4	15.2
Ringkøbing area % High habitat suitability of total Danish NS area	1.2	1.1	1.2	0.4
Mean density NS	0.208	0.188	0.282	0.2
Total number NS	12109	10945	16417	11643
Mean density Ringkøbing area	0.404	0.406	0.681	0.267
Total number Ringkøbing area	690	693	1162	456

Table 6 Statistics on the predicted abundance of Red-throated/Black-throated Diver *Gavia stellate/arctica* in the Jammerbugt development area in comparison to the rest of the Danish part of the North Sea

Area	Feb	Mar	Apr	May
Total number of grid cells	58216	58216	58216	58216
High habitat suitability	5885	5799	5633	5713
% High habitat suitability	10.1	10.0	9.7	9.8
Jammerbugt area (km^2)	262	262	262	262
Danish NS area (km^2)	58216	58216	58216	58216
Jammerbugt % area	0.5	0.5	0.5	0.5
Jammerbugt area High habitat suitability (km^2)	190	0	164	17
Jammerbugt area % High habitat suitability	72.5	0.0	62.6	6.5
Jammerbugt area % High habitat suitability of total Danish NS area	0.3	0.0	0.3	0.0
Mean density NS	0.208	0.188	0.282	0.2
Total number NS	12109	10945	16417	11643
Mean density Jammerbugt area	0.471	0.308	0.746	0.298
Total number Jammerbugt area	123	81	195	78

3.1.1.2 Common Scoter

The results of the distribution models for Common Scoter are shown in Appendix C.1.2. The presence/absence part clearly shows the species' preference for areas between 8m and 15m water depth with low current speed and intermediate salinity – characteristics which are typical for the Horns Rev area as well as the area adjacent to the Wadden Sea and close to the Jutland coast. The influence of Horns Rev 1 and 2 offshore wind farms on the presence of Common Scoter is uncertain, as the two response curves display different trends.

The different trends in relation to wind farms are also apparent in the positive part of the models, yet here water depth is by far the key factor determining the density of scoters. The density of the species also displays a negative relationship to shipping lanes. The relation to bottom salinity shows two peaks; one in low saline coastal water (<28 psu) and one in higher saline offshore waters (>32 psu). The validation of the model's predictive is illustrated in Figure 16, which shows that the predicted numbers of Common Scoters along the aerial transect lines in the North Sea are comparable to the observed numbers.

The predicted mean monthly densities in Figure 17 and Figure 18 and the areas of high habitat suitability in Figure 19 and Figure 20 show zones of persistent higher densities (> 50 birds/km^2) on the shallows off Blåvandshuk, along the coast of Jutland and at the western and north-western parts of Horns Rev. The densities peak during mid-winter (January). At the latitude of the Thor development area high densities and high habitat suitability to scoters are predicted very close to the coast, while the densities in the Thor area are very low. In the Ringkøbing area high habitat quality associated with the outer part of Horns Rev is predicted in the southwestern part of the area. In the Jammerbugt area higher densities are predicted to the southwest of the area and extending into the site. The overlap is largest during the month of April.

Figure 21, Figure 22, Figure 23 and Table 7, Table 8 and Table 9 provide more details on the importance of the Thor, Ringkøbing and Jammerbugt areas to Common Scoter. The two profiles across Thor confirm the low abundance of the species in the wind farm area, and medium densities (5 birds/km^2) are only predicted during January and March in a small sector of 20m depth located 4 km into the area at the eastern edge. The profile across the southern part of the Ringkøbing area confirms

that medium densities (7-13 birds/km^2) are predicted in the central offshore sector northwest of Horns Rev and south of Thor. Accordingly, although high habitat suitability is found in this sector densities exceeding 50 birds/km^2 are only predicted in the southernmost corner close to Horns Rev. The profiles across the Jammerbugt area confirm that medium densities (5-10 birds/km^2) of scoter are predicted in the southwestern part overlapping with the southern 50% of the wind farm area.

The model results document that although densities in the North Sea vary between months the birds show a remarkable fidelity to the same areas month-by-month with 10% of the Danish part of the North Sea classified as of high habitat suitability. The dynamics in the Thor and Ringkøbing areas in terms of high habitat suitability are also highly stable, whereas the proportion in Jammerbugt is much higher in April (56.9%) than during January-March (27.5%-29.4%).

The validation results (Appendix C) indicate that the presence-absence part of the model describes the input densities well with an AUC value of 0.74, while the predicted densities due to the high resolution only describes a small proportion of the variation in observed densities. The validation of the ability of the model to predict densities independently from the input data indicates that the model predictions provide a very reliable generalisation of the densities over the modelled region with a Sperman's correlation coefficient of 0.16.

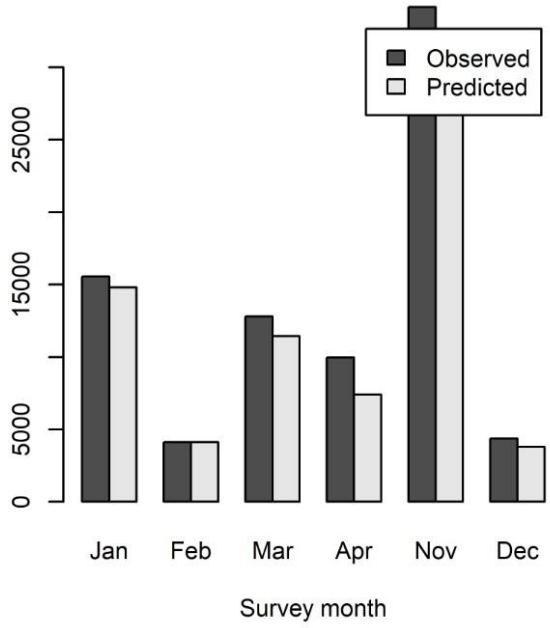

Figure 16 Comparison of predicted versus observed numbers of Common Scoter *Melanitta nigra* along the aerial transect lines in the North Sea.

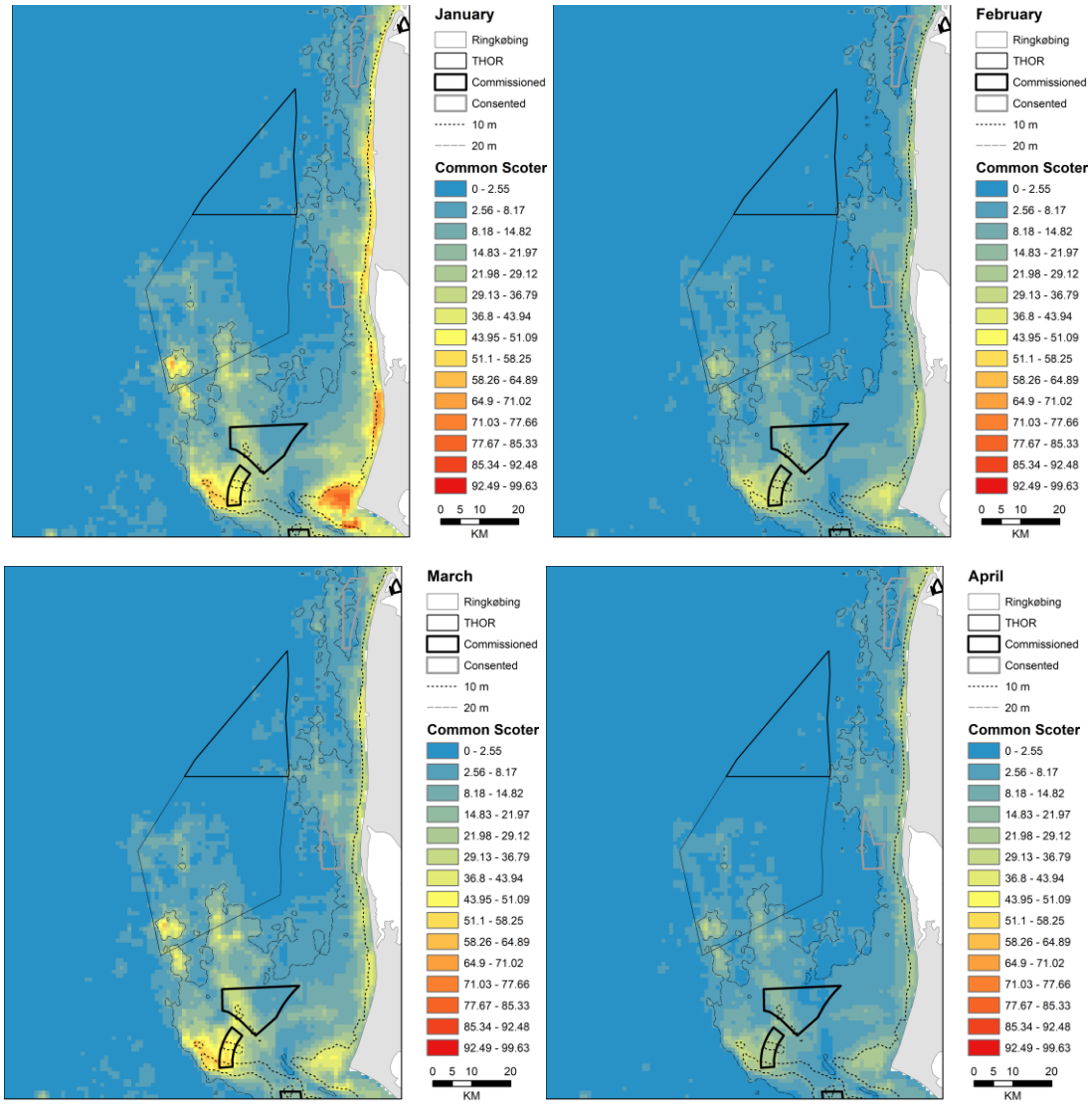

Figure 17 Predicted mean monthly density (n/km^2) of Common Scoter *Melanitta nigra* along the west coast of Denmark.

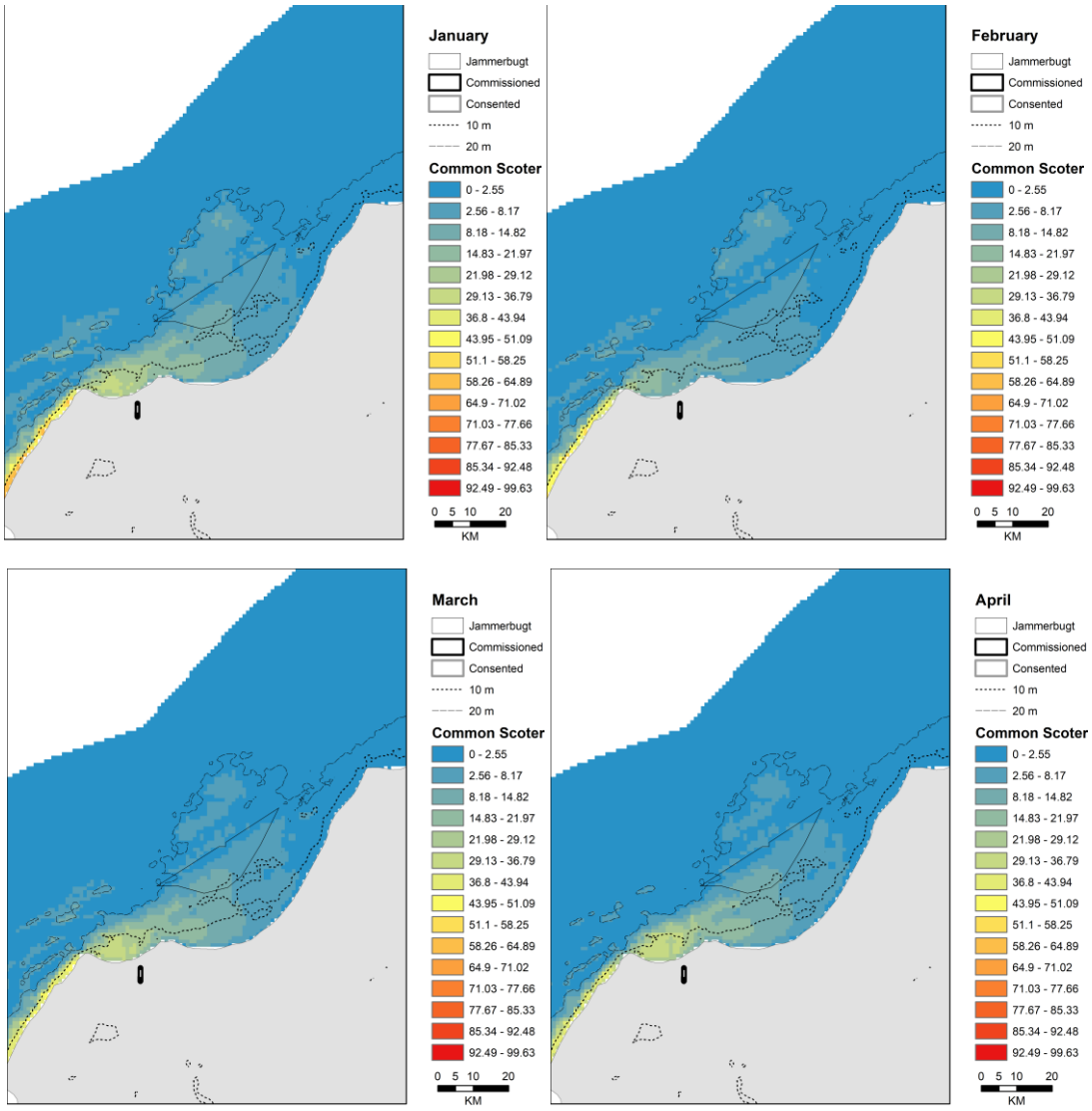

Figure 18 Predicted mean monthly density (n/km^2) of Common Scoter *Melanitta nigra* along the coast of Skagerrak.

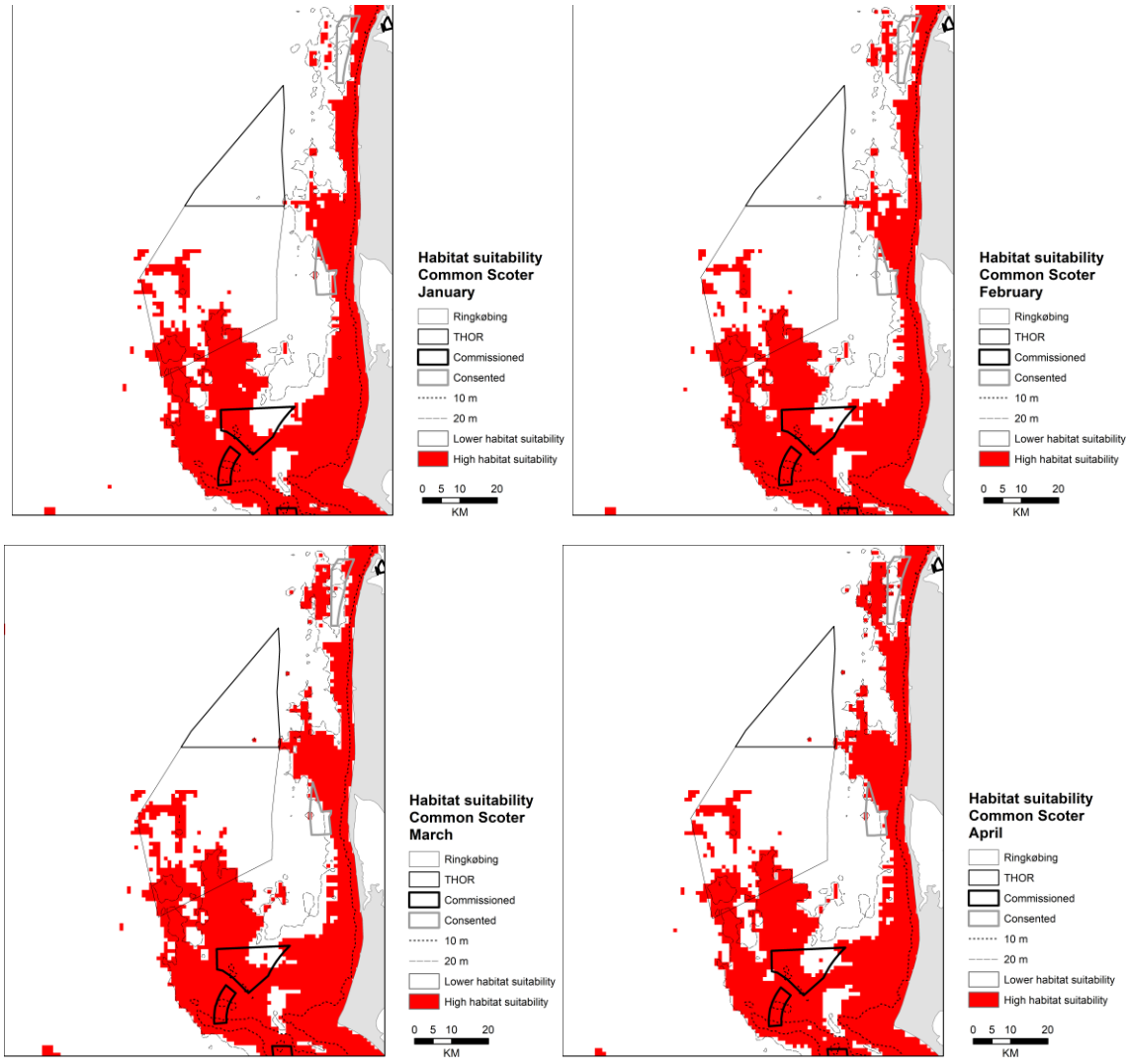

Figure 19 Areas of high habitat suitability to Common Scoter *Melanitta nigra* predicted during the main months of occurrence along the west coast of Denmark.

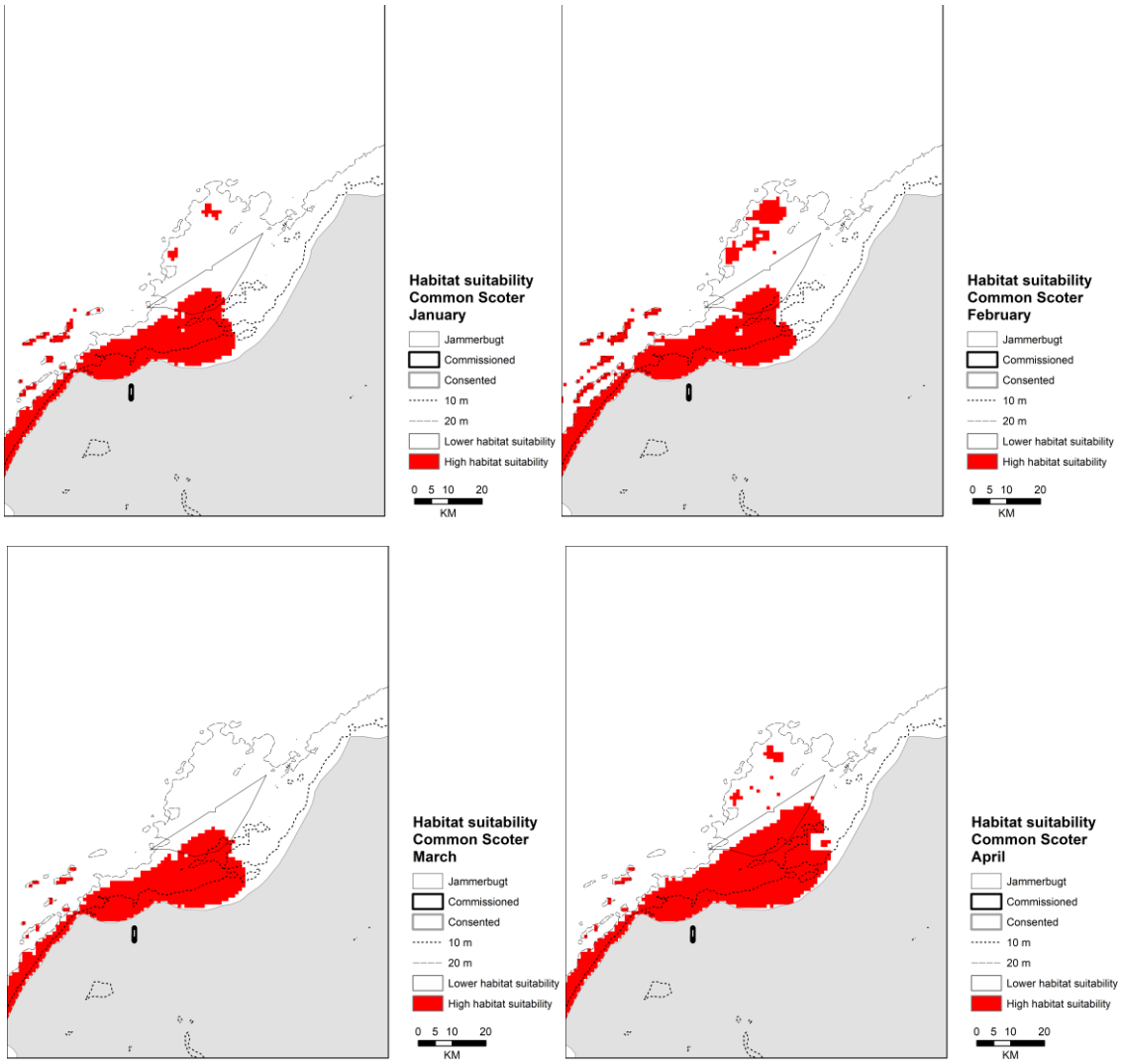

Figure 20 Areas of high habitat suitability to Common Scoter *Melanitta nigra* predicted during the main months of occurrence along the coast of Skagerrak.

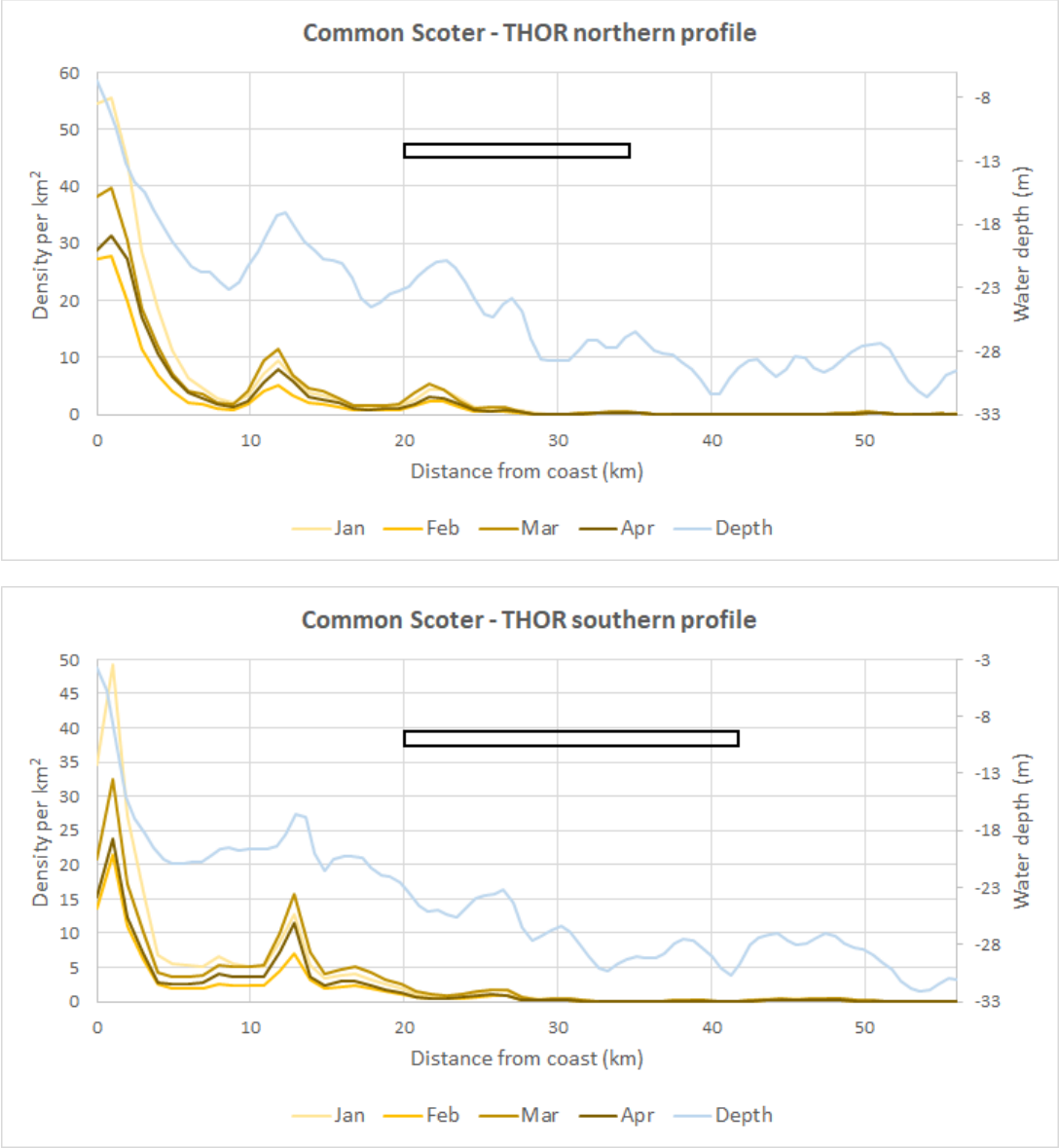

Figure 21 Predicted gradients in the mean monthly density (n/km^2) of Common Scoter *Melanitta nigra* along two profile lines crossing the Thor development area.

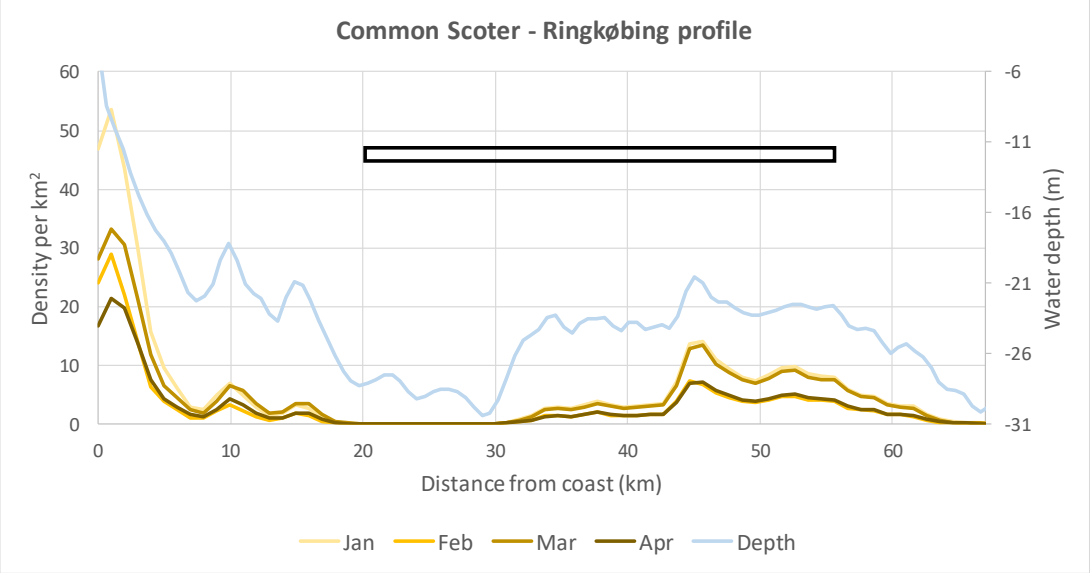

Figure 22 Predicted gradients in the mean monthly density (n/km^2) of Common Scoter *Melanitta nigra* along the profile line crossing the Ringkøbing development area.

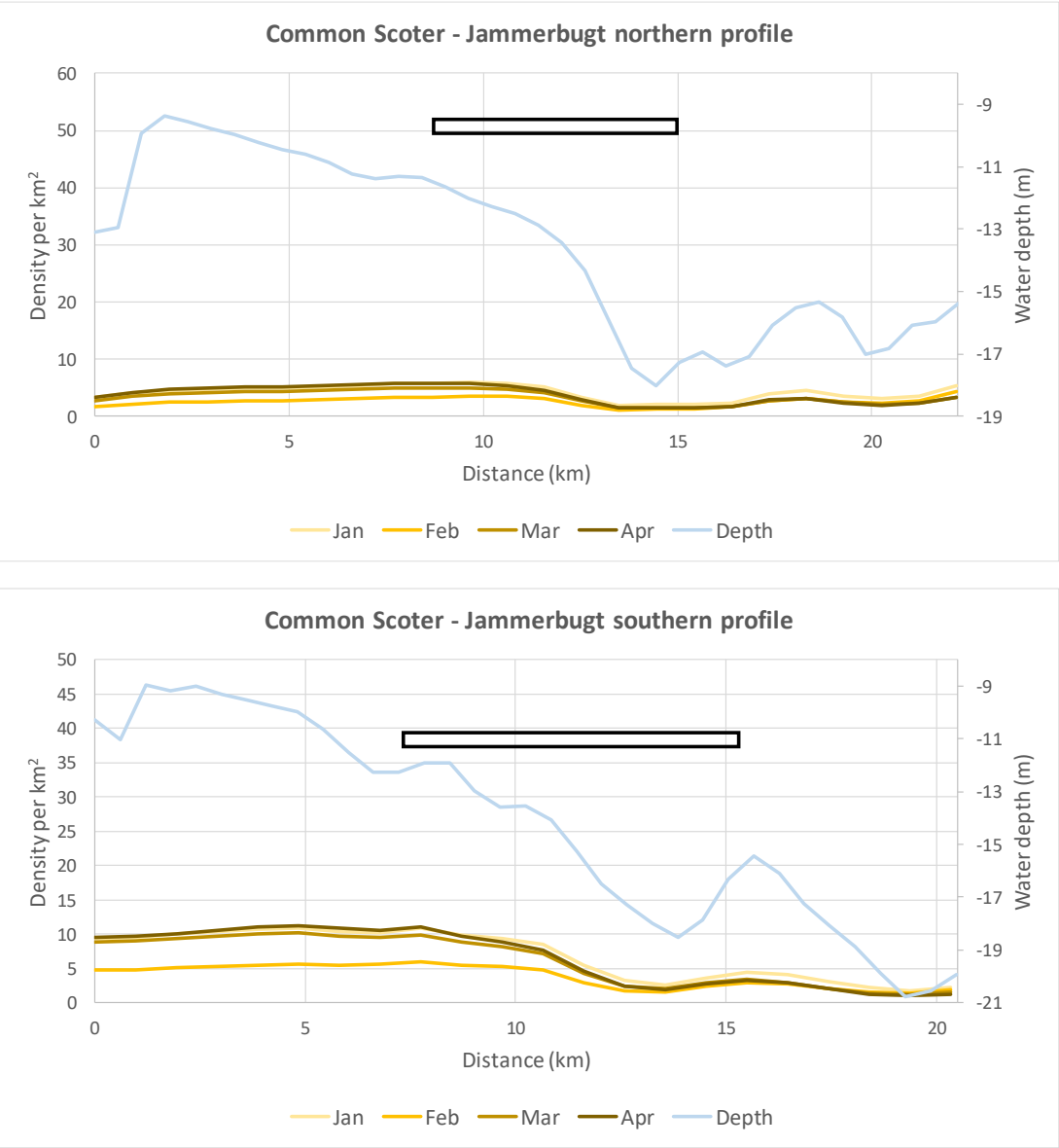

Figure 23 Predicted gradients in the mean monthly density (n/km^2) of Common Scoter *Melanitta nigra* along two profile lines crossing the Jammerbugt development area.

Table 7 Statistics on the predicted abundance of Common Scoter *Melanitta nigra* in the Thor development area in comparison to the rest of the Danish part of the North Sea.

Area	Jan	Feb	Mar	Apr
Total number of grid cells	58216	58216	58216	58216
High habitat suitability	5822	5822	5819	5822
% High habitat suitability	10.0	10.0	10.0	10.0
Thor area (km^2)	462.0	462.0	462.0	462.0
Danish NS area (km^2)	58216	58216	58216	58216
Thor % area	0.79	0.79	0.79	0.79
Thor area High habitat suitability (km^2)	1	4	4	4
Thor area % High habitat suitability	0.2	0.9	0.9	0.9
Thor area % High habitat suitability of total Danish NS area	0.02	0.07	0.07	0.07
Mean density NS	3.039	1.602	2.319	1.48
Total number NS	176918	93262	135003	86160
Mean density Thor area	1	0.536	1.1	0.627
Total number Thor area	462	248	508	290

Table 8 Statistics on the predicted abundance of Common Scoter *Melanitta nigra* in the Ringkøbing development area in comparison to the rest of the Danish part of the North Sea.

Area	Jan	Feb	Mar	Apr
Total number of grid cells	58216	58216	58216	58216
High habitat suitability	5822	5822	5819	5822
% High habitat suitability	10.0	10.0	10.0	10.0
Ringkøbing area (km^2)	1707	1707	1707	1707
Danish NS area (km^2)	58216	58216	58216	58216
Ringkøbing % area	2.93	2.93	2.93	2.93
Ringkøbing area High habitat suitability (km^2)	282	257	319	264
Ringkøbing area % High habitat suitability	16.5	15.1	18.7	15.5
Ringkøbing area % High habitat suitability of total Danish NS area	0.5	0.4	0.5	0.5
Mean density NS	3.039	1.602	2.319	1.48
Total number NS	176918	93262	135003	86160
Mean density Ringkøbing area	4.396	2.267	4.145	2.230
Total number Ringkøbing area	7504	3870	7076	3807

Table 9 Statistics on the predicted abundance of Common Scoter *Melanitta nigra* in the Jammerbugt development area in comparison to the rest of the Danish part of the North Sea.

Area	Jan	Feb	Mar	Apr
Total number of grid cells	58216	58216	58216	58216
High habitat suitability	5822	5822	5819	5822
% High habitat suitability	10.0	10.0	10.0	10.0
Jammerbugt area (km^2)	262	262	262	262
Danish NS area (km^2)	58216	58216	58216	58216
Jammerbugt % area	0.5	0.5	0.5	0.5
Jammerbugt area High habitat suitability (km^2)	72	74	77	149
Jammerbugt area % High habitat suitability	27.5	28.2	29.4	56.9
Jammerbugt area % High habitat suitability of total Danish NS area	0.1	0.1	0.1	0.3
Mean density NS	3.039	1.602	2.319	1.48
Total number NS	176918	93262	135003	86160
Mean density Jammerbugt area	5.504	5.042	3.308	5.859
Total number Jammerbugt area	1442	1321	867	1535

3.1.2 Southern Kattegat

3.1.2.1 Red-throated/Black-throated Diver

The results of the distribution models for Red-throated and Black-throated Diver are shown in Appendix C.2.1. The presence/absence part of the models indicate that the species prefer more saline areas with a water depth between 10 and 25 m and with low current speeds in the Kattegat. The positive part of the model mainly highlights the importance of areas with low eddy activity. The validation of the model's predictive power is illustrated in Figure 24, which shows that the predicted numbers of divers along the aerial transect lines in the southern Kattegat are comparable to the observed numbers.

The predicted mean monthly densities in Figure 25 and the areas of high habitat suitability in Figure 26 show zones of persistent medium-high densities (0.4-0.6 birds/km^2) and high habitat quality in the coastal areas shallower than 20 m north of Sjælland, around Anholt and in Skälderviken and Laholmsbugten. There is a pronounced influx of divers to the southern Kattegat in spring when densities and total numbers double compared to the winter season.

Both during winter and spring the Hesselø site is located in an area of low density of divers, and the closest areas of high habitat suitability are found at a minimum distance of 20 km north of Sjælland. The E-V profiles of modelled densities of divers across the site stress the occurrence of low densities in the area (Figure 27), and the table of abundance estimates documents the low abundance here (Table 10). The model results classify approximately 6% of the southern Kattegat as of high habitat suitability throughout winter and spring periods.

The validation results (Appendix C) indicate that the presence-absence part of the model describes the input densities well with an AUC value of 0.70, while the predicted densities due to the high resolution only describes a small proportion of the variation in observed densities. The validation of the ability of the model to predict densities independently from the input data indicates that the model predictions provide a reliable generalisation of the densities over the modelled region with a Sperman's correlation coefficient of 0.13.

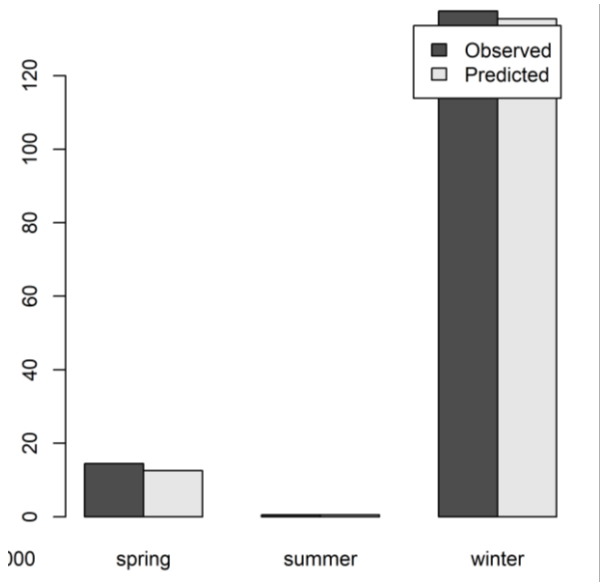

Figure 24 Comparison of predicted versus observed numbers of Red-throated/Black-throated Diver *Gavia stellata{arctica* along the aerial transect lines in the southern Kattegat.

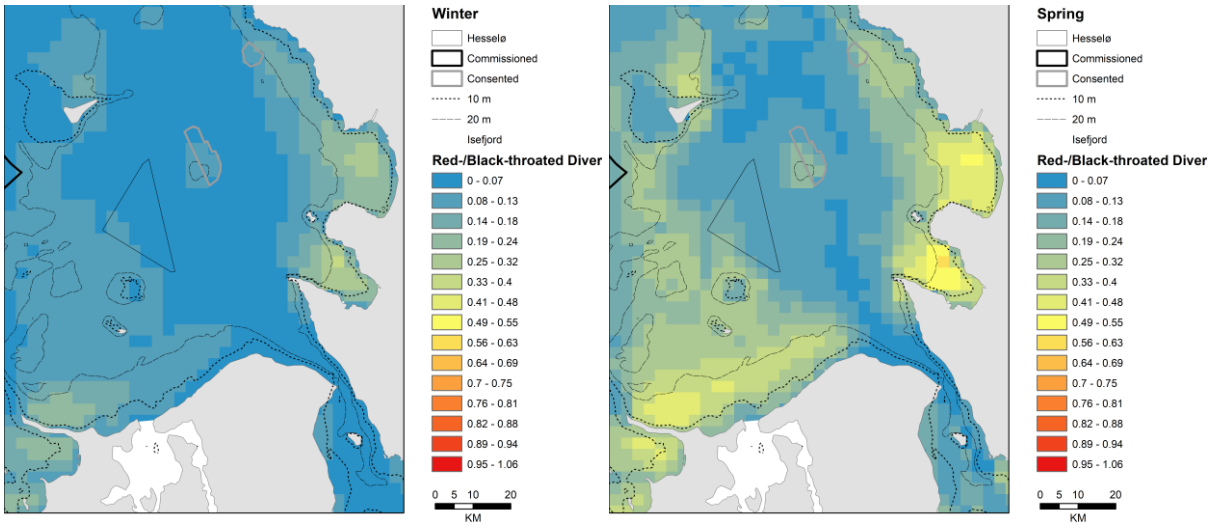

Figure 25 Predicted mean monthly density (n/km^2) of Red-throated/Black-throated Diver *Gavia stellata/arctica* in the southern Kattegat.

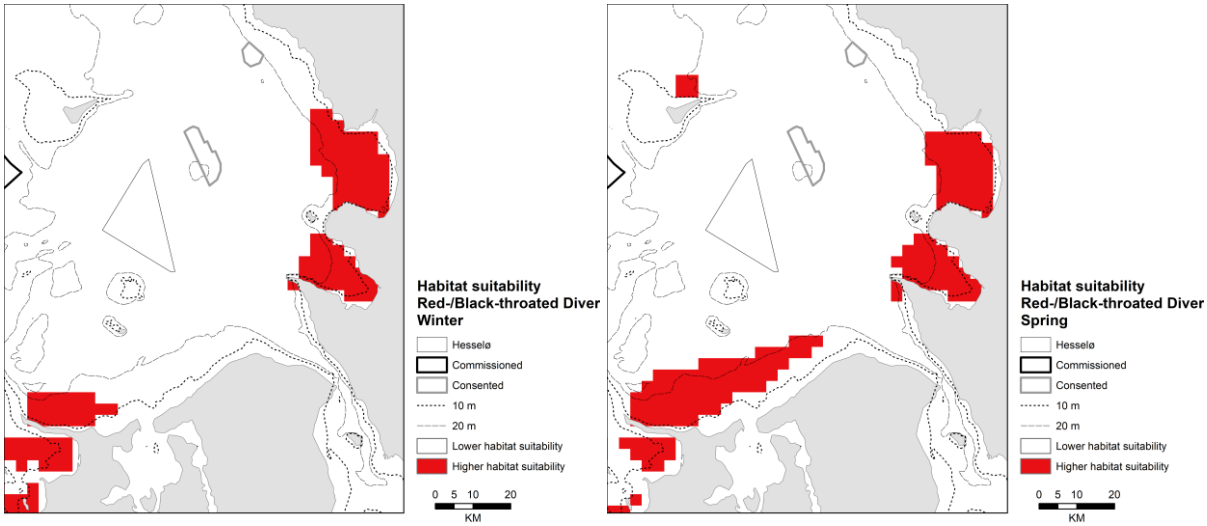

Figure 26 Areas of high habitat suitability to Red-throated/Black-throated Diver *Gavia stellata/arctica* predicted during the main months of occurrence in the southern Kattegat.

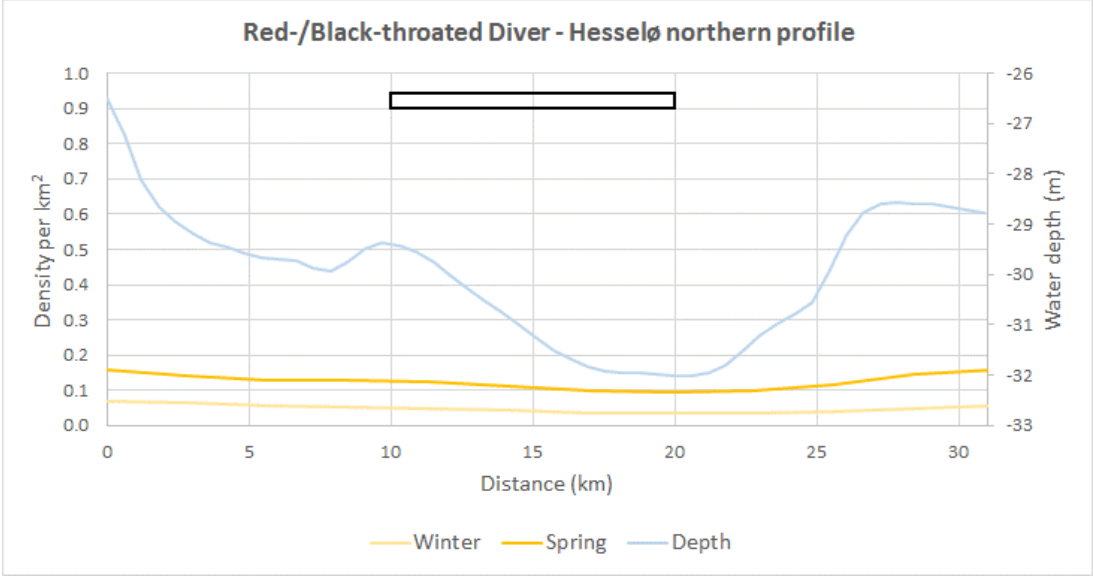

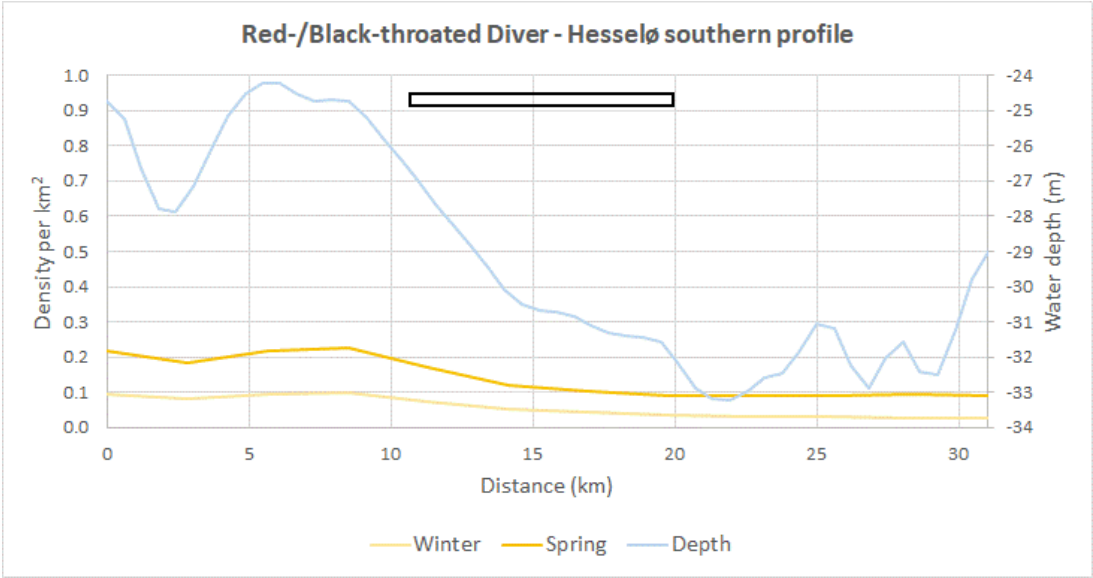

Figure 27 Predicted gradients in the mean monthly density (n/km^2) of Red-throated/Black-throated Diver *Gavia stellata/arctica* along two profile lines crossing the Hesselø development area.

Table 10 Statistics on the predicted abundance of Red-throated/Black-throated Diver *Gavia stellata/arctica* in the Hesselø development area in comparison to the rest of the southern Kattegat.

Area	Winter	Spring
Total number of grid cells	5695	5695
High habitat suitability	352	330
% High habitat suitability	6.2	5.8
Hesselø area (km^2)	262	262
Kattegat area (km^2)	30609	30609
Hesselø % area	0.9	0.9
Hesselø area High habitat suitability (km^2)	0	0
Hesselø area % High habitat suitability	0	0
Hesselø area % High habitat suitability of total Kattegat area	0	0
Mean density Kattegat	0.08	0.16
Total number Kattegat	2373	5034
Mean density Hesselø area	0.05	0.12
Total number Hesselø area	13	32

3.1.2.2 Common Eider

The results of the distribution models for Common Eider are shown in Appendix C.2.2. The presence/absence part of the models indicates that the species prefer areas in the southern Kattegat with the highest growth of mussels as reflected by the filter-feeder index. The birds also generally occur in areas of lower current speed. The positive part of the models shows that within the areas where Common Eiders mainly occur the highest densities are related to patches of relatively high current speed.

The validation of the model's predictive power is illustrated in Figure 28, which shows that the predicted numbers of eiders along the aerial transect lines in the southern Kattegat are comparable to the observed numbers.

The predicted mean monthly densities in Figure 29 and the areas of high habitat suitability in Figure 30show zones of medium-high densities (5-10 birds/km^2) and high habitat quality in the coastal areas shallower than 12 m in Sejerøbugten, around Anholt, the island Hesselø, Øresund and in Skälderviken. The densities are highest during winter and lowest during summer.

Throughout the year the Hesselø site is located in an area of low density of eiders, and the closest area of high habitat suitability is found at a minimum distance of 10 km at the island of Hesselø. The E-V profiles of modelled densities of eiders across the site stress the occurrence of low densities in the area (Figure 31), and the table of abundance estimates documents the low abundance here (Table 11). The model results classify approximately 6% of the southern Kattegat as of high habitat suitability throughout the year.

The validation results (Appendix C) indicate that the presence-absence part of the model describes the input densities well with an AUC value of 0.72, while the predicted densities due to the high resolution only describes a small proportion of the variation in observed densities. The validation of the ability of the model to predict densities independently from the input data indicates that the model predictions provide a very reliable generalisation of the densities over the modelled region with a Sperman's correlation coefficient of 0.17.

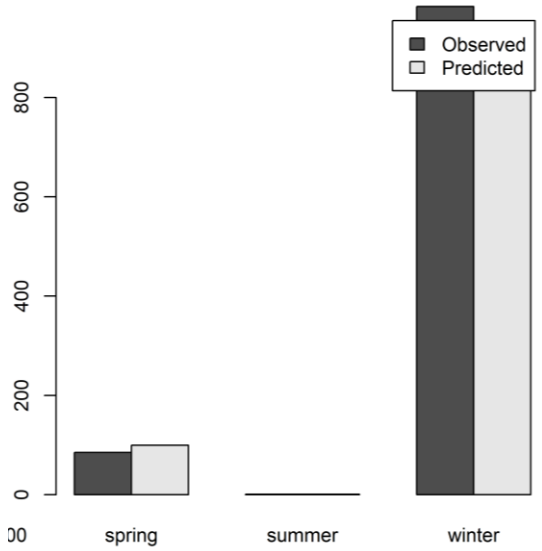

Figure 28 Comparison of predicted versus observed numbers of Common Eider *Somateria mollissima* along the aerial transect lines in the southern Kattegat.

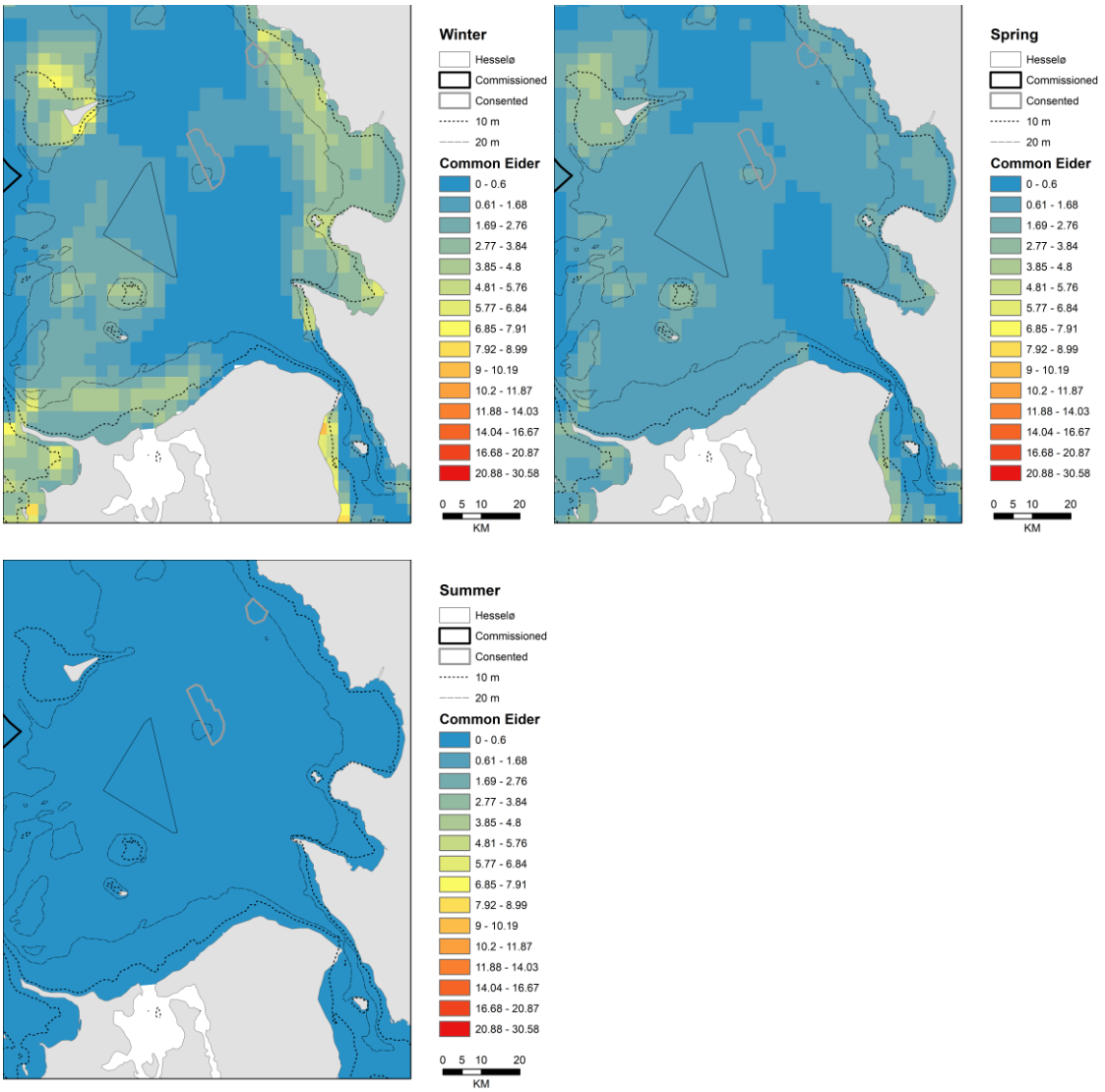

Figure 29 Predicted mean monthly density (n/km^2) of Common Eider *Somateria mollissima* in the southern Kattegat.

Figure 30 Areas of high habitat suitability to Common Eider *Somateria mollissima* predicted during the main months of occurrence in the southern Kattegat.

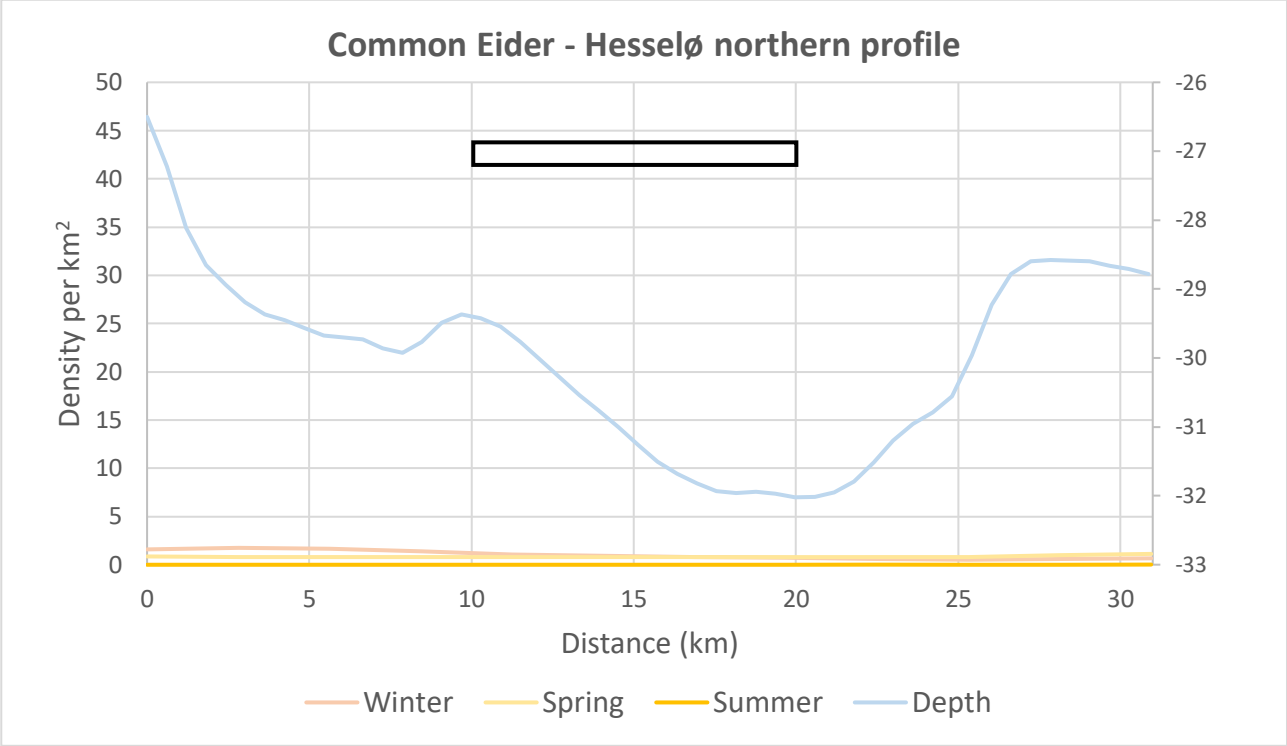

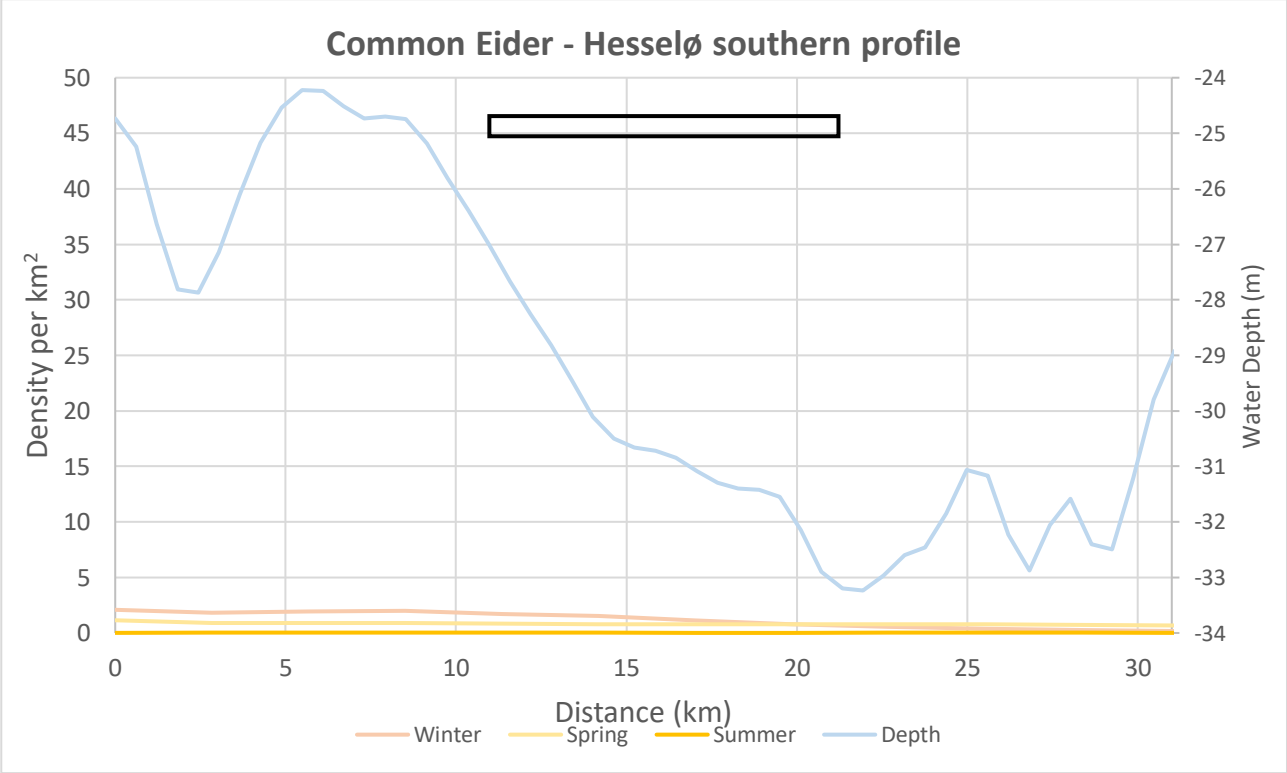

Figure 31 Predicted gradients in the mean monthly density (n/km^2) of Common Eider *Somateria mollissima* along two profile lines crossing the Hesselø development area.

Table 11 Statistics on the predicted abundance of Common Eider *Somateria mollissima* in the Hesselø development area in comparison to the rest of the southern Kattegat.

Area	Winter	Spring	Summer
Total number of grid cells	5695	5695	5695
High habitat suitability	339	341	335
% High habitat suitability	6.0	6.0	5.9
Hesselø area (km^2)	262	262	262
Kattegat area (km^2)	30609	30609	30609
Hesselø % area	0.9	0.9	0.9
Hesselø area High habitat suitability (km^2)	0	0	0
Hesselø area % High habitat suitability	0	0	0
Hesselø area % High habitat suitability of total Kattegat area	0	0	0
Mean density Kattegat	2.45	1.35	0.02
Total number Kattegat	75043	41293	498
Mean density Hesselø area	1.10	0.81	0.01
Total number Hesselø area	289	211	2

3.1.2.3 Common Scoter

The results of the distribution models for the Common Scoter are shown in Appendix C.2.3. As for the Common Eider, the presence/absence part of the models indicates that the species prefer areas in the southern Kattegat with the highest growth of mussels as reflected by the filter-feeder index. The birds also generally occur in areas of lower current speed. The positive part of the model shows that unlike the eiders Common Scoters are found in highest densities in areas away from shipping lanes.

The validation of the model's predictive power is illustrated in Figure 32, which shows that the predicted numbers of scoters along the aerial transect lines in the southern Kattegat are comparable to the observed numbers.

The predicted mean monthly densities in Figure 33 and the areas of high habitat suitability in Figure 34 show zones of medium-high densities (3-6 birds/km^2) and high habitat quality in the coastal areas shallower than 20 m at Sjællands Odde, Anholt, Øresund and at Kullen. The densities are highest during winter.

Throughout the year the Hesselø site is located in an area of low density of Common Scoter, and the closest area of high habitat suitability is found at a minimum distance of 25 km at Anholt. The E-V profiles of modelled densities of Common Scoter across the site stress the occurrence of low densities in the area (Figure 35), and the table of abundance estimates documents the low abundance here (Table 12). The model results classify approximately 6% of the southern Kattegat as of high habitat suitability throughout the year.

The validation results (Appendix C) indicate that the presence-absence part of the model describes the input densities very well with an AUC value of 0.81, while the predicted densities due to the high resolution only describes a small proportion of the variation in observed densities. The validation of the ability of the model to predict densities independently from the input data indicates that the model predictions provide a reasonable generalisation of the densities over the modelled region with a Sperman's correlation coefficient of 0.09.

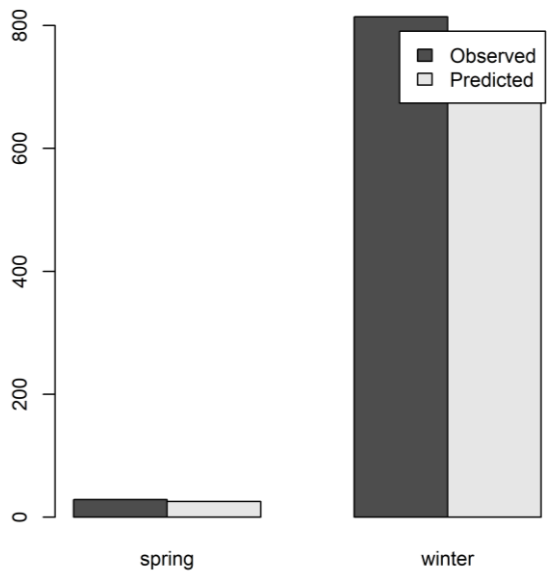

Figure 32 Comparison of predicted versus observed numbers of Common Scoter *Melanitta nigra* along the aerial transect lines in the southern Kattegat.

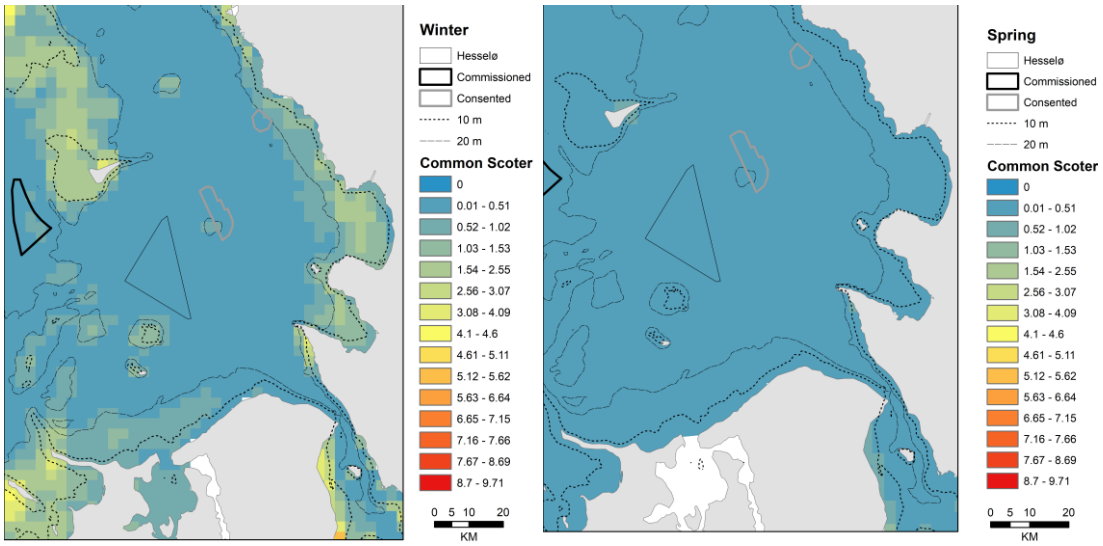

Figure 33 Predicted mean monthly density (n/km^2) of Common Scoter *Melanitta nigra* in the southern Kattegat.

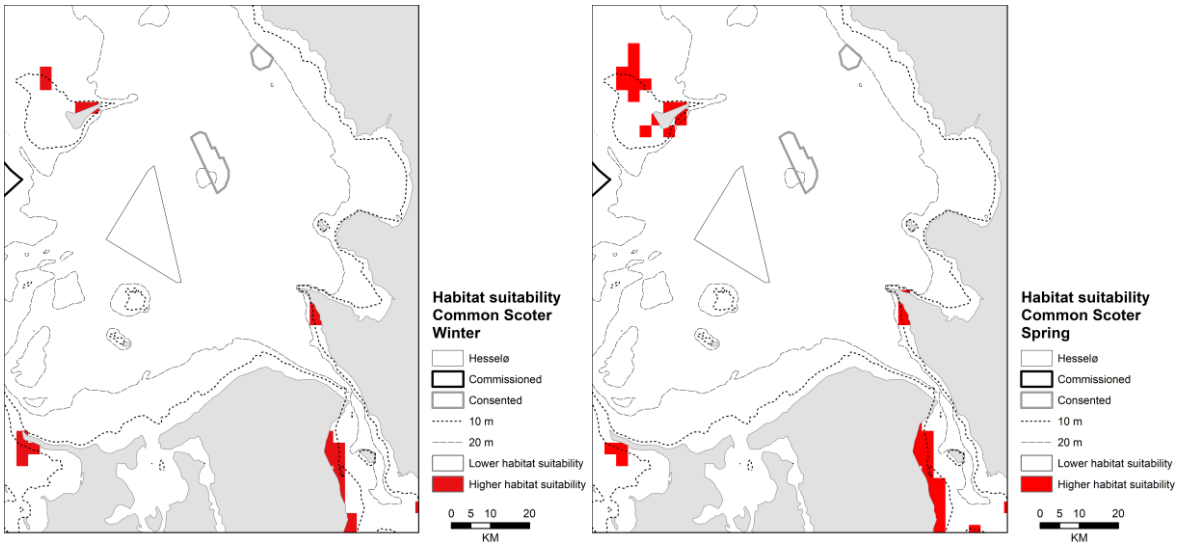

Figure 34 Areas of high habitat suitability to Common Scoter *Melanitta nigra* predicted during the main months of occurrence in the southern Kattegat.

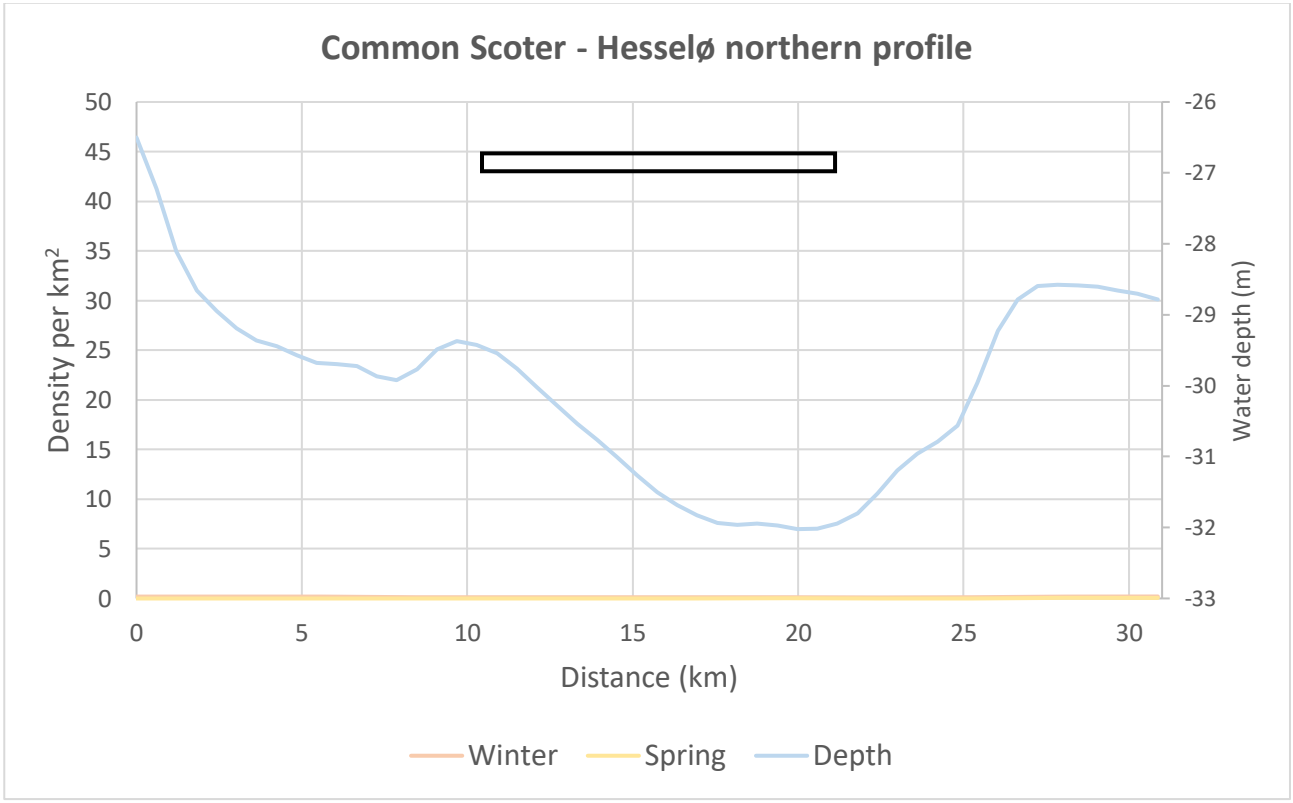

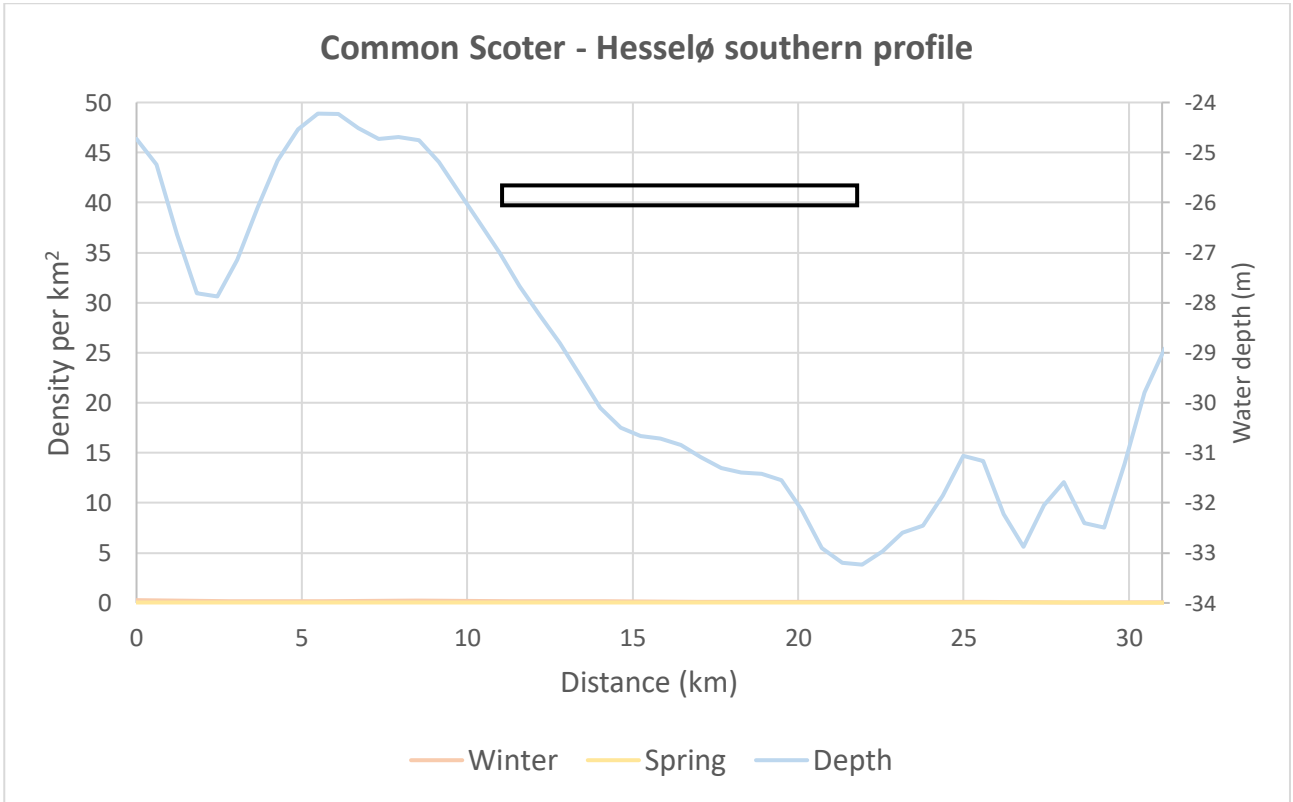

Figure 35 Predicted gradients in the mean monthly density (n/km^2) of Common Scoter *Melanitta nigra* along two profile lines crossing the Hesselø development area.

Table 12 Statistics on the predicted abundance of Common Scoter *Melanitta nigra* in the Hesselø development area in comparison to the rest of the southern Kattegat.

Area	Winter	Spring
Total number of grid cells	5695	5695
High habitat suitability	340	343
% High habitat suitability	6.0	6.0
Hesselø area (km^2)	262	262
Kattegat area (km^2)	30609	30609
Hesselø % area	0.9	0.9
Hesselø area High habitat suitability (km^2)	0	0
Hesselø area % High habitat suitability	0	0
Hesselø area % High habitat suitability of total Kattegat area	0	0
Mean density Kattegat	0.98	0.15
Total number Kattegat	30096	4628
Mean density Hesselø area	0.14	0.02
Total number Hesselø area	36	6

3.1.2.4 Velvet Scoter

The results of the distribution models for Velvet Scoter are shown in Appendix C.2.4, and resemble those for the Common Scoter with the presence/absence part showing a preference for areas in the southern Kattegat with the highest growth of mussels and lower current speed. The positive part of the model shows that unlike the Common Scoter the highest densities are mainly related to peak levels of potential mussel growth, while distance to shipping lanes has minor influence on the abundance of the species.

The validation of the model's predictive power is illustrated in Figure 36, which shows that the predicted numbers of scoters along the aerial transect lines in the southern Kattegat are comparable to the observed numbers.

The predicted mean monthly densities in Figure 37 and the areas of high habitat suitability in Figure 38 show zones of medium-high densities (1-3 birds/km^2) and high habitat quality in the coastal areas shallower than 20 m northwest of Anholt, in Øresund and at Kullen. The densities are highest during winter.

Throughout the year the Hesselø site is located in an area with very low densities or no Velvet Scoters, and the closest area of high habitat suitability is found at a minimum distance of 25 km at Anholt. The E-V profiles of modelled densities of Velvet Scoter across the site stress the occurrence of very low densities in the area (Figure 39), and the table of abundance estimates documents the very low abundance here (Table 13). The model results classify approximately 6% of the southern Kattegat as of high habitat suitability throughout the year.

The validation results (Appendix C) indicate that the presence-absence part of the model describes the input densities well with an AUC value of 0.78, while the predicted densities due to the high resolution only describes a small proportion of the variation in observed densities. The validation of the ability of the model to predict densities independently from the input data indicates that the model predictions provide a reasonable generalisation of the densities over the modelled region with a Sperman's correlation coefficient of 0.06.

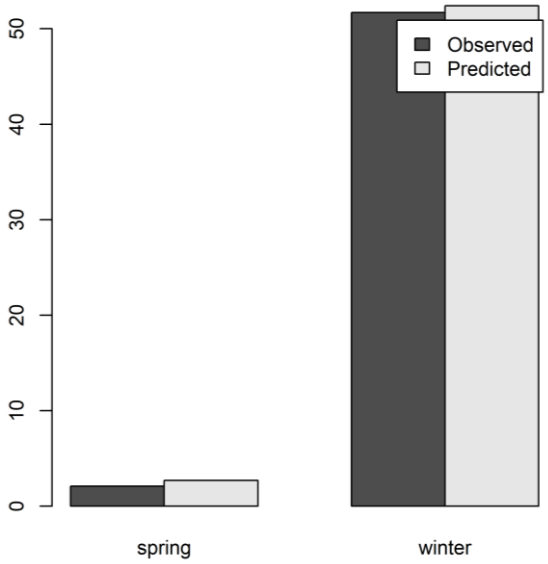

Figure 36 Comparison of predicted versus observed numbers of Velvet Scoter *Melanitta fusca* along the aerial transect lines in the southern Kattegat.

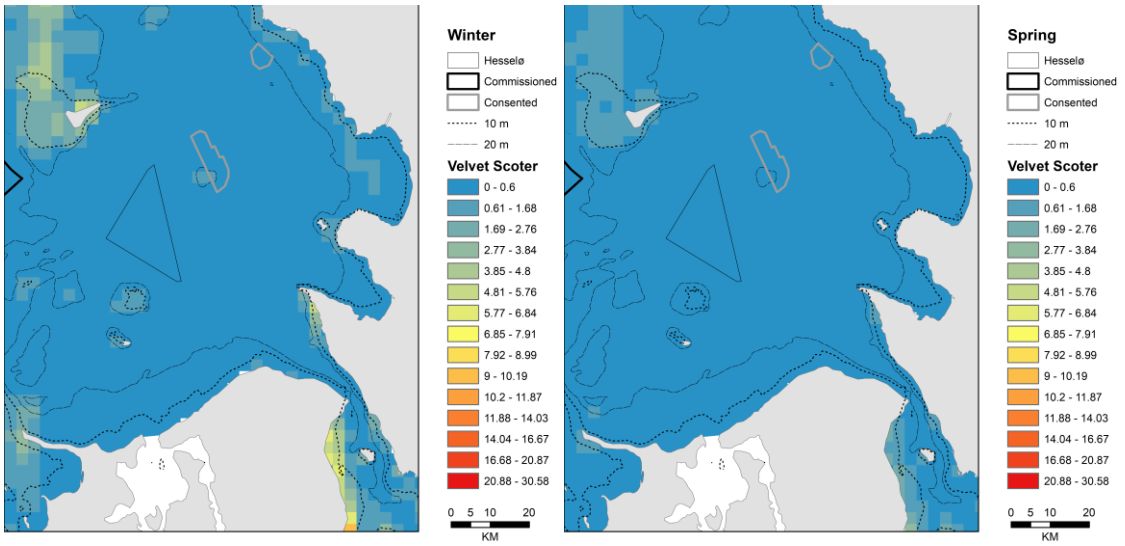

Figure 37 Predicted mean monthly density (n/km^2) of Velvet Scoter *Melanitta fusca* in the southern Kattegat.

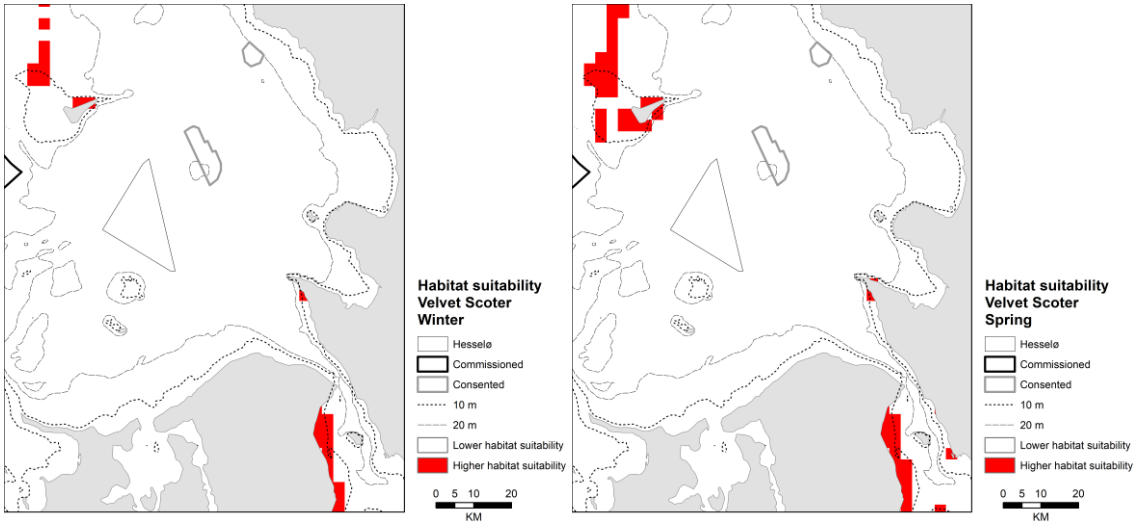

Figure 38 Areas of high habitat suitability to Velvet Scoter *Melanitta fusca* predicted during the main months of occurrence in the southern Kattegat.

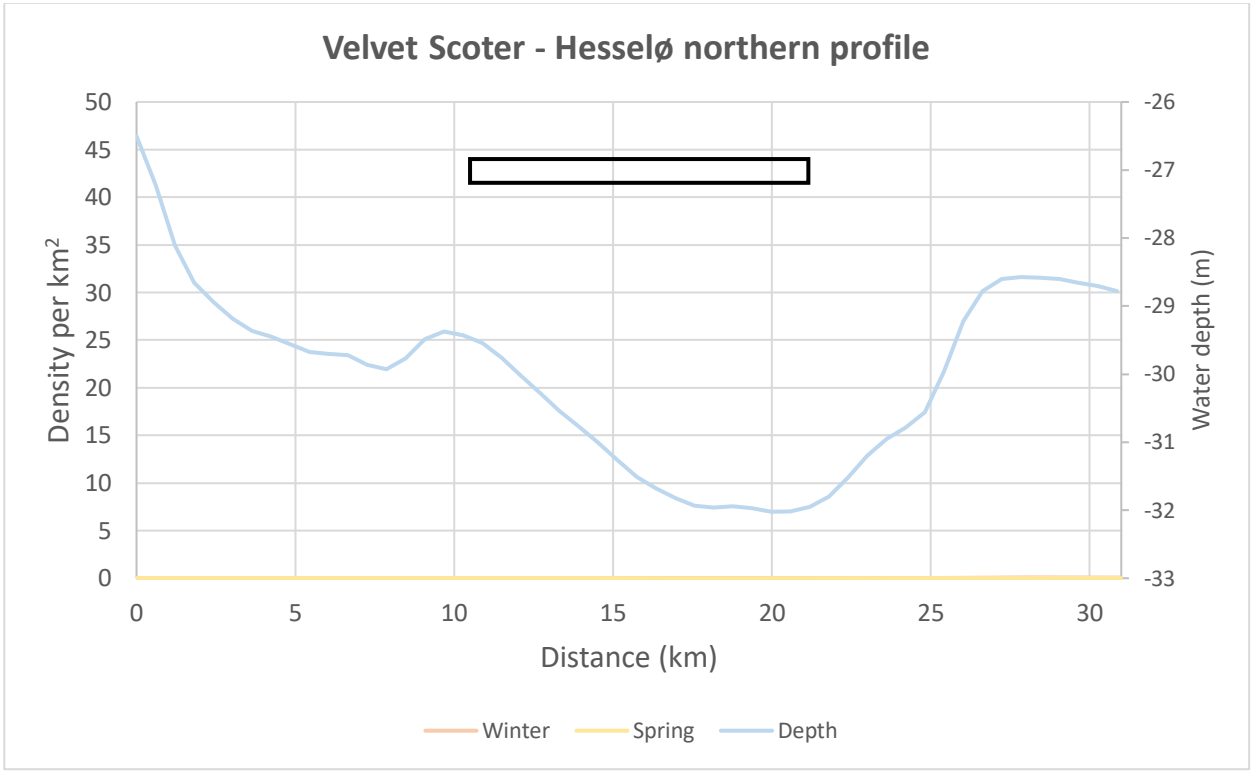

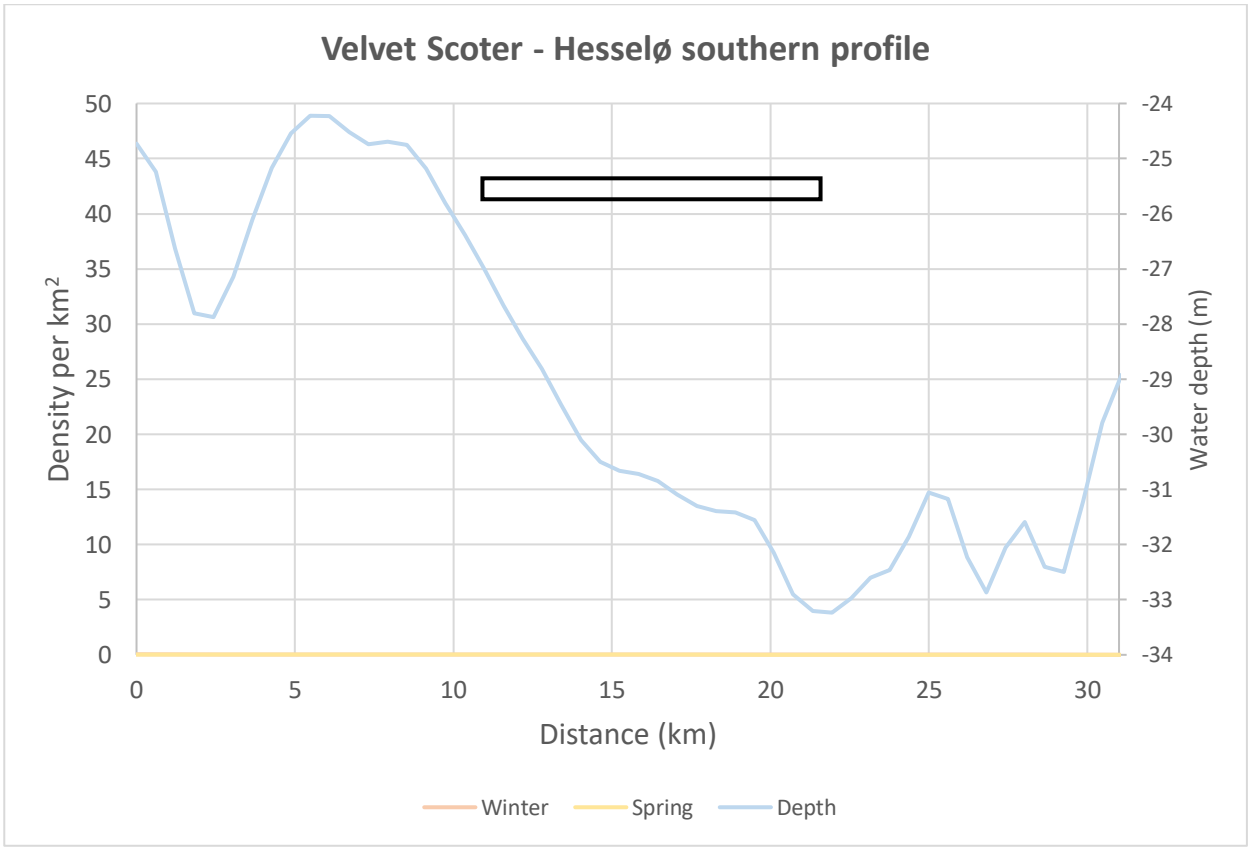

Figure 39 Predicted gradients in the mean monthly density (n/km^2) of Velvet Scoter *Melanitta fusca* along two profile lines crossing the Hesselø development area.

Table 13 Statistics on the predicted abundance of Velvet Scoter *Melanitta fusca* in the Hesselø development area in comparison to the rest of the southern Kattegat.

Area	Winter	Spring
Total number of grid cells	5695	5695
High habitat suitability	340	341
% High habitat suitability	6.0	6.0
Hesselø area (km²)	262	262
Kattegat area (km²)	30609	30609
Hesselø % area	0.9	0.9
Hesselø area High habitat suitability (km²)	0	0
Hesselø area % High habitat suitability	0	0
Hesselø area % High habitat suitability of total Kattegat area	0	0
Mean density Kattegat	1.11	0.30
Total number Kattegat	34031	9113
Mean density Hesselø area	0.01	0.002
Total number Hesselø area	2	1

3.1.2.5 Black-legged Kittiwake

The results of the distribution models for the Black-legged Kittiwake are shown in Appendix C.2.5**Error! Reference source not found.**. This species is occurring over a wide spectrum of surface salinity and water depth, but mainly in areas of intermediate current speed. As seen in the positive part of the model the kittiwake concentrates in areas with a depth between 30 m and 50 m.

The validation of the model's predictive power is illustrated in Figure 40, which shows that the predicted numbers of kittiwakes along the ship-based transect lines in the southern Kattegat are comparable to, yet slightly lower than the observed numbers.

The predicted mean monthly densities in Figure 41 and the areas of high habitat suitability in Figure 42 show zones of high densities (10-30 birds/km^2) and high habitat quality over the intermediate depths and slopes of the offshore banks in the eastern part of Kattegat. The densities are highest during winter, when the high-density zone extends into the Hesselø wind farm site.

During winter, the high-density zone covers the eastern part of the Hesselø site. The N-S profile of modelled densities of Black-legged Kittiwake across the site indicates decreasing densities from north to south during both autumn and winter seasons (Figure 43), and Table 14 documents that 72.1% of the site has high habitat suitability during winter.

The validation results (Appendix C) indicate that the presence-absence part of the model describes the input densities well with an AUC value of 0.72, while the predicted densities due to the high resolution only describes a small proportion of the variation in observed densities. The validation of the ability of the model to predict densities independently from the input data indicates that the model predictions provide a reliable generalisation of the densities over the modelled region with a Sperman's correlation coefficient of 0.14.

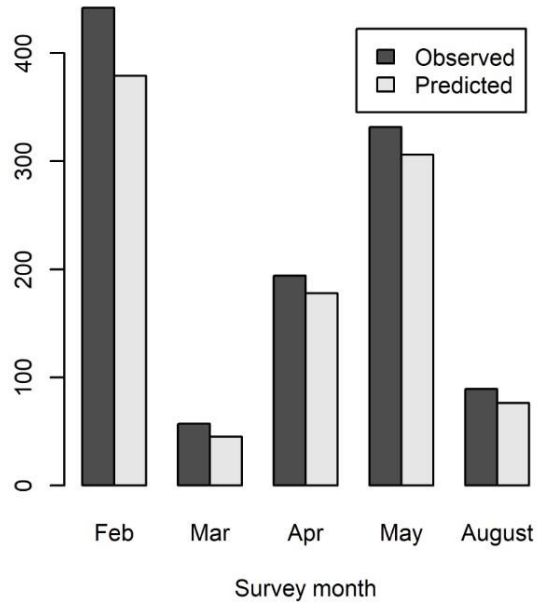

Figure 40 Comparison of predicted versus observed numbers of Black-legged Kittiwake *Rissa tridactyla* along the ship-based transect lines in the southern Kattegat.

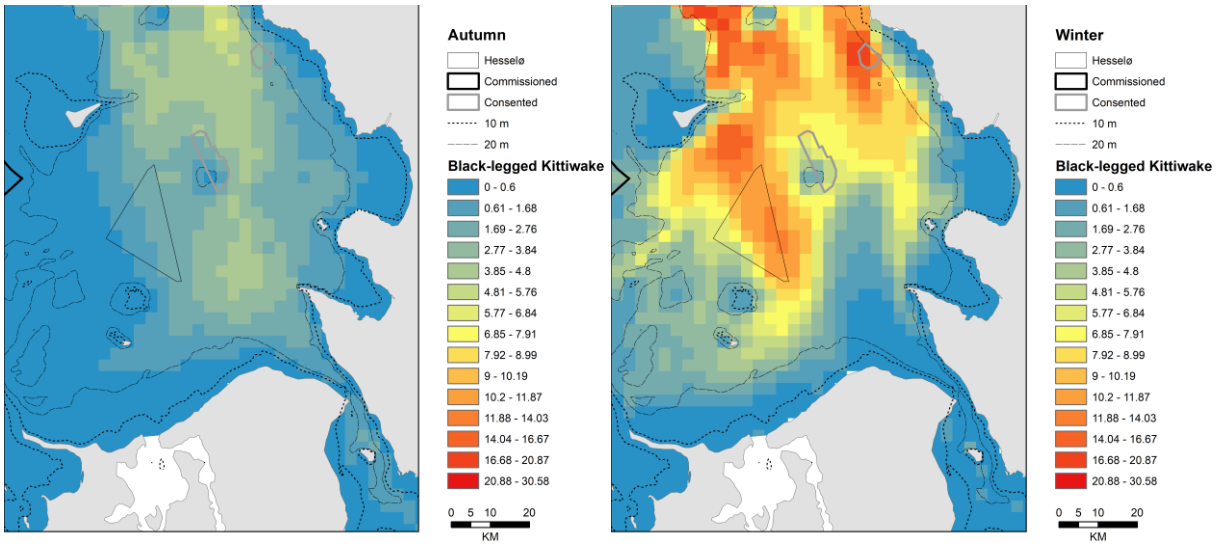

Figure 41 Predicted mean monthly density (n/km^2) of Black-legged Kittiwake *Rissa tridactyla* in the southern Kattegat.

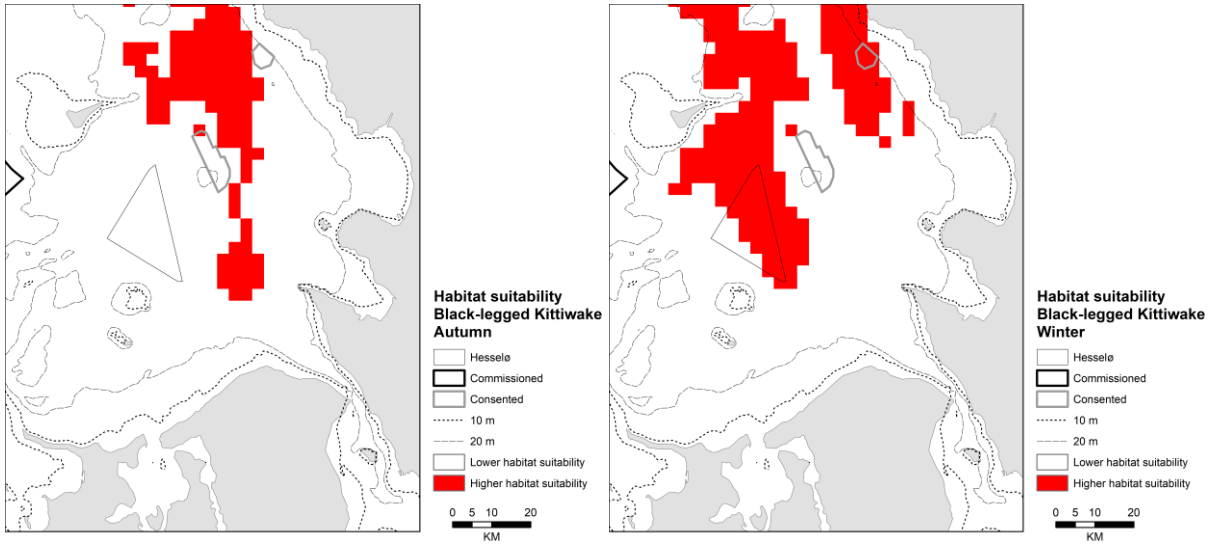

Figure 42 Areas of high habitat suitability to Black-legged Kittiwake *Rissa tridactyla* predicted during the main months of occurrence in the southern Kattegat.

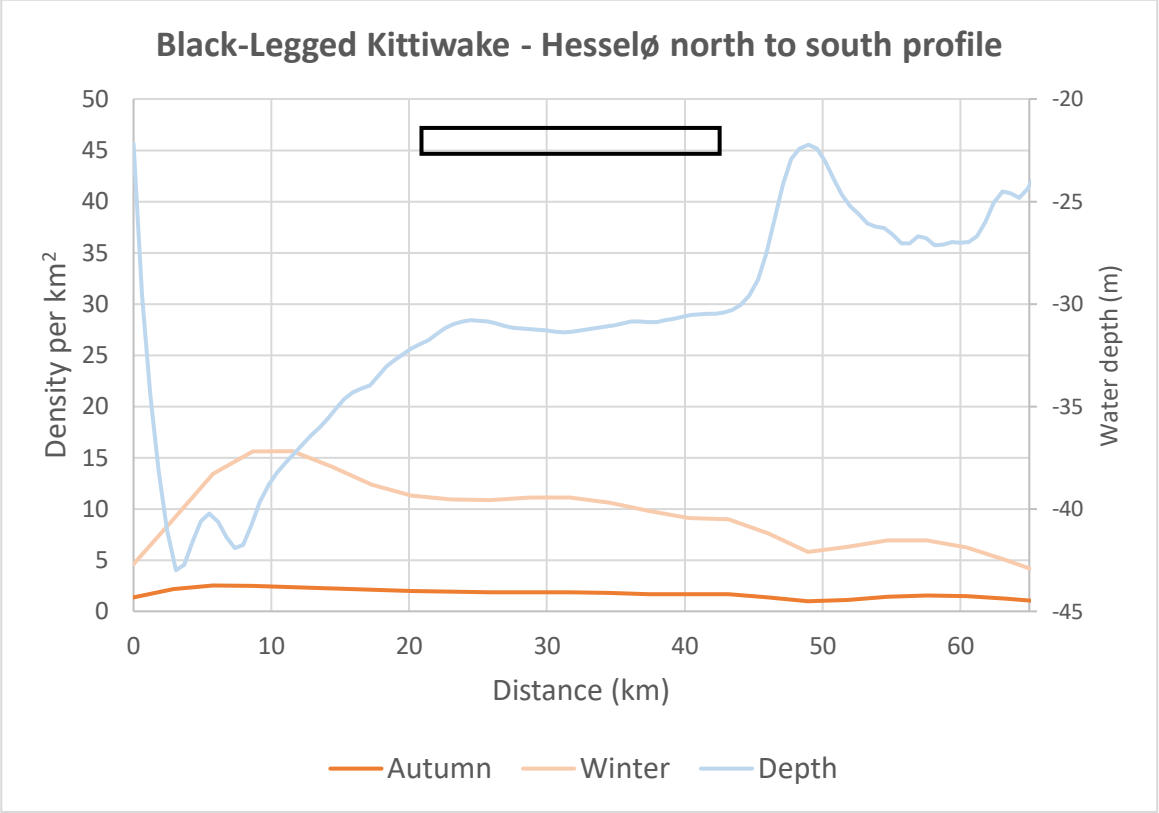

Figure 43 Predicted gradients in the mean monthly density (n/km^2) of Black-legged Kittiwake *Rissa tridactyla* along one profile line crossing the Hesselø development area.

Table 14 Statistics on the predicted abundance of Black-legged Kittiwake *Rissa tridactyla* in the Hesselø development area in comparison to the rest of the southern Kattegat.

Area	Autumn	Winter
Total number of grid cells	5695	5695
High habitat suitability	340	339
% High habitat suitability	6.0	6.0
Hesselø area (km^2)	262	262
Kattegat area (km^2)	30609	30609
Hesselø % area	0.9	0.9
Hesselø area High habitat suitability (km^2)	0	189
Hesselø area % High habitat suitability	0	72.1
Hesselø area % High habitat suitability of total Kattegat area	0	0.62
Mean density Kattegat	1.06	2.95
Total number Kattegat	32416	90271
Mean density Hesselø area	1.74	9.93
Total number Hesselø area	457	2603

3.1.2.6 Razorbill

The distribution model for the Razorbill was based entirely on topographic variables as well XY coordinates as none of the hydrodynamic seemed to have a strong influence on the distribution of the species. The results are shown in Appendix C.2.6**Error! Reference source not found.**. To some extent t he distribution of the Razorbill overlaps the distribution of the Black-legged Kittiwake with large concentrations over the slope areas with a water depth between 20 m and 50 m.

The validation of the model's predictive power is illustrated in Figure 44, which shows that the predicted numbers of razorbills along the ship-based transect lines in the southern Kattegat are comparable to, yet slightly lower than the observed numbers.

The predicted mean monthly densities in Figure 45 and the areas of high habitat suitability in Figure 46 show zones of high densities (25-50 birds/km^2) and high habitat quality over the intermediate depths and slopes of the offshore banks in the eastern part of Kattegat. Compared to the Black-legged Kittiwake the high-density zone does not extend as far south and just reaches the northern boundary of the proposed Hesselø wind farm site.

During autum, the high-density zone covers 3.4% of the Hesselø site. The N-S profile of modelled densities of Razorbill across the site strong decreasing trends in densities from north to south during both autumn and winter seasons (Figure 47), and Table 15 documents that 6% of the site has high habitat suitability during autumn and winter.

The validation results (Appendix C) indicate that the presence-absence part of the model describes the input densities reasonably well with an AUC value of 0.68, while the predicted densities due to the high resolution only describes a small proportion of the variation in observed densities. The validation of the ability of the model to predict densities independently from the input data indicates that the model predictions provide a reliable generalisation of the densities over the modelled region with a Sperman's correlation coefficient of 0.11.

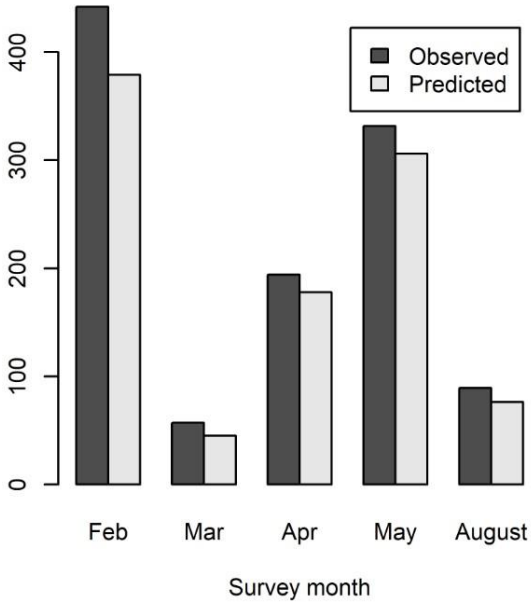

Figure 44 Comparison of predicted versus observed numbers of Razorbill *Alca torda* along the ship-based transect lines in the southern Kattegat.

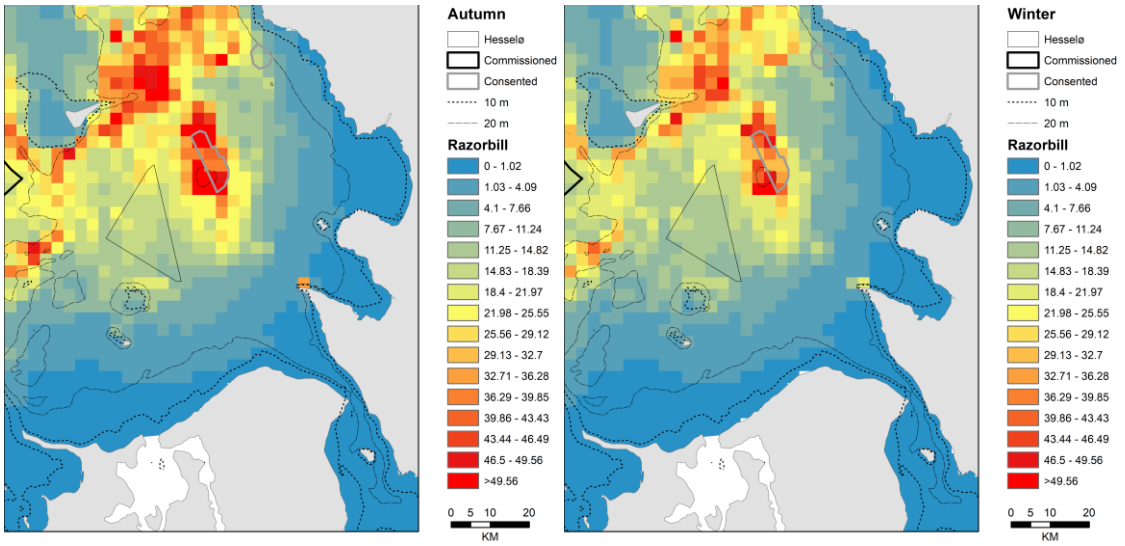

Figure 45 Predicted mean monthly density (n/km^2) of Razorbill *Alca torda* in the southern Kattegat.

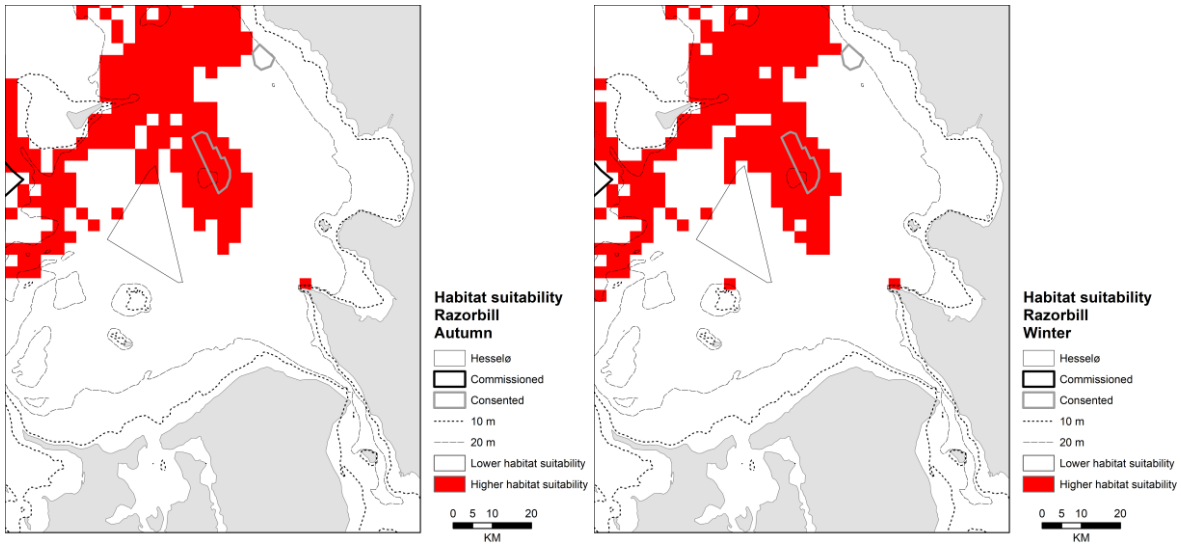

Figure 46 Areas of high habitat suitability to Razorbill *Alca torda* predicted during the main months of occurrence in the southern Kattegat.

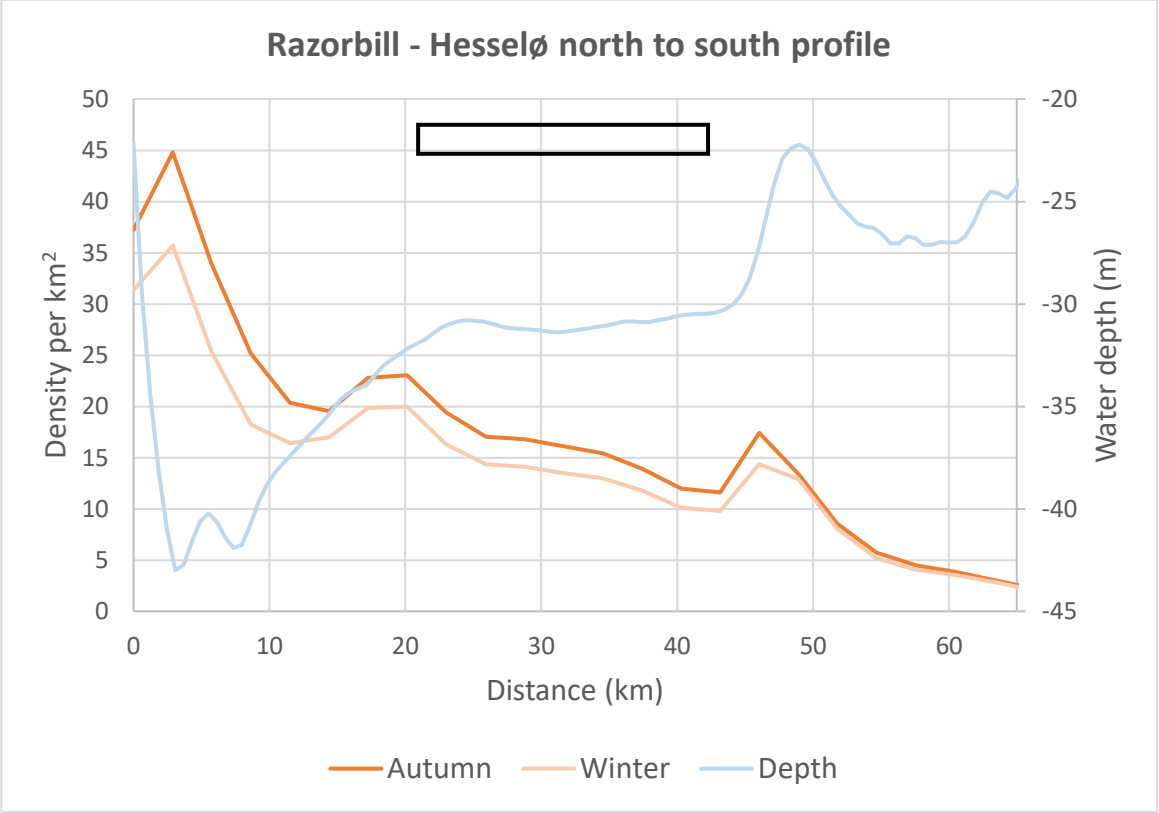

Figure 47 Predicted gradients in the mean monthly density (n/km^2) of Razorbill *Alca torda* along one profile line crossing the Hesselø development area.

Table 15 Statistics on the predicted abundance of Razorbill *Alca torda* in the Hesselø development area in comparison to the rest of the southern Kattegat.

Area	Autumn	Winter
Total number of grid cells	5695	5695
High habitat suitability	346	338
% High habitat suitability	6.1	5.9
Hesselø area (km^2)	262	262
Kattegat area (km^2)	30609	30609
Hesselø % area	0.9	0.9
Hesselø area High habitat suitability (km^2)	9	0
Hesselø area % High habitat suitability	3.4	0
Hesselø area % High habitat suitability of total Kattegat area	0.03	0
Mean density Kattegat	7.15	5.98
Total number Kattegat	218755	183018
Mean density Hesselø area	15.48	13.06
Total number Hesselø area	4056	3420

3.2 Thor, Ringkøbing and Jammerbugt areas

3.2.1 Red-throated/Black-throated Diver

As seen from the distribution model results in chapter 4.1.1 the Red-throated/Black-throated Divers concentrate in the interface between the Jutland Current and North Sea water mass. Although densities change between months, this pattern is persistent, and is also apparent in the observed densities collected during the various aerial surveys in the region after 2000 (Figure 48). The distribution pattern is mainly driven by the difference in salinity, yet productivity and water depth obviously also play a role as diver densities drop to low levels in areas with a water depth below 25 m.

The affinity to the interface or the salinity front in the modelled distribution of the two species in the Danish part of the North Sea is an extension of similar trends in the German Bight with the highest densities in the frontal zone along the 20 m curve off Sylt and at Amrum Bank (Skov & Prins 2001). Divers also displayed a relationship with areas of lower current speed which are consistent with the dominant conditions found in the northern part of the German Bight.

The interface between the Jutland Current and the North Sea water mass overlaps with parts of all three development areas along the Jutland coast, which gives rise to relatively high densities and high habitat suitability in the eastern 1/3 of Thor, in approximately 40% of the Ringkøbing area and in the central part of Jammerbugt wind farm area. While the extent of high habitat suitability varies between months in Thor and Jammerbugt areas, the extent is more stable in the Ringkøbing area. Despite the relatively high degree of spatial overlap between high habitat quality and the planned windfarm sites higher densities (> 0.75 birds/km^2) were only predicted during the month of April before the onset of spring migration. During the other months there is no evidence of larger areas of higher densities of diver overlapping the wind farm sites.

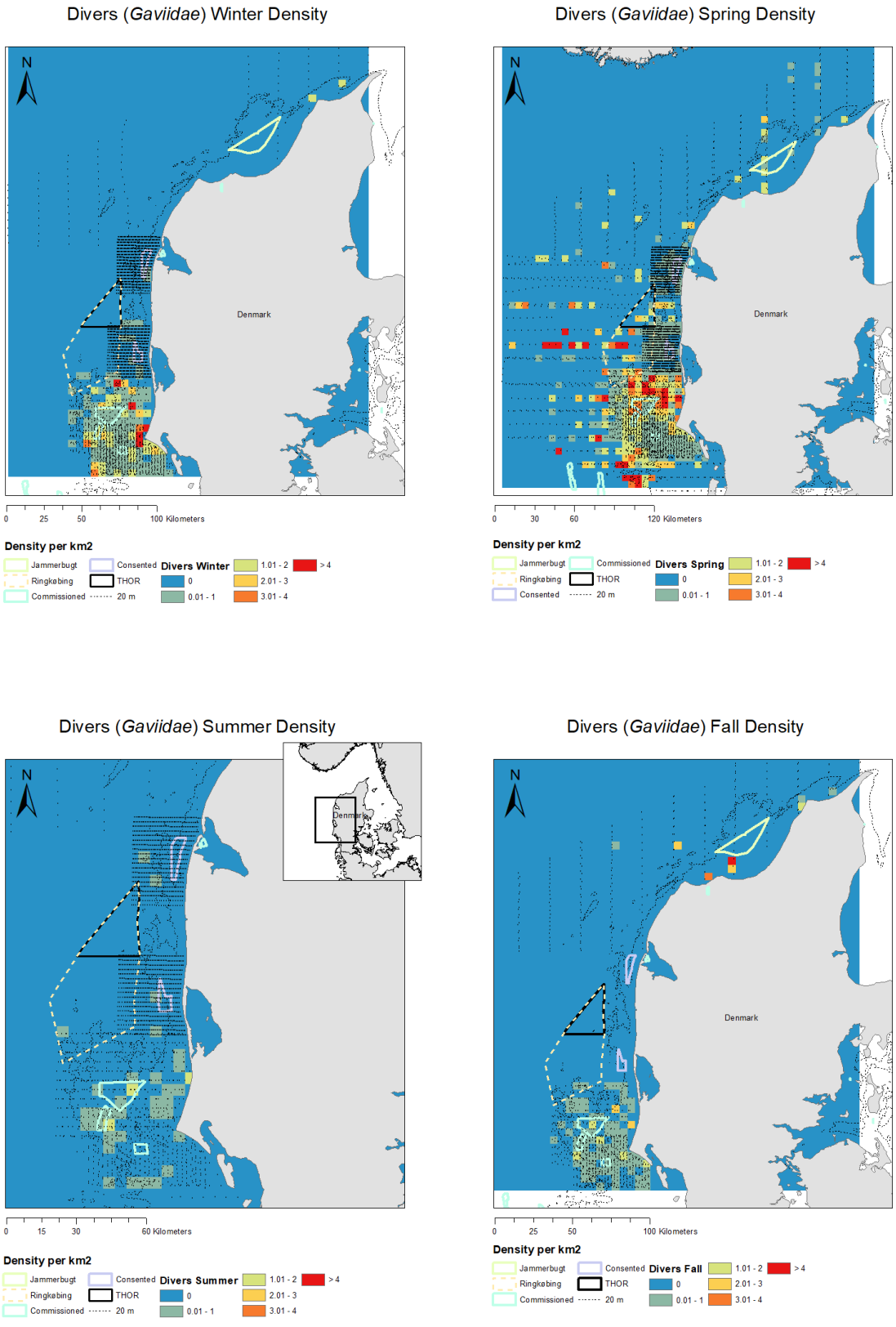

Figure 48 Observed densities of Red-throated/Black-throated Diver *Gavia stellate/arctica* split by season

3.2.2 Northern Gannet

As seen from the maps of observed densities during the aerial surveys in the North Sea (Figure 49) the distribution of the Northern Gannet is strongly related to the deeper areas with higher surface salinity. In the Danish part of the North Sea higher densities are typically observed around the western edge of Horns Rev and along the southern slopes of the Norwegian Trench during the dispersal from the colonies in the autumn season, while densities elsewhere are quite low. COWI's screening included the Northern Gannet as a potentially important species in relation to the Jammerbugt development area as it is listed in the IBA Skagerrak-Southwest Norwegian Trench by Skov et al. (1995, Hjorth 2018). However, as seen from Figure 49, higher densities are only infrequently observed in areas shallower than 20 m in the southern part of the Skagerrak. Accordingly, densities of this species are expected to be low-medium during autumn and low during the remainder of the year.

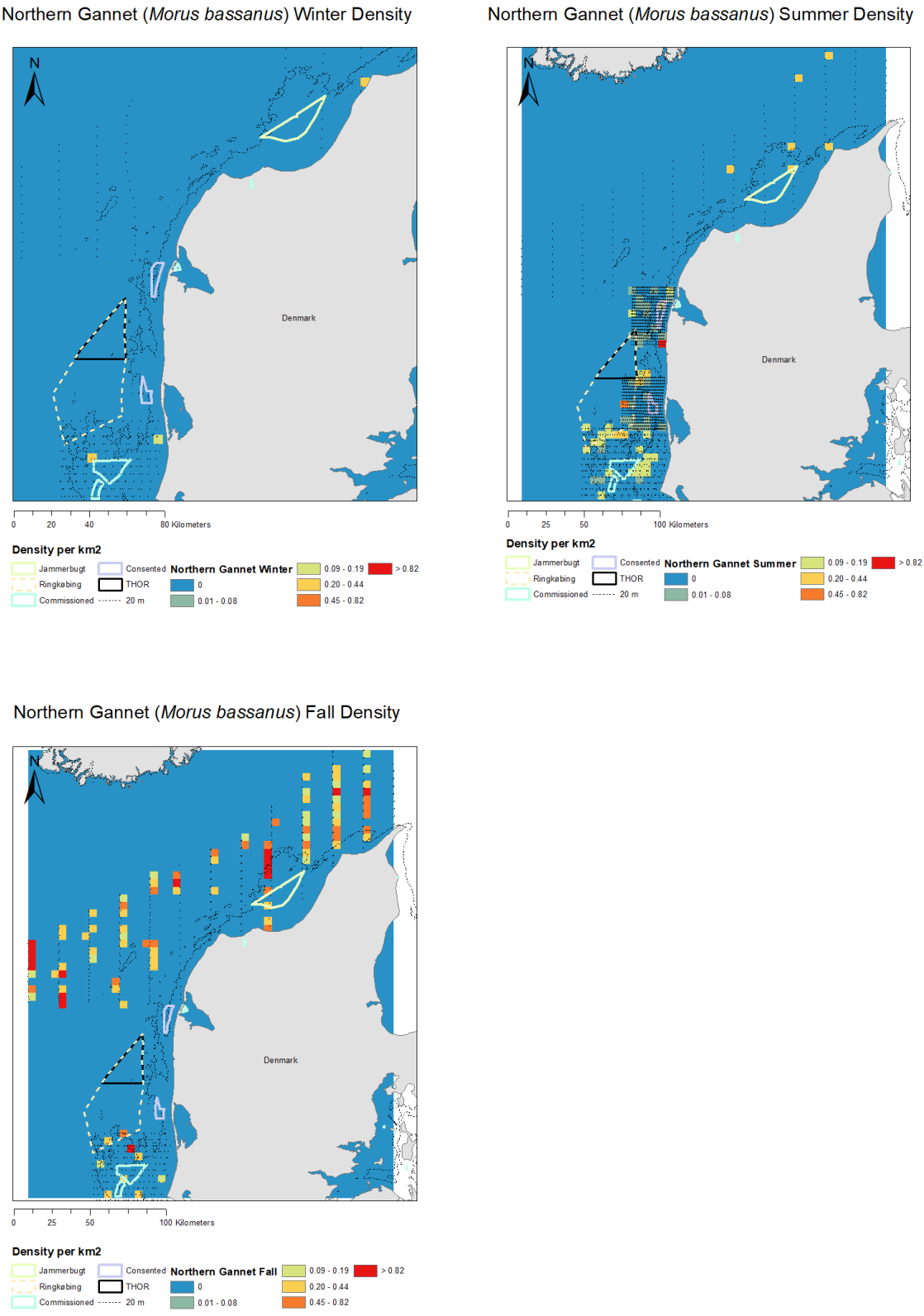

Figure 49 Observed densities of Northern Gannet *Morus bassanus* split by season.

3.2.3 Common Scoter

As seen from the distribution model results in chapter 4.1.1 the Common Scoters display a highly persistent distribution pattern along the west coast of Jutland with peak densities confined to areas of 8m to 15m water depth on the shallows off Blåvandshuk, along the coast of Jutland and at the western and north-western parts of Horns Rev. The densities peak during mid-winter (January). This pattern is also reflected in the aerial observations after 2000 (Figure 50), although few observations have been made in the Jammerbugt area. This, however, is most likely related to the relatively low survey effort in the area during the peak season (winter).

The predicted higher densities in the coastal zone do not overlap with the three wind farm areas. The predicted high densities in the western and north-western parts of Horns Rev overlap with the southwestern part of the Ringkøbing area with densities exceeding 50 birds/km^2. The area of high habitat quality extends over the southern part of the Ringkøbing and involve medium densities of 7-13 birds/km^2. The predicted good habitat conditions found in the southern half of the Jammerbugt area are related to medium densities (5-10 birds/km^2) of scoters.

The concentration of Common Scoter in the southwestern part of the Ringkøbing area which is related to the western and north-western parts of Horns Rev most likely form part of the group of scoters which has increased in the region and relying on the abundance of American razorclams *Ensis americanus* (Leonhard & Skov 2012).

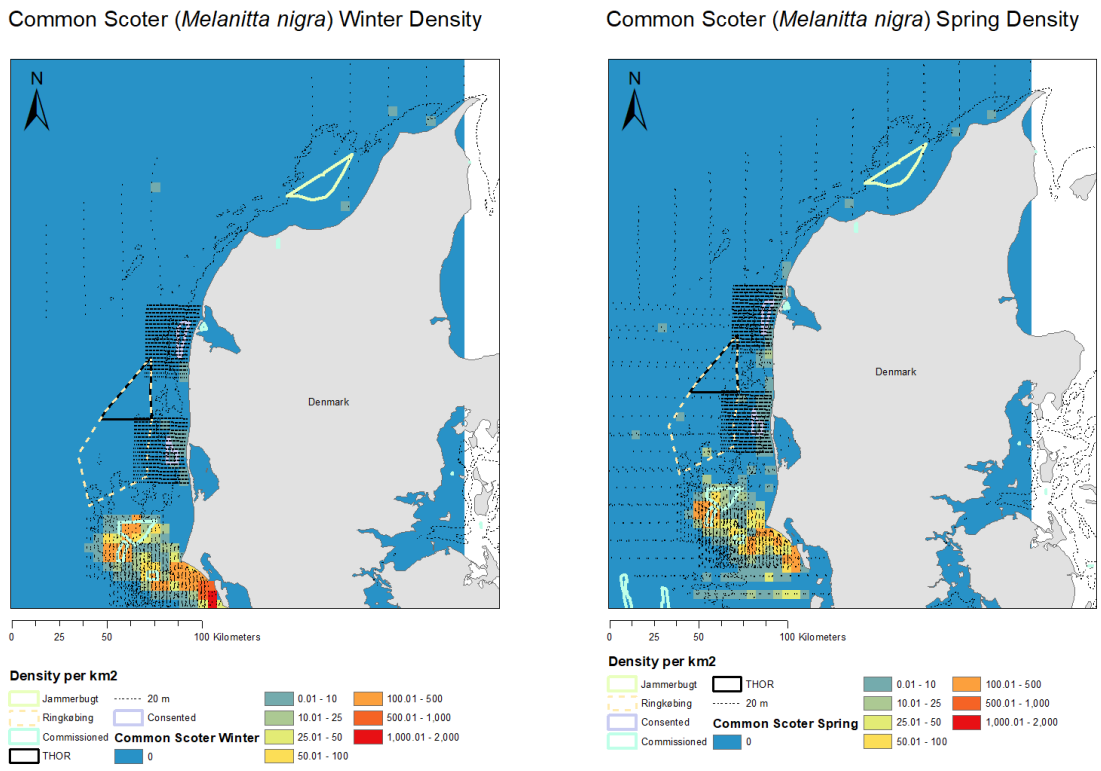

Figure 50 Observed densities of Common Scoter *Melanitta nigra* split by season.

3.2.4 Great Skua

Great Skuas are almost exclusively seen in the Danish part of the North Sea during the post-fledging dispersal in the autumn season. Although single individuals may be observed close to the coast during adverse weather conditions the majority of Great Skuas occur in the region of the Norwegian Trench in areas with a water depth exceeding 30 m. This is clearly seen from the maps of observed densities during the aerial surveys in the North Sea. COWI's screening included the Northern Gannet as a potentially important species in relation to the Jammerbugt development area as it is listed in the IBA Skagerrak-Southwest Norwegian Trench by Skov et al. (1995, Hjorth 2018). However, higher densities are only infrequently observed in areas shallower than 20 m in the southern part of the Skagerrak. Accordingly, densities of this species are expected to be low during autumn and very low during the remainder of the year.

3.2.5 Little Gull

On the basis of its relatively small population size in Western Palearctic the Little Gull is listed in Annex I of the EC Bird Directive. The species is also listed in the IBA German Bight by Skov et al. (1995, Hjorth 2018) due to concentrations occurring in shallower areas of lower salinity like Horns Rev. These concentrations are linked to the movement of almost the entire European population from its primary breeding areas in Belarus are to the wintering areas along the Atlantic coast of France and Spain (den Ouden & Stougie 1990). As this movement does not include areas north of Blåvandshuk to any great extent (Figure 51) higher densities are only expected to overlap with the southern part of the Ringkøbing development area.

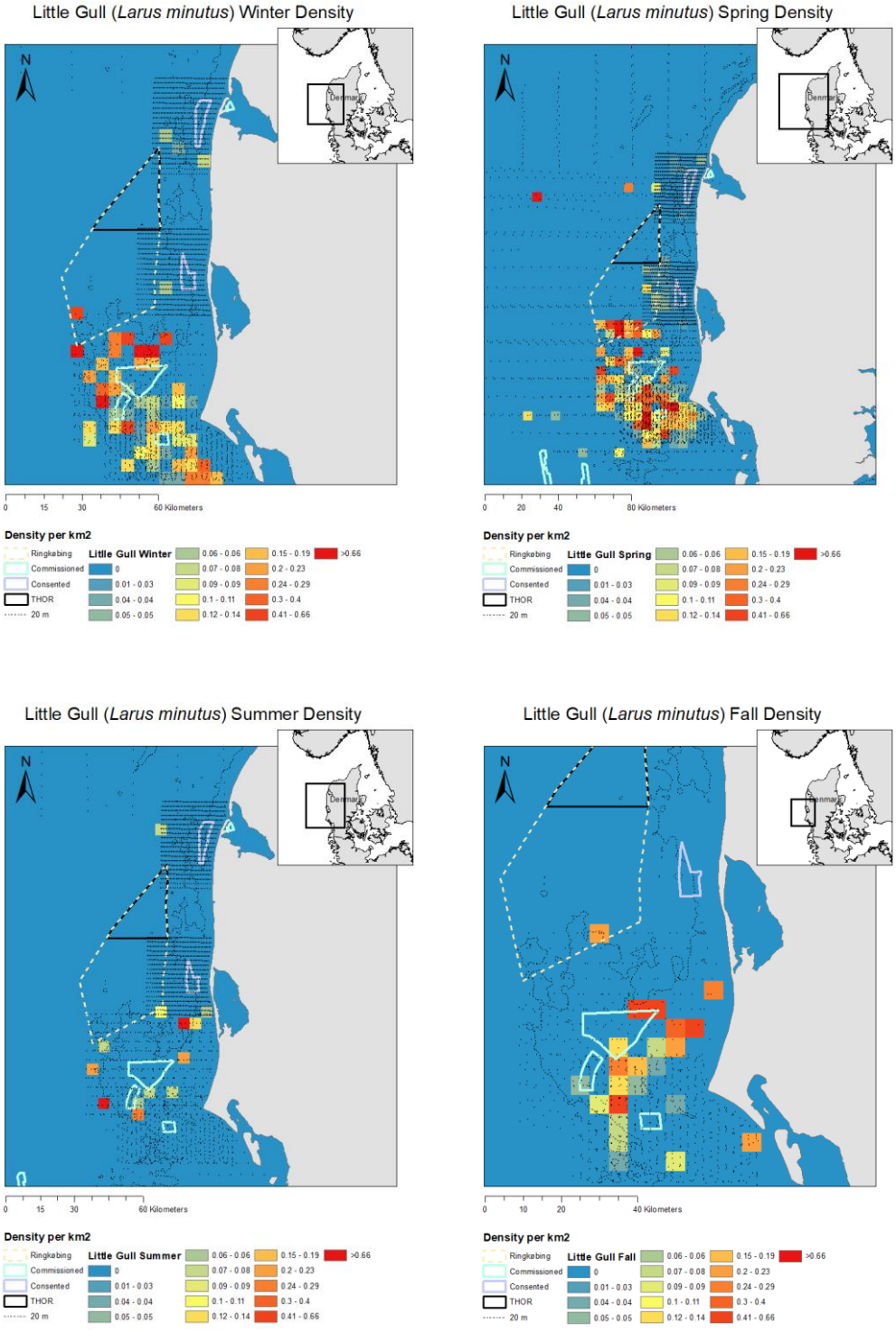

Figure 51 Observed densities of Little Gull *Hydrocoloeus minutus* split by season.

3.2.6 Common Gull

The Common Gull is listed in the IBA German Bight by Skov et al. (1995, Hjorth 2018) due to its abundance in the region during winter. In fact, the species is widespread in the shallower parts of the Jutland coast region with lower salinity and medium densities (1-10 birds/km^2) should be expected in the southern part of the Ringkøbing area.

3.2.7 Herring Gull

The Herring Gull is listed in the IBA Skagerrak-Southwest Norwegian Trench by Skov et al. (1995, Hjorth 2018) due to its abundance in the region during winter. As the high densities are found throughout shelf waters there is a potential for high densities (> 5 birds/km^2) occurring in the Jammerbugt area during this season.

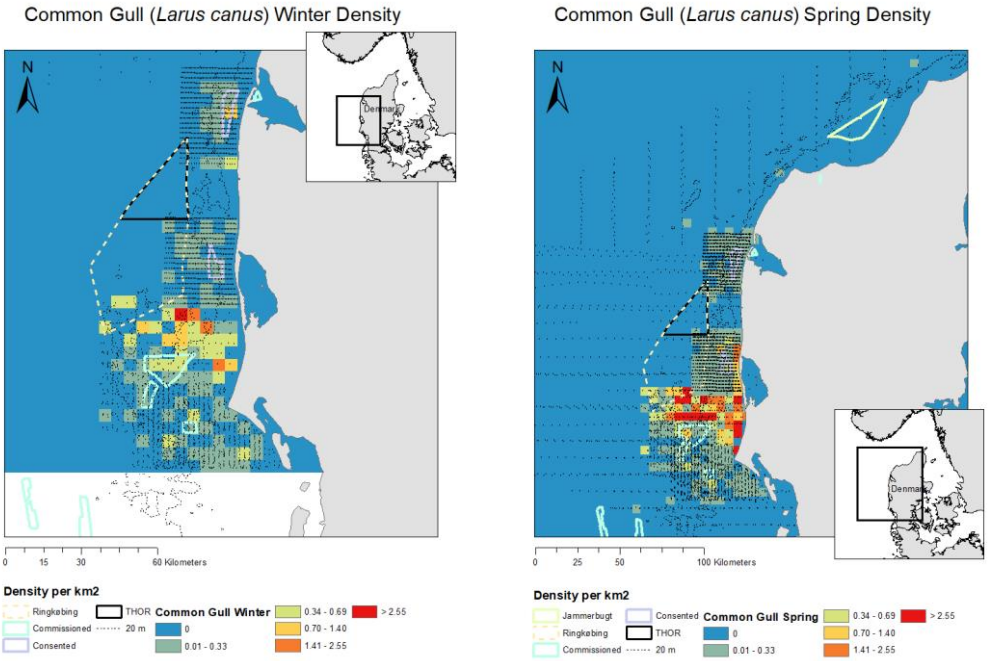

Figure 52 Observed densities of Common Gull *Larus canus* split by season.

3.2.8 Sandwich Tern

The Sandwich Tern is listed in the IBA German Bight by Skov et al. (1995, Hjorth 2018) due to feeding concentrations associated with the main breeding colonies. Due to the lack of large breeding colonies in the coastal areas adjoining the Ringkøbing and Thor area on low-medium densities (< 1/km^2) are typically recorded in these areas.

3.2.9 Common Guillemot

The Common Guillemot is listed in the IBA Skagerrak-Southwest Norwegian Trench by Skov et al. (1995, Hjorth 2018) due to its abundance in the region during late summer (moult), autumn and winter. Like many other pelagic seabird species the Common Guillemot's occurrence in the Skagerrak is related to the deeper areas with high salinity and good water clarity (Figure 53). This is especially the case during the swimming migration in July and August when large numbers of flightless adults with young arrive to the Norwegian Trench from breeding colonies in Scotland (Skov et al. 1992a). Following moult in the eastern Skagerrak the birds disperse to areas of 30-60m water depth in Kattegat and Skagerrak during late autumn and winter (Skov et al. 1992b).

It is therefore not likely that high densities (> 10 birds/km^2) occur regularly in the Jammerbugt wind farm area.

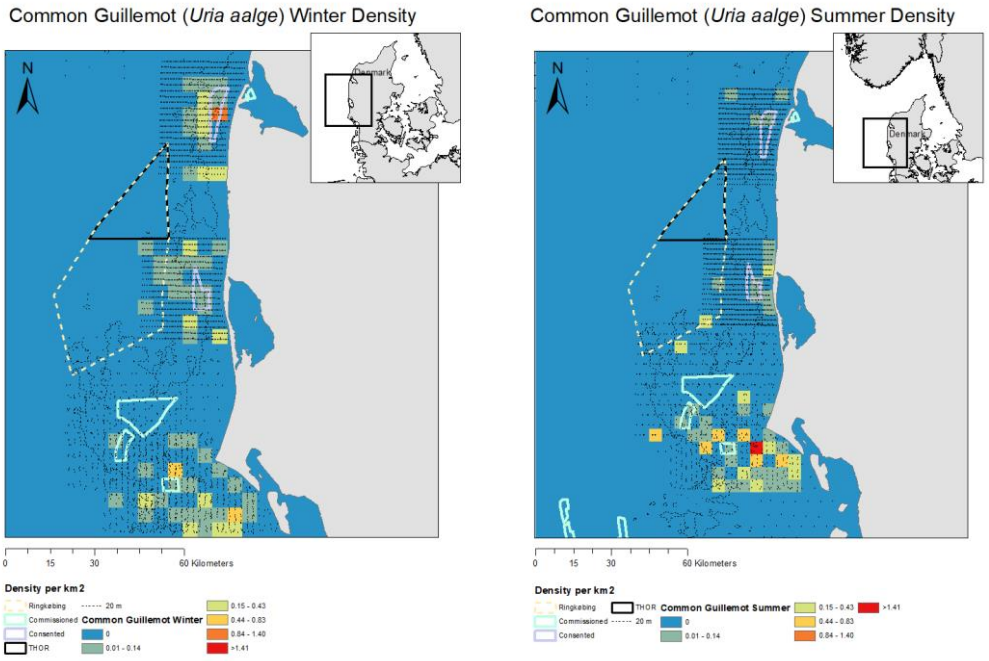

Figure 53 Observed densities of Common Guillemot *Uria aalge* split by season

3.2.10 Razorbill

The Razorbill is listed in the IBA Skagerrak-Southwest Norwegian Trench by Skov et al. (1995, Hjorth 2018) due to its abundance in the region during autumn and winter. Unlike the Common Guillemot which it often is seen co-occurring with the Razorbill does not moult in the Danish part of the North Sea but arrives in late October to the Skagerrak and northern Kattegat. The main wintering areas to this species are located in the central and eastern part of the Kattegat where the largest known winter concentrations of this species have been recorded (Laursen et al. 1989, Skov et al. 1995).

Like many other pelagic seabird species, the Razorbill's occurrence in the Skagerrak is related to the deeper areas with high salinity and good water clarity. It is therefore not likely that high densities (> 10 birds/km^2) occur regularly in the Jammerbugt wind farm area.

3.2.11 Little Auk

The Little Auk is listed in the IBA Skagerrak-Southwest Norwegian Trench by Skov et al. (1995, Hjorth 2018) due to its abundance in the region during winter. The Little Auk is however closely affined to the southern slopes of the Norwegian Trench, and rarely occurs in higher densities in areas shallower than 50m. It is therefore not likely that high densities (> 10 birds/km^2) occur regularly in the Jammerbugt wind farm area.

3.3 Hesselø Area

3.3.1 Red-throated/Black-throated Diver

The Red-throated/Black-throated Diver is mainly observed during the winter and spring seasons. Densities at the Hesselø site are generally low, while medium-high densities are observed in coastal areas shallower than 20 m (Figure 54).

Figure 54 Observed densities of Red-throated/Black-throated Diver *Gavia stellate/arctica* split by season

3.3.2 Red-necked Grebe

The Red-necked Grebe is mainly observed offshore in Kattegat during autumn and winter. Densities at the Hesselø site are low, whereas rather high densities compared to the small total size of the population are observed in the shallow area between Anholt and Jutland (Figure 55).

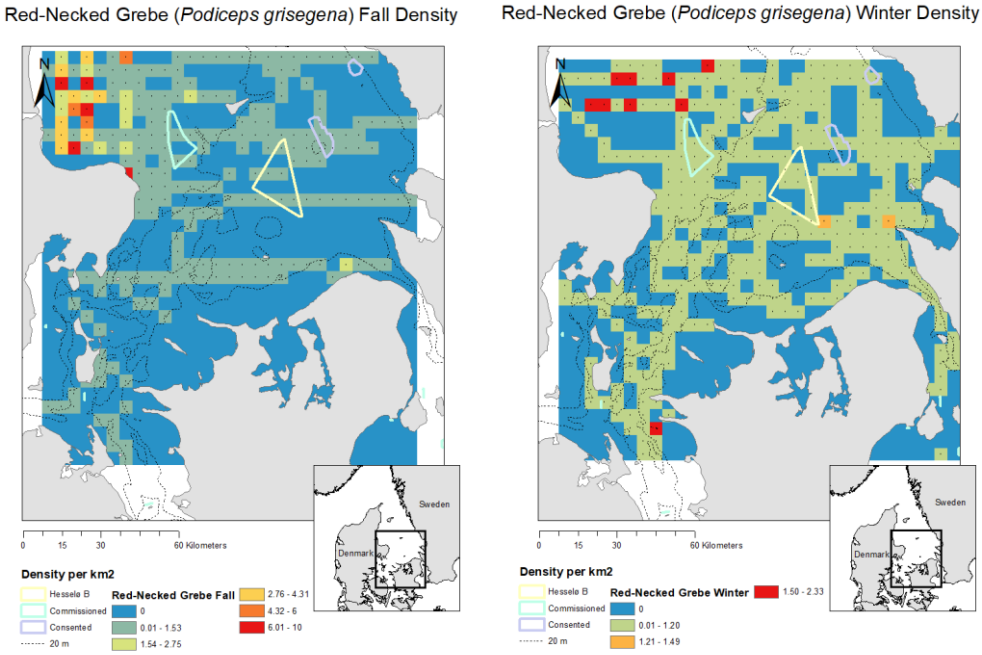

Figure 55 Observed densities of Red-necked Grebe *Podiceps grisegena* split by season.

3.3.3 Mute Swan, Common Goldeneye, Greater Scaup

The Mute Swan, Common Goldeneye and Greater Scaup are all chiefly found in near-shore or very shallow areas with a water depth less than 5 m.

3.3.4 Common Eider, Common Scoter, Velvet Scoter

Although single Common Eiders, Common Scoter and Velvet Scoter may be observed at the Hesselø site, higher densities of these species are only observed in areas shallower than 15 m.

3.3.5 Herring Gull, Great Black-backed Gull

Both species of large gulls are observed commonly over the offshore parts of the southern Kattegat, including in the Hesselø site (Figure 56). The distribution of both species shows a dispersed pattern of patches which reflects their strong association with fishing vessels.

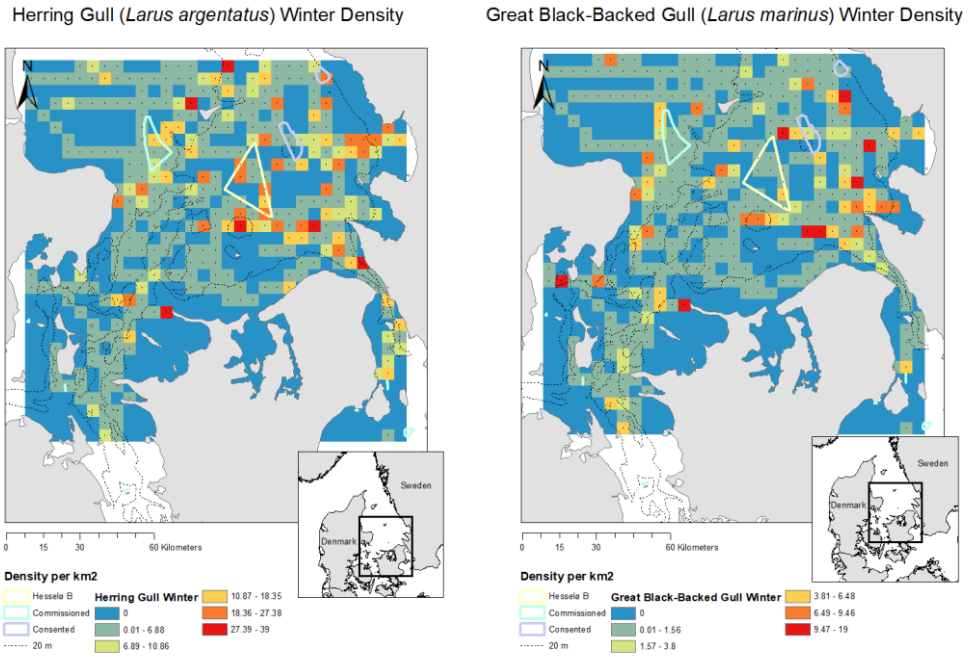

Figure 56 Observed densities of Herring Gull *Larus argentatus* and Great Black-backed Gull *Larus marinus* during winter.

3.3.6 Black-legged Kittiwake

As shown by the distribution models Black-legged Kittiwake is a very common winter guest to the eastern Kattegat, where it is mainly seen in high-density patches around shoals of schooling young herring. Although most kittiwakes in the region are seen around Lille Middelgrund the distribution extends south to the Hesselø site (Figure 57).

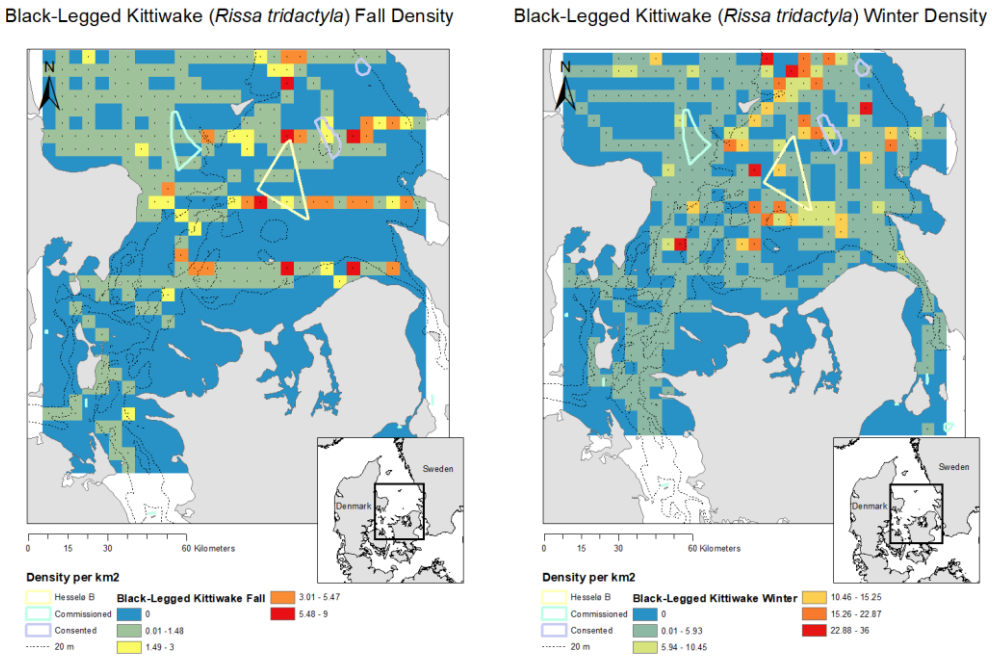

Figure 57 Observed densities of Black-legged Kittiwake *Rissa tridactyla* split by season.

3.3.7 Razorbill

The concentration of Razorbill in the Kattegat is the largest known concentration of the species during winter. The birds arrive Kattegat in late autumn where they are mainly seen between Djursland and Anholt and move in winter to the area of Lille Middelgrund (Figure 58). Low-medium densities are recorded at the Hesselø site.

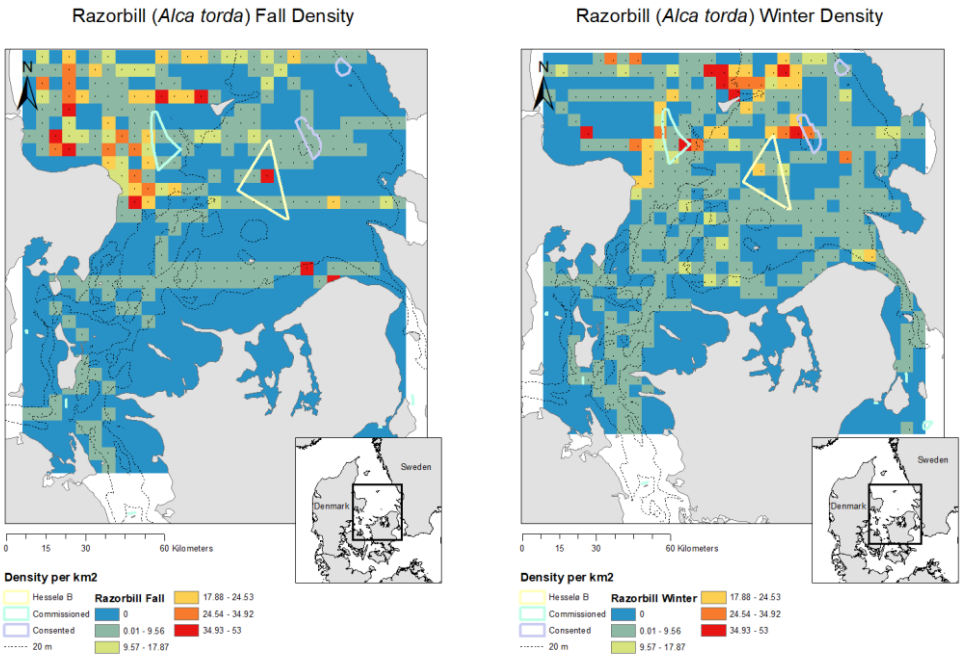

Figure 58 Observed densities of Razorbill *Alca torda* split by season.

3.4 Krieger's Flak Area

3.4.1 Migration intensity of Common Crane

The total Swedish and Norwegian populations (including juveniles) which pass the Arkona Basin is estimated at 84,000 individuals (Wetlands International 2012), and they cross the whole region between Bornholm and Falster over a broad front both during spring and autumn (Figure 59). The population in northern Europe has shown an increasing trend at least over the past 27 years; 0.84% per year from 1988-2012 and 2.43% per year from 2003-2012 (Wetlands International 2012).

3.4.2 Horizontal and vertical distribution of Common Crane

Even though the tracks obtained by satellite GPS telemetry during 2013-2014 indicate that most birds may cross centrally, telemetry data from the Swedish University of Agricultural Sciences from 2011-2012 show otherwise and stress that the birds indeed may cross anywhere between Bornholm and the coast of Zealand, Møn and Falster (Figure 60). During autumn most birds stage on wetlands in Rügen, Germany, while during spring most birds stage 50 km further west in the Darss area. Whether these changes in key staging areas give rise to different mean migration routes across the basin during spring and autumn is unknown. However, judged from a review of the historic locations of large observations of Common Crane along the Swedish south coast (2000-2012) the spatial variation in exit sites is mainly controlled by the wind direction (Skov et al. 2015). The vast majority of directions from Falsterbo recorded during the Kriegers Flak baseline investigations in autumn 2013 were concentrated around S in the direction of Rügen (Figure 61). During spring 2013, the mean direction of migrating Common Crane was 13°.

The patterns of flight altitude displayed by migrating Common Crane are very similar to those observed for raptors crossing between Sweden and Germany, yet a higher proportion of the Common Crane may cross Kriegers Flak at altitudes above 200 m. The general descend in flight altitude from the Swedish coast in autumn is nonetheless very clear (Figure 62). The GPS-tagged birds demonstrate how some Cranes (2 of 11 crossings) during optimal conditions can cross the Kriegers Flak region at heights above 400 m altitude (Figure 63).

The GAMM flight model for the Common Crane indicates that the birds descend in altitude after leaving the coast, and fly higher in clearer weather and decreasing humidity (Figure 64). The predictive accuracy of the GAMM was high, with a good agreement between observed and predicted altitudes and a Spearman's rank correlation of 0.40. During spring, most Common Crane arrive to Denmark and Sweden at altitudes between 150 and 200 m (Figure 64). During spring, the profile seems to depend on wind direction, with birds descending during tail winds and ascending during head winds. Thus, the Common Crane can use thermals drifting offshore to gain altitude at distances of up to 5 km from the coast.

During autumn steep descends are seen in both tail wind and head wind, the descend being slightly steeper in head winds. On average birds seem to cross the Arkona Basin at lower altitude during tail winds than head winds in autumn (Figure 64).

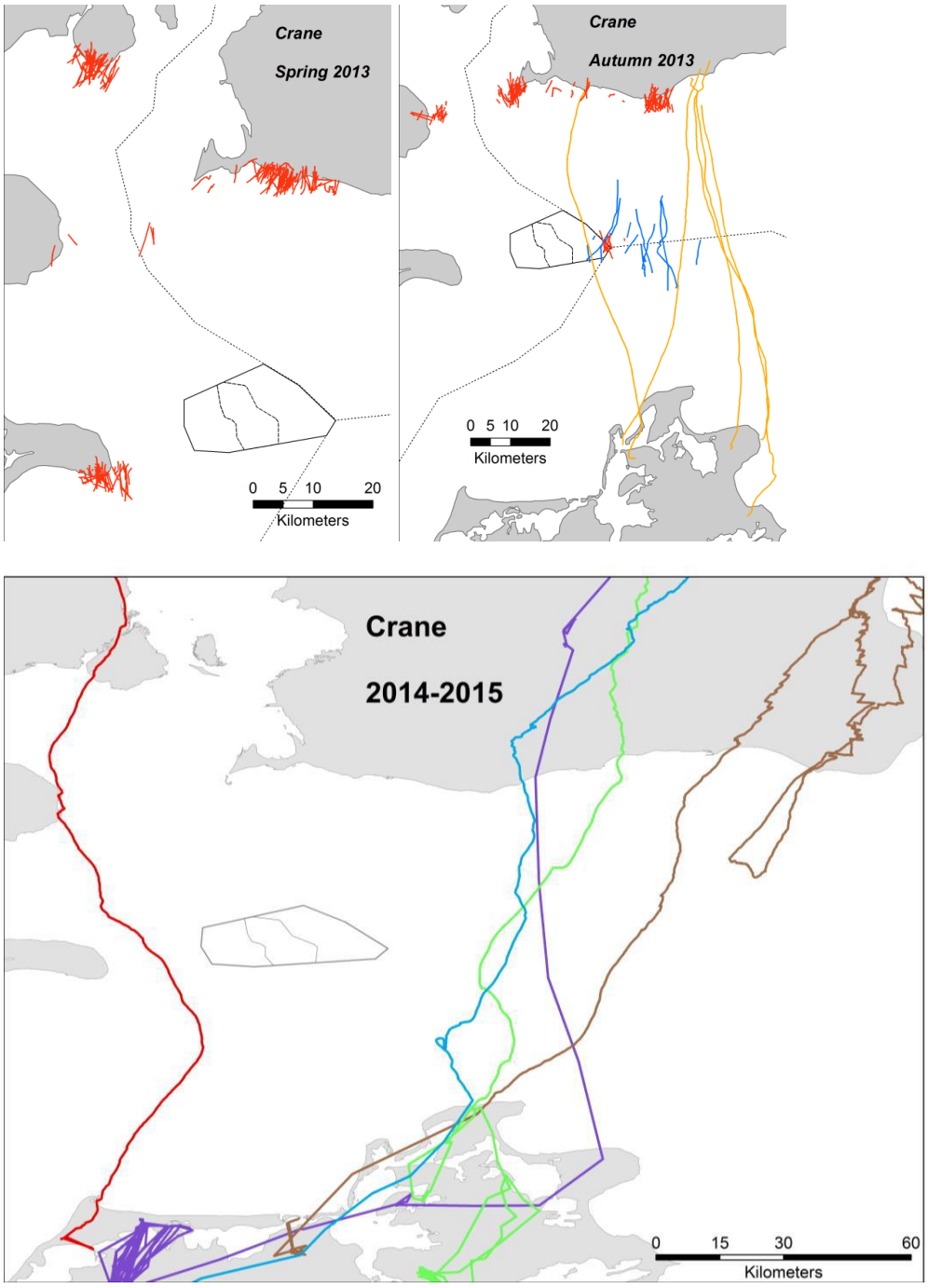

Figure 59 Migration tracks of Common Crane collected in the region during the Krieger's Flak baseline (Skov et al. 2015). Upper panel: spring and autumn 2013 - GPS-telemetry tagged birds are indicated by orange lines, radar-based tracks are marked by blue lines, and rangefinder-based tracks by red lines. Lower panel: GPS-telemetry tagged birds 2014-2015.

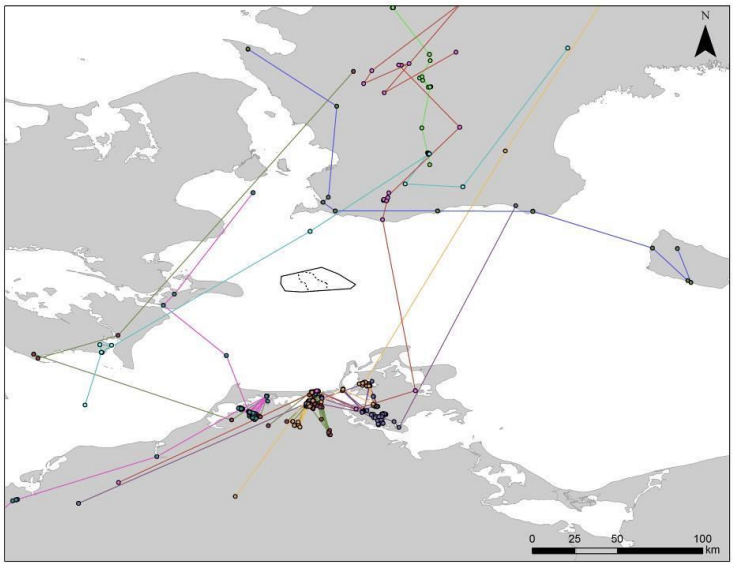

Figure 60 Migration tracks of ten GPS-tagged Common Crane collected in the study region during 2011-2012 (Courtesy Swedish University of Agricultural Sciences). Tracks over the sea are lines combining adjoining GPS positions logged on land, and do not show actual flight paths.

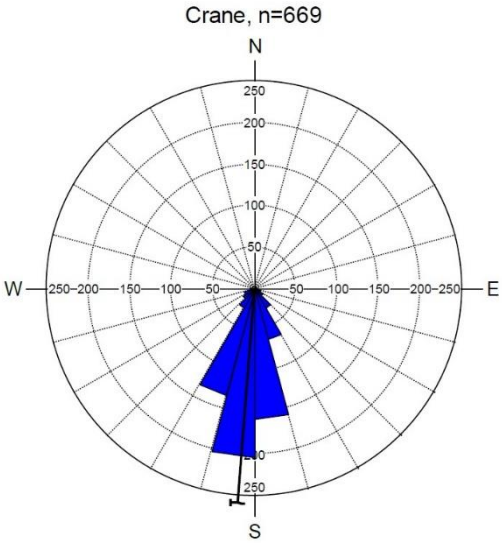

Figure 61 Sampled migration directions of Common Crane at Falsterbo, autumn 2013 (Skov et al. 2015). Numbers on the Y-axes refer to sample size (number of recordings by laser rangefinder). Each wedge represents a sector of 15°. The mean direction is indicated by the black line running from the centre of the graph to the outer edge. The arcs extending to either side represent the 95% confidence limits of the mean direction.

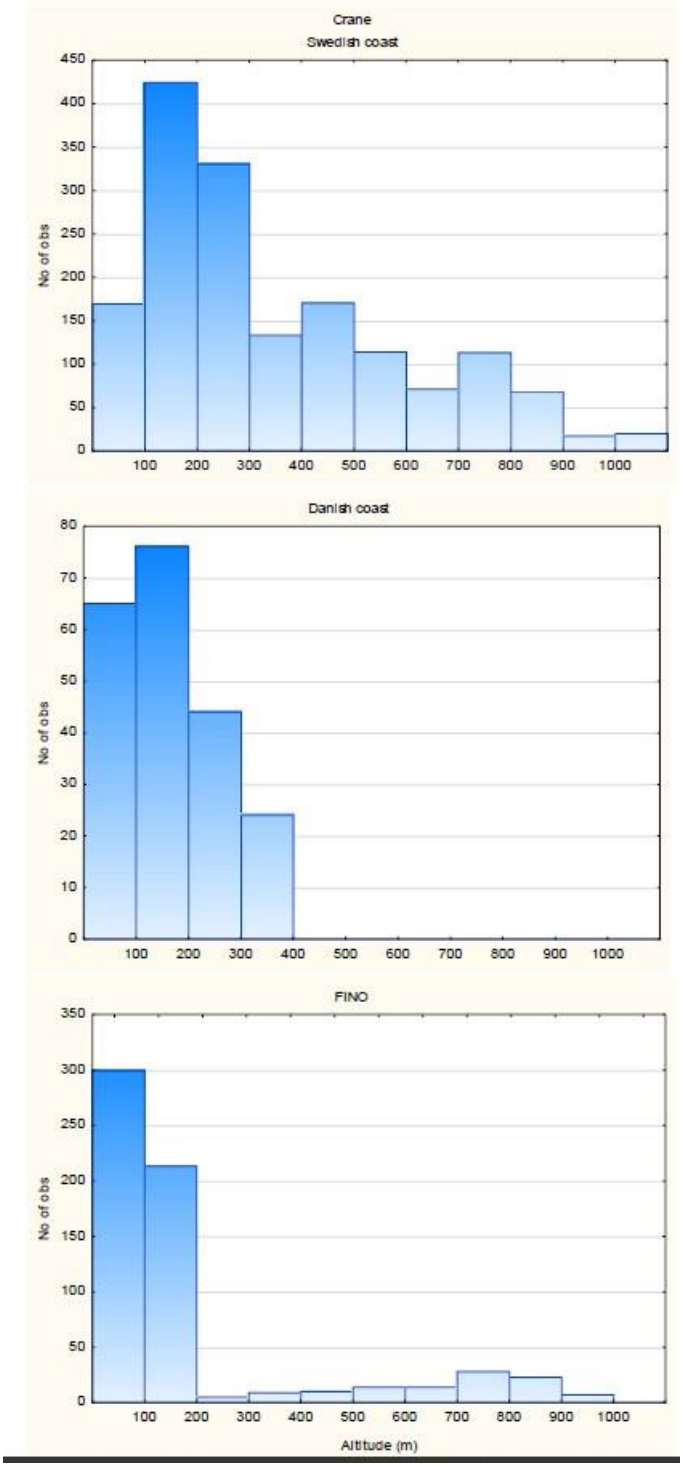

Figure 62 Frequency distribution of altitude measurements of Common Crane by laser rangefinder at the Swedish south coast, at the Danish coast and at FINO 2 during the Kriegers Flak baseline, autumn 2013 (Skov et al. 2015).

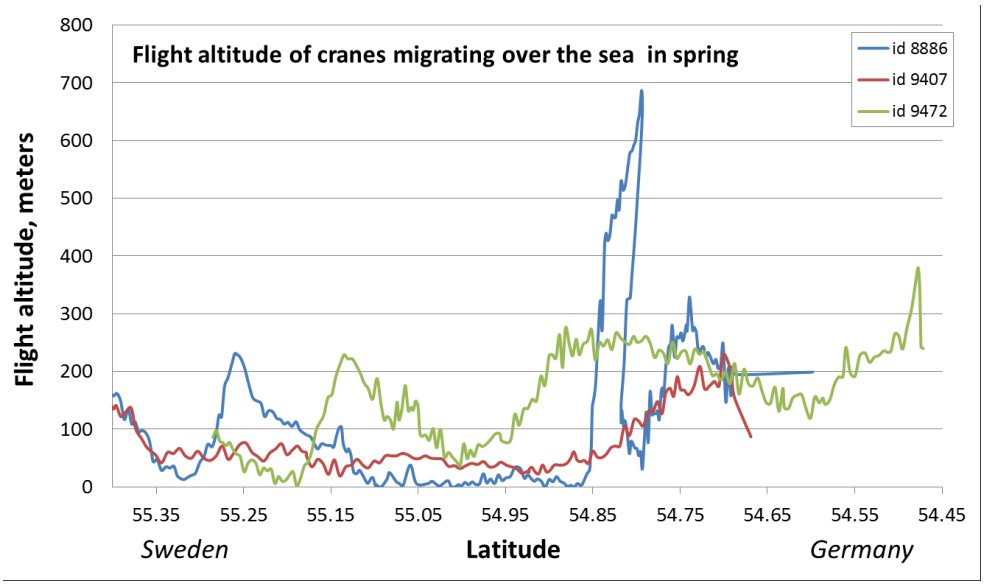

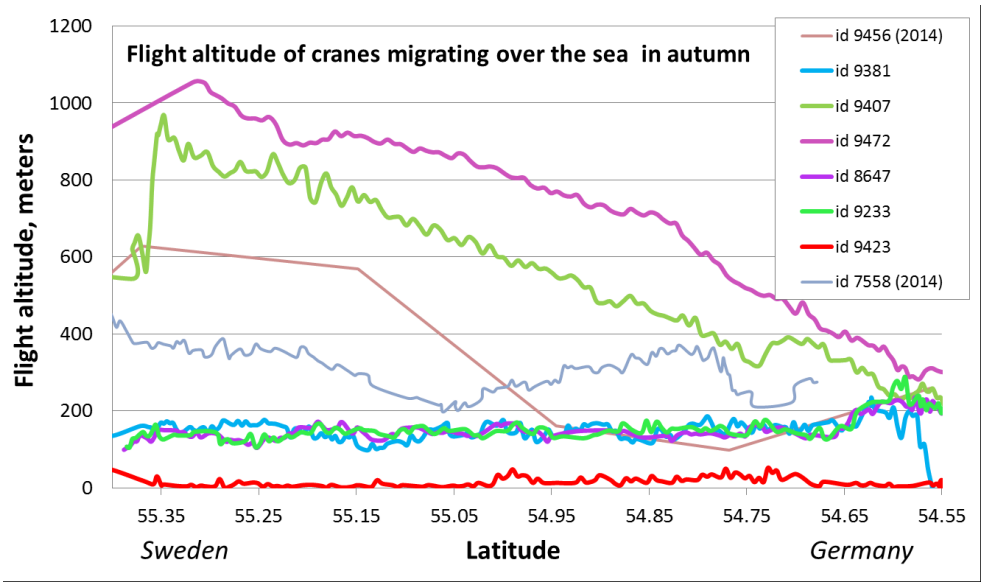

Figure 63 Height measurements of 11 GPS-tagged Common Crane 2013-2015. Krieger's Flak is located at latitude 55.00° N.

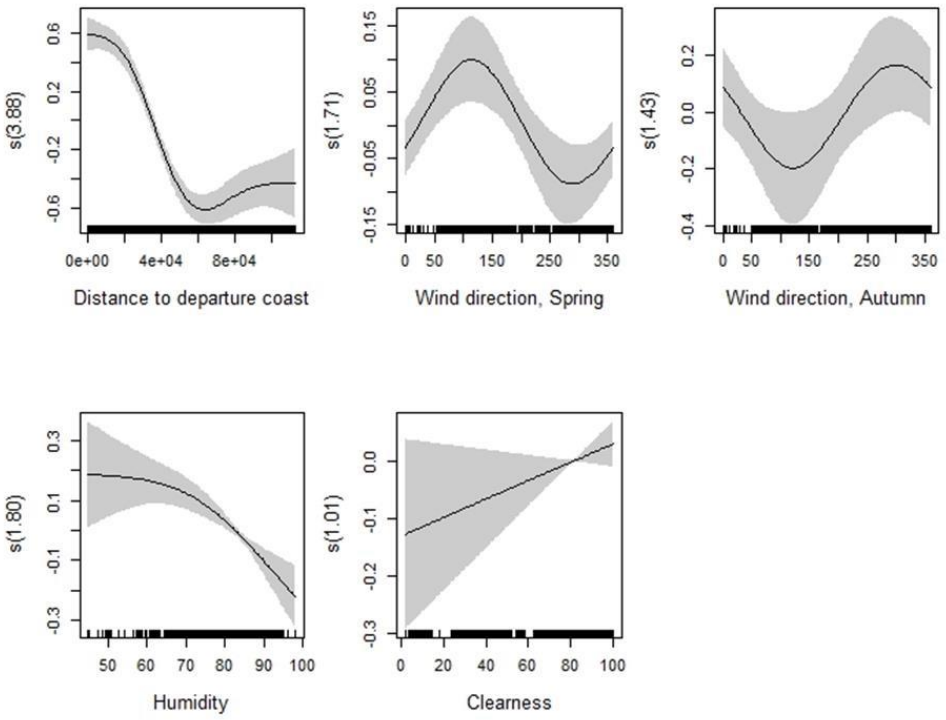

Figure 64 GAMM response curves for the Common Crane based on data from both spring and autumn collected during the Krieger's Flak baseline (Skov et al. 2015). The values of the environmental predictors are shown on the X-axis and the response on the Y-axis is on the scale of the linear predictor. The degree of smoothing is indicated in the title of the Y-axis. The shaded areas and the dotted lines show the 95% Bayesian confidence intervals.

3.4.3 Cumulative collision risk of Common Crane

We further used the GAMM flight model for Common Crane for predicting the average seasonal flight altitude at Krieger's Flak during average, poor and good visibility and during tail, head and cross winds. According to the predictions the birds fly on average at rotor height of the 10 MW turbines during all weather conditions and during both seasons but fly slightly lower in spring (Figure 65). According to the predictions the birds fly slightly above the 3 MW turbines during good visibility conditions in autumn and also during average visibility conditions in autumn with tail or westerly cross winds. During situations with poor visibility and during average visibility with head and easterly cross wind combinations the birds will fly at the height of the 3 MW rotor (Figure 65). On average, the birds fly slightly higher in tail wind and westerly cross winds in comparison to head winds and easterly crosswinds.

Based on the behavioural data collected at the Baltic2 Offshore Wind Farm as part of the baseline investigations for the Krieger's Flak wind farm in 2015 (Skov et al. 2015) the avoidance rate of Common Crane at Krieger's Flak can be assessed with the Band (2012) collision risk model using the input parameters in Table 13. A low level of responsive behaviour by Common Cranes to the perimeter of the Baltic 2 Offshore Wind Farm was recorded, as only one of 14 flocks approaching the wind farm avoided penetrating the front row of turbines. This resulted in a macro avoidance rate of 0.07. Once in the wind farm, Common Cranes displayed relatively strong horizontal and vertical meso avoidance behaviour. Of the 20 recorded flocks 16 avoided entering the rotor-swept zone, 7 of which made evasive horizontal movements while 9 avoided the rotor by increasing flight altitude (vertical meso avoidance). These behavioural characteristics resulted in a meso avoidance rate of 0.8. Combined with the recorded macro avoidance rate and the micro avoidance rate of 0.08 from Winkelmann (1992) a total avoidance rate of 0.83 was estimated.

Several wind farms are planned in the region of the Arkona Basin, of which four have been consented and six have been submitted or are in the process of submitting consent applications to the Danish, Swedish and German planning authorities (Figure 66, Table 12). Once built, each of these 18 wind farms will inevitably cause additive mortality to Common Cranes migrating between Germany and Sweden due to collisions, especially given the relatively low avoidance rate of 0.83. This will also be the case with the new Krieger's Flak project (referred to in Table 12 as Krieger's Flak IIIa and IIIb). However, in comparison to the PBR threshold for a sustainable annual additive mortality the collision mortality estimated for the new Krieger's Flak project alone (72 and 86 birds annually for sector A and B respectively) is of minor significance.

Yet, the cumulative impact from all projects in the region means that 1,466 Common Cranes have the potential to collide annually with the existing, consented and planned offshore wind farms in the near future (Figure 67). Compared to the estimated PBR threshold of 1,887 birds, the combined collision impact on the Swedish-Norwegian population of Common Crane equals 77.7 % of the PBR threshold. This means that the population most likely will be capable of compensating the loss of birds imposed by the 18 projects by 2023 (Figure 67). With additional offshore wind farm projects in the region the collision mortality may, however approach a level which is not sustainable by the population.

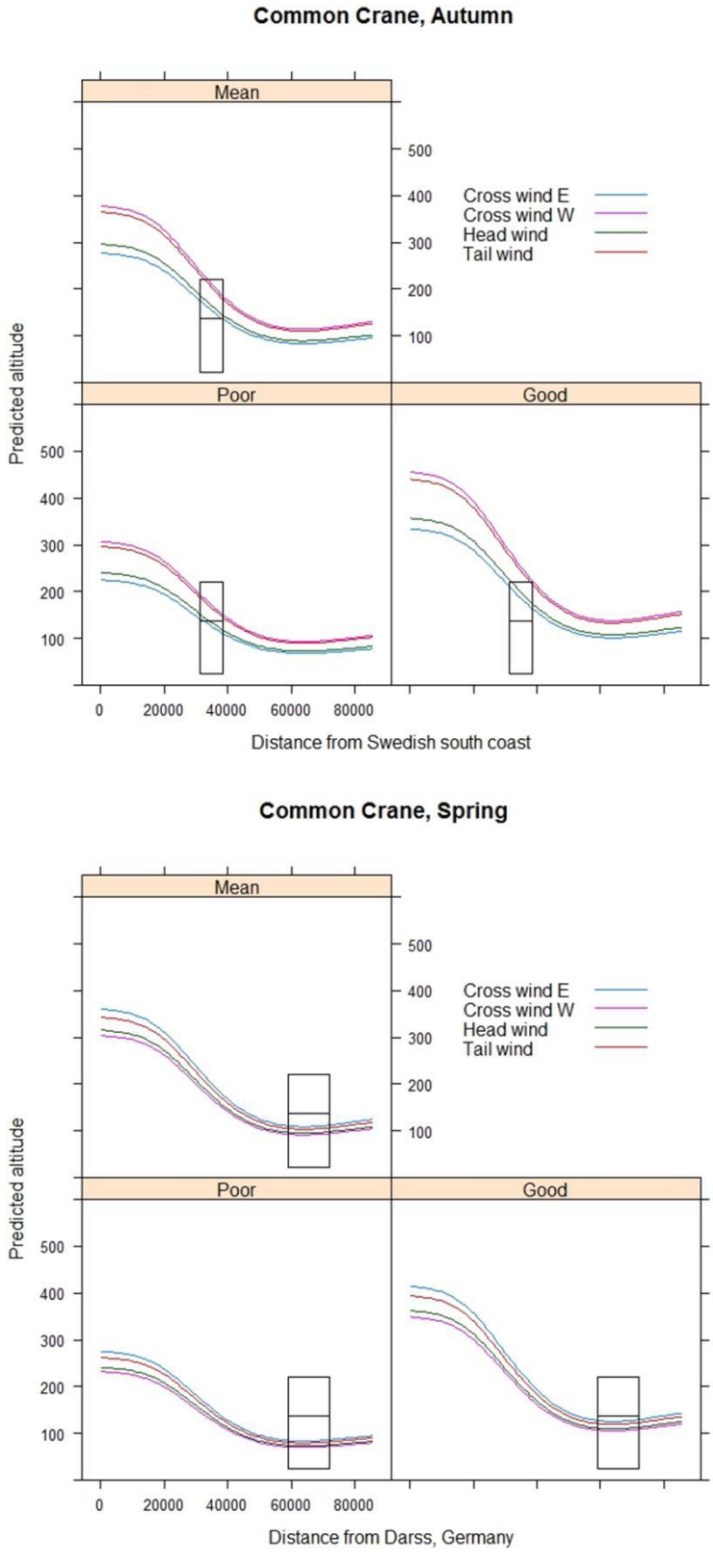

Figure 65 Average altitude for Common Crane in relation to distance from the coast of Sweden during autumn and from the coast of Germany during spring predicted during different visibility and wind directions for the spring and autumn seasons. All other predictor variables are set to mean values within the species-specific data set. The lines are the predicted flight altitudes and the black rectangle indicates the rotor swept area by 10 MW turbines. The line dividing the rectangle indicates the height of a 3 MW turbine.

Table 10 Overview of planned, consented and built offshore wind farm projects in the Arkona Basin.

Name	Country	Status	Year of construction	Turbine size	Number of turbines
Middelgrunden	DK	Built	2000	2	20
Lillgrund	SE	Built	2006	2.3	48
Breitling	DE	Built	2006	2.5	1
Baltic 1	DE	Built	2010	3	48
Avedøre Holme	DK	Built	2009	3.6	3
Baltic 2	DE	Built	2013	3.6	80
Wikinger Nord	DE	Built	2016	5	70
Arkona	DE	Built	2019	6	60
Arcadis Ost	DE	Consented	2020	4	58
Wikinger Süd	DE	Consented	2020	5	18
Gennaker	DE	Planned	2020	8	100
Kriegers Flak I	DK	Consented	2021	8	72
Nordre Flint	DK	Planned	2022	5	32
Aflandshage	DK	Planned	2022	5	50
Baltic Eagle	DE	Planned	2022	6	83
Kriegers Flak IIIa	DK	Planned	2022	8	46
Kriegers Flak IIIb	DK	Planned	2022	8	54
Kriegers Flak II	SE	Consented	2023	5	128

Table 11 Input parameters for the Band collision model. Measurements of bird length and wingspan was derived from www.dofbasen.dk and flight speed from Alerstam et al. (2007). Nocturnal activity and flight type is assumed based on expert knowledge. Proportion at rotor height and proportion of flight upwind during migration is based on the collected track data combined with historical meteorological measurements from Falsterbo, Sweden (www.smhi.se) and a 3.6 MW turbine with a maximum height of 141 m.

Parameter	
Avoidance rate	0.83
Bird length (m)	1.15
Wing span (m)	2.15
Flight speed (m/sec)	13.6
Nocturnal activity*	1
Flight type; gliding (G) or flapping (F)	F
Width of migration corridor (km)	140
Proportion at rotor height	79%
Proportion flight upwind	50%

* Degree of nocturnal activity indicated by a range from 1 (low) to 5 (high).

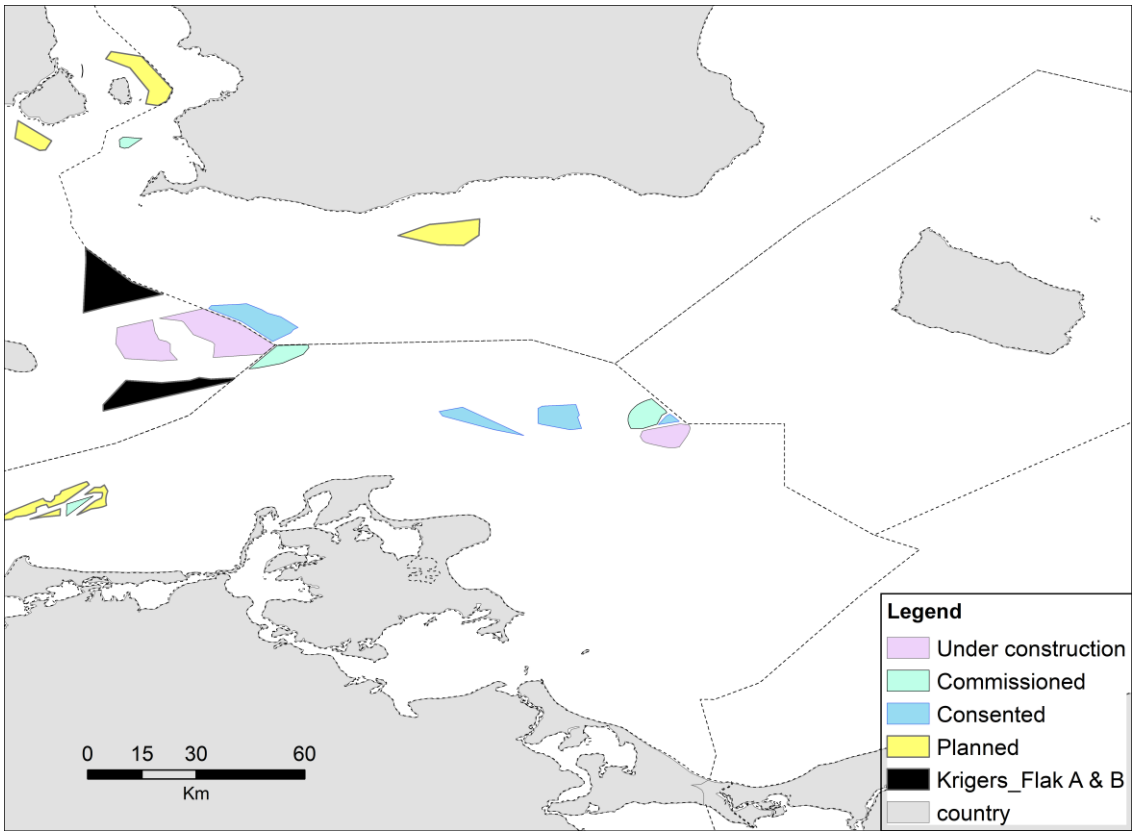

Figure 66 Overview of planned, consented and built offshore wind farms in the Arkona Basin.

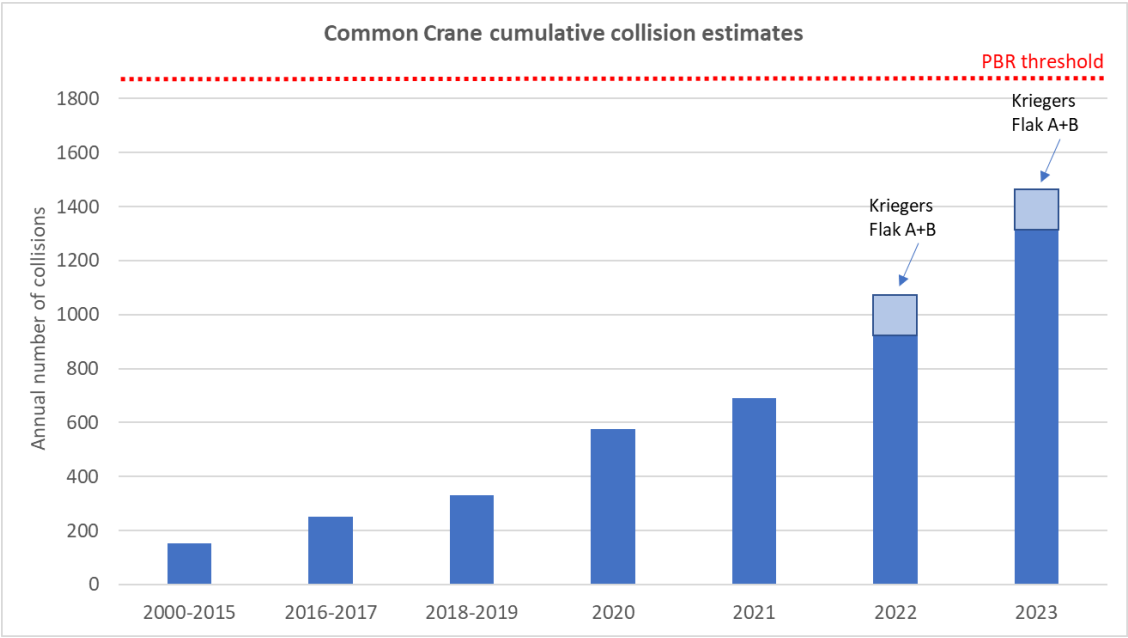

Figure 67 The cumulative number of Common Crane predicted to collide annually with wind farms in the Arkona Basin during different periods between 2000 and 2023. The Kriegers Flak A and B wind farms have been added to 2022 and 2023. The wind farms include all commissioned, consented and planned wind farms. The PBR threshold indicative of the limit for a sustainable mortality of Common Crane is indicated.

4 Conclusions

This review and analysis of existing seabird survey data from the Danish part of the North Sea and the central part of Kattegat has highlighted that although the data are dispersed and in most cases fragmented across areas and time the sheer volume of the data makes it possible to synthesize the information into maps of average seasonal densities useful for spatial planning of offshore wind farms. In the North Sea alone the combined data from aerial surveys contain 1.2 million records, and at least a similar amount of historic (primarily pre-2000) ship-based survey data are available. The survey data collected in combination with hydrodynamic model data on the oceanographic conditions during each of the many surveys are assessed as sufficient for describing the distribution and abundance of seabirds in the developing areas for the prospected Thor, Ringkøbing and Hesselø wind farms. The large amount of flight data on migrating Common Crane collected during the baseline for the Krieger's Flak I wind farm has enabled a robust assessment of the cumulative collision risk to this species of the prospected Krieger's Flak IIIa and IIIb wind farms with all planned, consented and commissioned wind farms in the region of the Arkona Basin.

The validation of the developed models shows that a high predictive accuracy has been achieved in the distribution models of the Red-throated and Black-throated Diver and the Common Scoter in the areas targeted for offshore wind farms in the Danish part of the North Sea.

4.1 Thor and Ringkøbing areas

The Thor wind farm area constitutes the northernmost part of the much larger Ringkøbing area, which extends to the northwestern Horns Rev area. As both divers and Common Scoter display highest densities towards the northwestern Horns Rev the southern half of the Ringkøbing area overlaps with high densities of divers (>0.75 birds/km^2) and scoters (>50 birds/km^2), hold relatively large numbers of birds and therefore has a high risk for severe displacement of these species. Densities of scoters are much lower in the northern part of the Ringkøbing and Thor areas, and high densities of divers in Thor are limited to the easternmost 5 km of the dedicated wind farm area.

Although the concentration of Common Scoter in Ringkøbing and Thor areas is predicted to be persistent across seasons the densities of divers in both areas only reach densities above 0.75 birds/km^2 during the period preceding spring migration in April. Yet, although peak numbers are limited in time potential population effects of displacement may still be significant depending on available food resources in the areas which the birds are displaced into.

4.2 Jammerbugt area

The dedicated wind farm area in Jammerbugt is located in the same type of marine habitat as the northeastern part of the Ringkøbing area and the Thor area, and densities of divers and scoters are therefore similar. Accordingly, densities of divers are comparable to these areas, and higher densities of divers in the Jammerbugt area are also confined to the month of April. More than half of the central part of the wind farm area has high habitat quality to divers during April. The densities of Common Scoter reach medium level in the southern half of the wind farm area.

4.3 Hesselø area

With the exception of Black-legged Kittiwake during the winter period the dedicated wind farm area Hesselø hosts low densities of seabirds, including divers and seaducks. As the Black-legged Kittiwake has low sensitivity towards displacement from offshore wind farms the Hesselø site should be considered as the most suitable of the four proposed sites due to overall low levels of impacts on birds foreseen for this site.

4.4 Krieger's Flak area

The cumulative impact from all projects in the region means that 1,466 Common Cranes have the potential to collide annually with the existing, consented and planned offshore wind farms in the near future. Compared to the estimated PBR threshold of 1,887 birds, the combined collision impact on the Swedish-Norwegian population of Common Crane equals 77.7 % of the PBR threshold. As the collision mortality is clearly below the PBR threshold the population will most likely be capable of compensating the loss of birds imposed by the 18 projects by 2023. With additional offshore wind farm projects in the region the collision mortality may, however approach a level which is not sustainable by the population.

5 References

Bailey H, Thompson PM. 2009. Using marine mammal habitat modelling to identify priority conservation zones within a marine protected area. Mar Ecol Prog Ser 378: 279−287

Becker, G. A., Fiuza, A. F. G., James, I. D. 1983. Water mass analysis in the German Blght during MARSEN, Phase I. J. geophys. Res. 88(C14): 9865-9870.

Buckland, S. T., D. R. Anderson, K. P. Burnham, J. L. Laake, D. L. Borchers, and L. Thomas. 2001. Introduction to Distance Sampling: Estimating Abundance of Biological Populations. Oxford University Press, Oxford, UK.

Burnham, K. P., and D. R. Anderson. 2002. Model Selection and Multimodel Inference: A Practical Information-Theoretic Approach, second edition. Springer-Verlag, New York, USA.

Cama, A., Abellana, R., Christel, I., Ferrer, X., Vieites, DR. 2012. Living on predictability: modelling the density distribution of efficient foraging seabirds. Ecography 35: 912−921

Cook, A.S.C.P., Humphreys, E.M., Masden, E.A. and Burton, N.H.K. 2014. The avoidance rates of collision between birds and offshore turbines. BTO Research Report No. 656. British Trust for Ornithology, Thetford, 273pp.

Embling, C.R., Gillibrand, P.R., Gordon, J., Shrimpton, J., Stevick, P.T., Hammond, P.S. 2010. Using Habitat Models to Identify Suitable Sites for Marine Protected Areas for Harbour Porpoises (Phocoena phocoena). Biological Conservation 143: 267 – 279.

Fauchald, P., Skov, H., Skern-Mauritzen, M., Hausner, V.H., Johns, D., Tveraa, T. 2011. Scale-dependent response diversity of seabirds to prey in the North Sea. Ecology 92: 228−239

Heinänen, S., Skov, H. 2018. Offshore Wind Farm Eneco Luchterduinen - Ecological Monitoring of Seabirds. T3 (Final) Report. Commissioned by Eneco. DHI report.

Lee, A. J. 1980. North Sea: Physical Oceanography. Pp. 467-493 in: Banner, F.T., Collins, M.B. & Massie, K.S. (Eds.). The sea and the sea bed in motion, Elsevier Oceanography Series 24B. Elsevier. Amsterdam.

MacLeod, CD, Zuur, AF. 2005. Habitat utilisation by Blain-ville's beaked whales off Great Abaco, northern Bahamas, in relation to seabed topography. Mar Biol 147: 1−11

Maxwell DL, Stelzenmüller V, Eastwood PD, Rogers SI. 2009 Modelling the spatial distribution of plaice (Pleuronectes platessa), sole (Solea solea) and thornback ray (Raja clavata) in UK waters for marine management and planning. J Sea Res 61: 258−267

May, R.F. 2015. A unifying framework for the underlying mechanisms of avian avoidance of wind turbines. Biological Conservation 190: 179 – 187. http://dx.doi.org/10.1016/j.biocon.2015.06.004.

Milner-Gulland, E.J. & Akçakaya, H.R. 2001. Sustainability indices for exploited populations under uncertainty. Trends in Ecology and Evolution 16: 686-692.Cook & Robinson 2015

Niel, C. and Lebreton, J.D. 2005. Using demographic invariants to detect over-harvested bird populationsfrom incomplete data. Conservation Biology, 19, 826–835.

Robinson LM, Elith J, Hobday AJ, Pearson RG, Kendall BE, Possingham HP, Richardson AJ. 2011. Pushing the limits in marine species distribution modelling: lessons from the land present challenges and opportunities. Glob Ecol Biogeogr 20: 789−802

Schneider, D.C., Duffy, D.C. 1985. Scale-dependent variability in seabird abundance. Mar Ecol Prog Ser 25: 211−218

Skov, H., Prins, E. 2001. Impact of estuarine fronts on the dispersal of piscivorous birds in the German Bight. Mar Ecol Prog Ser 214: 279−287

Skov, H., Durinck, J., Bloch, D. 2003. Habitat characteristics of the shelf distribution of the harbour porpoise (Phocoena phocoena) in the waters around the Faroe Islands during summer. NAMMCO Sci Publ 5: 31−40

Swanberg. P.O. c. 1985. Migration routes of Swedish Common Cranes (Grus grus) present knowledge. Link: http://epa.uz.ua/01600/01603/00075/pdf/Aquila_EPA-01603_1986-1987_063-073.pdf

Taylor, B.L., Wade, P.R., DeMaster, D.P., and Barlow, J. 2000. Incorporating uncertainty into management models for marine mammals. Conservation Biology, 14, 1243–1252.

Wade, P.R. 1998. Calculating limits to the allowable human-caused mortality of cetaceans and pinnipeds. Marine Mammal Science, 14, 1–37.

Winiarski, K. J., M. L. Burt, E. Rexstad, D. L. Miller, C. L. Trocki, P. W. C. Paton, and S. R. McWilliams. 2014. Integrating aerial and ship surveys of marine birds into a combined density surface model: A case study of wintering Common Loons. The Condor: Ornithological Applications 116:149–161.

Winkelman, J.E. 1992. De invloed van de Sep-proefwindcentrale te Oosterbierum (Friesland) op vogels, 1: Aanvaringsslachtoffers. RIN-rapport 92/2, IBN-DLO, Arnhem, The Netherlands.

Wood, S.N. (2004) Stable and efficient multiple smoothing parameter estimation for generalized additive models. J. Amer. Statist. Ass. 99:673-686.

Wood, S.N. 2006. Generalized Additive Models: An introduction with R. Chapman and Hall, London, UK.

Zuur, A.F., Saveliev, A.A., Ieno, E.N., 2012. Zero inflated models and generalized linear mixed models with R. Newburgh: Highland Statistics Ltd

APPENDICES

A APPENDIX A – Hydrodynamic model – UKNS2

A.1 Water level

The DHI North Sea hydrodynamic model has been validated against measured water levels from select tide gauge stations within the model domain, including the station at Helgoland. In Figure A- 1 the water level comparisons for Helgoland are shown. Notice that the plots have been adjusted for the difference in the vertical datum between the tide gauge and the model. It is observed in the plots that the North Sea model compares well to the measurements in terms of both tidal amplitudes and phases as well as residual (non-tidal) variability. The performance measures in the figure also show a good agreement between measurements and model results.

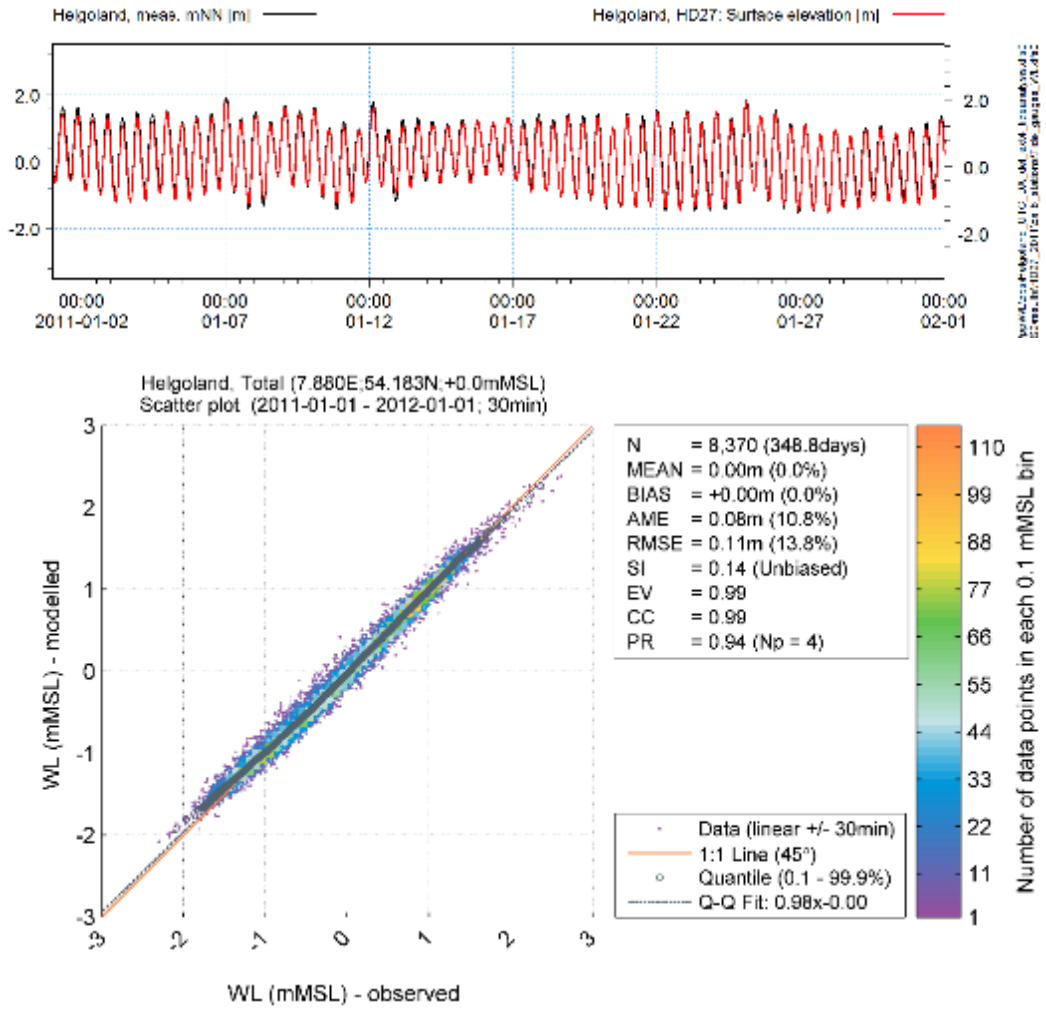

Figure A- 1 Comparison of measured and modelled water level at Helgoland. In the lower panel bias-corrected scatter plot and performance measures for the year 2011 are given.

A.2 Currents

The DHI North Sea model has been validated against measured currents from the FINO1 and FINO 3 research platforms. In both stations a surface and a bottom layer comparison is presented. In Figure A-2 and Figure A- 3 surface and bottom current comparisons at FINO1 are shown. It is observed in the plots that the currents here are dominated by the E-W going tide with magnitudes of 0-0.8 m/s. The measurements, particularly the surface measurements, contain infrequent high current magnitudes between 0.8 and 2.0 m/s, which are not captured by the model. Whether these represent processes not included in the model or measurement errors is not clear. Overall the model compares well to the measurements for the lower magnitudes (0-0.5 m/s) and underestimates to some degree for the higher magnitudes (above 0.5 m/s). With respect to current directions the model compares well to the measurements as observed in the dual current rose plots.

In Figure A- 4 and Figure A- 5 surface and bottom current comparisons at FINO3 are shown. It is observed in the plots that the currents here are dominated by the relatively weak SE-NW going tide with magnitudes of 0-0.5 m/s. Also here the measurements contain a few significantly higher magnitudes, but much less than the FINO1 measurements. The model compares well to the measurements for the lower magnitudes (0-0.4 m/s) and underestimates slightly for the higher magnitudes. The current directions are reproduced well by the model.

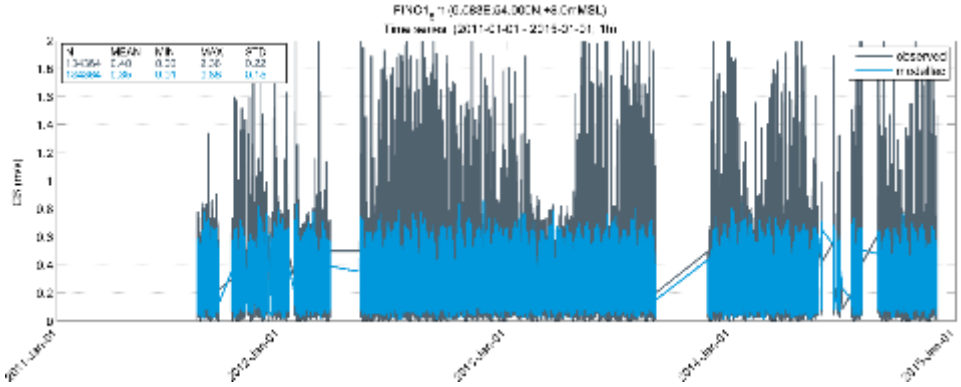

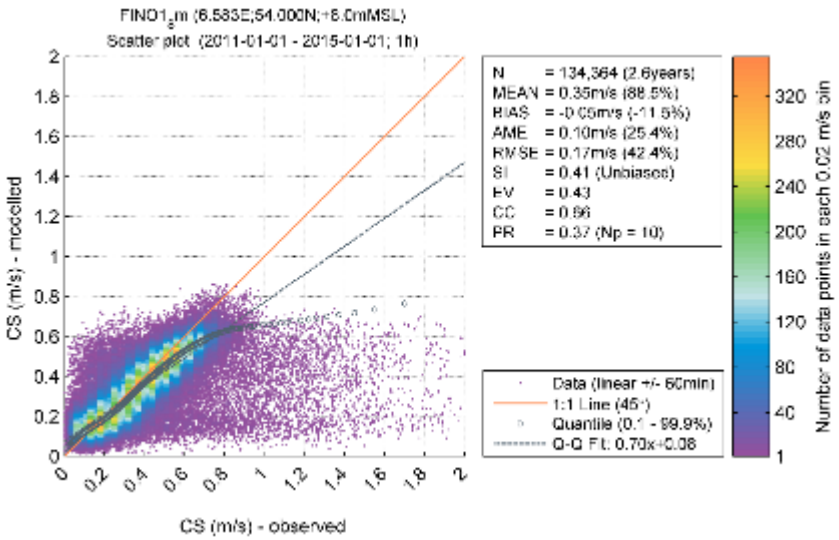

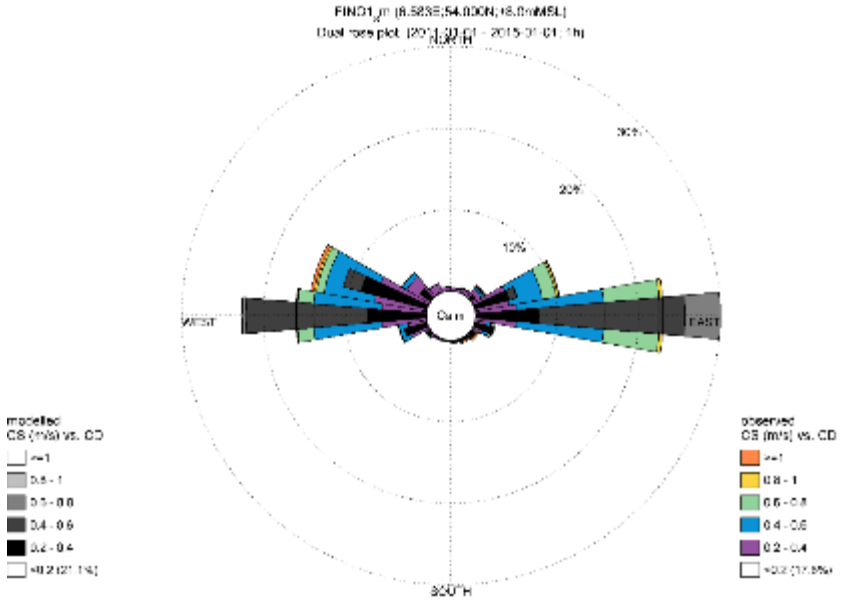

Figure A- 2 Comparison of observed and modelled currents at FINO1 in the subsurface layer (at 8m depth). Data source: FINO1 ©Bundesamt für Seeschifffahrt und Hydrographie (BSH), Germany, sponsored by BMWi (Bundesministerium für Wirtschaft und Energie) and PTJ (Projektträger Jülich, Forschungszentrum Jülich).

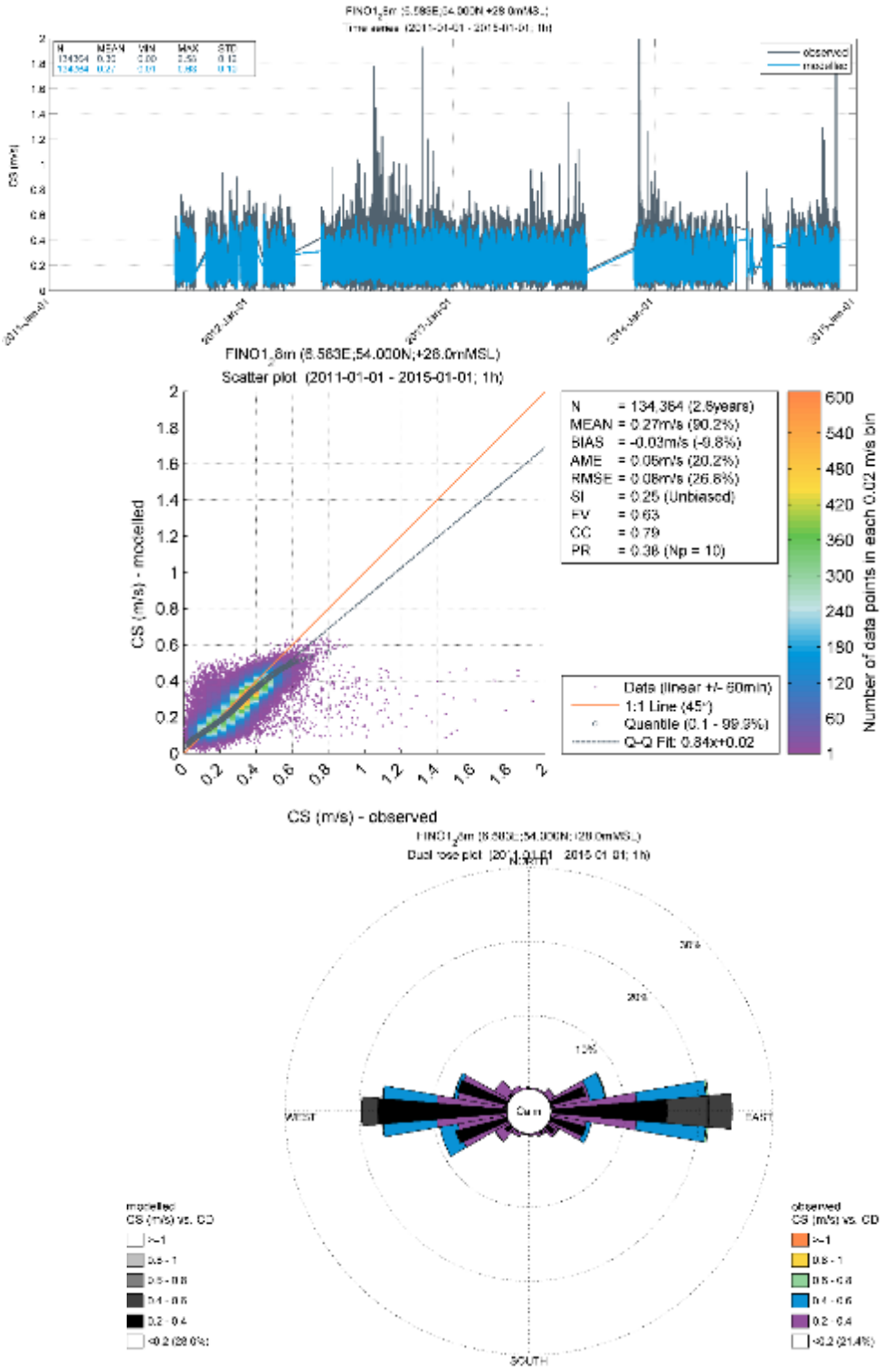

Figure A- 3 Comparison of observed and modelled currents at FINO1 in the bottom layer (at 28m depth). Data source: FINO1 ©Bundesamt für Seeschifffahrt und Hydrographie (BSH), Germany, sponsored by BMWi (Bundesministerium für Wirtschaft und Energie) and PTJ (Projektträger Jülich, Forschungszentrum Jülich).

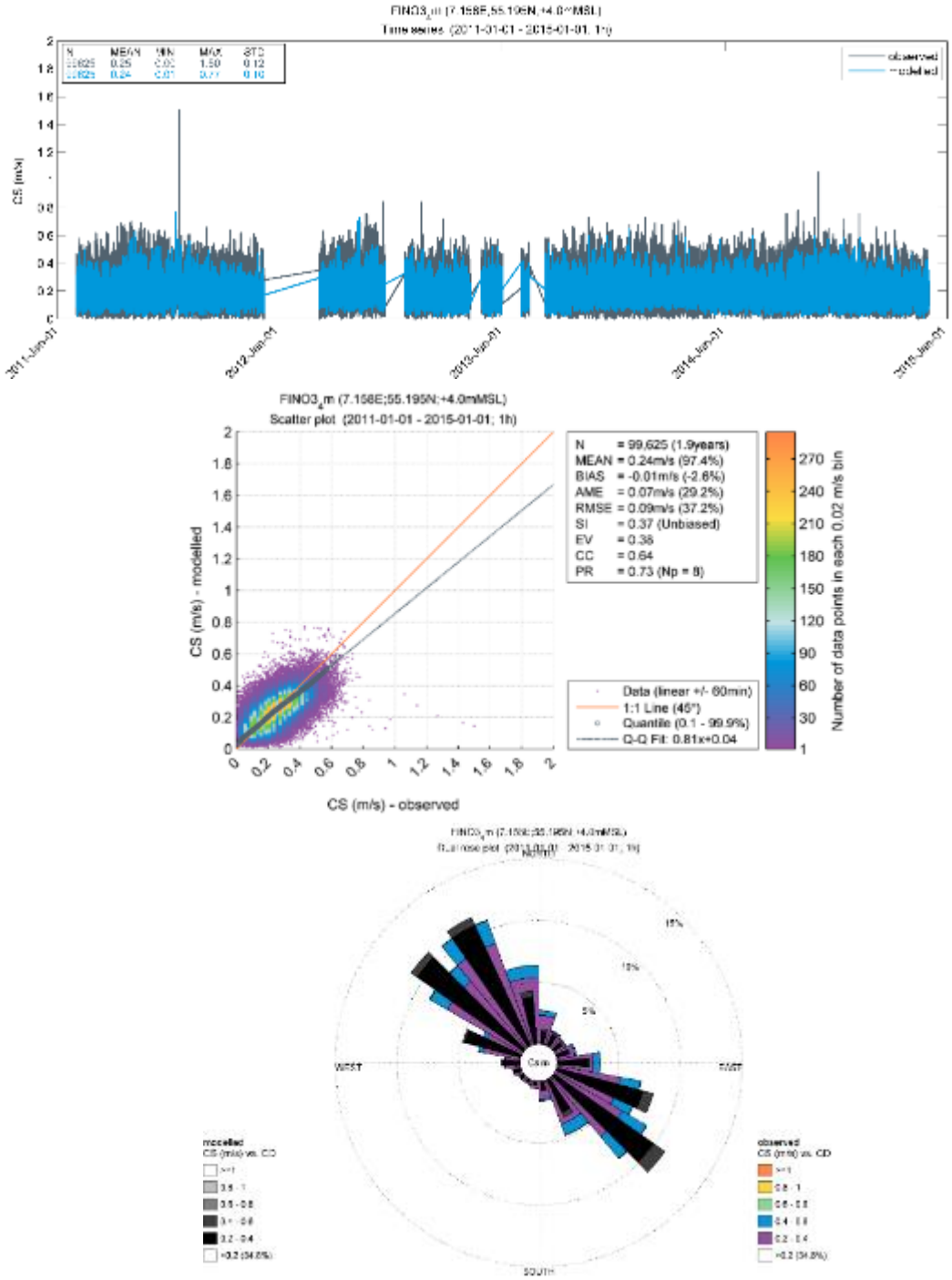

Figure A- 4 Comparison of observed and modelled currents at FINO3 in the surface layer (at 4m depth). Data source: FINO3 ©Bundesamt für Seeschifffahrt und Hydrographie (BSH), Germany, sponsored by BMWi (Bundesministerium für Wirtschaft und Energie), PTJ (Projektträger Jülich, Forschungszentrum Jülich), SH (Schleswig-Holstein) and EU (European Union).

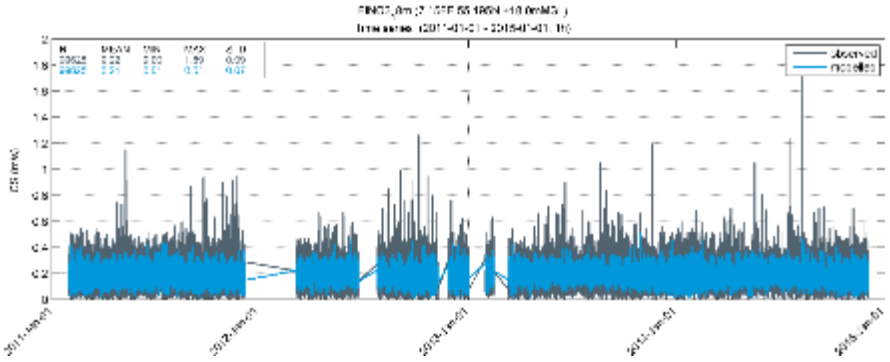

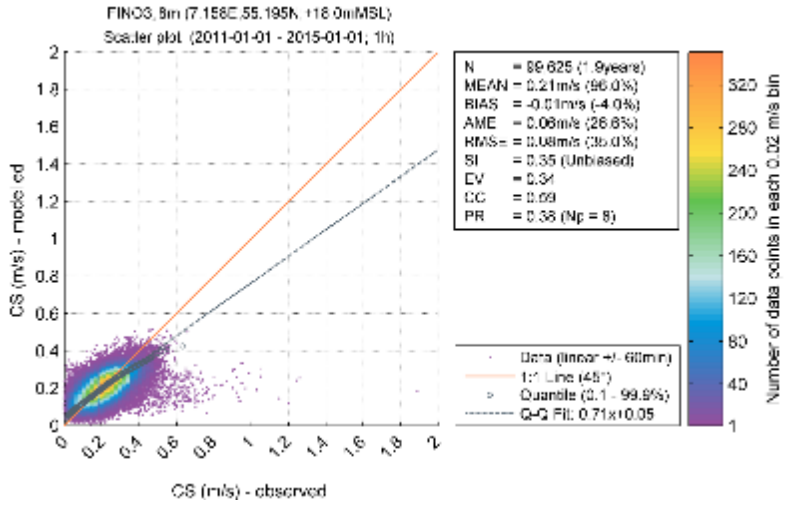

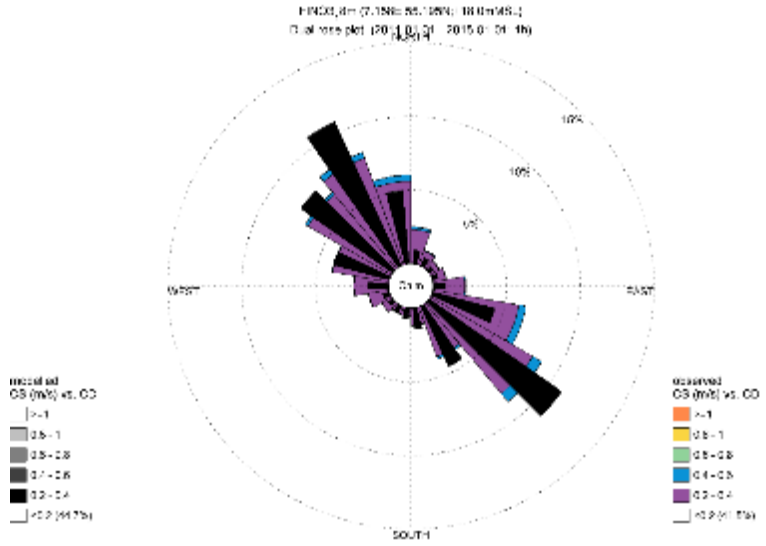

Figure A- 5 Comparison of observed and modelled currents at FINO3 in the bottom layer (at 18m depth). Data source: FINO3 ©Bundesamt für Seeschifffahrt und Hydrographie (BSH), Germany, sponsored by BMWi (Bundesministerium für Wirtschaft und Energie), PTJ (Projektträger Jülich, Forschungszentrum Jülich), SH (Schleswig-Holstein) and EU (European Union).

A.3 Salinity and water temperature

Modelled salinity and water temperature time series have been compared to measurements in a number of stations, including FINO1. In Figure A- 6 the time series comparisons are shown. Notice that the figures compare both surface and bottom salinities and temperatures. The comparisons show a good agreement between the measurements and the North Sea model for both salinity and temperature.

For salinity, the absolute salinity levels as well as the stratification and the variability and seasonality of the surface layer salinity are well represented by the model. For water temperature, the absolute levels and seasonality are well represented by the model. Also the seasonality of the thermal stratification is well represented, and both the summer stratification and autumn mixing of the water column are captured well by the model.

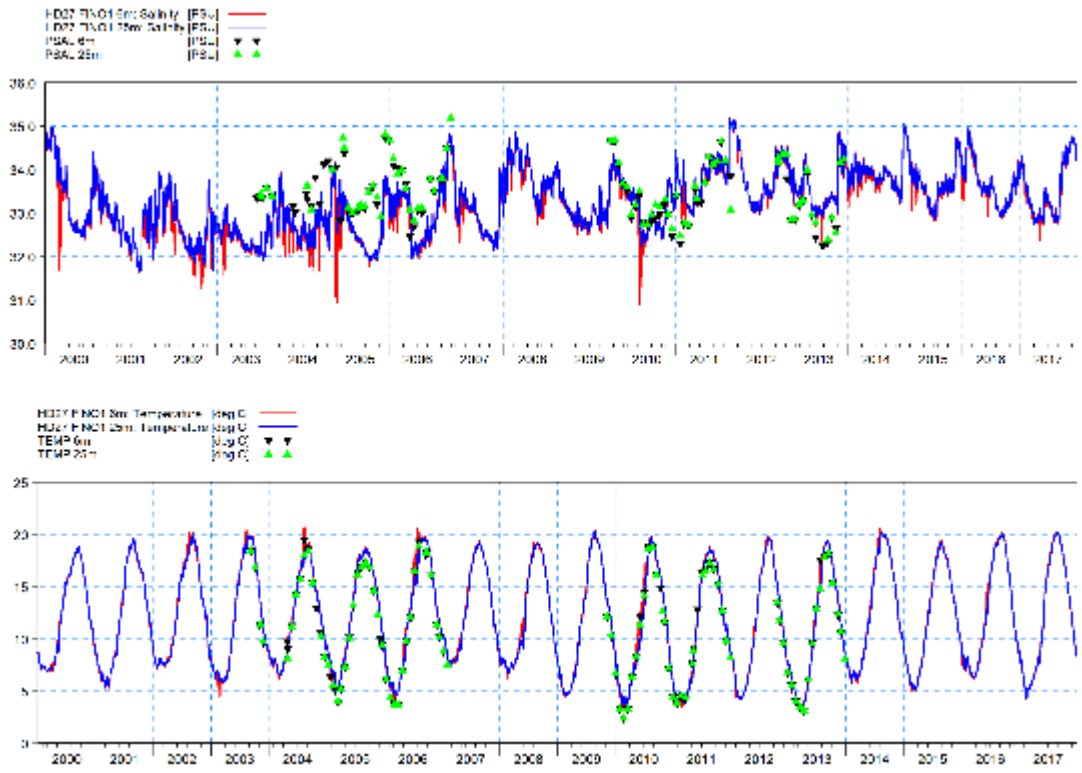

Figure A- 6 Comparison of measured and modelled salinity (top) and water temperature (bottom) at FINO1 station

The hydrodynamic variables surface salinity, surface current speed, upwelling, eddy potential (vorticity), surface current gradient, surface salinity gradient and vertical temperature gradient were extracted from the hydrodynamic model time series to the survey data based on exact position and time, interpolated between timesteps (Table A- 1). The spatio-temporal characteristics of these variables are detailed in chapter 8.

Table A- 1List of predictor variables included in the initial distribution models

Variable	Description	Rationale for inclusion
Surface salinity	Salinity (psu)	Water mass characteristics
Surface current speed	Magnitude of horizontal current speed (m/s)	Hydrodynamic structure determining variation in prey availability
Upwelling	Vertical current vector (w)	Hydrodynamic structure concentrating prey
Eddy potential (vorticity)	Eddy activity measured as the local vorticity (m/s/m depth) integrated over the whole water column	Hydrodynamic structure concentrating prey
Surface current gradient	Horizontal gradient of currents (m/s/m depth)	Hydrodynamic structure concentrating prey
Surface salinity gradient	Horizontal gradient of salinity (psu)	Hydrodynamic structure concentrating prey
Vertical salinity gradient	Vertical gradient of salinity (psu)	Stratification characteristics
Vertical temperature gradient	Vertical gradient of temperature (C˚)	Stratification characteristics

B APPENDIX B – Hydrodynamic model – DKBS2

B.1 Water Level

B.1.1 Measured water level

The DKBS2 hydrodynamic model has been validated against measured water levels from select tide gauge stations within the model domain.

In Figure B- 1 the location of the tide gauge stations is shown. The water level comparisons are shown in figures below. Notice that the plots have been adjusted for the difference in the vertical datum between the tide gauge and the model.

It is observed in the plots that the DKBS2 model compares well to the measurements in terms of both tidal amplitudes and phases (mainly in Skagerrak, Kattegat and Belt Sea) and residual (non-tidal) variability.

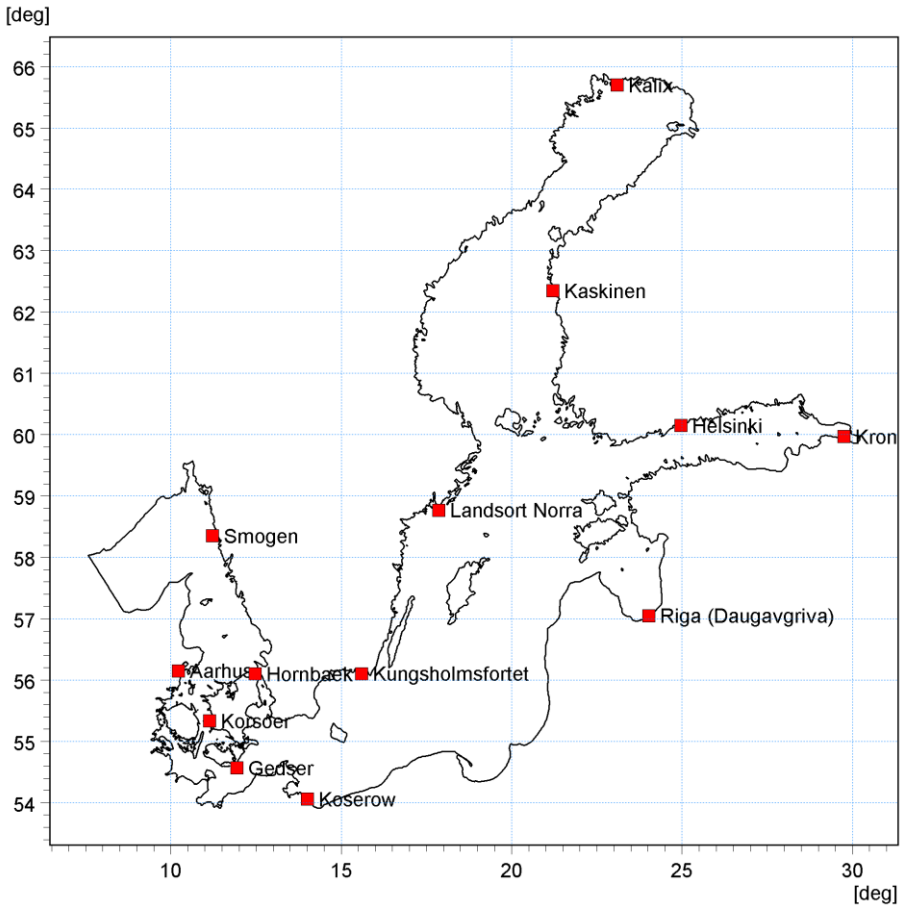

Figure B- 1 Location of applied tide gauge stations

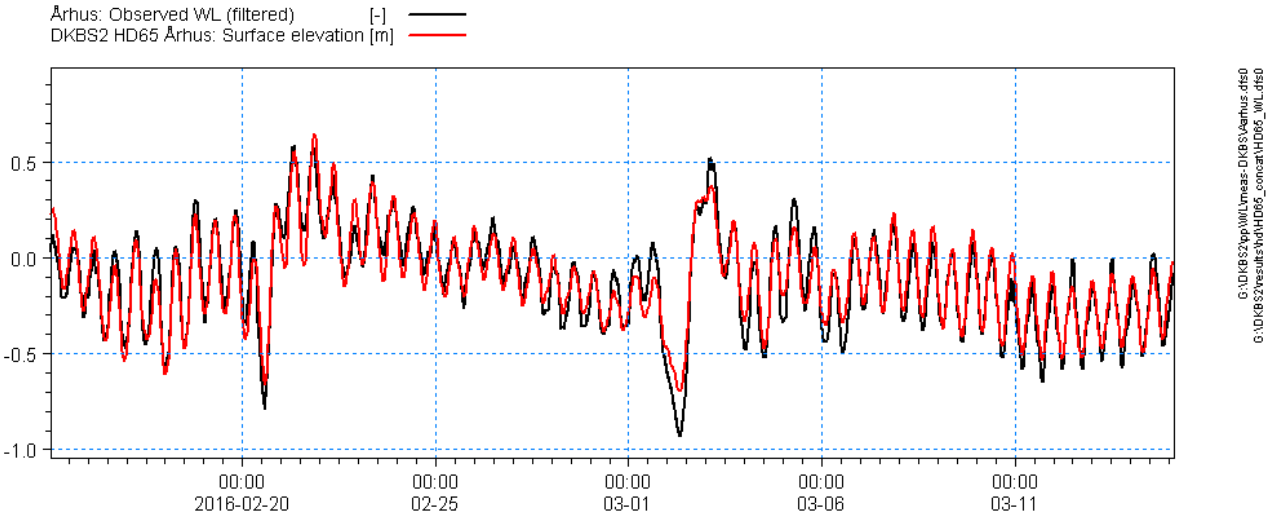

Figure B- 2 Comparison of measured and modelled water level at Aarhus

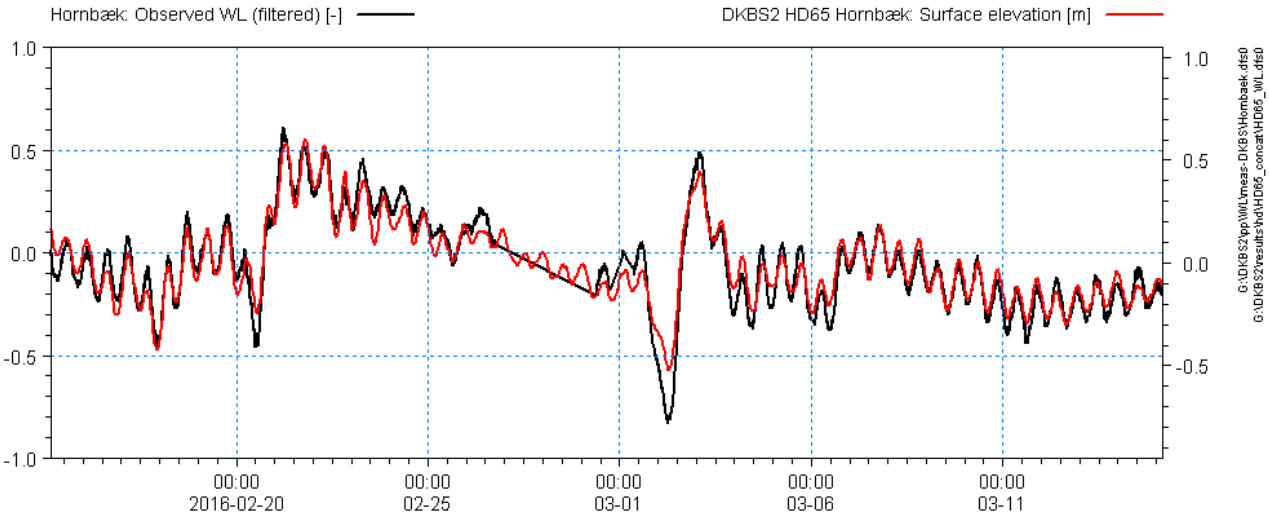

Figure B- 3 Comparison of measured and modelled water level at Hornbæk

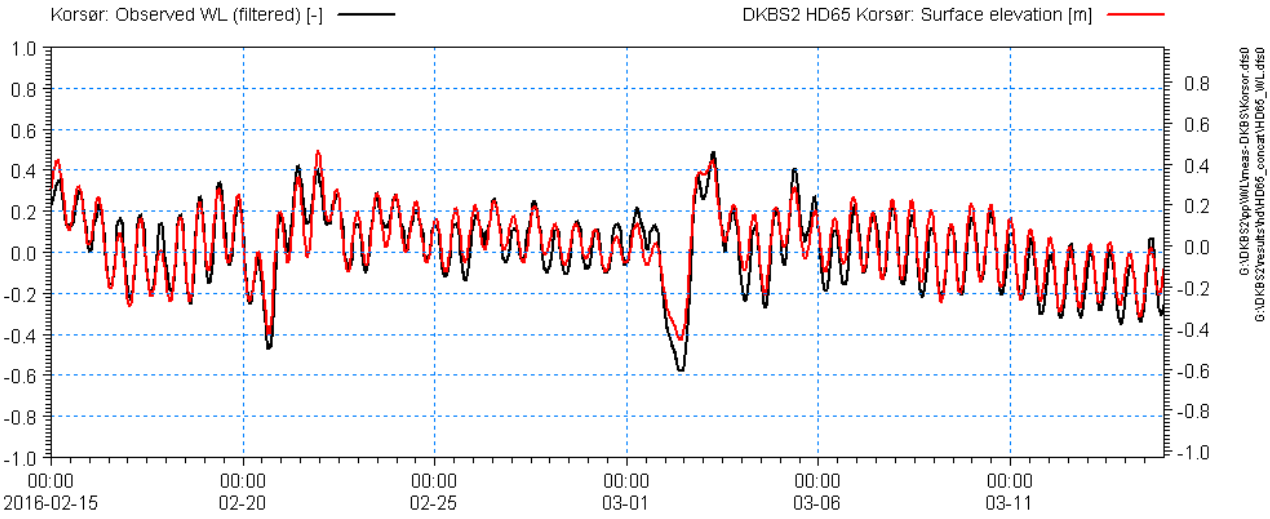

Figure B- 4 Comparison of measured and modelled water level at Korsør

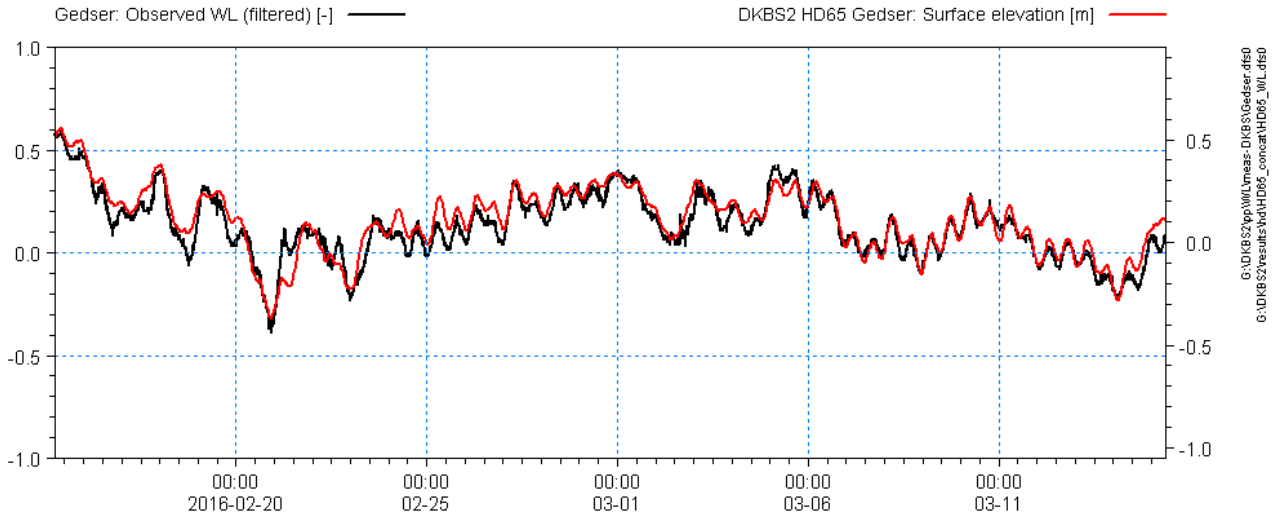

Figure B- 5Comparison of measured and modelled water level at Gedser

B.2 Circulation

B.2.1 Discharge through Danish straits

In Figure B- 6 the water discharge through Great Belt, Øresund and Little Belt in 2011 is shown. The modelled mean outflow for the period 2008-2017 is 533 km^3/year, which is in accordance with the value of about 500 km^3/year established in the literature.

In Figure B- 7 linear regressions between instantaneous discharge at Great Belt and Øresund, and Great Belt and Little Belt, respectively are shown. The slope terms from the regressions are in fair agreement with the established ration of 1:7:3 between Little Belt, Great Belt and Øresund respectively.

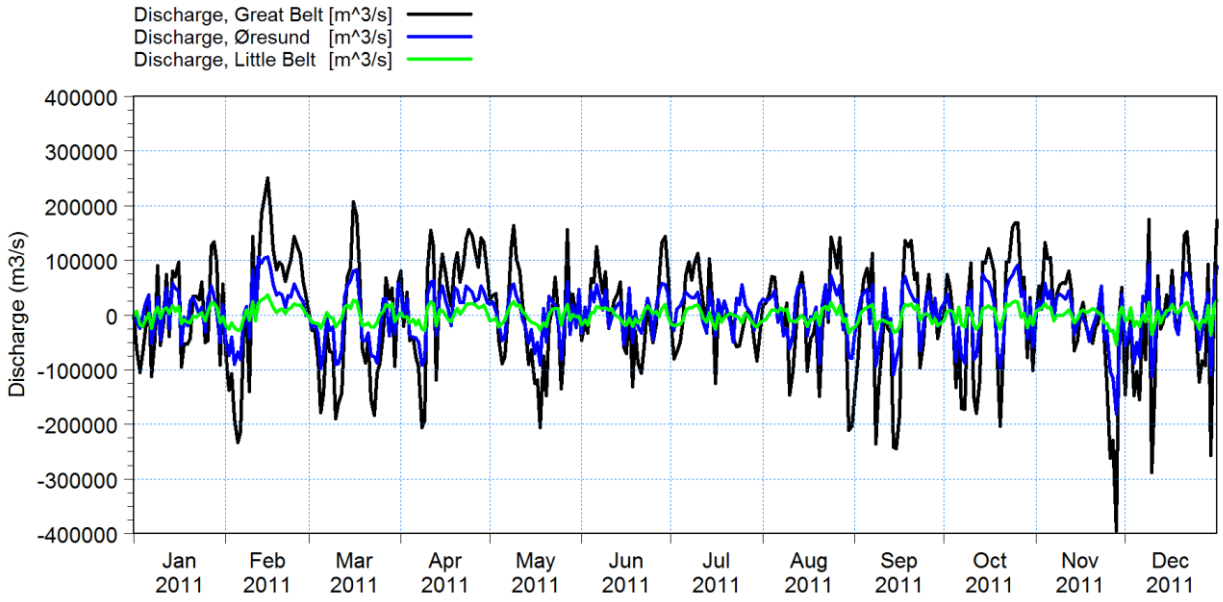

Figure B- 6 Instantaneous discharge at Great Belt, Øresund and Little Belt shown exemplary for 2011. Positive numbers represent outflow (northward), negative numbers inflow (southward) events.

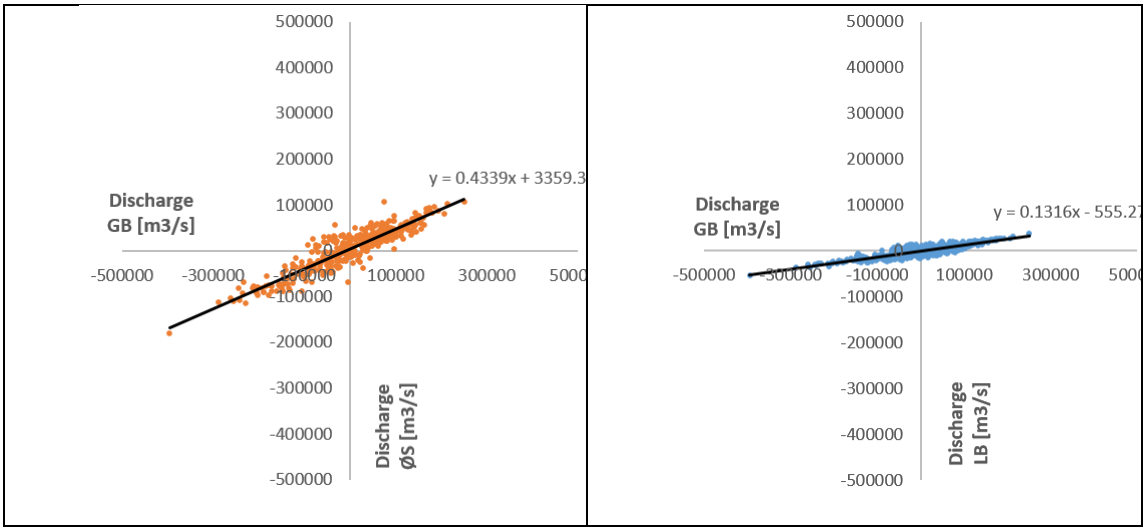

Figure B- 7 Scatter plots of instantaneous discharges at Great Belt (horizontal axes) vs Øresund and Little Belt (vertical axes) for the year 2011.

B.2.2 Measured current

The DKBS2 hydrodynamic model has been validated against measured current from available measurement stations within the model domain.

In Figure B- 8 the location of the measurement stations is shown. The current comparisons are shown in the figures below.

The measurements and model results show a fair agreement hereby demonstrating the ability of the model to simulate the current strength, variability and directionality.

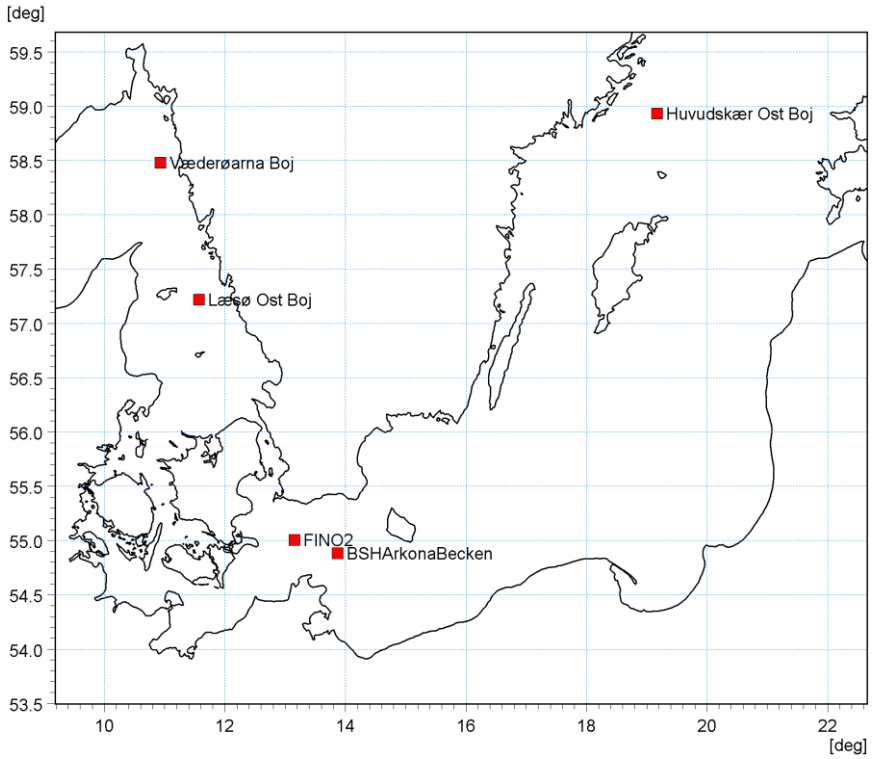

Figure B- 8 Location of available current measurement stations.

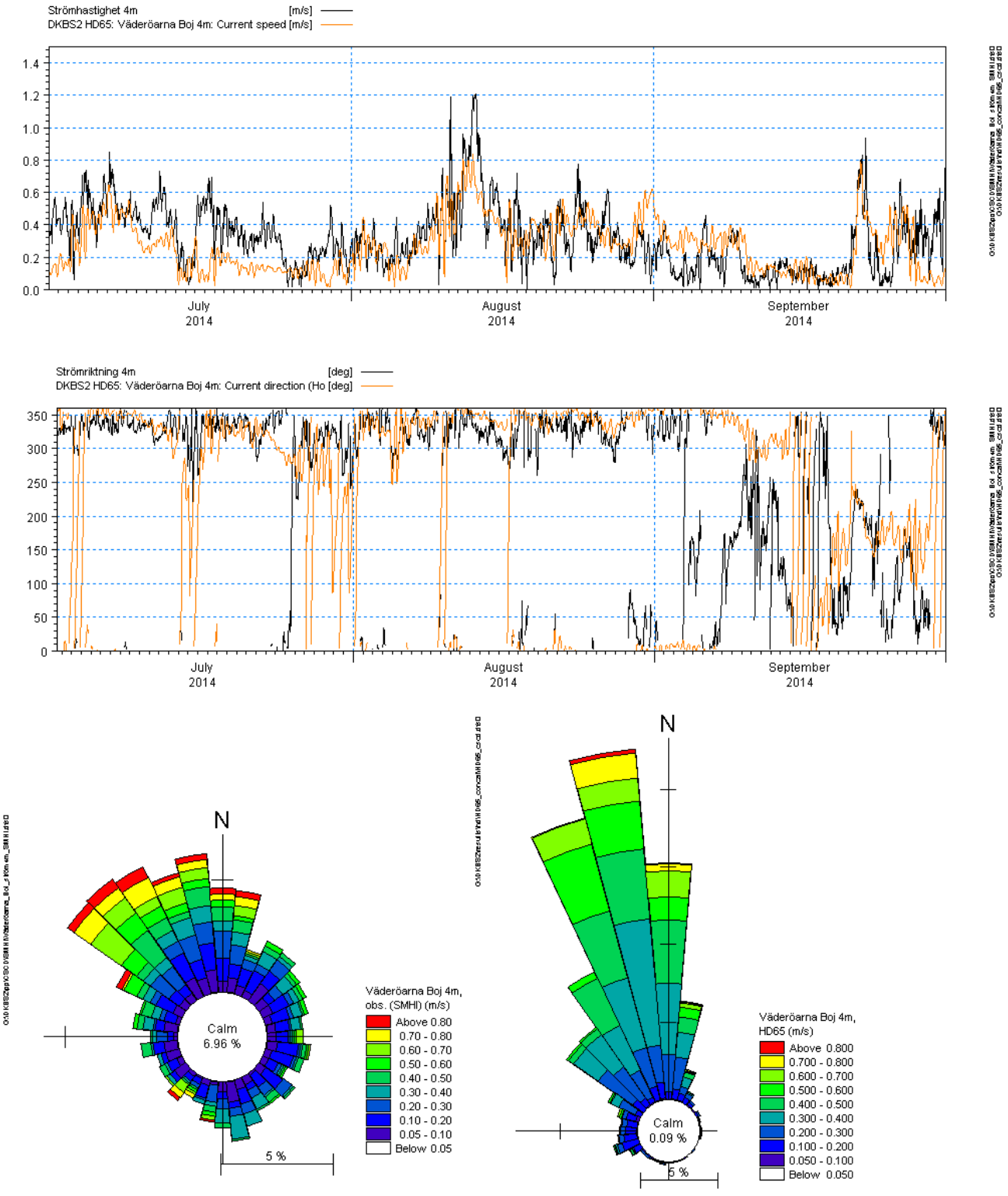

Figure B- 9 Comparison of measured and modelled current at Väderöarna station at depth 4m.

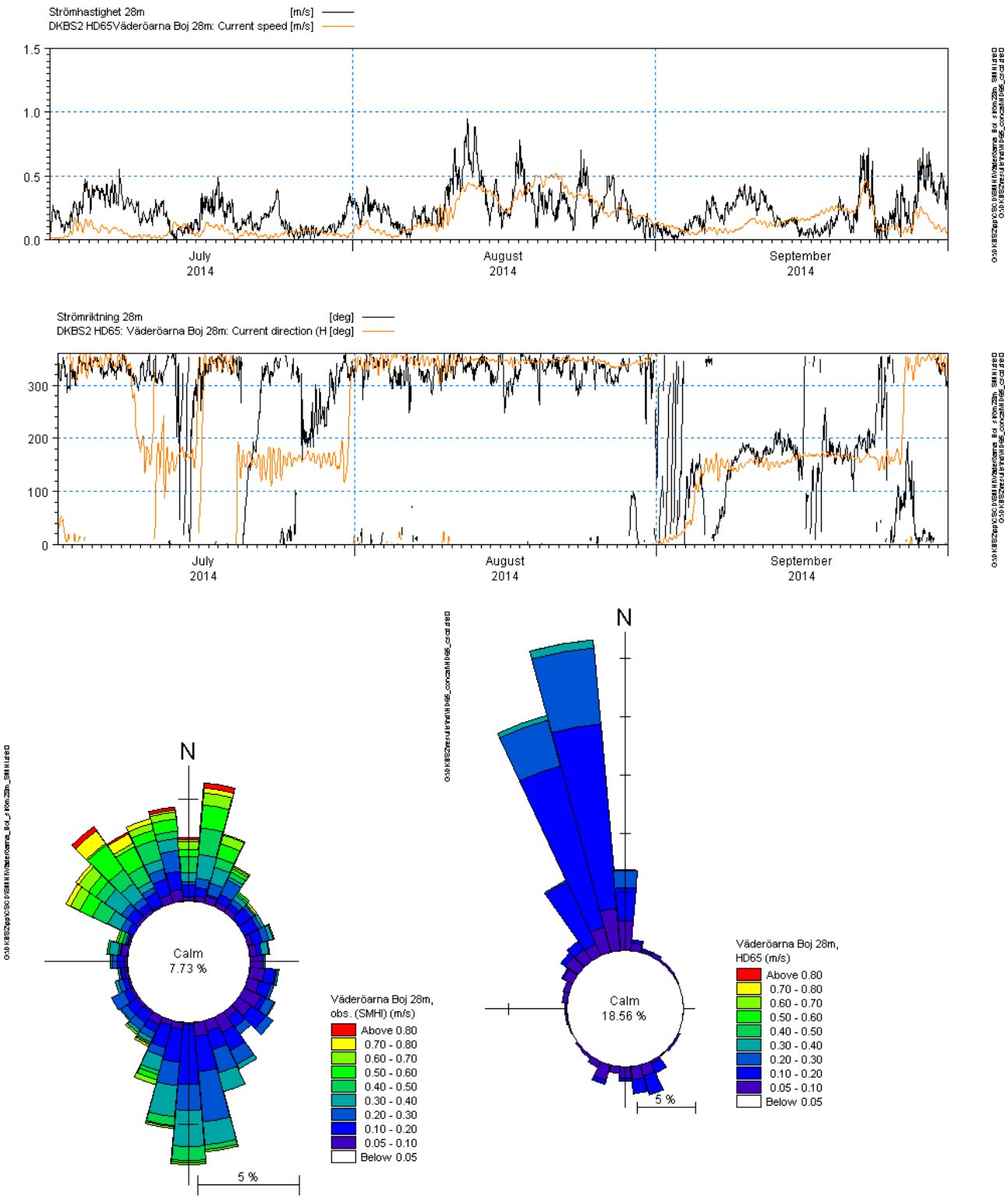

Figure B- 10 Comparison of measured and modelled current at Väderöarna station at depth 28m.

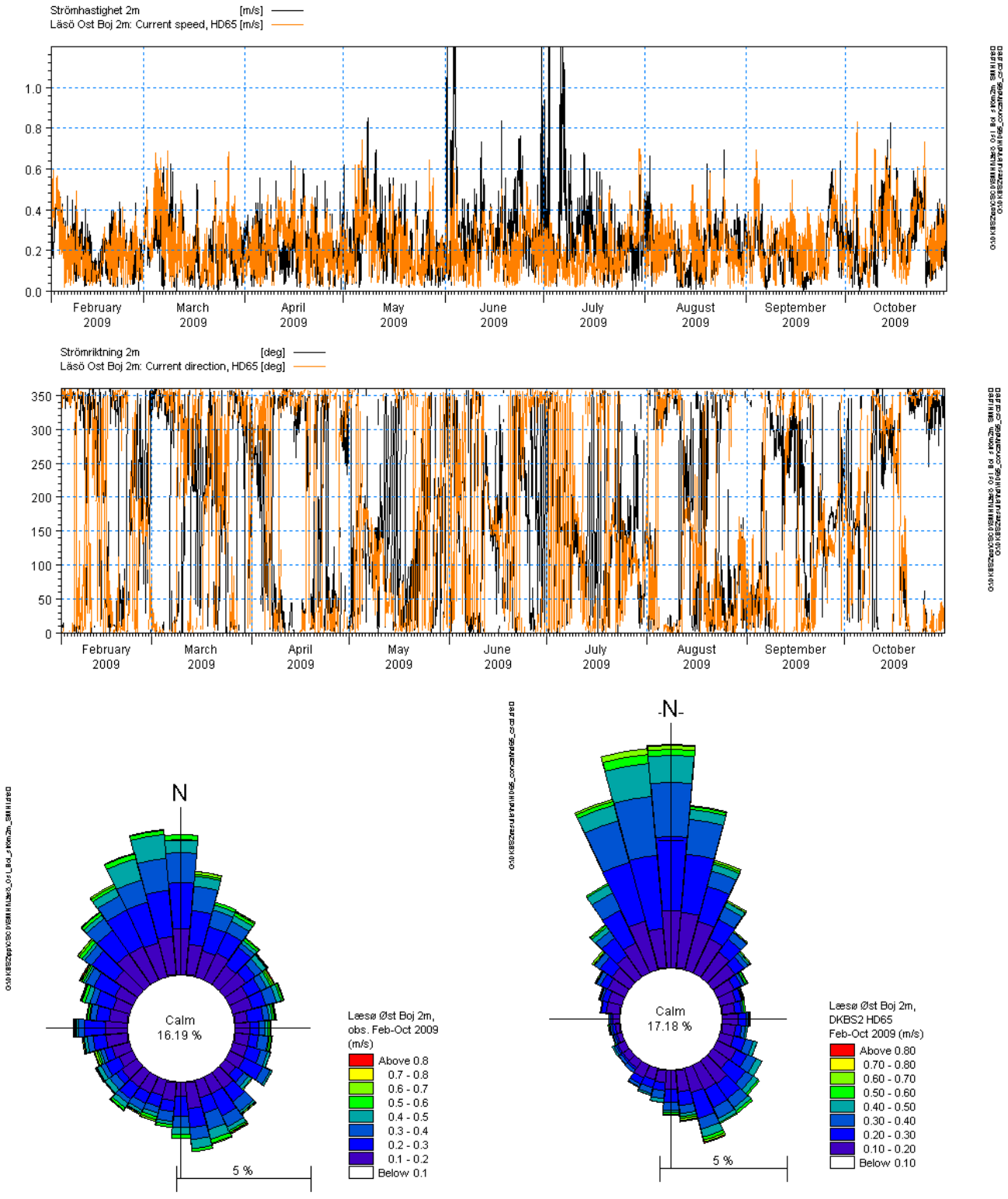

Figure B- 11 Comparison of measured and modelled current at Läsö Ost Boj at depth 2m.

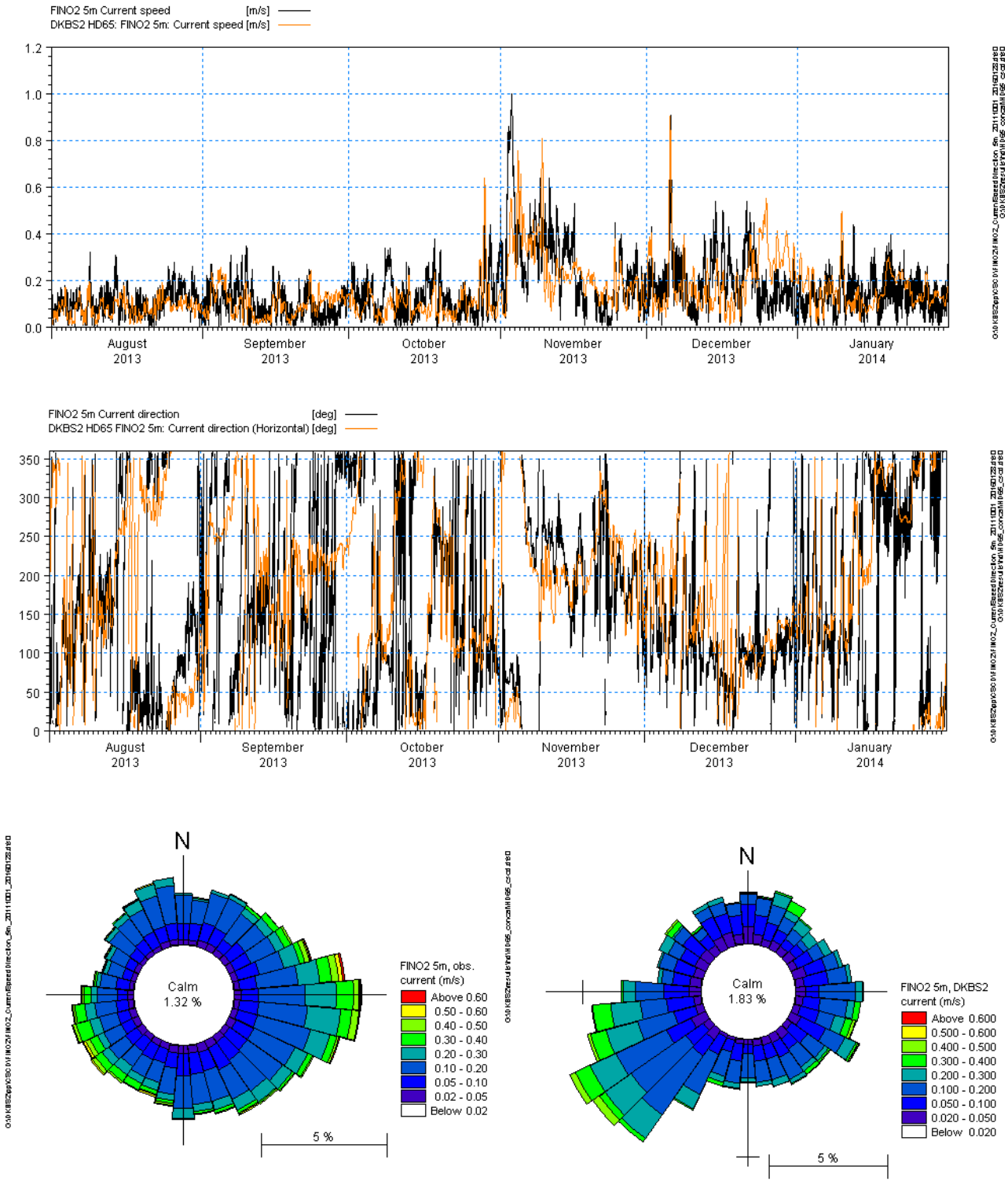

Figure B- 12 Comparison of measured and modelled current at FINO2 station at depth 5m.

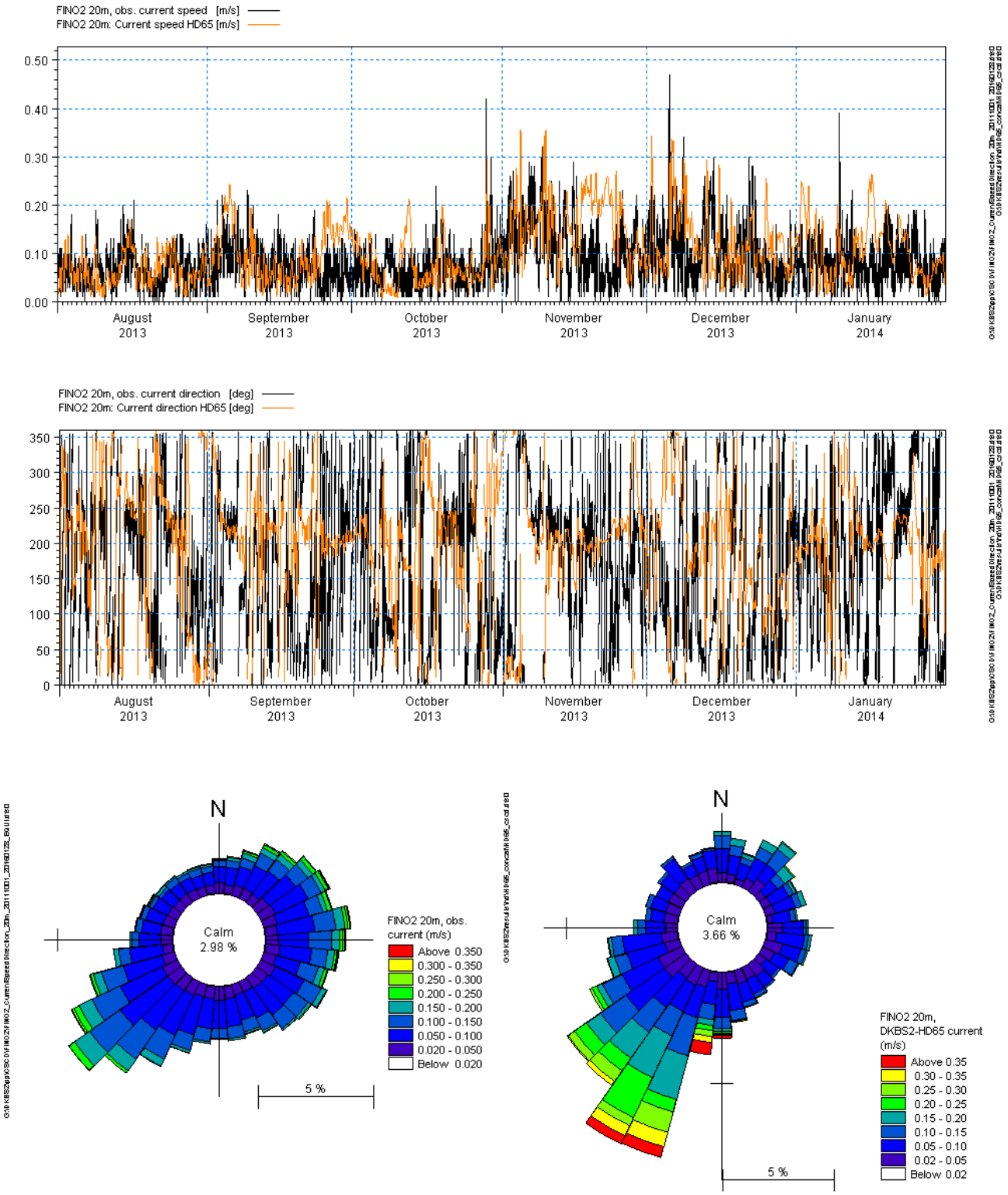

Figure B- 13 Comparison of measured and modelled current at FINO2 station at depth 20m

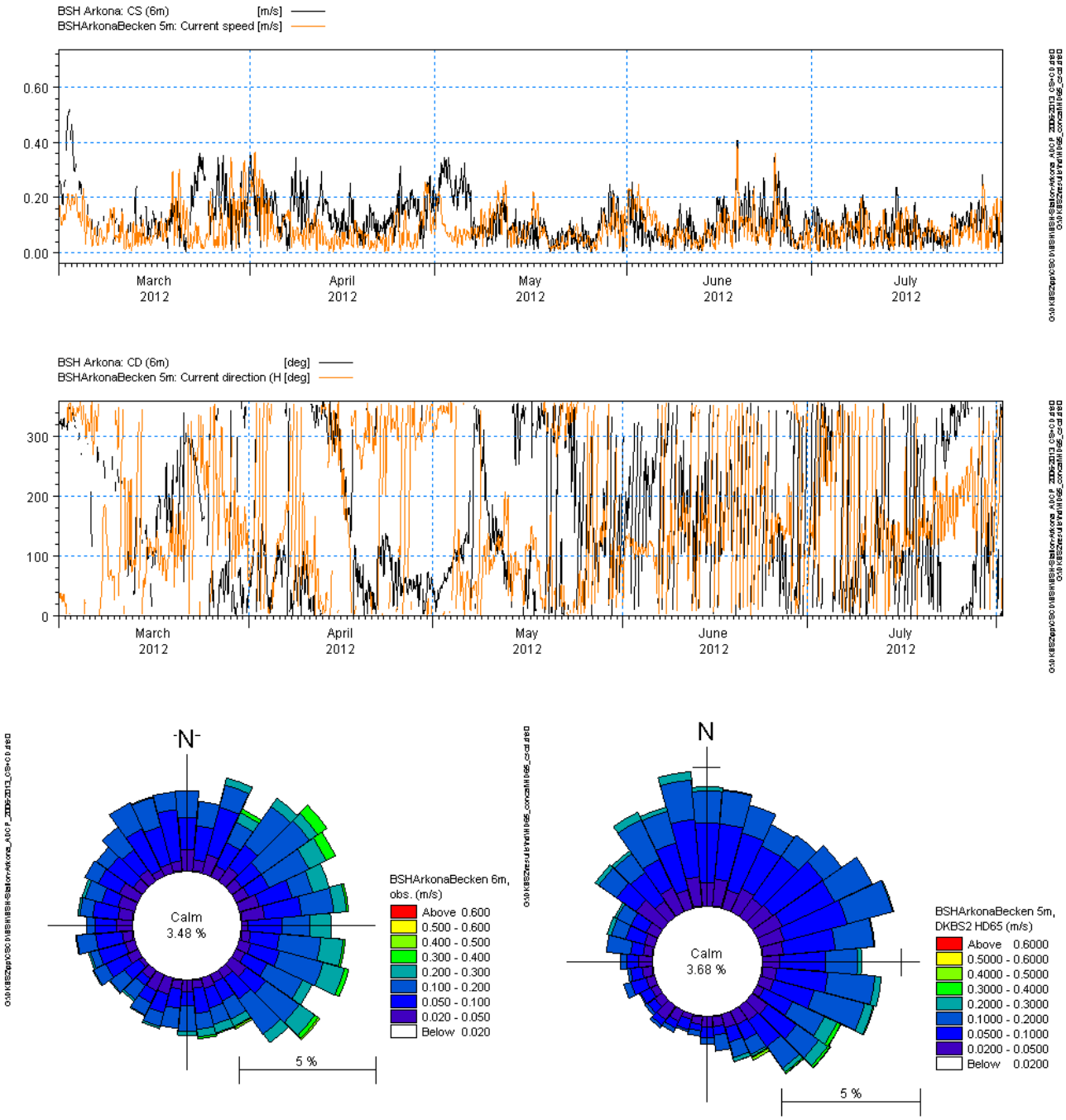

Figure B- 14 Comparison of measured and modelled current at BSH Arkona Becken station at depth 5-6m

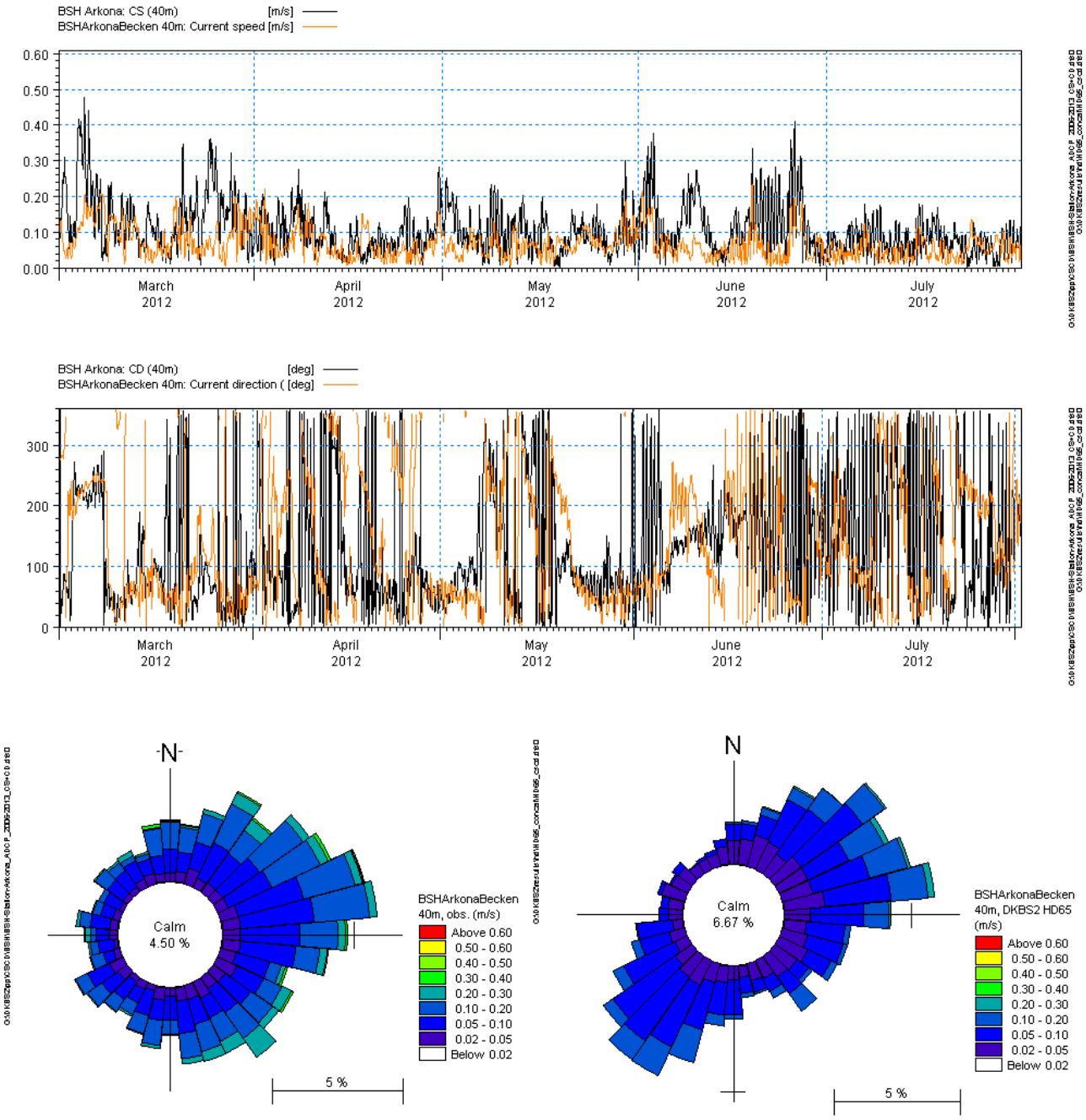

Figure B- 15 Comparison of measured and modelled current at BSH Arkona Becken station at depth 40m.

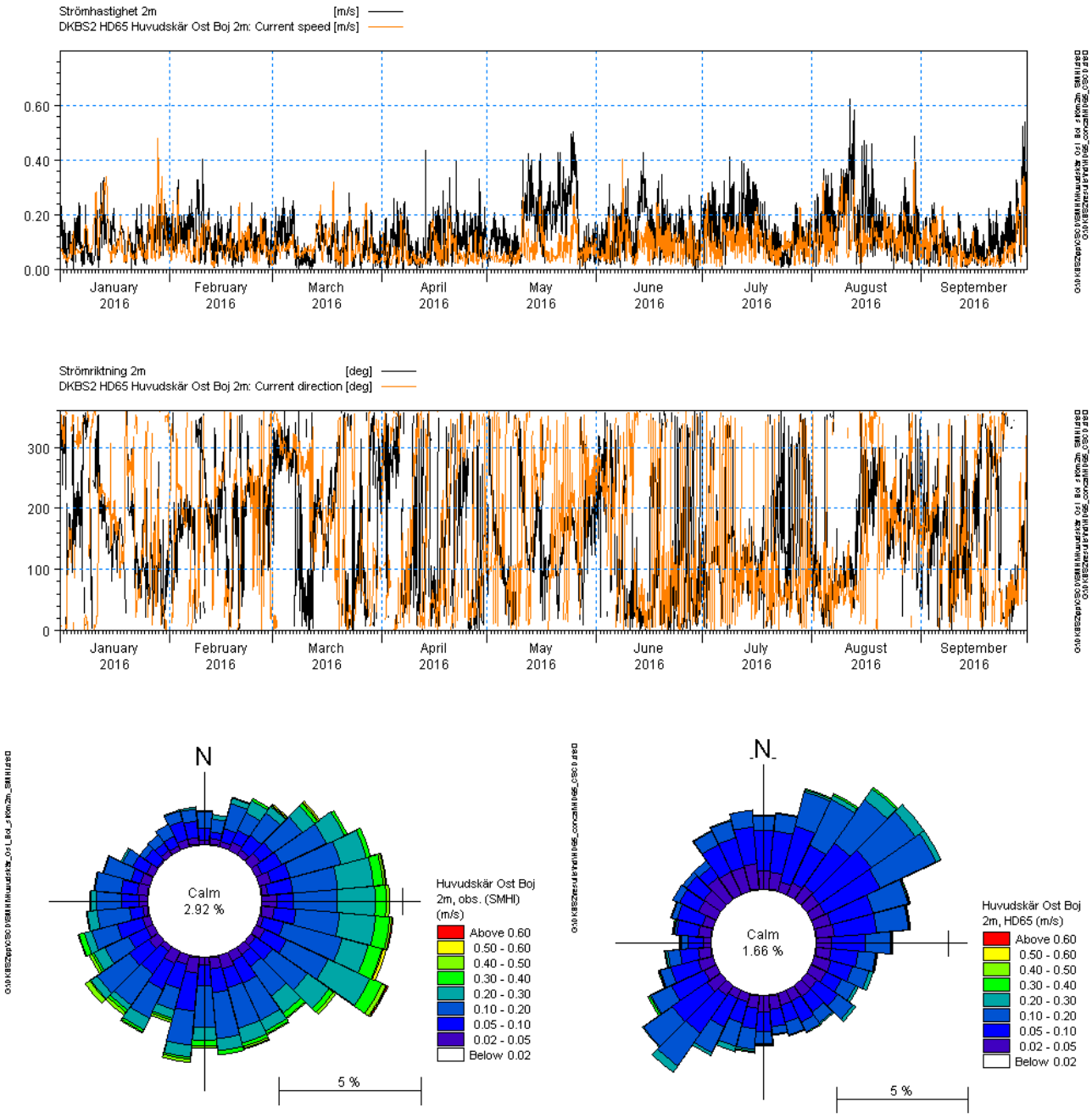

Figure B- 16 Comparison of measured and modelled current at Huvudskär Ost Boj at depth 2m.

B.3 Stratification

B.3.1 Measured salinity and water temperature

Modelled salinity and water temperature time series have been compared to measurements in a number of stations. In Figure B- 17 the location of the salinity and water temperature measurement stations is shown, and the time series comparisons are shown in the figures below.

Notice that all figures compare both surface and bottom values, and some also compare medium depth values.

The measurements and model results show a good agreement hereby demonstrating the ability of the model to simulate the water temperature and salinity in terms of both short-term, seasonal and inter-annual variability, gradients from east to west as well as the pronounced stratification within the model area.

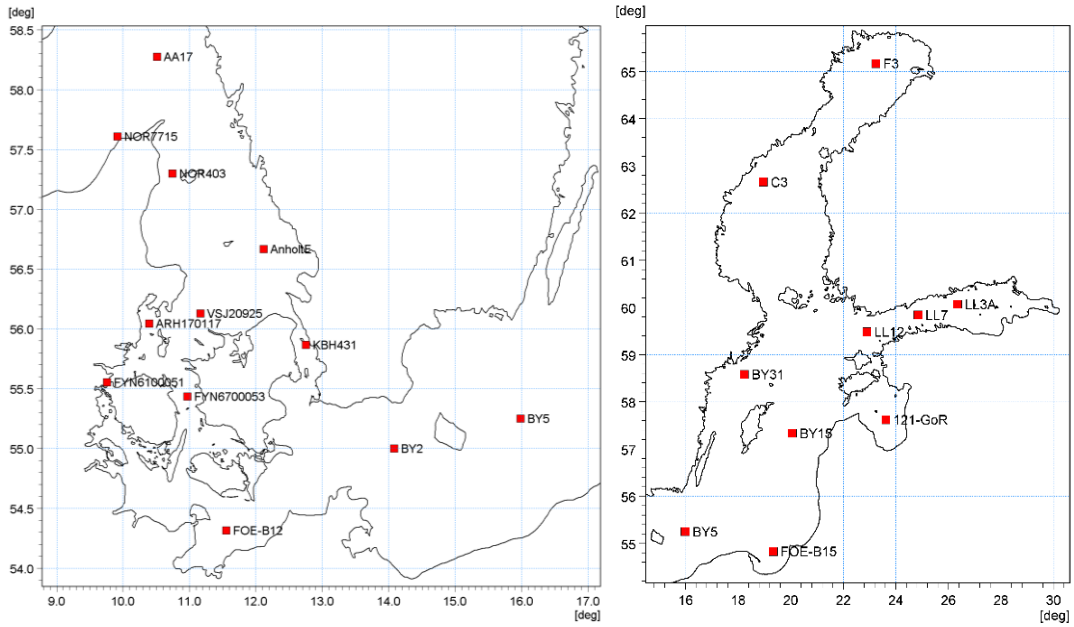

Figure B- 17 Location of salinity and temperature measurement stations.

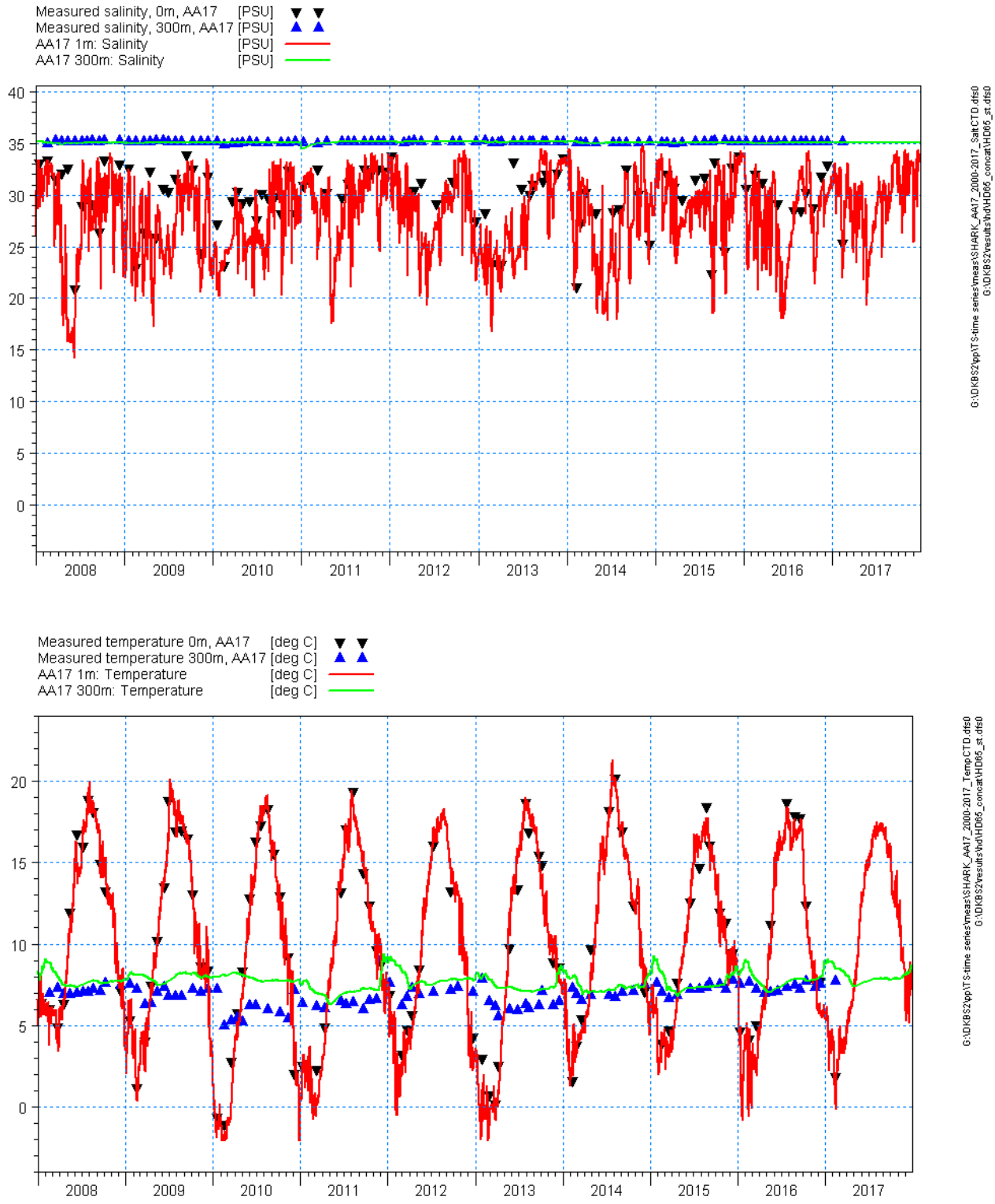

Figure B- 18 Comparison of measured and modelled salinity (top) and water temperature (bottom) at AA17 station.

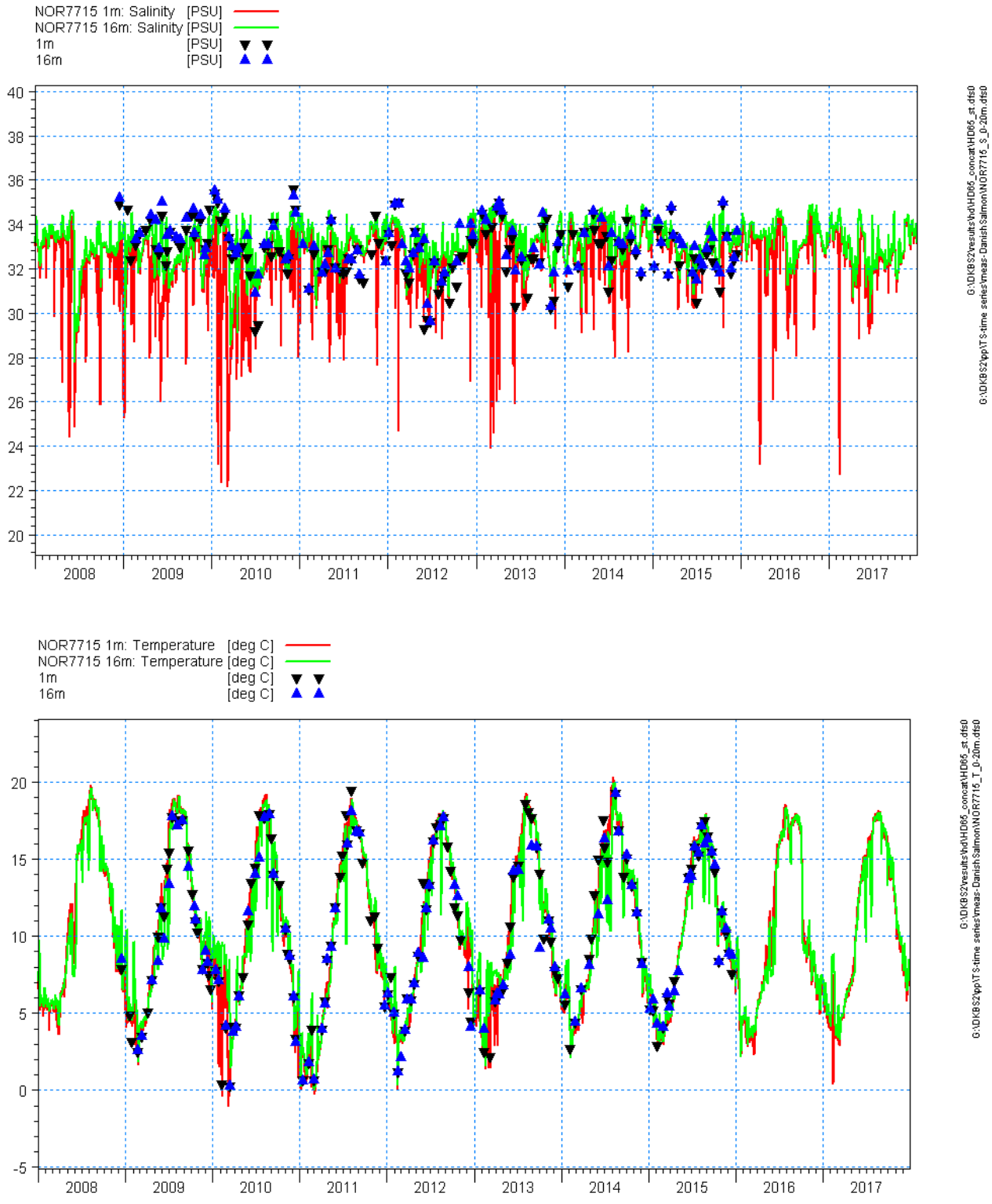

Figure B- 19 Comparison of measured and modelled salinity (top) and water temperature (bottom) at NOR7715 station

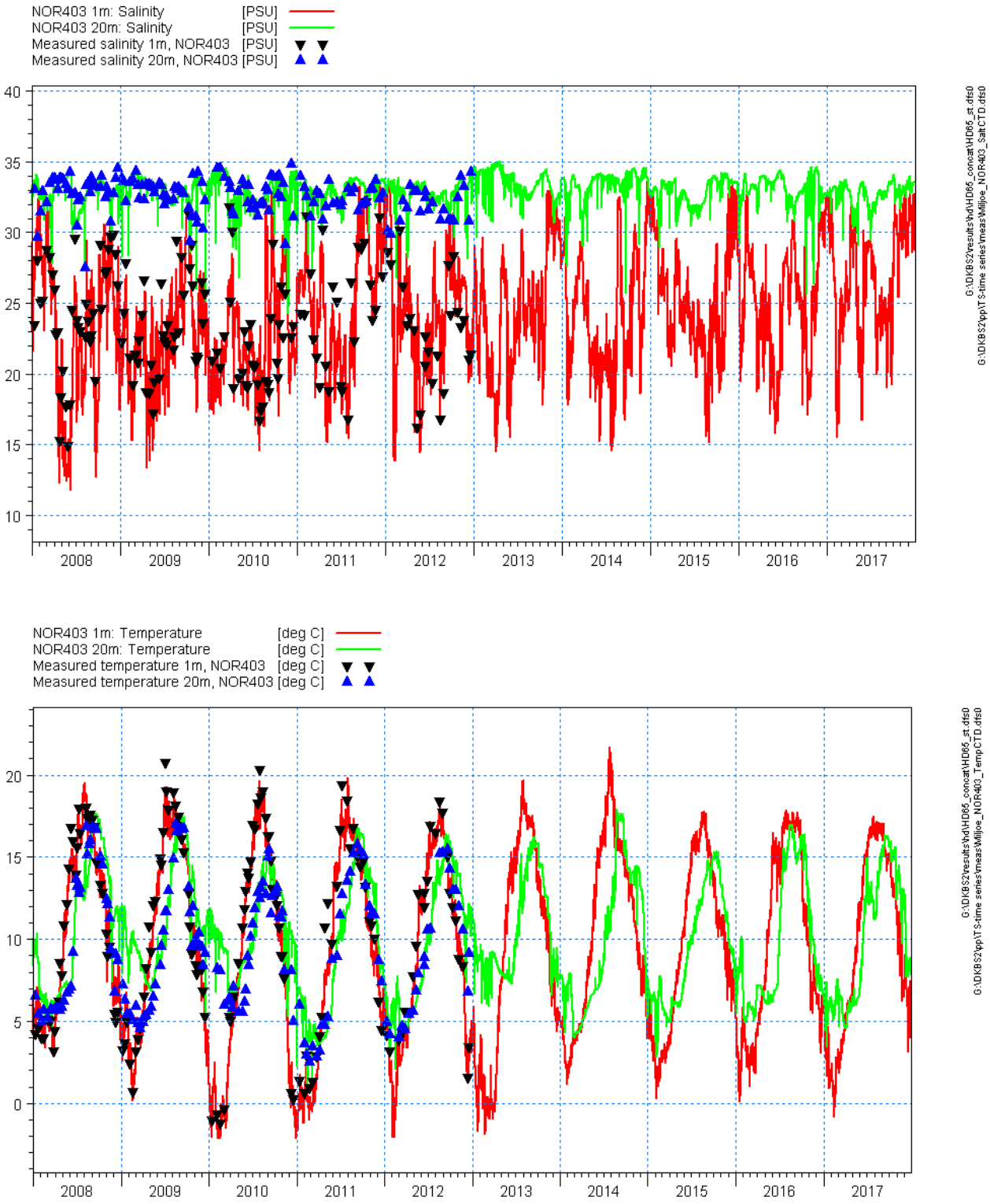

Figure B- 20 Comparison of measured and modelled salinity (top) and water temperature (bottom) at NOR403 station

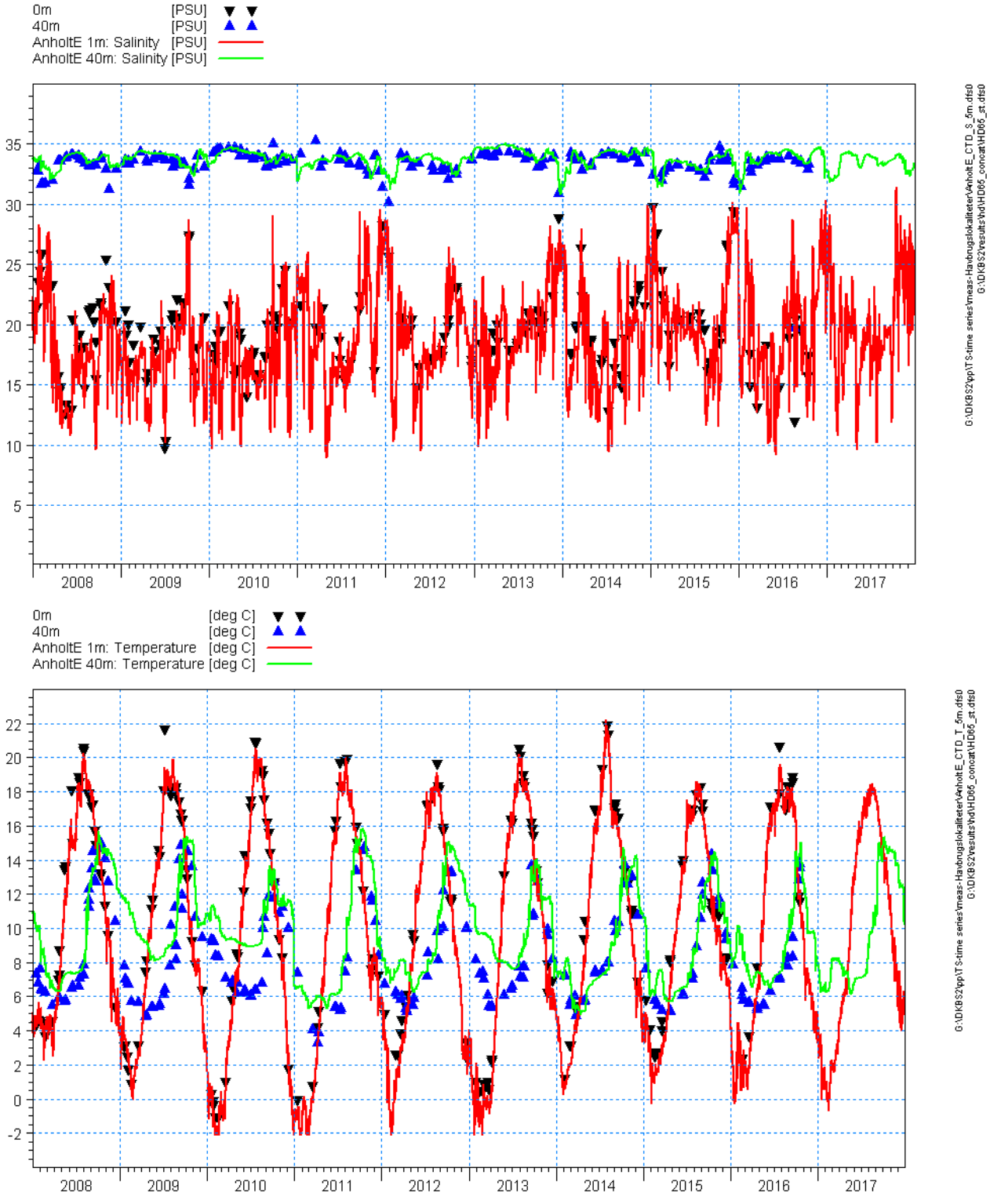

Figure B- 21 Comparison of measured and modelled salinity (top) and water temperature (bottom) at Anholt E station

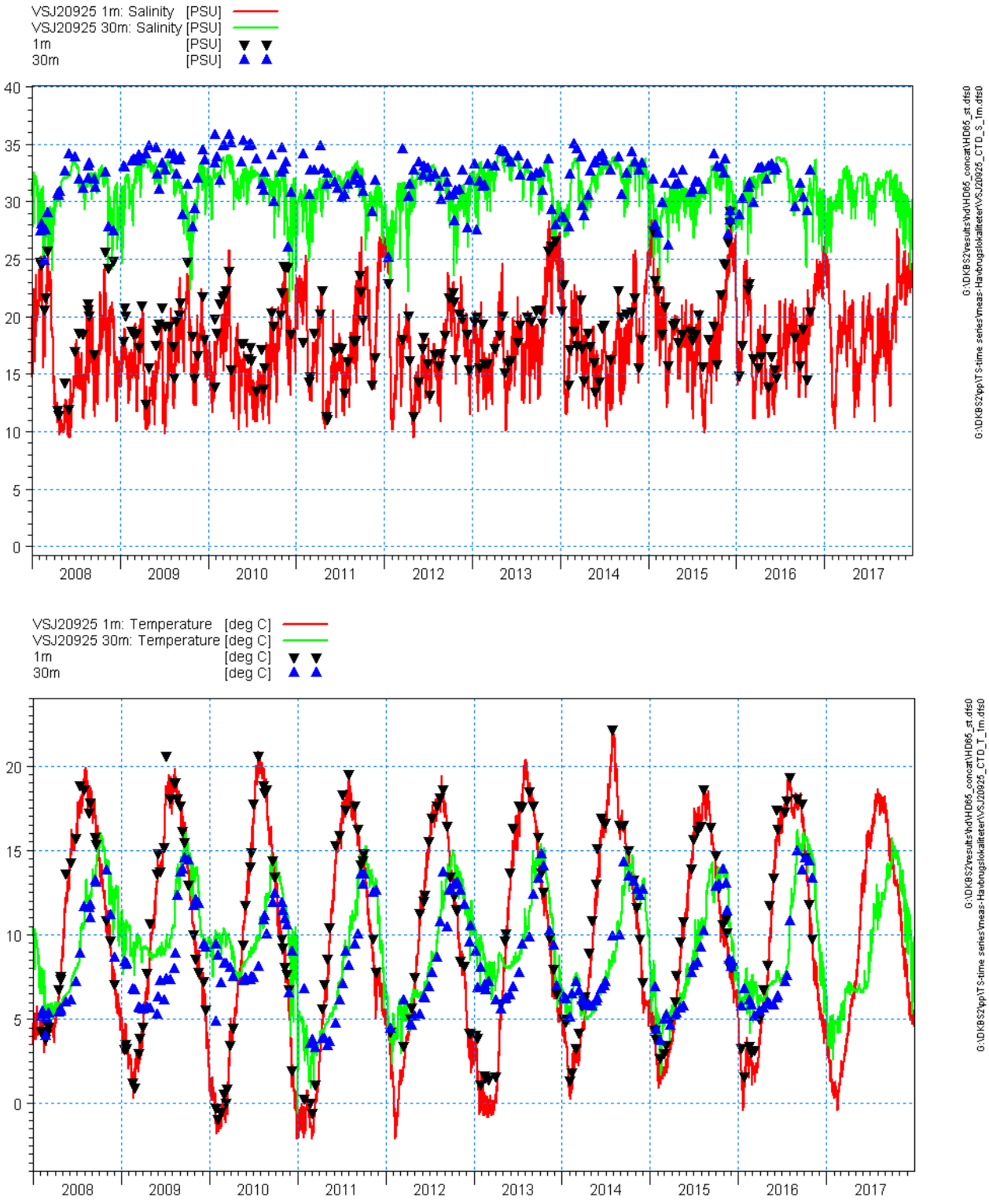

Figure B- 22 Comparison of measured and modelled salinity (top) and water temperature (bottom) at VSJ20925 station

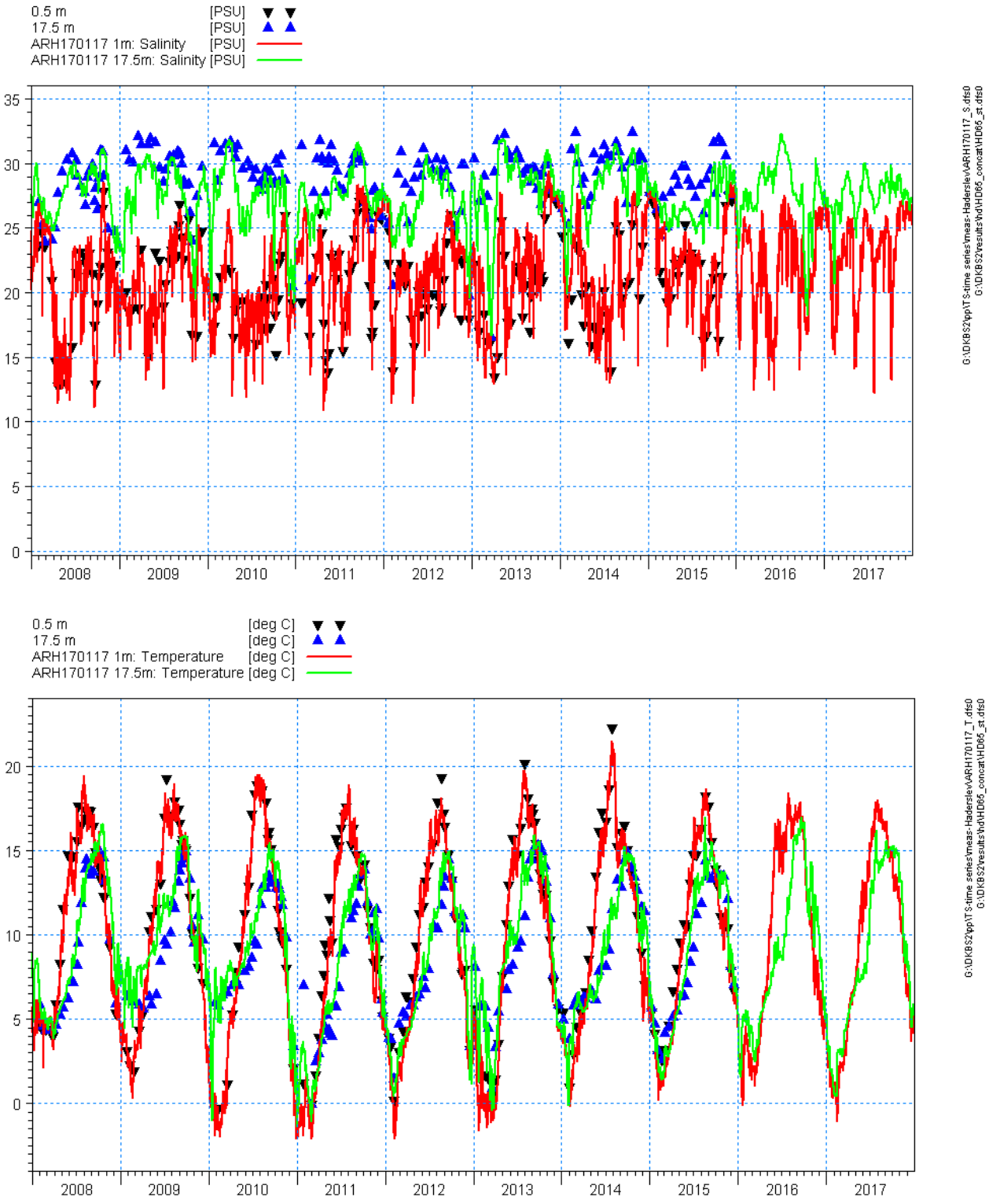

Figure B- 23 Comparison of measured and modelled salinity (top) and water temperature (bottom) at ARH70117 station

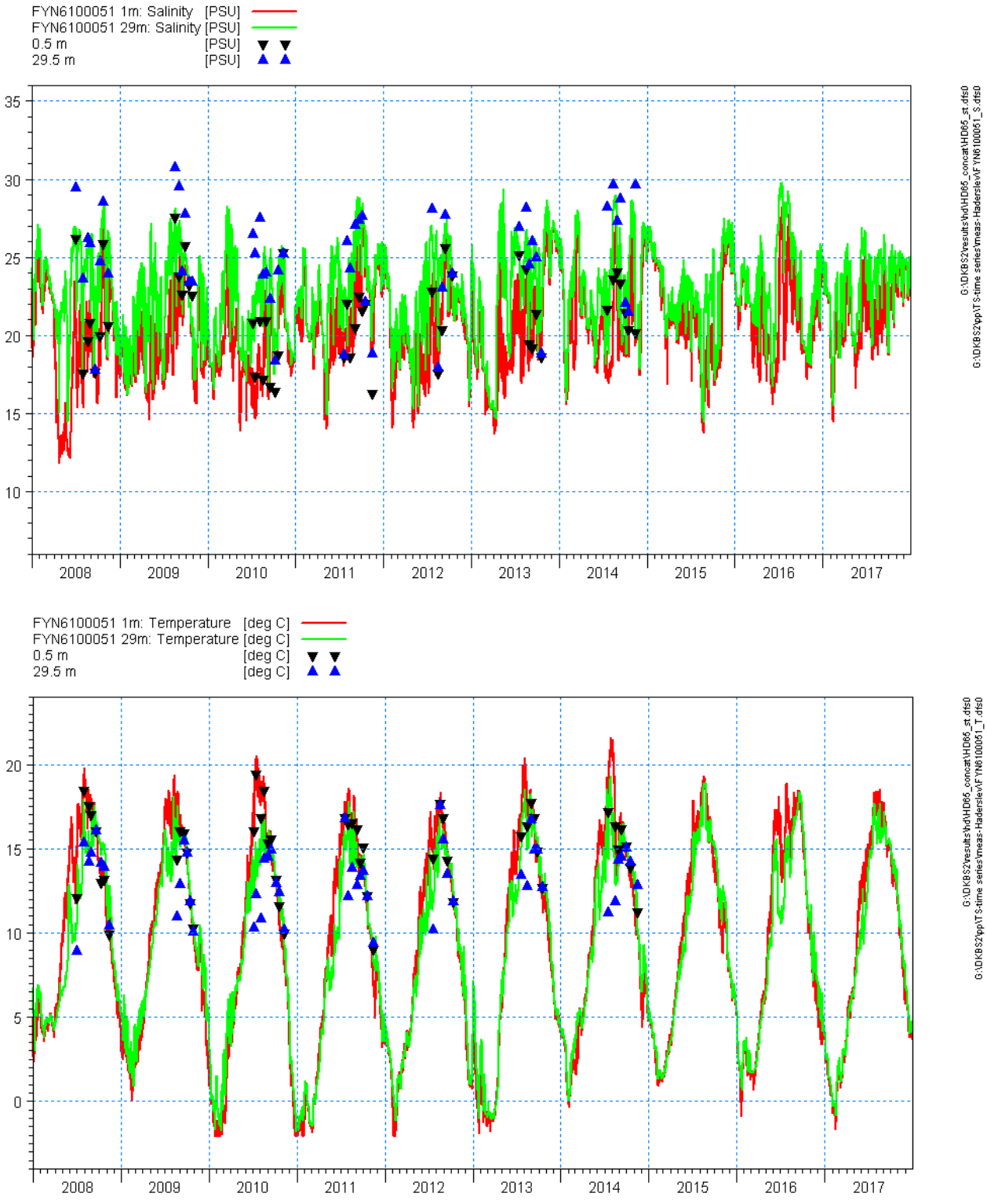

Figure B- 24 Comparison of measured and modelled salinity (top) and water temperature (bottom) at FYN6100051 station

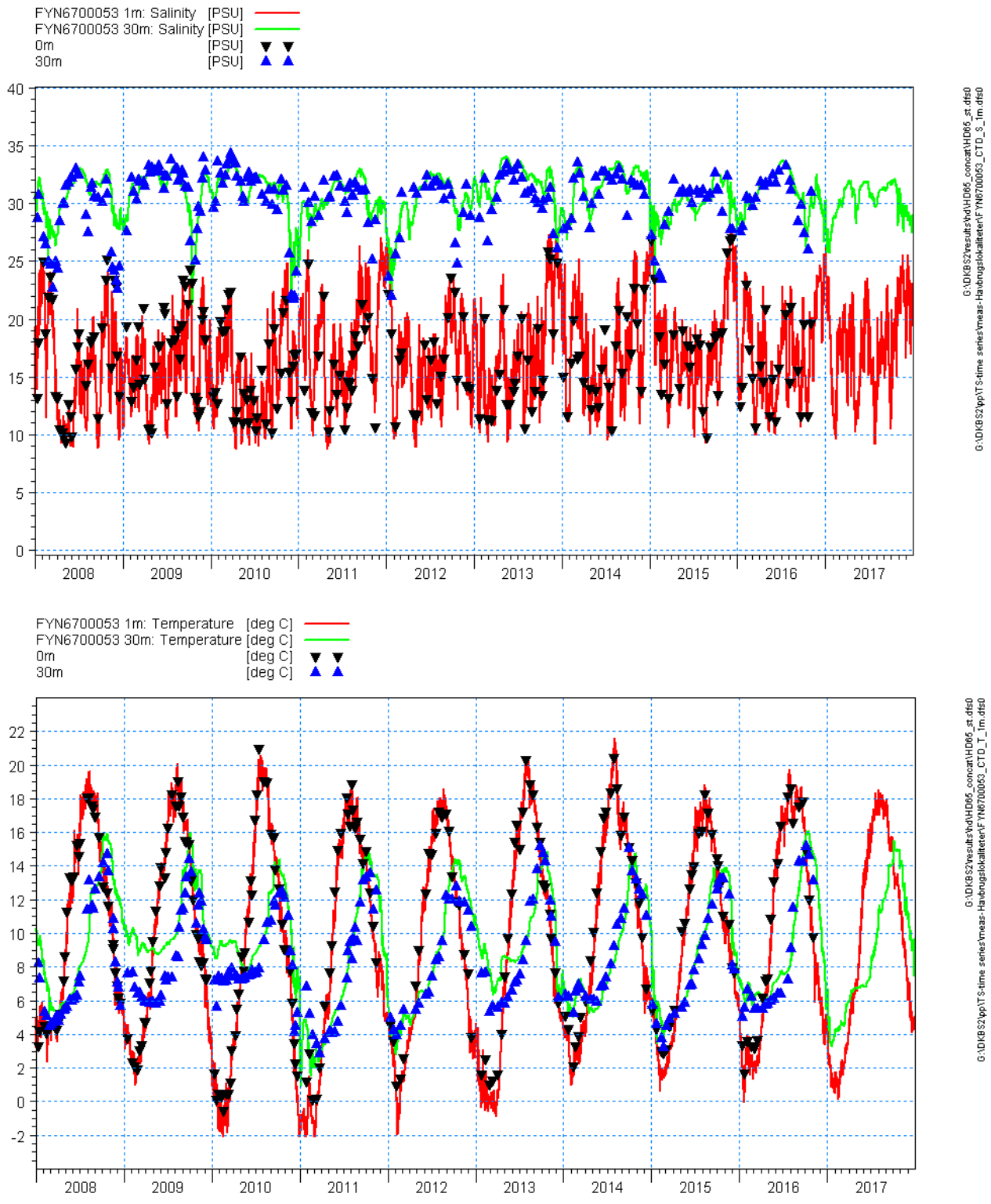

Figure B- 25 Comparison of measured and modelled salinity (top) and water temperature (bottom) at FYN6700053 station

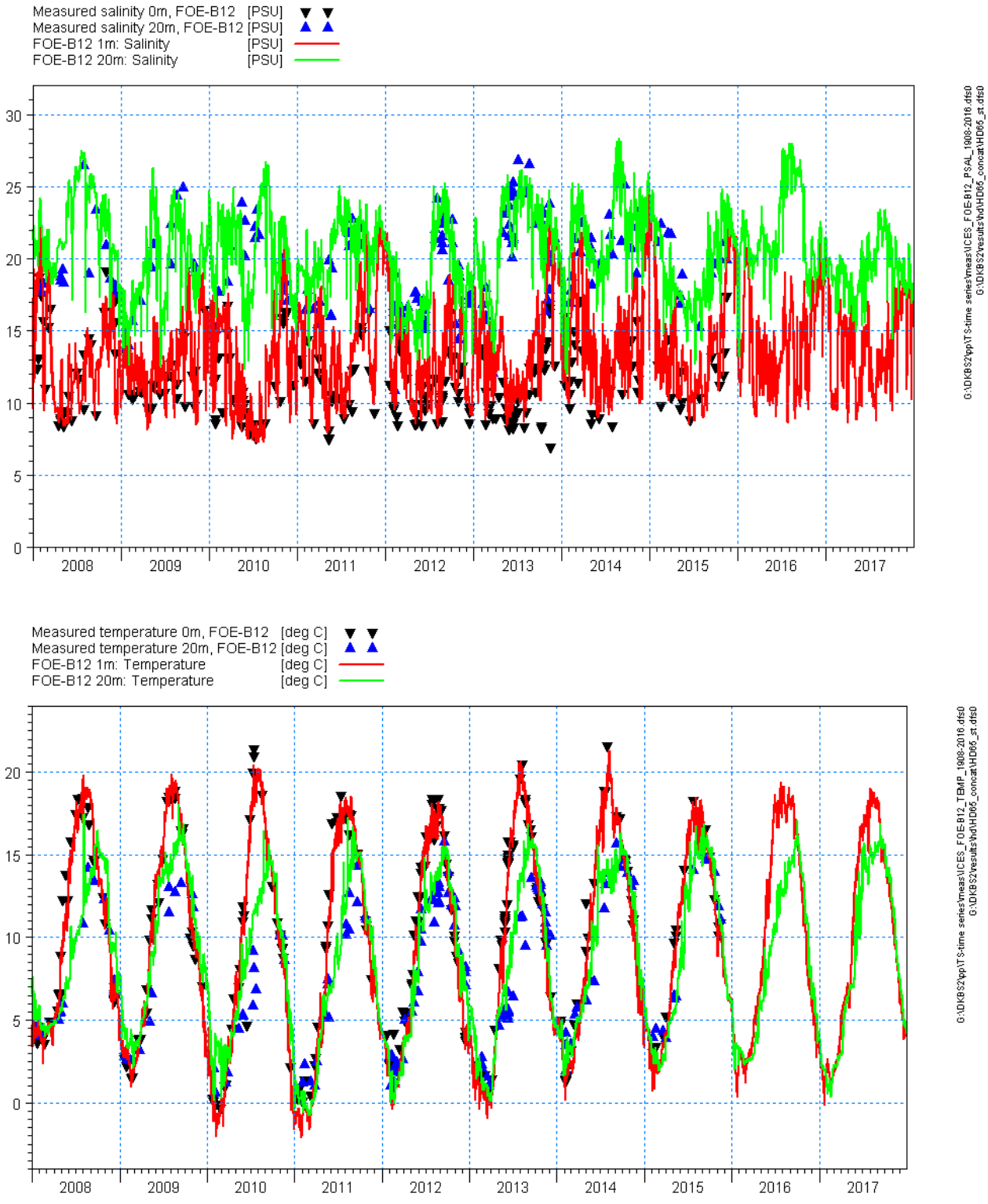

Figure B- 26 Comparison of measured and modelled salinity (top) and water temperature (bottom) at FOE-B12 station

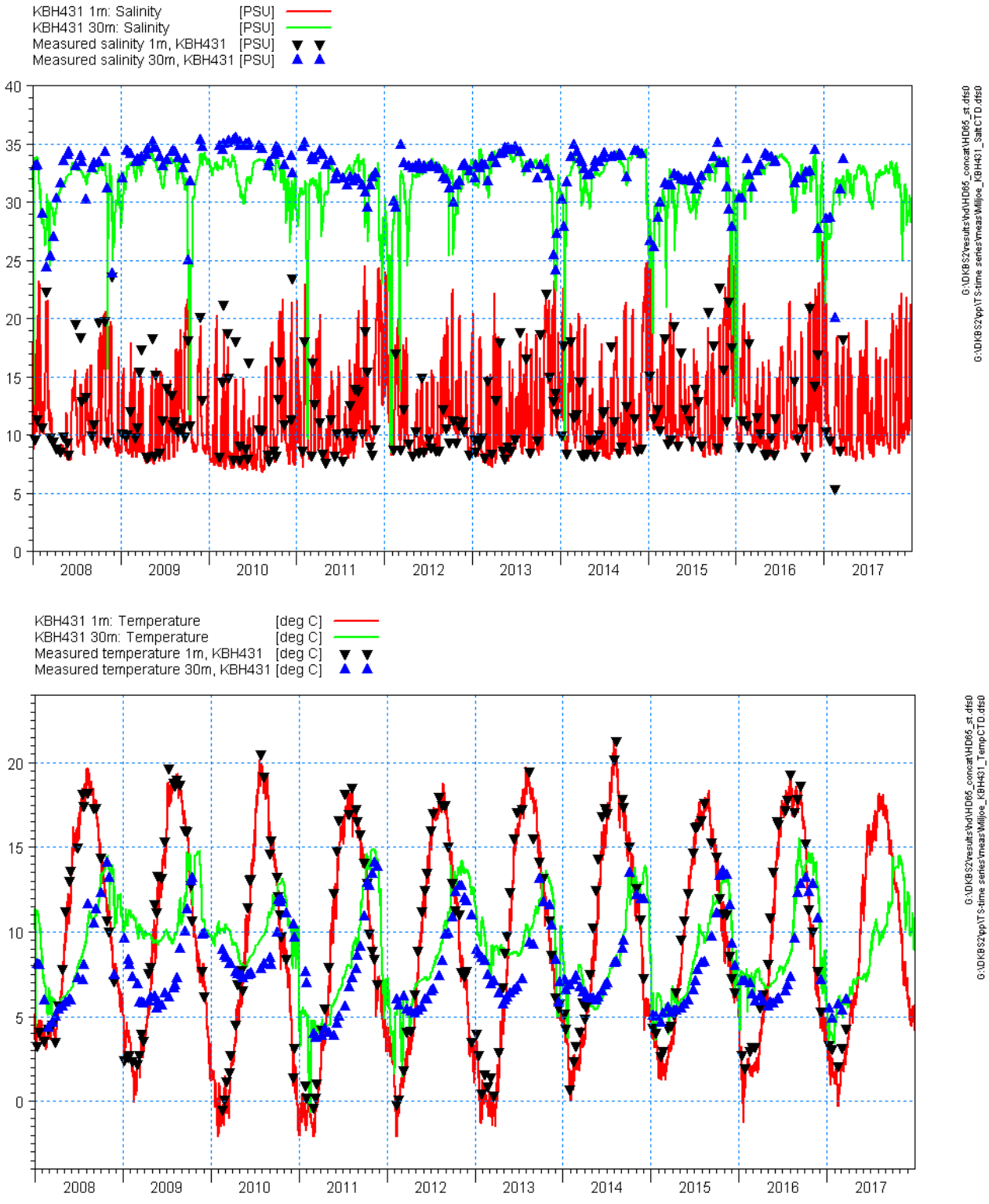

Figure B- 27Comparison of measured and modelled salinity (top) and water temperature (bottom) at KBH431 station.

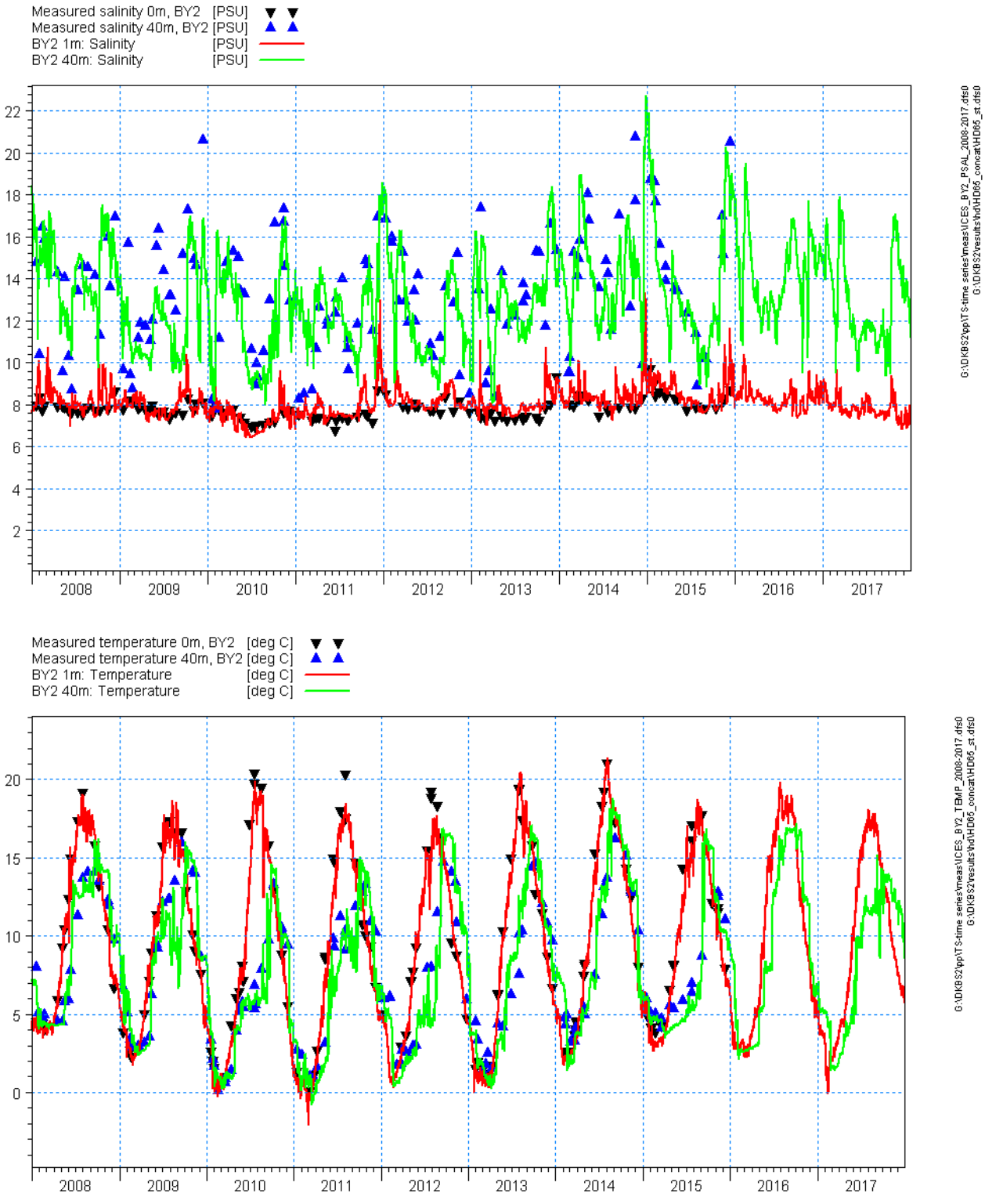

Figure B- 28 Comparison of measured and modelled salinity (top) and water temperature (bottom) at BY2 station.

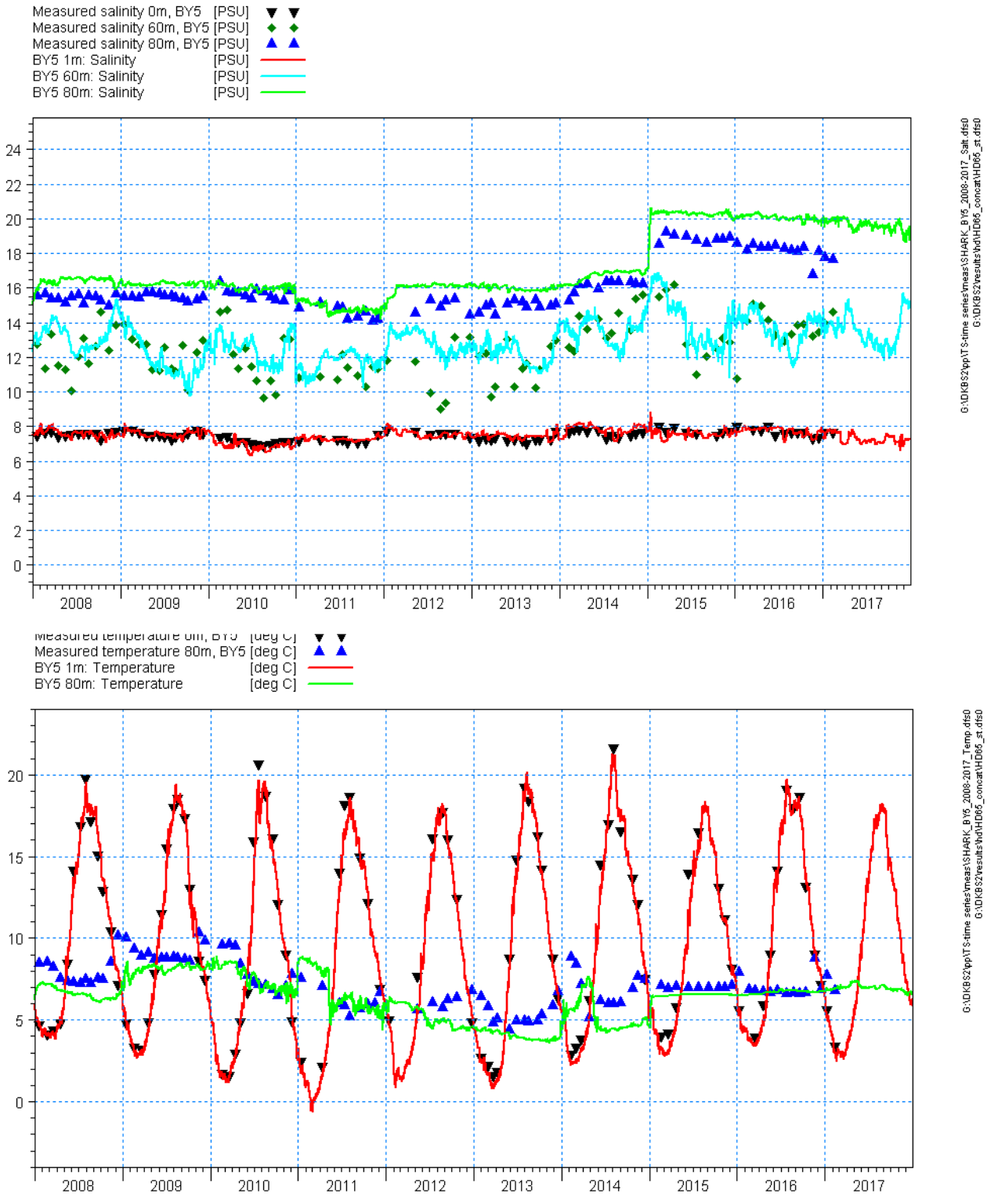

Figure B- 29 Comparison of measured and modelled salinity (top) and water temperature (bottom) at BY5 station.

B.4 Conclusion

A new version of DHI's Kattegat, Belt Sea and Baltic Sea model called DKBS2 has been established and validated.

The model has been executed for the period 2008-2017 (10 years). The present report summarizes the model setup and demonstrates the ability of the model to simulate water level variation, circulation and stratification of the system.

B.5 References

Cheng Y. and O.B. Andersen (2010). Improvement in global ocean tide model in shallow water regions. Altimetry for Oceans and Hydrology OST-ST Meeting, Lisbon (2010) (Poster, SV.1-68 45)

DHI (2017). MIKE 21 & MIKE 3 FLOW MODEL FM, Hydrodynamic and Transport Module, Scientific Documentation. MIKE Powered by DHI 2017.

FEHY 2011. Fehmarnbelt Fixed Link EIA. Marine Water Baseline. Hydrography of the Fehmarnbelt area. Report No E1TR0028. August 2011

Flather, R. A. (1976). A tidal model of the northwest European continental shelf. Memo. Soc. Roy. Sci. Liege, 6 (10), 141–164.

C APPENDIX C – Model Results

C.1 North Sea

C.1.1 Red-throated/Black-throated Diver

Table C- 1 Smooth terms, adjusted R-squared and evaluation statistics for the distribution models for Red-throated/Black-throated Diver *Gavia stellate/arctica* in the North Sea. F statistics and the approximate significance for the smooth terms and t-statistic and the significance for the parametric terms are shown.

	Presence/absence			Positive density		
	Estimate	t	p-value	Estimate	t	p-value
Parametric terms						
March	-0.167	-2.004	0.045	-0.004	-0.036	0.971
April	0.362	2.656	0.008	-0.214	-1.321	0.187
May	0.026	0.200	0.842	-0.316	-1.996	0.046
August	-0.981	-8.864	0	-0.13	-0.714	0.475
		F	p-value		F	p-value
Salinity (surface)		27.383	0		4.967	0.026
Current speed (surface)		8.416	0			
Distance shipping lane		28.760	0			
Depth		14.016	0		8.006	0
Distance HR1		39.149	0		2.865	0.091
Chlorophyll *a*		13.873	0		13.214	0
R-sq.(adj)	0.025			0.014		
AUC	0.629					
Spearman´s corr.				0.100		
Sample (n)	19227			2199		

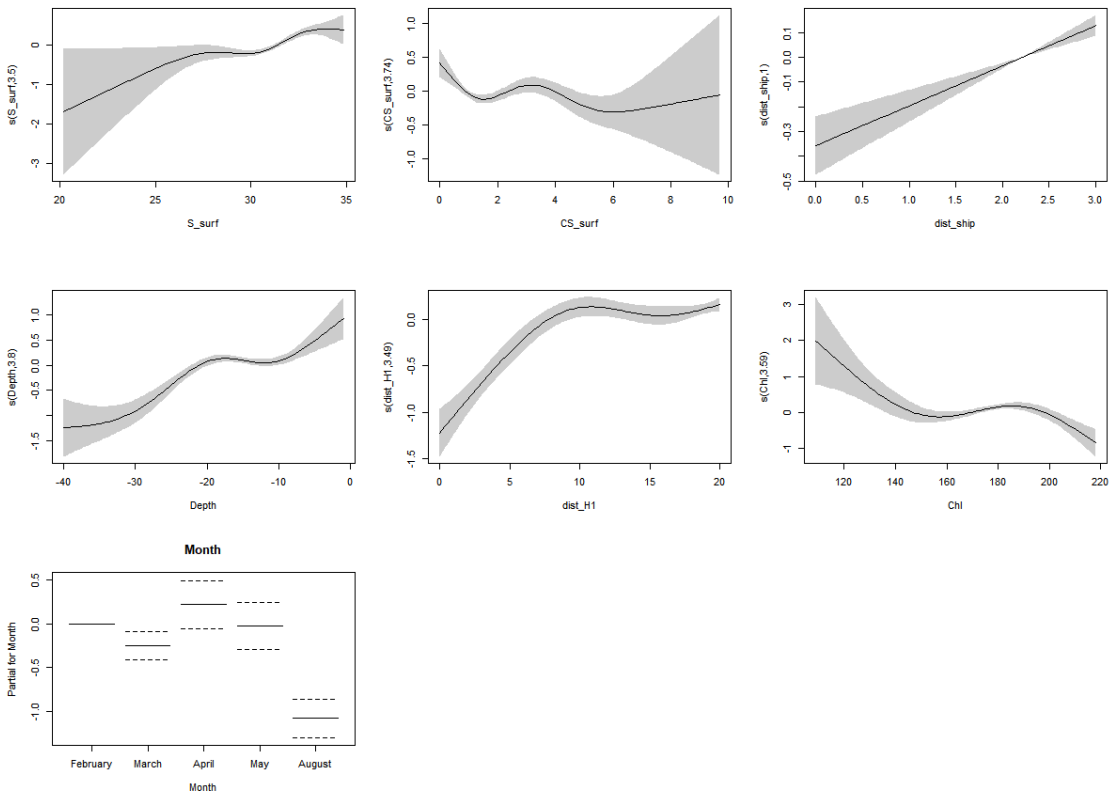

Figure C- 1 Response curves for presence absence model parts for Red-throated/Black-throated Diver *Gavia stellate/arctica* in the North Sea.

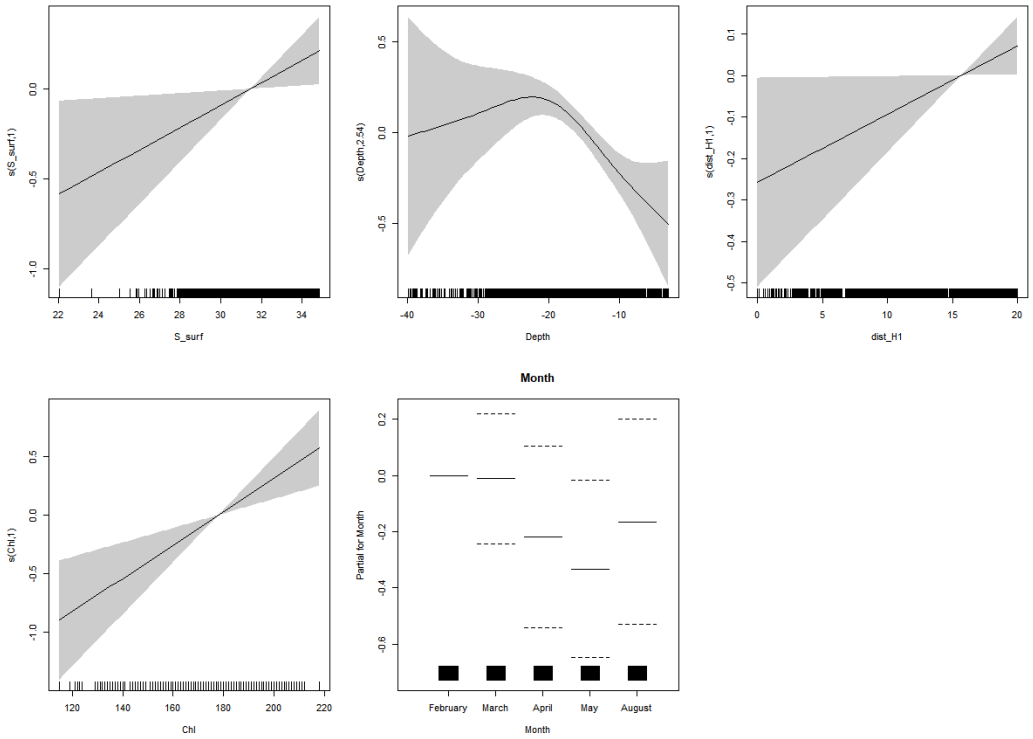

Figure C- 2 Response curves for positive model parts for Red-throated/Black-throated Diver *Gavia stellate/arctica* in the North Sea.

C.1.2 Common Scoter

Table C- 2 Smooth terms, adjusted R-squared and evaluation statistics for the distribution models for Common Scoter *Melanitta nigra* in the North Sea. F statistics and the approximate significance for the smooth terms and t-statistic and the significance for the parametric terms are shown.

	Presence/absence			Positive density		
	Estimate	t	p-value	Estimate	t	p-value
Parametric terms						
February	-0.550	-4.930	0	-0.238	-1.607	0.108
March	-0.455	-4.249	0	0.089	0.660	0.509
April	-1.011	-9.313	0	-0.017	-0.116	0.908
November	-1.004	-8.178	0	-0.415	-2.339	0.019
December	-0.695	-5.017	0	-0.032	-0.167	0.867
		F	p-value		F	p-value
Salinity (bottom)		16.273	0		6.122	0.001
Current speed (bottom)		6.746	0		11.422	0
Depth		1481.053	0		23.424	0
Distance shipping lane					13.619	0
Distance HR1		40.126	0			
Distance HR2		9.274	0		7.973	0
X coordinate					12.007	0
R-sq.(adj	0.100			0.039		
AUC	0.740					
Spearman´s corr.				0.156		
Sample (n)	20632			3649		

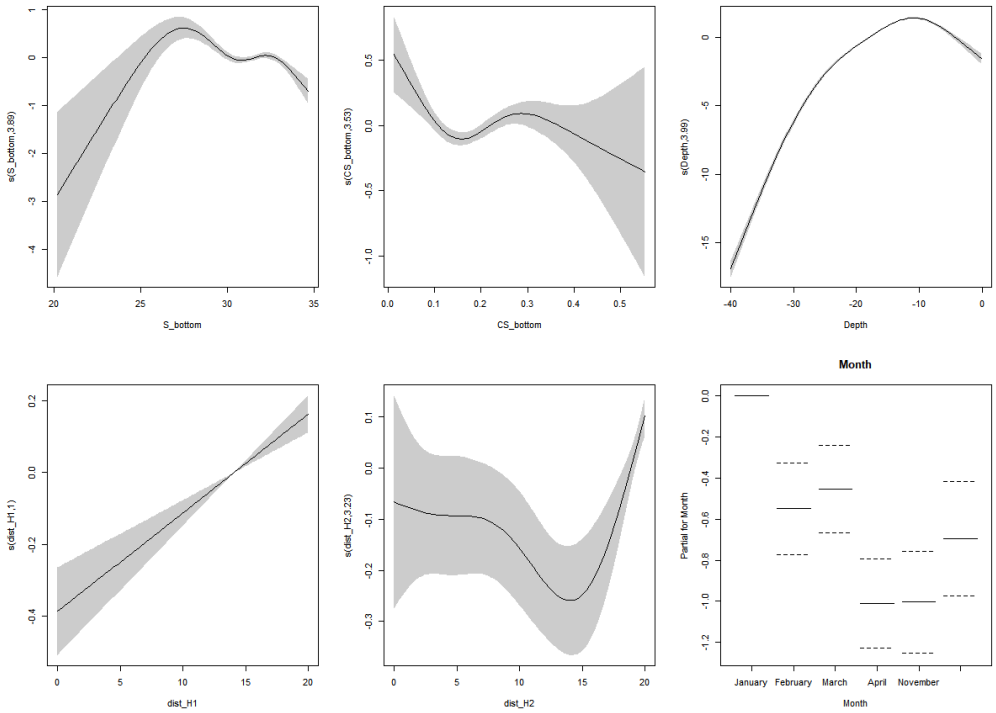

Figure C- 3 Response curves for presence absence model parts for Common Scoter *Melanitta nigra* in the North Sea.

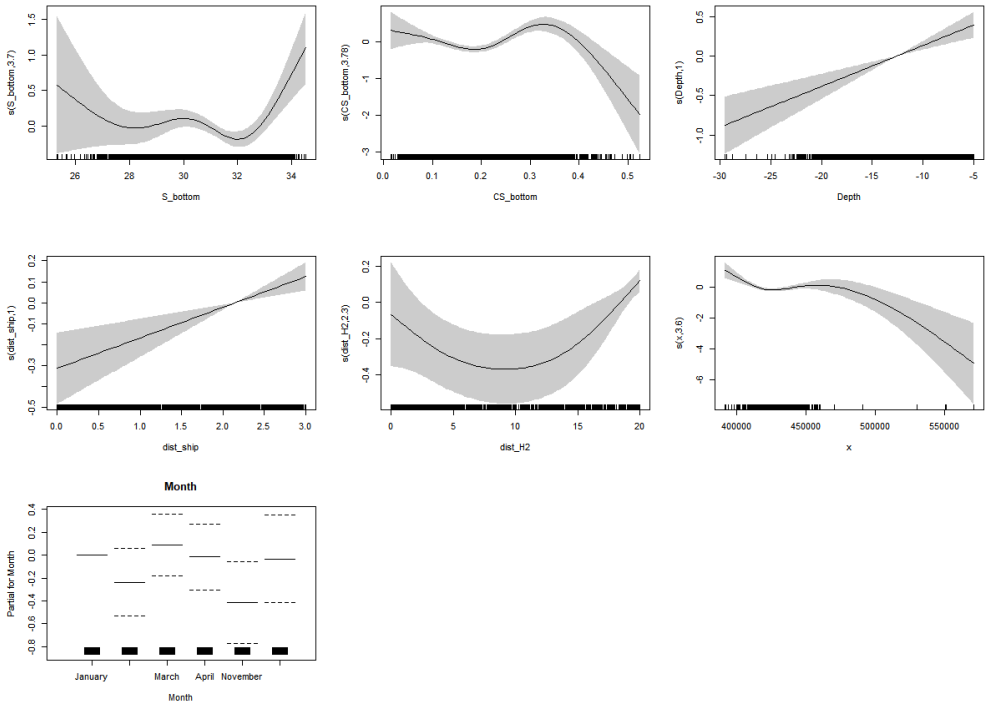

Figure C- 4 Response curves for positive model parts for Common Scoter *Melanitta nigra* in the North Sea.

C.2 Kattegat

C.2.1 Red-throated/Black-throated Diver

Table C- 3 Smooth terms, adjusted R-squared and evaluation statistics for the distribution models for Red-throated/Black-throated Diver *Gavia stellata/arctica* in the southern Kattegat. F statistics and the approximate significance for the smooth terms and t-statistic and the significance for the parametric terms are shown.

	Presence/absence			Positive density		
	Estimate	t	p-value	Estimate	t	p-value
Parametric terms						
Winter	-2.970	-16.135	0	1.307	12.313	0
Spring	0.490	0.713	0.476	0.15	0.213	0.832
Summer	-2.853	-6.073	0	-1.23	-1.985	0.049
		F	p-value		F	p-value
Salinity (surface)		3.161	0.076		3.023	0.052
Current speed (surface)		7.481	0.006			
Eddy activity					3.877	0.018
Depth		4.766	0.001			
R-sq.(adj)	0.020			0.026		
AUC	0.702					
Spearman´s corr.				0.129		
Sample (n)	3155			157		

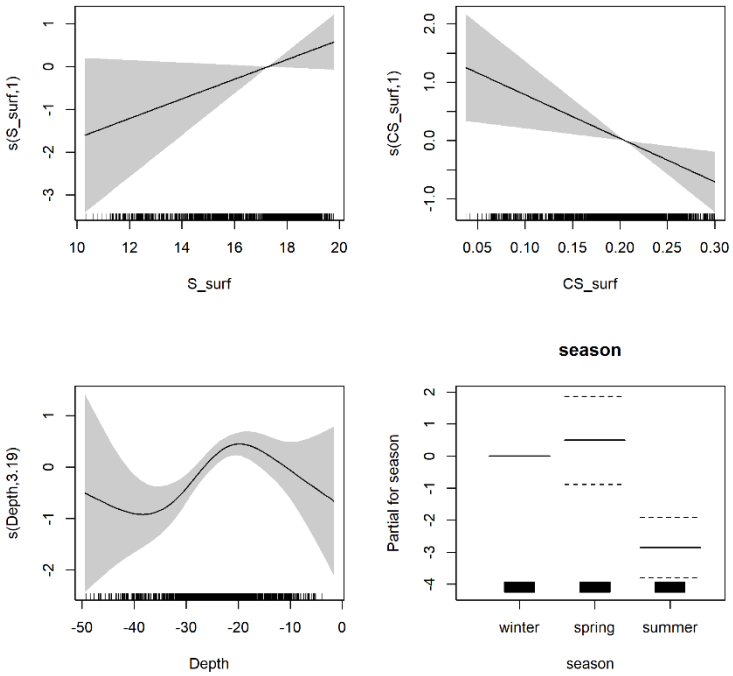

Figure C- 5 Response curves for presence absence model parts for Red-throated/Black-throated Diver *Gavia stellata/arctica* in the southern Kattegat.

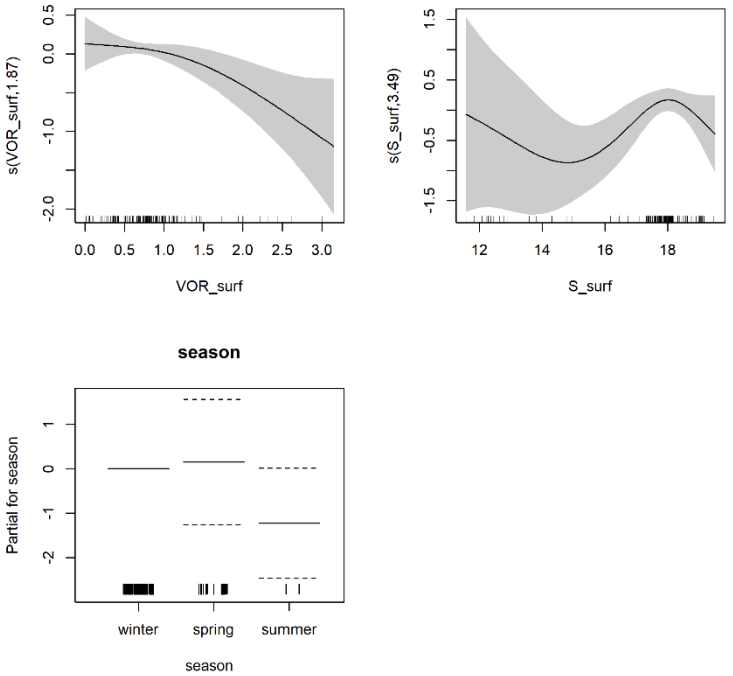

Figure C- 6 Response curves for positive model parts for Red-throated/Black-throated Diver *Gavia stellata/arctica* in the southern Kattegat.

C.2.2 Common Eider

Table C- 4 Smooth terms, adjusted R-squared and evaluation statistics for the distribution models for Common Eider *Somateria mollissima* in the southern Kattegat. F statistics and the approximate significance for the smooth terms and t-statistic and the significance for the parametric terms are shown.

	Presence/absence			Positive density		
	Estimate	t	p-value	Estimate	t	p-value
Parametric terms						
Winter	-2.172	-13.225	0	2.593	28.515	0
Spring	-1.294	-3.126	0.002	0.185	0.424	0.672
Summer	-3.898	-8.857	0	-1.883	-1.297	0.196
		F	p-value		F	p-value
Current speed (surface)		21.188	0		7.856	0
Filter feeder index		26.162	0			
R-sq.(adj)	0.051			0.053		
AUC	0.717					
Spearman´s corr.				0.171		
Sample (n)	3173			287		

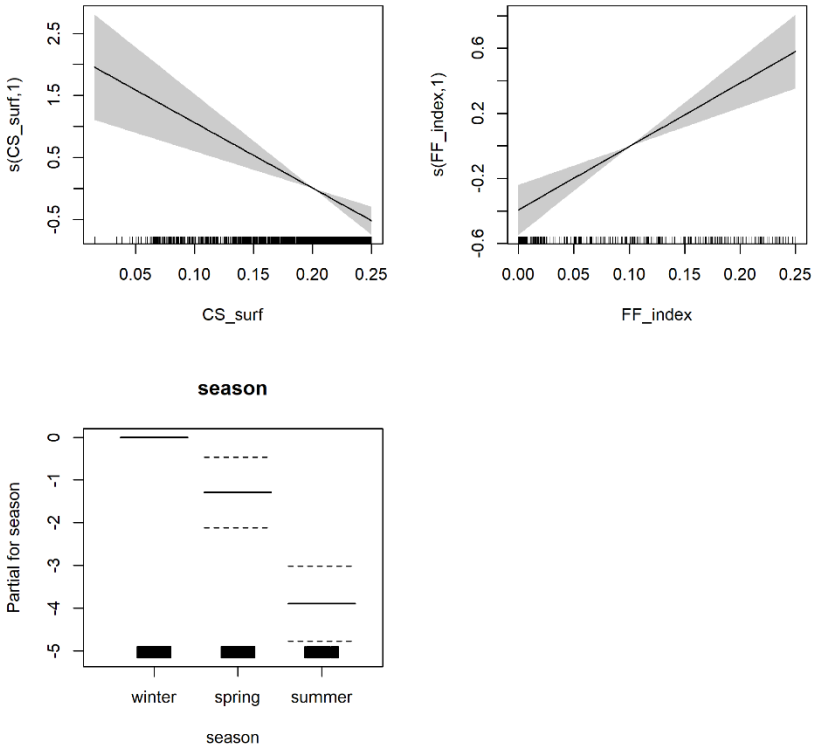

Figure C- 7 Response curves for presence absence model parts for Common Eider *Somateria mollissima*

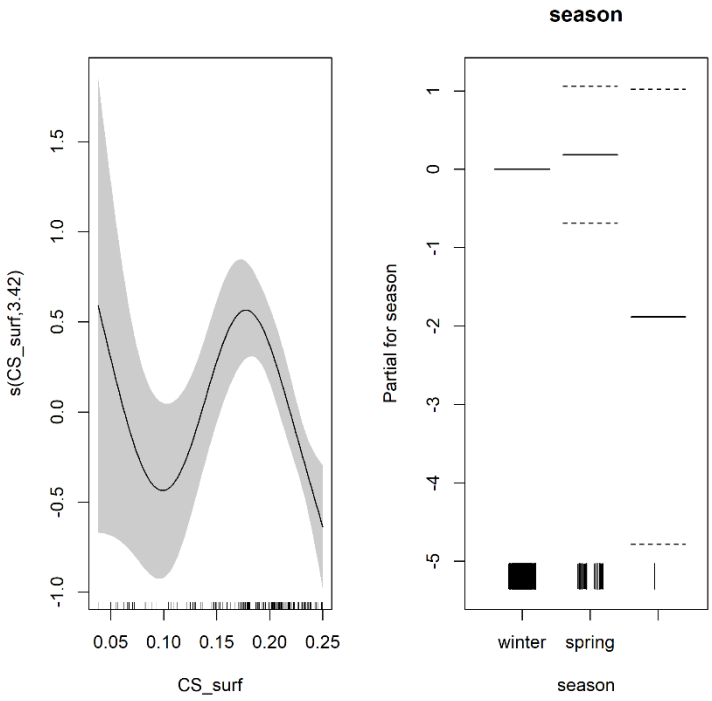

Figure C- 8 Response curves for positive model parts for Common Eider *Somateria mollissima*

C.2.3 Common Scoter

Table C- 5 Smooth terms, adjusted R-squared and evaluation statistics for the distribution models for Common Scoter *Melanitta nigra* in the southern Kattegat. F statistics and the approximate significance for the smooth terms and t-statistic and the significance for the parametric terms are shown.

	Presence/absence			Positive density		
	Estimate	t	p-value	Estimate	t	p-value
Parametric terms						
Winter	-3.884	-15.79	0	3.788	17.004	0
Spring	-1.354	-1.996	0.046	-0.879	-1.181	0.241
		F	p-value		F	p-value
Current speed (surface)		13.146	0			
Filter feeding index		20.653	0			
Distance shipping lane					1.55	0.217
R-sq.(adj)	0.030			-0.009		
AUC	0.809					
Spearman´s corr.				0.085		
Sample (n)	2889			78		

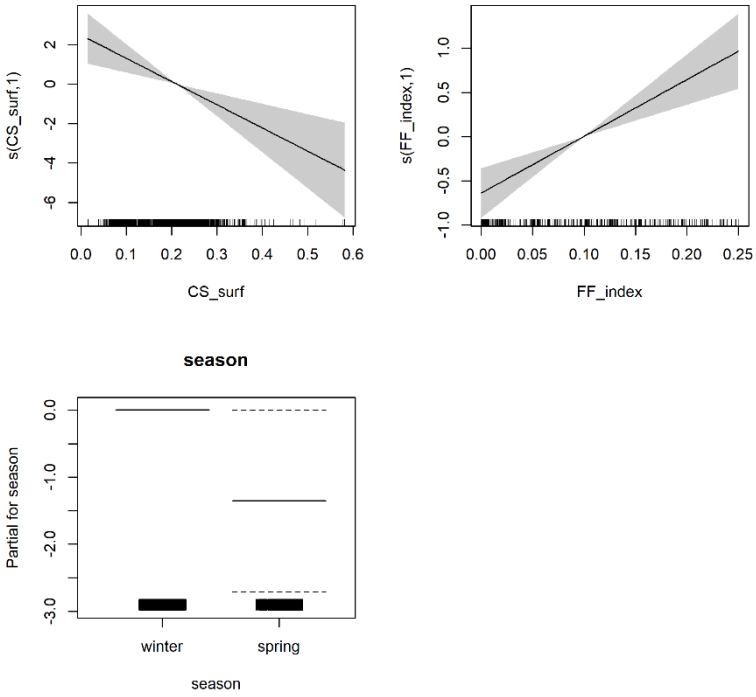

Figure C- 9 Response curves for presence absence model parts for Common Scoter *Melanitta nigra*

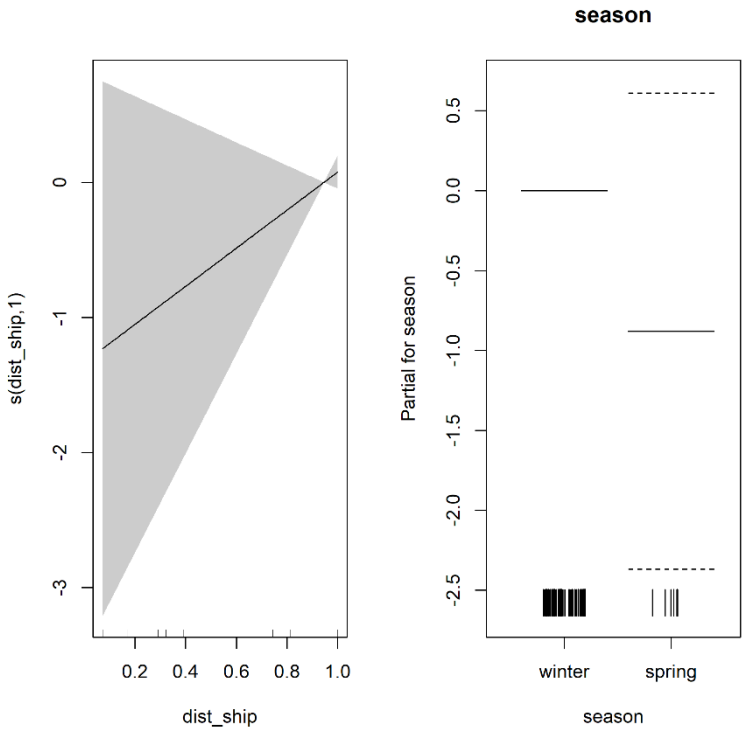

Figure C- 10 Response curves for positive model parts for Common Scoter *Melanitta nigra*

C.2.4 Velvet Scoter

Table C- 6 Smooth terms, adjusted R-squared and evaluation statistics for the distribution models for Velvet Scoter *Melanitta fusca* in the southern Kattegat. F statistics and the approximate significance for the smooth terms and t-statistic and the significance for the parametric terms are shown.

	Presence/absence			Positive density		
	Estimate	z	p-value	Estimate	t	p-value
Parametric terms						
Winter	-5.181	-16.791	0	2.092	10.546	0
Spring	-0.663	-0.968	0.333	-0.825	-1.416	0.171
		Chi.sq	p-value		F	p-value
Current speed (surface)		7.983	0.005			
Filter feeding index		9.283	0.008		8.144	0.009
R-sq.(adj)	0.004			0.031		
AUC	0.782					
Spearman´s corr.				0.061		
Sample (n)	2885			25		

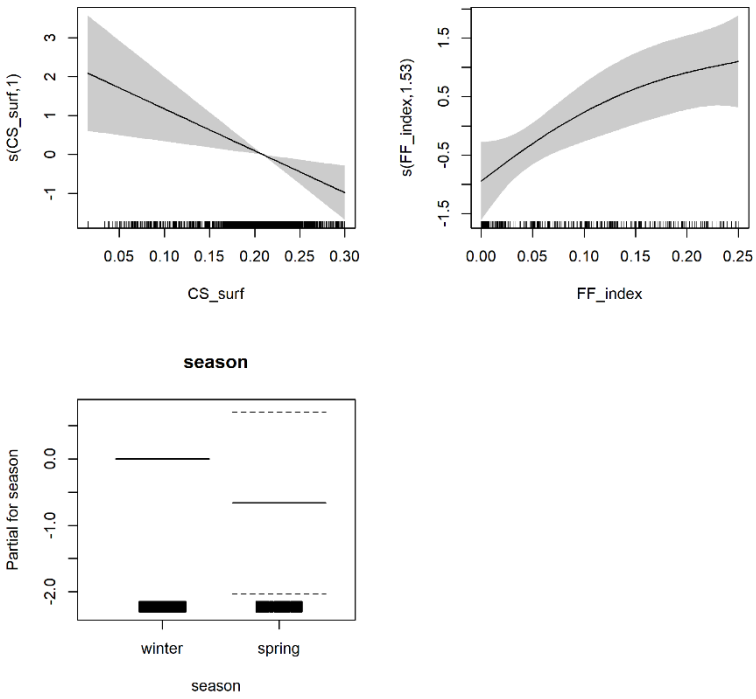

Figure C- 11 Response curves for presence absence model parts for Velvet Scoter *Melanitta fusca*

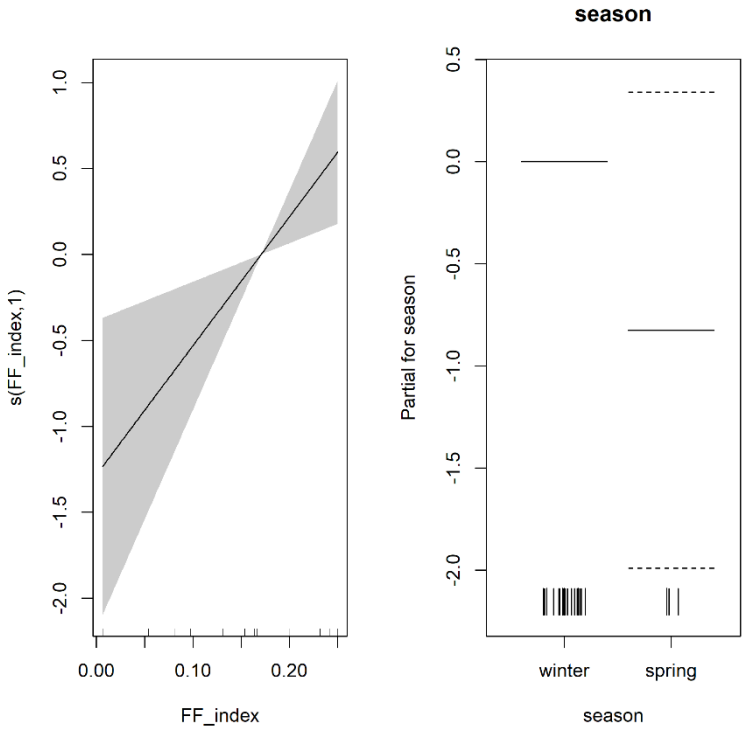

Figure C- 12 Response curves for positive model parts for Velvet Scoter *Melanitta fusca*

C.2.5 Black-legged Kittiwake

Table C- 7 Smooth terms, adjusted R-squared and evaluation statistics for the distribution models for Black-legged Kittiwake *Rissa tridactyla*. F statistics and the approximate significance for the smooth terms and t-statistic and the significance for the parametric terms are shown.

	Presence/absence			Positive density		
	Estimate	t	p-value	Estimate	t	p-value
Parametric terms						
Winter	-0.786	-1.179	0.238	-10.117	-1.823	0.069
Autumn	-0.220	-0.310	0.756	37.940	2.235	0.026
Salinity (surface)	-0.156	-1.453	0.146			
Depth	0.005	0.512	0.608			
Interaction salinity (surface): depth	-0.005	-4.341	0			
		F	p-value		F	p-value
Current speed (surface)		19.587	0		4.230	0.004
Salinity (surface)					3.944	0.004
Depth					6.733	0
R-sq.(adj)	0.114			0.044		
AUC	0.721					
Spearman´s corr.				0.139		
Sample (n)	2539			624		

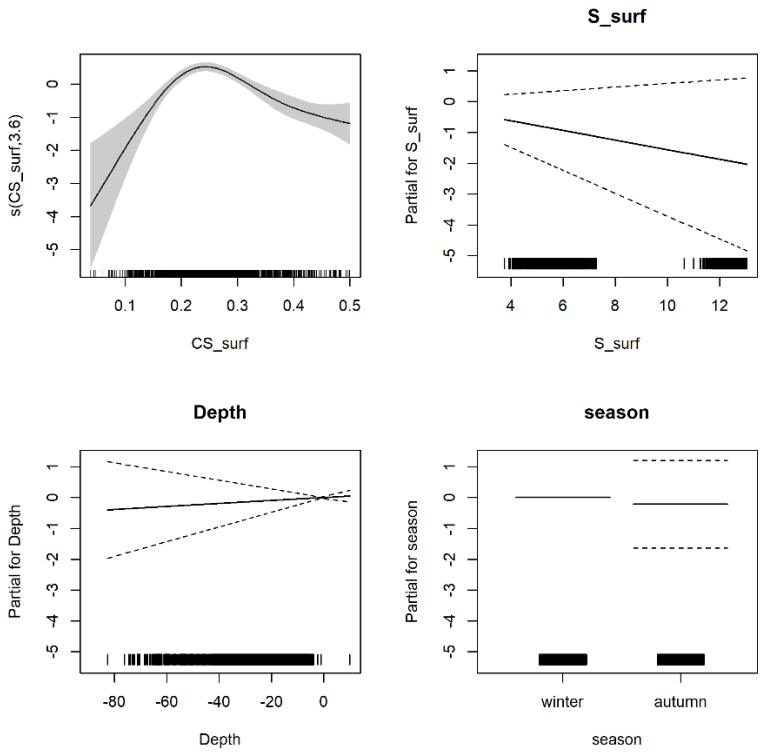

Figure C- 13 Response curves for presence absence model parts for Black-legged Kittiwake *Rissa tridactyla*

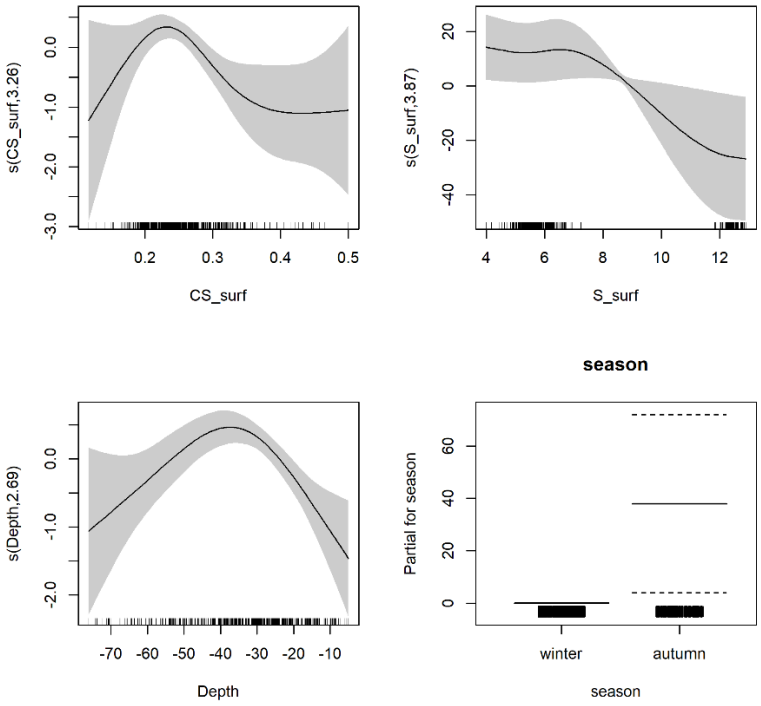

Figure C- 14 Response curves for positive model parts for Black-legged Kittiwake Rissa tridactyla

C.2.6 Razorbill

Table C- 8 Smooth terms, adjusted R-squared and evaluation statistics for the distribution models for Razorbill *Alca torda* in the southern Kattegat. F statistics and the approximate significance for the smooth terms and t-statistic and the significance for the parametric terms are shown.

	Presence/absence			Positive density		
	Estimate	z	p-value	Estimate	t	p-value
Parametric terms						
Winter	-1.086	-15.239	0	3.193	26.903	0
Autumn	-0.308	-3.030	0.002	0.384	1.868	0.062
		Chi.sq	p-value		F	p-value
Depth		4.678	0.031		6.449	0
Slope		4.967	0.09		3.296	0.009
Curve					2.606	0.053
X coordinate		36.221	0		11.157	0
Y coordinate		122.603	0		12.549	0
R-sq.(adj)	0.088			0.052		
AUC	0.676					
Spearman´s corr.				0.105		
Sample (n)	2448			658		

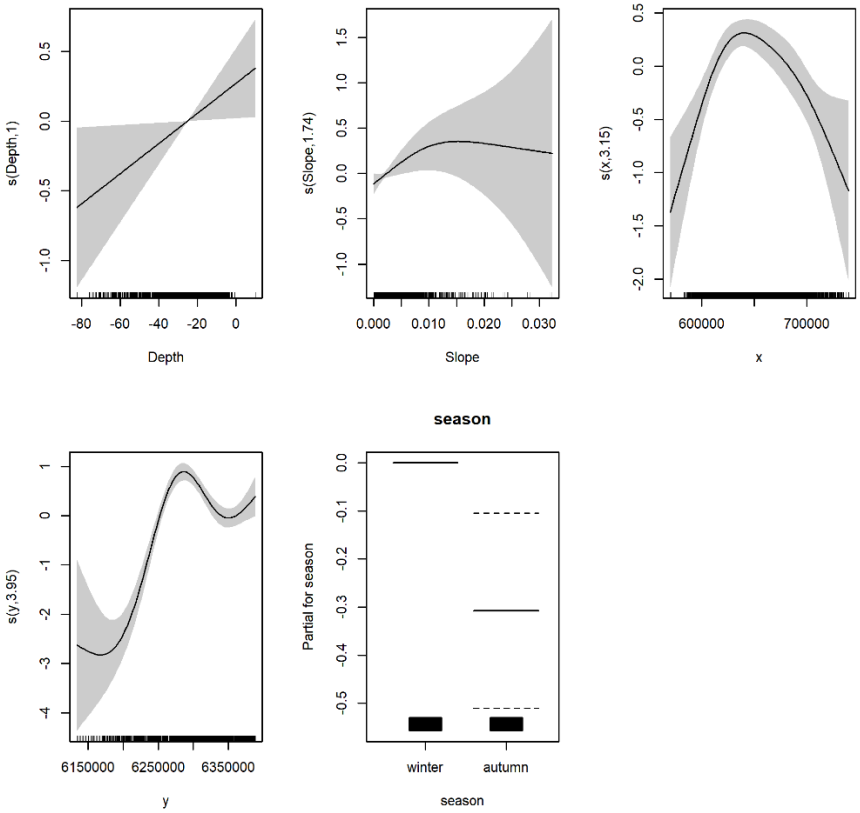

Figure C- 15 Response curves for presence absence model parts for Razorbill *Alca torda*

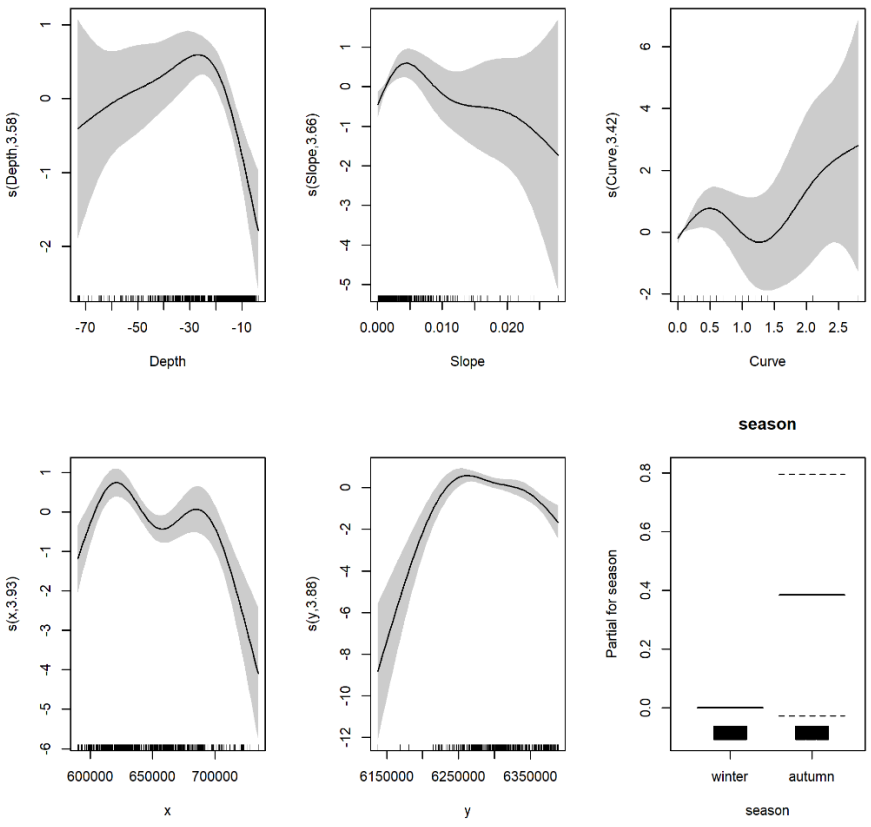

Figure C- 16 Response curves for positive model parts for Razorbill *Alca torda*

D APPENDIX D – Meta Data

D.1 North Sea – west coast

ENS – Investigation of density and abundance of seabirds in Danish waters
Project no. 11823165
Responsible consultant: DHI A/S
Metadata for the following file: North_Sea_west_coast.mpk Skov, H. Mortensen, L.O., Tuhuteru, N. (2019) ”Site selection for offshore wind farms in Danish waters; investigations of bird distribution and abundance”. Report for Energistyrelsen.
File map: The file is a map package including rasters on predicted marine bird distribution in the North Sea west coast, which include: Common Scoter (Melanitta nigra): January, February, March and April Red- and Black-throated Divers (Gavia stellata and Gavia arctica): February, March, April and May   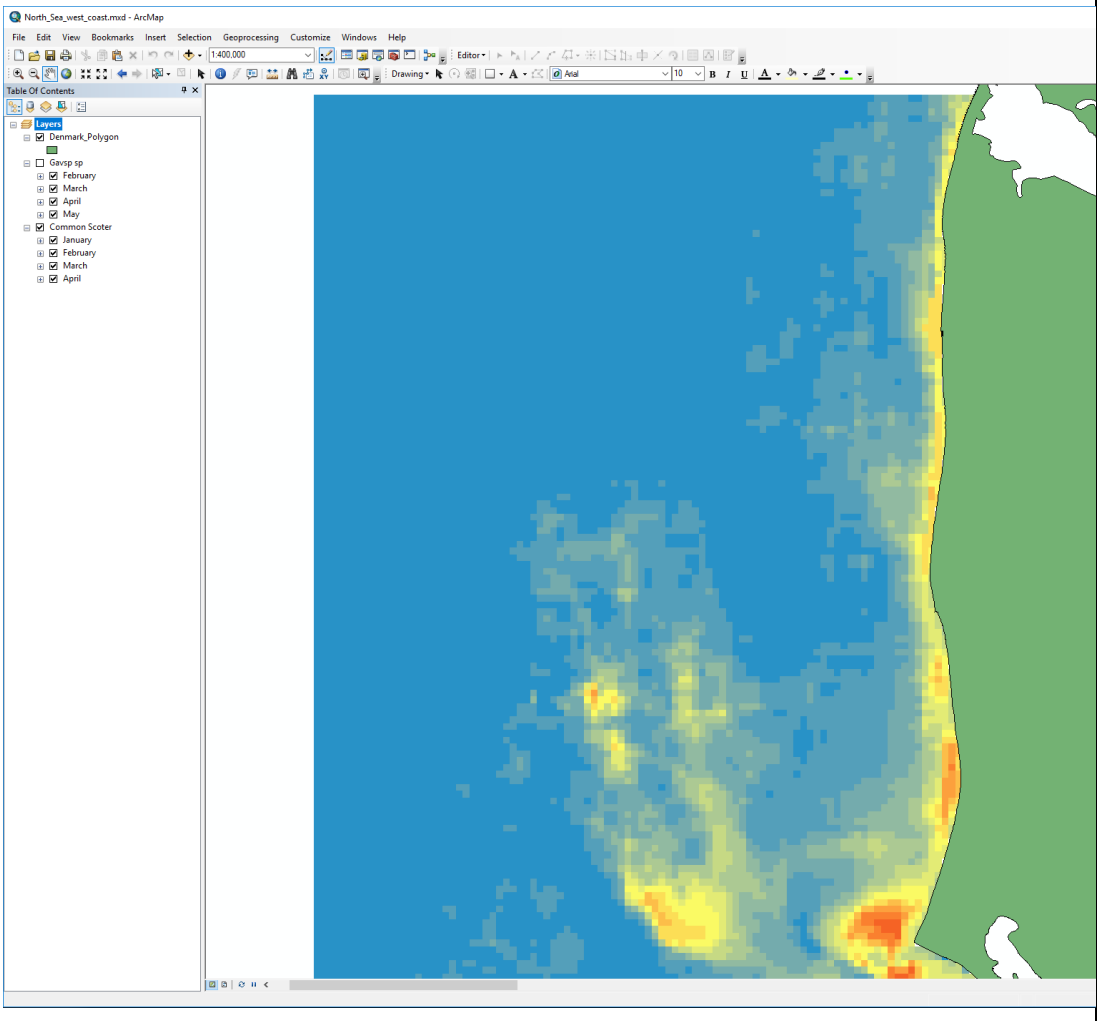

ENS – Investigation of density and abundance of seabirds in Danish waters
Sources: Models has been created based on survey data supplied from Aarhus University (years: 1999, 2000, 2001, 2002, 2003, 2004, 2005, 2006, 2007, 2008, 2009, 2011, 2012, 2013, 2016), Orbicon (2013) and NIRAS (2013,2014) Predictive data has been derived from the MIKE by DHI Hydrodynamic models
Geo-reference: UTM 32 WGS 84
Date of delivery from sources: Jan-Apr 2019
Special conditions: Raster data have been clipped to match published maps in Skov et al. 2019
Description of data: Data are rasters of the predicted mean density of seabirds at the North Sea west coast divided into months of the year. The density is predicted based on predictive modelling, conducted on arial line transect surveys in the North Sea. The resolution of rasters is 3000 meters and values are expressed in numbers per km^2.

D.2 Jammerbugten

ENS – Investigation of density and abundance of seabirds in Danish waters
Project no. 11823165
Responsible consultant: DHI A/S
Metadata for the following file: Jammerbugten.mpk Skov, H. Mortensen, L.O., Tuhuteru, N. (2019) ”Site selection for offshore wind farms in Danish waters; investigations of bird distribution and abundance”. Report for Energistyrelsen.
File map: The file is a map package including rasters on predicted marine bird distribution in Jammerbugten, which include: Common Scoter (Melanitta nigra): January, February, March and April Red- and Black-throated Divers (Gavia stellata and Gavia arctica): February, March, April and May   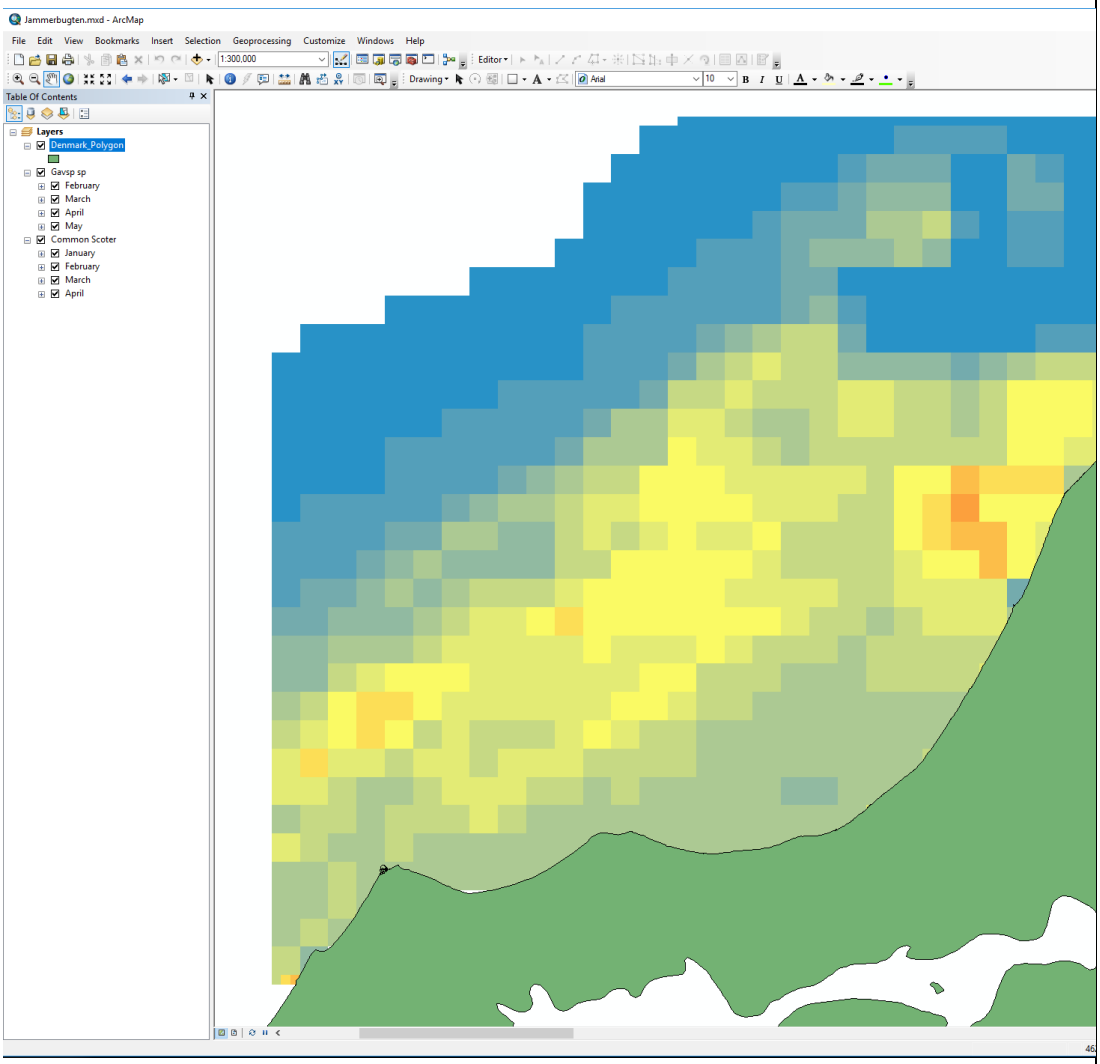

ENS – Investigation of density and abundance of seabirds in Danish waters
Sources: Models has been created based on survey data supplied from Aarhus University (years: 1999, 2000, 2001, 2002, 2003, 2004, 2005, 2006, 2007, 2008, 2009, 2011, 2012, 2013, 2016), Orbicon (2013) and NIRAS (2013,2014) Predictive data has been derived from the MIKE by DHI Hydrodynamic models
Geo-reference: UTM 32 WGS 84
Date of delivery from sources: Jan-Apr 2019
Special conditions: Raster data have been clipped to match published maps in Skov et al. 2019
Description of data: Data are rasters of the predicted mean density of seabirds at the North Sea west coast divided into months of the year. The density is predicted based on predictive modelling, conducted on aerial line transect surveys in the North Sea. The resolution of rasters is 3000 meters and values are expressed in numbers per km^2.

D.3 Kattegat

ENS – Investigation of density and abundance of seabirds in Danish waters
Project no. 11823165
Responsible consultant: DHI A/S
Metadata for the following file: Kattegat_Predictions.mpk Skov, H. Mortensen, L.O., Tuhuteru, N. (2019) ”Site selection for offshore wind farms in Danish waters; investigations of bird distribution and abundance”. Report for Energistyrelsen.
File map: The file is a map package including rasters on predicted marine bird distribution in southern Kattegat, which include: Common Eider (Somateria mollissima): spring, summer and winter Common Scoter (Melanitta nigra): spring and winter Red- and Black-throated Divers (Gavia stellata and Gavia arctica): spring, summer and winter Black-legged Kittiwake (Rissa tridactyla): autumn and winter Razorbill (Alca torda): autumn and winter Velvet Scoter (Melanitta fusca): spring and winter   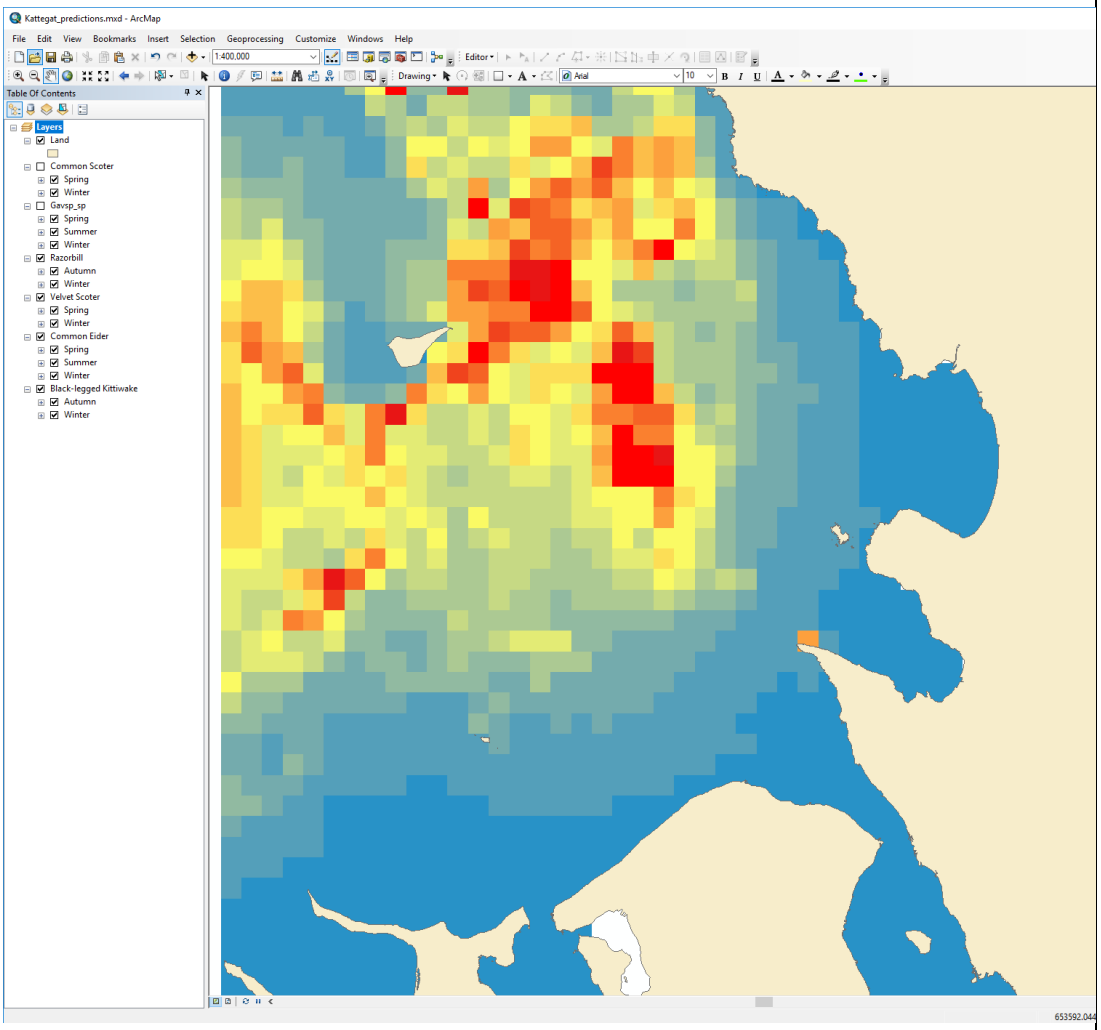

ENS – Investigation of density and abundance of seabirds in Danish waters
Sources: Models have been created based on survey data supplied from Aarhus University (years 2004, 2008, 2012, 2013, 2016), Lund University (years 2017, 2018, 2019) and the "European Seabirds at Sea" data base. Predictive data have been derived from MIKE by DHI Hydrodynamic models.
Geo-reference: UTM 32 WGS 84
Date of delivery from sources: Jan-Apr 2019
Special conditions: Raster data have been clipped to match published maps in Skov et al. 2019
Description of data: Data is rasters of the predicted mean density of seabirds in Kattegat divided into seasons. The density is predicted based on predictive modelling, conducted on aerial and ship-based line transect surveys in Kattegat. The resolution of rasters is 3000 meters and values are expressed in numbers per km^2.